University College London

Department of Physics & Astronomy

Variational calculations of rotation-vibration spectra for small molecules of astrophysical interest

Alec Owens

A thesis submitted for the degree of Doctor of Philosophy

March 29, 2017

I, Alec Owens, confirm that the work presented in this thesis is my own. Where information has been derived from other sources, I confirm that this has been indicated in the thesis.

Abstract

Variational calculations of rotation-vibration spectra are presented for a range of four- and five-atom molecules of atmospheric and astrophysical importance. Using state-of-the-art electronic structure methods, new nine-dimensional potential energy and dipole moment surfaces are constructed for methyl chloride (CH_3Cl), silane (SiH_4), and methane (CH_4). The respective surfaces are rigorously evaluated against high-resolution spectroscopic data from a variety of experimental sources. The *ab initio* potential energy surfaces represent some of the most accurate to date, whilst intensity simulations utilizing the dipole moment surfaces show good agreement with experiment.

A novel application of rotation-vibration computations is introduced to investigate the sensitivity of spectral lines to a possible space-time variation of the proton-to-electron mass ratio μ. The approach relies on finding the mass dependence of the computed energy levels and is only possible because of the remarkable accuracy of variational calculations. Highly sensitive transitions are uncovered for ammonia (NH_3) and the hydronium cation (H_3O^+) which could lead to a tighter constraint on a varying μ. An advantage of the variational approach is that Einstein A coefficients can be determined to help guide future laboratory and astronomical observations.

This thesis demonstrates the current capabilities of variational calculations of rotation-vibration spectra and highlights the challenges faced by the field.

Publications

The work in this thesis is based on the following publications:

Chapter 4

Accurate *ab initio* vibrational energies of methyl chloride
A. Owens, S. N. Yurchenko, A. Yachmenev, J. Tennyson, and W. Thiel, J. Chem. Phys. **142**, 244306 (2015).

A global *ab initio* dipole moment surface for methyl chloride
A. Owens, S. N. Yurchenko, A. Yachmenev, J. Tennyson, and W. Thiel, J. Quant. Spectrosc. Radiat. Transf. **184**, 100 (2016).

Chapter 5

A global potential energy surface and dipole moment surface for silane
A. Owens, S. N. Yurchenko, A. Yachmenev, and W. Thiel, J. Chem. Phys. **143**, 244317 (2015).

Chapter 6

A highly accurate *ab initio* potential energy surface for methane
A. Owens, S. N. Yurchenko, A. Yachmenev, J. Tennyson, and W. Thiel, J. Chem. Phys. **145**, 104305 (2016).

Chapter 7

Accurate prediction of the ammonia probes of a variable proton-to-electron mass ratio
A. Owens, S. N. Yurchenko, W. Thiel, and, V. Špirko, Mon. Not. R. Astron. Soc. **450**, 3191 (2015).

Enhanced sensitivity to a possible variation of the proton-to-electron mass ratio in ammonia
A. Owens, S. N. Yurchenko, W. Thiel, and, V. Špirko, Phys. Rev. A **93**, 052506 (2016).

Accurate prediction of H_3O^+ and D_3O^+ sensitivity coefficients to probe a variable proton-to-electron mass ratio
A. Owens, S. N. Yurchenko, O. L. Polyansky, R. I. Ovsyannikov, W. Thiel, and, V. Špirko, Mon. Not. R. Astron. Soc. **454**, 2292 (2015).

Acknowledgements

I would like to thank my supervisors Dr. Sergey Yurchenko at UCL and Prof. Walter Thiel at the Max-Planck-Institut für Kohlenforschung. In addition I am grateful to Prof. Jonathan Tennyson for acting as a subsidiary supervisor at UCL, Dr. Andrey Yachmenev, and Prof. Vladimir Špirko.

Contents

List of Figures

List of Tables

1 Introduction

Accurate *ab initio* electronic structure calculations combined with a variational treatment of nuclear motion are playing an increasingly important role in high-resolution molecular spectroscopy. Nowadays, the process of generating comprehensive line lists detailing millions of transitions for small polyatomic molecules is relatively straightforward. The resulting datasets can be used for rigorous spectral analysis with applications in both terrestrial and astrophysical studies.

To calculate the rotation-vibration spectrum of a molecule from first principles it is necessary to solve the non-relativistic, time-independent Schrödinger equation,

$$H\Psi = E\Psi. \tag{1.1}$$

For all but the simplest systems an exact solution is not possible. Instead, levels of approximation must be introduced to obtain a satisfactory result. The most significant of these is the Born-Oppenheimer (BO) approximation [1–3]. Here, the total wavefunction Ψ of the molecular system is separated into a product of the electronic and nuclear wavefunctions,

$$\Psi(\mathbf{r}_i, \mathbf{R}_A) = \psi^{\text{elec}}(\mathbf{r}_i; \mathbf{R}_A)\psi^{\text{nuc}}(\mathbf{R}_A). \tag{1.2}$$

The nuclear wavefunction ψ^{nuc} depends on the nuclear coordinates $\mathbf{R}_A$, whilst the electronic wavefunction ψ^{elec} depends explicitly on the electronic coordinates $\mathbf{r}_i$, and parametrically on the nuclear coordinates $\mathbf{R}_A$. It is this separation that has allowed the theoretical study of atoms and molecules to flourish.

Because the masses of the nuclei are much larger than those of the electrons, the nuclei are considered fixed in space with respect to electron motion. For each fixed nuclear geometry the corresponding electronic Schrödinger equation can be solved

to give the electronic energy. Repeating this for numerous nuclear configurations produces a potential energy surface (PES) along which the nuclei move. The BO approximation works because of the very strong coupling between electrons and nuclei; a change in nuclear geometry causes an instantaneous change of electron motion.

For a molecule containing N atoms and n electrons, the molecular Hamiltonian in atomic units ($m_e = e = \hbar = 4\pi\epsilon_0 = 1$) is expressed as

$$\begin{aligned} H = &-\frac{1}{2}\sum_{i=1}^{n}\nabla_i^2 - \sum_{A=1}^{N}\frac{1}{2M_A}\nabla_A^2 - \sum_{i=1}^{n}\sum_{A=1}^{N}\frac{Z_A}{|\mathbf{r}_i - \mathbf{R}_A|} \\ &+ \sum_{i=1}^{n}\sum_{j>i}^{n}\frac{1}{|\mathbf{r}_i - \mathbf{r}_j|} + \sum_{A=1}^{N}\sum_{B>A}^{N}\frac{Z_A Z_B}{|\mathbf{R}_A - \mathbf{R}_B|}, \end{aligned} \tag{1.3}$$

where lower case subscripts refer to electrons, upper case subscripts to nuclei, and M_A and Z_A are the mass and charge of the nuclei, respectively. In a more compact form and dropping the coordinate indices,

$$H = T_e(\mathbf{r}) + T_N(\mathbf{R}) + V_{eN}(\mathbf{r}, \mathbf{R}) + V_{ee}(\mathbf{r}) + V_{NN}(\mathbf{R}), \tag{1.4}$$

where there is a kinetic energy operator T for electrons e and nuclei N, and a potential energy V from eN Coulombic attraction, and ee/NN Coulombic repulsion.

Selecting a fixed nuclear configuration, the electronic Hamiltonian is

$$H_{\text{elec}} = T_e(\mathbf{r}) + V_{eN}(\mathbf{r}; \mathbf{R}) + V_{ee}(\mathbf{r}) + V_{NN}(\mathbf{R}), \tag{1.5}$$

where $V_{NN}(\mathbf{R})$ is a constant value for a chosen $\mathbf{R}$, such that

$$H_{\text{elec}}(\mathbf{r}; \mathbf{R})\psi^{\text{elec}}(\mathbf{r}; \mathbf{R}) = E_{\text{elec}}(\mathbf{R})\psi^{\text{elec}}(\mathbf{r}; \mathbf{R}). \tag{1.6}$$

Repeatedly solving Eq. (1.6) to get the electronic energy E_{elec} for a selection of nuclear geometries gives the Born-Oppenheimer PES, $V_{\text{BO}}(\mathbf{R})$. It is independent of the masses of the nuclei and is applicable to all isotopologues of a given molecule.

Once $V_{\mathrm{BO}}(\mathbf{R})$ is known we can solve for the nuclear motion,

$$(T_N + V_{\mathrm{BO}})\psi^{\mathrm{nuc}} = E\psi^{\mathrm{nuc}}, \tag{1.7}$$

to get the total energy E of the system in the electronic state defined by the PES. In this thesis we only consider rotations and vibrations in the ground electronic state.

Note that in the BO approximation the contribution from the nuclear kinetic energy operator T_N acting on $\psi^{\mathrm{elec}}(\mathbf{r};\mathbf{R})$ is neglected. The terms which arise from allowing T_N to act on $\psi^{\mathrm{elec}}(\mathbf{r};\mathbf{R})$ can improve the description of the PES. The most straightforward to compute is the diagonal Born-Oppenheimer correction (DBOC) or adiabatic correction (discussed in Sec. 2.4.4). Further residual errors arising from the wavefunction separation of Eq. (1.2) are treated with so-called nonadiabatic corrections. However, their calculation is a more complicated affair and formally requires a summation over all electronic states of a molecule. It has been argued that the use of atomic mass values in rovibrational calculations can to some extent compensate for the errors of the BO approximation [4], and this approach is often employed in high-accuracy studies.

The energies and eigenfunctions obtained from solving Eq. (1.7) are the necessary quantities for simulating rovibrational spectra. In Fig 1.1, a general outline of the stages involved is presented. Symmetry and selection rules will govern the allowed transitions between different energy levels, however, to compute the corresponding transition intensities requires knowledge of the molecular dipole moment surface (DMS). The DMS describes the charge distribution of a molecule as a function of nuclear geometry and, like the PES, can be routinely calculated using electronic structure methods. Once known it is utilized with the rovibrational eigenfunctions to determine intensities.

In this thesis, rotation-vibration calculations will be performed on a range of four- and five-atom molecules of astrophysical importance. The molecular systems considered are: methyl chloride (CH_3Cl), silane (SiH_4), methane (CH_4), ammonia (NH_3) and hydronium (H_3O^+). New potential energy and dipole moment surfaces

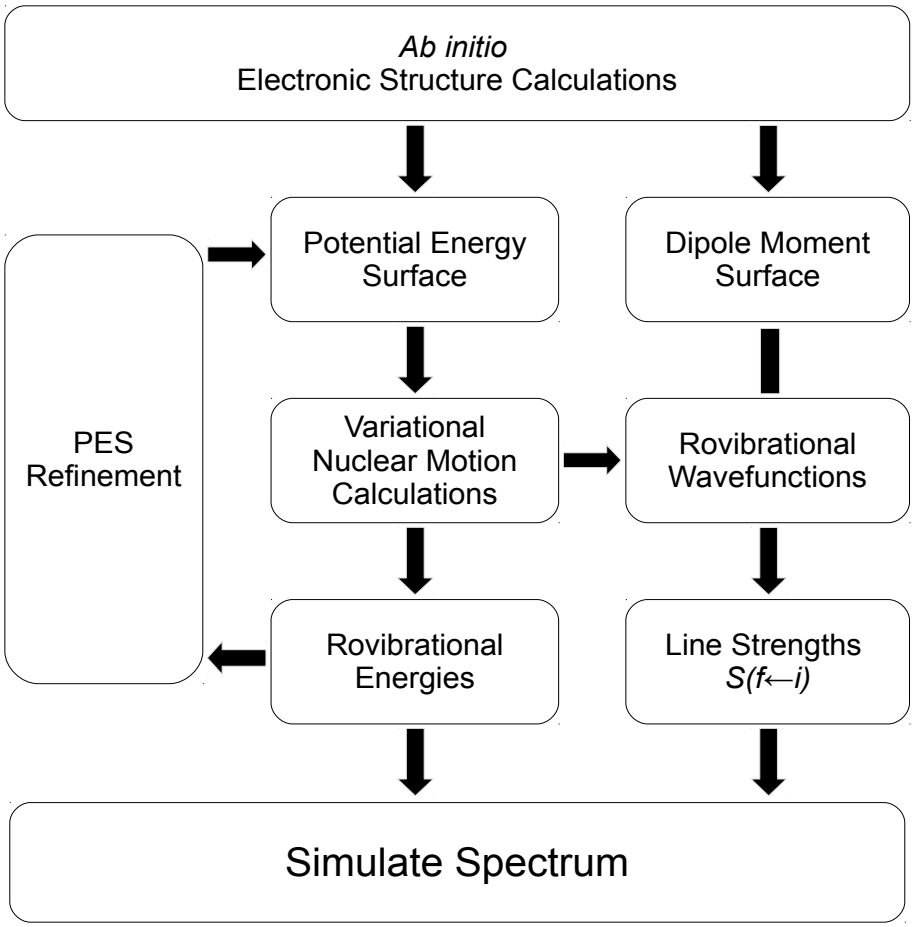

Figure 1.1: Overview of computing a rotation-vibration spectrum for a small polyatomic molecule from first principles.

for CH_3Cl, SiH_4 and CH_4 will be generated using state-of-the-art *ab initio* theory. Using variational calculations the respective surfaces will be rigorously evaluated at the current threshold of what is computationally possible for high-accuracy studies of five-atom systems. For NH_3 and H_3O^+, existing surfaces will be used to investigate the sensitivity of spectral lines to a possible variation of the proton-to-electron mass ratio μ. The approach presented is a novel application of variational calculations of rovibrational spectra.

A key motivation for the present work has been the discovery of over 3000 planets outside of our solar system. Termed exoplanets (short for extrasolar planets), characterizing their atmospheric composition has created a huge demand for spectroscopic data, the majority of which has not been catalogued. Unlike spectra recorded

in the laboratory at room temperature, exoplanets are likely to be much hotter objects with temperatures up to 2000 K. There is a dramatic increase in the number of molecular transitions at higher temperatures; for example a recent methane hot line list, 10to10 [5], applicable for temperatures up to 1500 K contained 9.8 billion transitions. Obtaining this kind of coverage from laboratory measurements is impractical and a far more viable solution is to employ theory, especially now the methods are well established. The successful characterization of exoplanet atmospheres also requires a range of molecular species to be considered. HITEMP [6] was the only spectroscopic database dealing exclusively with hot spectra but contained only five molecules (H_2O, CO_2, CO, OH, NO) and their isotopologues.

The ExoMol project [7, 8] was set up to address these issues and is actively computing key spectroscopic data for the study of exoplanet and other hot atmospheres. Using high-level *ab initio* methods as part of a robust theoretical model, comprehensive rotation-vibration line lists and spectra are being constructed for important diatomic and polyatomic species. A degree of empirical tuning is usually incorporated into the process by refining the PES to experimental data. This step is necessary to reach the level of accuracy required by high-resolution spectroscopy. Whilst some molecules such as CH_3Cl have to be started from scratch, other systems can use existing potential energy and dipole moment surfaces if available.

A portion of the work presented in this thesis is inspired by a growing field of research concerned with spectroscopic tests of fundamental physics. Molecules provide an attractive testing ground for probing possible variations of the fundamental constants of nature. In particular, rotation-vibration transitions are sensitive to the proton-to-electron mass ratio. If any variation did exist it would cause observable shifts in the transition frequencies of certain molecules. Not all transitions are suitable however. To determine the most favourable, the sensitivity of a transition can be quantified, via the calculation of a sensitivity coefficient, once the mass dependence of the involved energy levels is known. Variational calculations are comprehensive and accurate and this presents the opportunity to investigate promising candidate

systems such as NH_3 and H_3O^+.

However, before any molecules are considered it is important to discuss the theoretical methods required to accurately solve the non-relativistic, time-independent Schrödinger equation. As seen earlier, solution of Eq. (1.1) is done in two stages. First we have to treat the electronic Schrödinger equation and this is the subject of Chapter 2. Here the focus will be on highly accurate electronic structure methods suitable for small, closed-shell molecules. After establishing the Hartree-Fock wavefunction and the definition of electron correlation, we will work towards explicitly correlated F12 coupled cluster theory which is a very powerful approach. However, the electronic structure method is meaningless without the correct choice of one-particle basis set. The concepts behind basis set construction will therefore be introduced before focusing on the correlation-consistent class of basis sets and their F12-optimized counterparts. Further improvements in accuracy come from basis set extrapolation and the treatment of additional higher-level corrections to the electronic energy. These topics will also be discussed.

In Chapter 3 we turn to solving the nuclear Schrödinger equation. For high-accuracy work a complete treatment of the nuclear motion problem is offered by variational approaches. In this thesis we use the computer program TROVE [9]. Therefore we will focus only on the methodology of TROVE and how it achieves its generality. The limitations of electronic structure theory means empirical refinement of the PES is a necessary step and we examine the implementation in TROVE. We will then move on to the topic of line intensities and the procedure used to compute the line strength of a transition for a given molecular DMS. Spectral lines have a definite shape and it is important to be aware of the physical factors which cause line broadening. We conclude by looking at these effects and how best to model them using shape functions.

Having reviewed the theoretical basis for simulating rotation-vibration spectra from first principles, the first system we will consider is methyl chloride in Chapter 4. This molecule is of the form XY_3Z — a structure which had not previously been

implemented in TROVE. Chapter 4 should therefore illustrate the entire process of generating a spectrum from scratch. This begins with the application of high-level *ab initio* theory to compute an accurate PES and DMS. Once suitable analytic representations have been defined to represent the *ab initio* data, the respective surfaces can be rigorously tested. A reliable assessment is only possible with well converged term values but the increasing size of matrices which must be considered can often make this problematic computationally. A way of circumventing this issue in TROVE is to employ a complete vibrational basis set extrapolation and this will be described with respect to CH_3Cl. We will then go on to compute vibrational energies, the equilibrium geometry of CH_3Cl, pure rotational energies, vibrational transition moments, absolute line intensities, and a preliminary rotation-vibration line list.

The next system we treat is silane in Chapter 5 and this will be more straightforward having dealt with CH_3Cl, and because XY_4-type molecules have been previously implemented in TROVE. A key consideration in this chapter will be the approach to the electronic structure calculations, notably the PES. Generating a highly accurate *ab initio* PES can be a computationally intensive task due to the consideration of additional higher-level corrections to the electronic energy. For SiH_4 we take a slightly different approach to that of CH_3Cl and we employ certain approximations to be more time-effective. A new nine-dimensional DMS is constructed before both surfaces are evaluated with variational calculations. The equilibrium bond length, pure rotational energies, vibrational energies, vibrational transition moments, absolute line intensities, and an overview of the rotation-vibration spectrum of silane are all computed and compared with experiment.

With the knowledge acquired from constructing *ab initio* PESs for CH_3Cl and SiH_4, we turn our attention to the atmospherically important methane molecule in Chapter 6. A highly accurate *ab initio* PES for CH_4 is presented and we calculate vibrational energies, the equilibrium geometry, and pure rotational energies to compare with experiment. This chapter represents a culmination of the techniques

learnt over the previous two chapters.

In Chapter 7 we explore the mass sensitivity of rotation-vibration energy levels of XY_3-type molecules. This is done to investigate a possible variation of the proton-to-electron mass ratio and is possible because of the remarkable accuracy of variational calculations. After a brief introduction to the field of spectroscopic tests of fundamental physics, we look at other methods used to compute sensitivity coefficients before introducing a new, variational approach. A comprehensive study of ammonia and the hydronium cation will then be carried out with the aim of uncovering particularly sensitive transitions which could help guide future observations.

Concluding remarks on the work presented in this thesis are given in Chapter 8.

2 Solving the electronic Schrödinger equation

2.1 Introduction

A considerable amount of chemistry is determined by the interactions between electrons. As a result, tremendous progress has been made in the development of clever approximations to solve the electronic Schrödinger equation. The field of quantum chemistry is a very active area of research and shows no sign of slowing down. A range of electronic structure methods are available to treat molecular systems of varying size and structure. For small molecules, highly accurate wave-function based approaches offer a systematic route towards the correct result and we focus on this class of methods in this chapter.

Computing the rotation-vibration spectrum of a molecule requires knowledge of the molecular PES and DMS. These are constructed on extensive grids of nuclear geometries which can contain, for example, around $100,000$ points for a five-atom molecule. Given the huge number of calculations which are required, selecting the most suitable method and one-particle basis set to solve the electronic Schrödinger equation is not always straightforward. It is important to strike a balance between accuracy and computational expense.

The PES is the foundation of rovibrational energy level calculations and its quality not only dictates the accuracy of line positions but can be crucial for improvements in computed band intensities [10]. The DMS reflects the charge distribution of a molecule as a function of nuclear geometry. Because the electric dipole moment $\boldsymbol{\mu}$ is a vector quantity, three surfaces (corresponding to the Cartesian components μ_X, μ_Y and μ_Z) are required. The dipole moment is equal to the first derivative of

the electronic energy with respect to external electric field strength ϵ. In component form,

$$\mu_A = -\left(\frac{dE}{d\epsilon_A}\right)_{\epsilon_A=0}, \tag{2.1}$$

where the Cartesian coordinate axis $A = X, Y, Z$. It is straightforward to evaluate Eq. (2.1) using finite differences as the derivatives can be approximated using the expression,

$$\frac{dE}{d\epsilon_A} \approx \frac{E(\epsilon_A) - E(-\epsilon_A)}{2\epsilon_A}. \tag{2.2}$$

The finite-field approach, where an electric field is applied along each coordinate axis, is flexible as any electronic structure method can be employed. There is also the capability of incorporating additional higher-level corrections (discussed in Sec. 2.4) to the DMS to improve its accuracy. However, the finite differentiation technique is expensive as seven calculations are required for each nuclear geometry (two for each coordinate axis and a field-free calculation for the electronic energy). Alternatively, Eq. (2.1) can be evaluated using analytical derivatives which are more accurate but only available in certain quantum chemistry codes. A final option is to compute the DMS as the expectation value of the dipole moment operator but this holds only for truly variational wavefunctions. Regardless of the method chosen, theoretical intensity simulations which rely on an *ab initio* DMS are nowadays competitive with experiment [11].

The choice then of theoretical method and basis set to compute the PES and DMS is extremely important as it will heavily influence the quality of the final line list. In this chapter we will discuss the theoretical basis for solving the electronic Schrödinger equation and the preferred *ab initio* theory and one-particle basis sets for doing this. The aim is to provide an understanding of electronic structure methods so that they can be confidently used in practical high-accuracy calculations. Only the fundamental concepts which I consider important are presented as there are numerous books and review articles which detail the working equations.

2.2 Electronic structure methods

2.2.1 Hartree-Fock theory

In Hartree-Fock theory each electron moves in an average field created by the other electrons with no independent interactions. A system of N electrons is represented as a single Slater determinant

$$\Psi_{\mathrm{SD}}(\mathbf{x}_1, \mathbf{x}_2, \ldots, \mathbf{x}_N) = \frac{1}{\sqrt{N!}} \begin{vmatrix} \chi_1(\mathbf{x}_1) & \chi_2(\mathbf{x}_1) & \cdots & \chi_N(\mathbf{x}_1) \\ \chi_1(\mathbf{x}_2) & \chi_2(\mathbf{x}_2) & \cdots & \chi_N(\mathbf{x}_2) \\ \vdots & \vdots & \ddots & \vdots \\ \chi_1(\mathbf{x}_N) & \chi_2(\mathbf{x}_N) & \cdots & \chi_N(\mathbf{x}_N) \end{vmatrix}, \tag{2.3}$$

which is antisymmetric with respect to the interchange of the coordinates of any two electrons, hence satisfying the Pauli exclusion principle. Here, χ_i is a spin-orbital with the spatial ($\mathbf{r}$) and spin (ω) degrees of freedom expressed as the space-spin coordinate $\mathbf{x}_i = (\mathbf{r}_i, \omega_i)$.

The Hartree-Fock method, or self-consistent-field (SCF) procedure, is concerned with finding the optimum set of spin-orbitals to give the Slater determinant with the lowest energy. This is done by solving the Hartree-Fock equations. It is an iterative procedure based on the variational principle such that

$$E_{\mathrm{HF}} = \frac{\langle \Psi_{\mathrm{SD}} | H_{\mathrm{elec}} | \Psi_{\mathrm{SD}} \rangle}{\langle \Psi_{\mathrm{SD}} | \Psi_{\mathrm{SD}} \rangle} \geq E_{\mathrm{exact}}. \tag{2.4}$$

The HF energy E_{HF} provides an upper bound to the exact ground state energy E_{exact}, with the corresponding HF wavefunction being the best single determinant approximation to the electronic ground state of the system. It is this wavefunction that forms the basis of many post-Hartree-Fock methods. Despite the fact HF is able to recover around 99.9% of the exact ground state energy, it is simply not accurate enough.

Quantum chemical methods are instead focused on recovering the correlation

energy, defined as

$$E_{\text{corr}} = E_{\text{exact}} - E_{\text{HF}}. \tag{2.5}$$

For many-electron systems this quantity is always negative. It can be understood as the contribution from electron-electron interactions not accounted for by the mean-field approach of Hartree-Fock. The correlation energy is often partitioned into two contributions: static and dynamic correlation. In certain situations, for example bond breaking, multiple Slater determinants are needed to get an reasonable zeroth-order description of the wavefunction. A single HF reference is not sufficient and the resulting difference in energy between these two representations is called static correlation. Dynamic correlation is attributed to the motion of the electrons and is short-range in origin. In most cases the distinction between the two is not well defined and the partitioning can be somewhat arbitrary.

2.2.2 Configuration interaction

The most straightforward post-HF method is configuration interaction (CI). Here, the CI wavefunction is represented as a linear combination of Slater determinants,

$$\Psi_{\text{CI}} = c_0\Psi_{\text{HF}} + \sum_{i,a} c_i^a \Psi_i^a + \sum_{i<j,a<b} c_{ij}^{ab}\Psi_{ij}^{ab} + \ldots, \tag{2.6}$$

where Ψ_i^a is the Slater determinant (or configuration) obtained by exciting an electron in spin-orbital i to spin-orbital a in Ψ_{HF}. The indices $i, j, \ldots$ and $a, b, \ldots$ denote occupied and unoccupied spin-orbitals, respectively. The expansion coefficients $c_0, c_i^a, c_{ij}^{ab}, \ldots$ are optimized in a variational procedure.

If all possible configurations are constructed for an N-electron system, we have full configuration interaction (FCI). This corresponds to solving the electronic Schrödinger equation exactly for a given one-particle basis set (introduced in Sec. 2.3) and represents the most accurate treatment one can hope for. However, in all but the smallest systems FCI is not possible due to the steep computational scaling of the method as the number of configurations in the expansion increases. Instead the CI

expansion must be truncated at some level of excitation. For example, CI with only single and double excitations, i.e. the terms shown in Eq. (2.6), is known as CISD.

Many multireference electronic structure methods employ the form of the CI wavefunction (a linear combination of Slater determinants). These approaches select the most important configurations and are motivated by the inadequacy of the HF determinant to reliably describe the system. Multireference configuration interaction (MRCI) is often used to compute global PESs as it provides accurate energies towards dissociation. For closed-shell molecules near equilibrium however, the HF determinant dominates the wavefunction and coupled-cluster methods are preferred.

2.2.3 Coupled-cluster theory

Coupled-cluster (CC) theory originated in nuclear physics in the 1950s but largely went unnoticed. It was the application to atomic and molecular electronic structure combined with the growth in computing power which enabled CC theory to become a powerful method to treat electron correlation (see Bartlett and Musial [12] and references therein for a historical overview). The success of CC theory is rooted in its exponential ansatz,

$$\begin{aligned}\Psi_{\mathrm{CC}} &= \exp(T)\Psi_{\mathrm{HF}} \\ &= (1 + T + T^2/2 + T^3/3! + \ldots)\Psi_{\mathrm{HF}}.\end{aligned} \tag{2.7}$$

Here, the cluster operator is given by

$$T = T_1 + T_2 + T_3 + \ldots + T_N, \tag{2.8}$$

with all single excitation operators represented by the term T_1, all double excitations by T_2, triples by T_3, etc. That is,

$$T = \sum_{\mu} t_\mu \tau_\mu, \tag{2.9}$$

with each excitation operator τ_μ having an associated cluster amplitude t_μ. The general index μ labels spin-orbitals for an N-electron system.

An exact solution to the Schrödinger equation in a given one-particle basis set is obtained by including all possible excitations in the cluster operator. This is equivalent to FCI in the same basis. For the majority of systems such an approach is not feasible computationally so the level of excitation in the cluster operator is truncated. This produces the well-known acronyms CCSD, CCSDT, CCSDTQ,... where the addition of another letter corresponds to the inclusion of higher excitations.

Let us consider CCSD (coupled-cluster with all single and double excitations) i.e. $T = T_1 + T_2$. The singly-excited determinants are described by the connected term

$$T_1\Psi_{\mathrm{HF}} = \sum_{i,a} t_i^a \Psi_i^a, \tag{2.10}$$

whilst for doubly-excited determinants there is a contribution from a connected and disconnected term

$$(T_2 + \frac{1}{2}T_1^2)\Psi_{\mathrm{HF}} = \sum_{i<j,a<b} t_{ij}^{ab}\Psi_{ij}^{ab} + \frac{1}{2}\sum_{i,a}\sum_{j,b} t_i^a t_j^b \Psi_{ij}^{ab}. \tag{2.11}$$

Two disconnected terms $(T_1T_2 + \frac{1}{6}T_1^3)$ contribute to the triply-excited determinants, and so on. We see that by using an exponential ansatz, all possible determinants which enter the FCI wavefunction are generated for a given basis set. The description of these determinants (through the cluster amplitudes t_μ) is what changes and improves by adding higher levels of excitation to T. To determine the cluster amplitudes, a nonlinear set of equations is solved in an iterative procedure. If the HF determinant is a good zeroth-order reference, the series rapidly converges to the exact energy within the chosen basis.

If $\mathcal{N}$ is a measure of molecular size, CCSD calculations are of the order $\mathcal{O}(\mathcal{N}^6)$, whilst CCSDT scales as $\mathcal{O}(\mathcal{N}^8)$. Such steep computational scaling led to the development of approximate ways to treat the triples contribution. The most successful of these is the popular CCSD(T) [coupled cluster with all singles and doubles and

a perturbational estimate of connected triple excitations].

Although CCSD(T) is considered the gold standard of quantum chemistry, it can only be used for small to medium sized systems (up to 20 atoms) as the computational cost is still prohibitive [$\mathcal{O}(\mathcal{N}^7)$]. This challenge is being overcome with the development of local coupled-cluster methods. The success of local CC methods is based on the short-range origin of dynamic electron correlation. Already CCSD(T) calculations have been carried out on an entire protein containing 644 atoms [13]. I expect these methods to become prevalent in the near future.

More limiting for high-accuracy work (even for small molecules) is the slow convergence of the correlation energy with respect to basis set size. As the interelectronic distance $r_{12} \to 0$ a cusp occurs in the wavefunction. Accurately describing the shape of this cusp using an expansion in products of Gaussian-type orbitals (the most common one-electron functions) is problematic, hence the slow convergence. This issue has been addressed with the development of explicitly correlated methods which will be discussed in Sec. 2.2.4.

Note that CC methods are size-extensive [14]. This means that the exact energy scales correctly (linearly) with the number of particles in the system. It is a formal scaling property of the energy applicable to any geometry and ensures accurate relative energies along a PES. It is closely related to, but more general than, the concept of size-consistency [15]. A size-consistent method for system AB must satisfy

$$E_{AB}(r \to \infty) = E_A + E_B, \tag{2.12}$$

where subsystems A and B are separated by distance r. Hartree-Fock, many-body perturbation theory and coupled-cluster theory are all size-extensive methods but they are only size-consistent if the reference wavefunction they are based on has correct dissociation behaviour. Truncated CI approaches are neither size-extensive, nor size-consistent.

2.2.4 Explicitly correlated coupled-cluster methods

Explicitly correlated F12 methods are at the forefront of practical high-accuracy calculations and offer a far more efficient way to compute reliable results. They overcome the slow convergence of the correlation energy with basis set size by introducing an explicit dependence on the interelectronic distance r_{12} into the wavefunction. The idea dates back over 85 years to Hylleraas and the helium atom [16], but only recently has the methodology developed enough for molecular systems to be routinely treated (see Helgaker et al. [17] for a history). So far there have been explicitly correlated extensions to configuration interaction, perturbation theory, and coupled-cluster methods.

Considering the CCSD-F12 wavefunction,

$$\Psi_{\mathrm{CCSD-F12}} = \exp(T)\Psi_{\mathrm{HF}} = \exp(T_1 + T_2 + T_{2'})\Psi_{\mathrm{HF}}, \tag{2.13}$$

an additional operator $T_{2'}$ is present. This term introduces the explicitly correlated contribution whilst the operators T_1 and T_2 are the same as in standard CCSD theory. The resulting wavefunction is augmented with an additional expansion using F12 basis functions (geminals) that are able to describe the shape of the cusp region because of their explicit dependence on r_{12}. As a result, the basis set error of a calculation can be reduced by an order of magnitude compared to standard CCSD.

The most efficient way of introducing r_{12} is through a Slater-type function [18],

$$f_{12} = -\beta^{-1}\exp(-\beta r_{12}), \tag{2.14}$$

where β (sometimes γ in the literature) is a length-scale parameter with a value around $1.0\,a_0^{-1}$ where a_0 is the Bohr radius. Different choices of f_{12} have been used in the past such as the linear correlation factor $f_{12} = r_{12}$ (known as the R12 class of methods). However, Eq. (2.14) has been shown to be close to the optimal factor for incorporating the interelectronic distance [19].

Certain key developments allowed explicitly correlated methods to become computationally feasible. The numerous many-electron integrals could be reduced into sums of products of two-electron integrals by successively inserting an approximate resolution of the identity (RI) [20]. In early methods the RI was approximated using the orbital basis but this needed an extremely large one-particle basis set in calculations. The proposal of an additional complementary auxiliary basis set (CABS) to be used with the orbital basis improved the accuracy of the approximate RI and gave simpler working equations [21]. This approach is now used in all modern implementations. Integral evaluation also became more efficient with the use of density fitting [22, 23]. Accompanying these advances were the design of correlation consistent F12-optimized basis sets which we will discuss in Sec. 2.3.

As of yet, no explicitly correlated treatment of the perturbative triples (T) contribution has been implemented and it is computed using standard CC techniques. There exist several approximate CCSD(T)-F12 models and an overview of the different variants has been given by Tew et al. [24]. In calculations I employed the CCSD(T)-F12x ($x = a, b$) approach of Werner and coworkers [25–27]. These methods retain only the dominant F12 contributions. Compared to standard CCSD(T), there is a slight increase in computational effort when using CCSD(T)-F12x which arises from an initial explicitly correlated second-order Møller-Plesset (MP2-F12) perturbation theory calculation (of the order $\mathcal{O}(\mathcal{N}^5)$). Marginal differences in energy occur if $x = a$ or b but relative energies are of a similar accuracy.

It is worth noting that the basis set error in the CCSD-F12 correlation energy is reduced to such an extent that the respective error in the HF energy becomes significant. To compensate, a perturbative CABS singles correction [25] was introduced which reduces the HF basis set error by an order of magnitude so that the accuracy of the HF energy is equivalent to the CCSD-F12 correlation energy.

2.3 One-particle basis sets

If a FCI wavefunction was expanded in an infinite one-particle basis set we would arrive at the exact, non-relativistic energy of the system. Of course this is not possible. The basis set has to be truncated at some level which introduces an error into the calculation. Effective one-particle basis sets try to make this error as small as possible and if it can somehow be reduced to zero, we are working at the complete basis set (CBS) limit. The theoretical study of atoms and molecules is concerned with these two aspects: a wavefunction as close to FCI as possible, and a one-particle basis set at the CBS limit.

The computational resources, theoretical method, molecular system and property in question will influence the choice of basis set. There is no such thing as an optimum basis set suitable for all scenarios. In practical molecular wavefunction calculations Gaussian basis sets are preferred because of their computational efficiency; the many-centre integrals which arise can be factorised into products of one-centre integrals (a result of the Gaussian Product Theorem) and these are far easier to compute.

Considering only the spatial degrees of freedom of the spin-orbitals from Eq. (2.3), the unknown orbitals $\chi_i(\mathbf{r})$ can be expanded using M known one-electron functions $\phi_\mu(\mathbf{r})$, such that

$$\chi_i(\mathbf{r}) = \sum_{\mu}^{M} c_{i\mu}\phi_\mu(\mathbf{r}). \tag{2.15}$$

The expansion coefficients $c_{i\mu}$ are determined from the iterative SCF procedure with the one-particle basis set defined by $\sum \phi_\mu(\mathbf{r})$.

Gaussian basis sets are constructed from primitive Cartesian functions of the form,

$$\phi_a^{\mathrm{GTO}}(\mathbf{r}_A) = N(x-X)^l(y-Y)^m(z-Z)^n \exp(-\zeta_a(\mathbf{r}-\mathbf{R}_A)^2), \tag{2.16}$$

with centre (usually nuclear) $\mathbf{R}_A = (X_A, Y_A, Z_A)$, normalization constant N, orbital

exponent ζ_a which defines the radial extent of the function, and the total angular momentum $l+m+n$ which is used to classify the function. For $l+m+n = 0, 1, 2, 3$ we have s, p, d, f-type functions, respectively. Functions with a large exponent are known as tight, whilst those with a low exponent are termed diffuse. Calculations employ linear combinations or contractions of the primitive Gaussian-type orbitals (GTOs),

$$\phi_\mu^{\mathrm{cGTO}}(\mathbf{r}_A) = \sum_a^K C_{\mu a} \phi_a^{\mathrm{GTO}}(\mathbf{r}_A), \tag{2.17}$$

where $C_{\mu a}$ are contraction coefficients to be decided and $K < M$. Contraction gives a more compact basis set and there are different approaches for how this is done. The two main schemes are general and segmented contraction but we will not discuss these further. The interested reader is referred to Ref. [28] (and references therein).

The number and subsequent contraction of the primitive GTOs defines the basis set. There are a huge number of Gaussian basis sets each assembled using slightly different principles (see Refs. [28, 29] for an overview). In this thesis I only employ the correlation-consistent basis sets of Dunning and coworkers [30–35] and their explicitly correlated F12 counterparts [36–38]. For this reason I limit the discussion to these two classes of basis set only.

2.3.1 Correlation-consistent basis sets

The correlation-consistent polarized valence basis sets, denoted cc-pVXZ where basis set size increases with the cardinal number X = D, T, Q, 5, 6, 7, are widely used for high-accuracy work. Initially proposed by Dunning [30] for first and second row atoms, the cc-pVXZ basis sets offer a systematic route towards the CBS limit for correlated methods. Generally speaking, at each step up in the cardinal number X, functions of different angular momentum are added in a structured manner to recover more of the correlation energy.

Dunning was inspired by the success of the atomic natural orbital (ANO) basis sets [39] and subsequently analysed the energy contribution of different basis functions for oxygen at the CISD level of theory. Including functions with higher

angular momentum than those of the occupied atomic orbitals, known as polarization functions, was necessary to describe correlation effects. The idea then was to add successively larger shells of polarization functions, which in this case are primitive Gaussians optimized at the correlated CISD level, to a core set of SCF optimized functions. Here, a shell is a set of functions with the same contraction coefficient, exponent, centre and total angular momentum. Increasing the cardinal number X adds another shell to the basis set which contributes a very similar amount of correlation energy.

As the 'V' in the name implies, the cc-pVXZ basis sets are concerned only with the valence electron correlation energy. For all-electron calculations which compute the correlation contribution from core electrons, it is necessary to use specially designed core-valence cc-pCVXZ, or weighted core-valence cc-pwCVXZ basis sets [33, 35]. Here, tight functions with large exponents are included to describe the region closer to the nuclei. In second-row atoms it was later shown that including an additional *d*-function with a larger exponent improved results, giving rise to the cc-pV(X+*d*)Z basis sets [34]. Also widely employed are the augmented correlation-consistent basis sets, aug-cc-pVXZ [31]. In this class, a set of diffuse functions are added for each value of total angular momentum present in the basis. Because of the small exponent, diffuse functions decay slowly with distance from the nucleus and provide a better description of the long-range portion of the wavefunction. This is important for computing a DMS because the dipole moment operator accentuates the contribution from diffuse parts of the wavefunction.

The variety of correlation-consistent basis sets highlights the fact that particular chemical situations or molecular properties have different basis set requirements. They are all, however, built on the principle of reducing the basis set error in a smooth and predictable way. This has led to the use of extrapolation techniques to achieve results at the CBS limit and we will discuss this further in Sec. 2.3.3.

2.3.2 F12-optimized and auxiliary basis sets

The development of explicitly correlated CC methods was followed by the introduction of new F12-optimized correlation-consistent basis sets, denoted cc-pVXZ-F12 where X = D, T, Q, 5 [36, 38]. Originally, the cc-pVXZ basis sets were designed to describe both the short-range electron-electron cusp and longer-range correlation effects of the electronic wavefunction. Inclusion of a nonlinear r_{12} factor into the wavefunction which could accurately account for the cusp region changed the requirements of the one-particle basis set.

The F12-optimized basis sets were constructed following a similar procedure to the standard cc-pVXZ basis sets. Again, the idea is to identify and form shells of polarization functions that lower the correlation energy in a systematic manner. These can then be added to a core set of SCF optimized functions. Using both atomic and molecular systems from the first and second row, basis sets were optimized at the MP2-F12 level of theory. The main difference between the cc-pVXZ-F12 and standard cc-pVXZ basis sets is that at each step up in the cardinal number X, at least two shells of the new angular momentum value are added. The F12-optimized basis sets are slightly larger than their standard Dunning counterparts but show markedly better performance with explicitly correlated methods. New F12-optimized core-valence basis sets, cc-pCVXZ-F12 [37], are also available.

The majority of explicitly correlated methods require three additional auxiliary basis sets (ABS); two for density fitting approximations of two-electron repulsion integrals, and a complementary auxiliary basis set (CABS) for the RI approximation of three-electron integrals (and in some cases four-electron integrals). The OptRI ABS [40] have been designed for use with the cc-pVXZ-F12 basis sets and minimize the RI errors. For density fitting of the exchange and Fock integrals the JKFIT ABS of Weigend [41] are often used, whilst for the remaining two-electron integrals the MP2FIT ABS of Hättig [42] are known to be reliable. New MP2FIT ABS [43] have recently been optimized for use with the cc-pVXZ-F12 and cc-pCVXZ-F12 basis sets

and it is expected that these will become the standard in future F12 calculations. Guidelines for the construction of ABS in Ref. [43] suggest the number of auxiliary basis functions should be no more than six times the number of functions in the one-particle basis set.

2.3.3 Basis set extrapolation

Given the systematic behaviour of the correlation-consistent basis sets it was inevitable that methods to extrapolate results to the CBS limit would emerge. By running a series of calculations with increasing cardinal number X, the computed energies can be fitted with an expression and a value at the CBS limit estimated. Numerous formulas have been put forward but there is no general consensus as to which one is the best (see Ref. [44] for a recent comparison).

To obtain an accurate energy at the CBS limit it is sufficient to use two or three separate calculations. The extrapolation is more reliable if larger basis sets are utilized. As different contributions to the total energy converge at different rates with respect to basis set size, some strategies extrapolate the various contributions separately. For example, in a CCSD(T) calculation one formula would be applied to the HF energy, another to the CCSD energy, and another to the (T) contribution.

Since the introduction of robust F12 methods only one parameterized two-point, Schwenke-style [45] formula applicable for MP2-F12 and CCSD(T)-F12b has been suggested [46],

$$E^C_{\mathrm{CBS}} = (E_{n+1} - E_n)F^C_{n+1} + E_n. \tag{2.18}$$

The coefficient F^C_{n+1} is specific to the C = MP2-F12, CCSD-F12b or (T) energy contribution E, whilst n and $n+1$ refer to the smaller and larger basis set, respectively. Optimized coefficients have been determined for the cc-pVXZ-F12 and aug-cc-pVXZ classes of basis set. The reliability of extrapolating CCSD(T)-F12b results has however been questioned [47], and with the development of the cc-pV5Z-F12 basis set [38] extrapolation may no longer be necessary for small molecules. Explicitly correlated methods are relatively new and will no doubt undergo further

development and testing. New basis sets and extrapolation formulas are likely to be proposed along the way.

2.4 Additional higher-level corrections

Achieving "spectroscopic accuracy" (better than $\pm 1\,\mathrm{cm}^{-1}$) in rovibrational energy level calculations using a purely *ab initio* PES is extremely challenging due to the limitations of electronic structure methods. To do so one must account for higher-level (HL) electron correlation beyond the initial coupled cluster method when generating the PES and use a one-particle basis set near the CBS limit. Core-valence (CV) electron correlation, higher-order (HO) electron correlation, scalar relativistic (SR) effects and the diagonal Born-Oppenheimer correction (DBOC) are considered to be the leading HL contributions [17, 48]. Although expensive to compute, their inclusion can significantly improve calculated rotation-vibration energy levels. There are also certain approximations which can be utilized to reduce computational time as we will see in Chapter. 4, 5 and 6.

2.4.1 Core-valence electron correlation

The behaviour of valence electrons dominates our understanding of chemistry. Core electrons are responsible for the absolute energy of a molecule but are largely unperturbed by vibrations and as such, are not expected to significantly alter the shape of the PES. It is usually sufficient to freeze core electrons when generating the PES, known as the frozen-core (fc) approximation. By doing this calculations are significantly cheaper which is an important consideration when computing the electronic energy at tens of thousands of nuclear geometries.

For high accuracy studies, however, it is necessary to go beyond the fc approximation by considering the contribution from correlating core electrons. This is computed as the difference between an all-electron (ae) and frozen-core calculation within a given level of theory, i.e. $\Delta E_{\mathrm{CV}} = E(\mathrm{ae}) - E(\mathrm{fc})$. Including the CV cor-

rection usually causes an energy bias in the PES and it is necessary to also consider HO electron correlation, which contributes to the electronic energy with the opposite sign.

2.4.2 Higher-order electron correlation

Energy corrections beyond the standard CCSD(T) treatment are usually termed as HO electron correlation. Often these are estimated using the hierarchy of coupled-cluster methods CCSDT, CCSDT(Q), CCSDTQ, and so on. The HO correction can be written as

$$\Delta E_{\mathrm{HO}} = \Delta E_{\mathrm{T}} + \Delta E_{(\mathrm{Q})} + \ldots, \tag{2.19}$$

where $\Delta E_{\mathrm{T}} = E_{\mathrm{CCSDT}} - E_{\mathrm{CCSD(T)}}$ and $\Delta E_{(\mathrm{Q})} = E_{\mathrm{CCSDT(Q)}} - E_{\mathrm{CCSDT}}$. One could calculate $E_{\mathrm{CCSDT(Q)}} - E_{\mathrm{CCSD(T)}}$ but by splitting up the contribution it is possible to use successively smaller basis sets at each step up in excitation level due to faster convergence [49]. This significantly reduces the computational expense of determining ΔE_{HO}.

Corrections for HO electron correlation are not restricted to the hierarchy of coupled cluster theory. Any appropriate (multireference) method can be used to compute, or at least recover some of, the energy difference between FCI and CCSD(T). For example, a high-level *ab initio* PES for ammonia used the internally contracted averaged coupled-pair functional (ic-ACPF) method [50, 51] such that, $\Delta E_{\mathrm{HO}} = (E_{\mathrm{ACPF}} - E_{\mathrm{CCSD(T)}})$ [52]. The ic-ACPF method is a modification of the internally contracted multi-reference configuration interaction (ic-MRCI) method and has the advantage of being approximately size-extensive.

2.4.3 Relativistic effects

A rigorous relativistic treatment of a molecule using the Dirac-Coulomb-Breit Hamiltonian is computationally demanding and unnecessary for light systems (containing elements H–Ar). It is usually sufficient to treat the effects of relativity in an approximate manner based on the Dirac equation. Relativistic effects in quantum

chemistry are classed as either (i) scalar relativistic (SR) effects, or (ii) spin-orbit (SO) coupling. This classification is essentially a divide between contributions which do not split the energy levels (i.e SR), and those which do (i.e. SO).

SR effects, associated with the relativistic mass increase of electrons, can be computed using the one-electron mass-velocity (MV) and Darwin (D1) operators

$$H^{\mathrm{MV}} = -\frac{1}{8c^2}\sum_i \mathbf{p}_i^4, \tag{2.20}$$

$$H^{\mathrm{D1}} = -\frac{\pi}{2c^2}\sum_{i,A} Z_A \delta(|\mathbf{r}_i - \mathbf{R}_A|), \tag{2.21}$$

from the Breit-Pauli Hamiltonian in first-order perturbation theory [53]. Here, the momentum operator $\mathbf{p} = -i\hbar\nabla$ and c is the speed of light. Corrections at the one-electron MVD1 level tend to provide a reliable description of SR effects in light systems and the two-electron Darwin term (D2) need not be considered.

Alternatively, the second-order Douglas-Kroll-Hess (DKH) approach [54, 55] can be used. The DKH approach employs a series of unitary transformations to effectively decouple or separate out the negative energy states (positrons) from the Dirac equation. The remaining 'electron-only' Hamiltonian can then be approximated to arbitrary order. Second-order (denoted DKH2) is usually sufficient. These two methods are widely available in quantum chemistry codes.

For light, closed-shell molecules, which are the focus of this thesis, the spin-orbit interaction can be safely neglected in spectroscopic calculations [56]. I have not considered smaller relativistic corrections arising from the Gaunt and Breit interactions, or the Lamb shift. The effects of these on small, light molecules is discussed in Ref. [56].

The field of relativistic quantum chemistry is a very active area of research. We have only touched upon the key aspects relevant for this thesis. Other methods such as the zero-order regular approximation (ZORA) scheme or direct perturbation theory (DPT) approach have also been developed to compute SR effects. I refer the reader to Refs. [17, 56] (and references therein) for an overview.

2.4.4 Diagonal Born-Oppenheimer correction

As shown in Eq. (1.2), the Born-Oppenheimer approximation separates the nuclear and electronic degrees of freedom. There is however a second assumption made and that is to neglect the contribution of the nuclear kinetic energy operator acting on the electronic wavefunction [3]. To first-order this contribution has the form

$$\Delta E_{\mathrm{DBOC}} = \langle \psi_{\mathrm{elec}} | \sum_{A} -\frac{\hbar^2}{2M_A} \nabla_A^2 | \psi_{\mathrm{elec}} \rangle, \tag{2.22}$$

and is known as the DBOC. It can be routinely calculated in quantum chemical packages and its inclusion in the PES leads to the so-called adiabatic approximation. The PES becomes mass-dependent and applicable only for a single isotopologue. Note that the DBOC is largest for molecules containing hydrogen, seen by considering the denominator in Eq. (2.22).

2.5 Chapter summary

The preferred *ab initio* theory and one-particle basis sets to solve the electronic Schrödinger equation for small, closed-shell molecules have been detailed in this chapter. The focus was on high-accuracy methods, basis sets and techniques to recover as much of the correlation energy as possible. Ideally we would employ FCI with an infinitely large basis set to get the exact, non-relativistic electronic energy. However, this is simply not possible and levels of approximation must be introduced. For molecular systems where a single HF determinant dominates the wavefunction, coupled cluster theory is well suited to tackle the problem. When combined with explicit correlation we have very powerful methods at our disposal.

These methods are ineffective without a suitable choice of one-particle basis set. Whilst a huge number have been designed in the past, arguably the most successful are the correlation-consistent basis sets of Dunning and coworkers as they offer a

systematic route towards the CBS limit. Basis set extrapolation can be exploited and the basis set truncation error rendered negligible. The development of explicitly correlated methods has slightly shifted the requirements of the one-particle basis set and as a result, new F12-optimized correlation-consistent basis sets are now available. This is also the case for the additional ABS necessary for an explicitly correlated calculation.

Even with all these advances, to obtain the best possible *ab initio* PES one must go beyond the initial coupled cluster approach by considering additional HL energy corrections. The main contributions are CV electron correlation, HO electron correlation, SR effects and the DBOC. This last term is mass dependent and its inclusion causes the PES to become applicable for only one isotopologue. The computational effort needed to generate the PES and DMS can quickly escalate when considering these extra terms. There are ways of reducing the computational burden and we will see examples of this for CH_3Cl in Chapter 4, SiH_4 in Chapter 5 and CH_4 in Chapter 6. Before doing this however, we must study the nuclear motion problem to see how the PES and DMS are used in rotation-vibration calculations.

3 Solving the nuclear Schrödinger equation

3.1 Introduction

The choice of coordinate system to describe molecular motion is crucial for obtaining a tractable solution to the nuclear Schrödinger equation. An intelligent selection can greatly simplify the form of the rovibrational Hamiltonian and accelerate convergence towards the correct result. In a laboratory-fixed frame using Cartesian coordinates, a molecule with N atoms requires $3N$ coordinates to specify the positions of its atoms. These $3N$ coordinates do not however distinguish between the different types of molecular motion: translation of the whole molecule through space, rotation of the molecule and vibration or internal motion of the nuclei.

Translational motion in free space gives rise to a continuous spectrum which is not useful for spectroscopy. The three centre-of-mass motion coordinates can be removed to leave $3N-3$ coordinates describing a space-fixed axis system. From here we are able to distinguish the rotational and vibrational motion by transforming to a suitable molecule-fixed frame (also referred to as a body-fixed frame). The Euler angles (θ, ϕ, χ) define the orientation of the molecule-fixed xyz axis system with respect to the space-fixed axis system and ultimately describe the overall rotation of the molecule. The remaining $3N-6$ coordinates ($3N-5$ for linear molecules) define vibrational motion of the nuclei. How these internal coordinates are chosen will to some extent depend on molecular structure. Over the years numerous coordinate choices and Hamiltonians for different types of molecule have been reported in the literature, each usually accompanied with a computer program to solve the nuclear motion problem. This lack of generality is an issue and much effort has therefore

been directed towards developing self-contained, numerical approaches which do not require pre-derivation of the rovibrational Hamiltonian.

After coordinate choice and Hamiltonian have been established the next consideration is how to solve the rotation-vibration Schrödinger equation. For high-accuracy studies the only real option is variationally. Variational methods offer a complete treatment of the nuclear motion problem and can achieve unparalleled accuracy in their results. There is however a considerable computational cost associated with these approaches and treating molecules containing five atoms or more is extremely challenging.

Perturbation theory was long preferred in high-resolution spectroscopy but is known to become unreliable in certain situations; for example in floppy molecules which undergo large-amplitude motion such as ammonia. Alternative purely vibrational methods are actively being developed such as vibrational configuration interaction (VCI) or vibrational coupled cluster (VCC) theory. Inspired by progress in electronic structure theory these approaches may become more widespread in the future (see Refs. [57, 58] for an overview).

In this thesis I use the variational nuclear motion program TROVE [9] for all spectroscopic calculations. TROVE is designed to compute the rotation-vibration energy levels and corresponding transition intensities for a polyatomic molecule of arbitrary structure in an isolated electronic state; a "black-box" for calculating rovibrational spectra. This generality has allowed a range of molecular systems containing up to five atoms to be treated [10, 59–68]. In this chapter we will focus on the methodology and recent developments in TROVE (a detailed review was recently given by Tennyson and Yurchenko [69]). We will then discuss the simulation of rovibrational spectra before offering concluding remarks.

3.2 TROVE

3.2.1 General methodology

In TROVE, solution of the rotation-vibration Schrödinger equation is achieved by numerical diagonalization of the respective Hamiltonian constructed in terms of a symmetry adapted basis set. The rovibrational Hamiltonian is represented in product form as a truncated power series expansion around some reference molecular configuration, usually chosen as the equilibrium geometry or some non-rigid flexible configuration. The expansion itself is in terms of user defined internal coordinates.

In a general and compact form, the kinetic energy operator (KEO) for a molecule with M vibrational degrees of freedom can be expressed in terms of the vibrational coordinates $\boldsymbol{\xi} = \{\xi_1, \xi_2, \ldots, \xi_M\}$ as

$$T_N = \frac{1}{2} \sum_{\lambda,\mu=1}^{M+3} \Pi_\lambda^\dagger G_{\lambda\mu}(\boldsymbol{\xi}) \Pi_\mu + U(\boldsymbol{\xi}). \tag{3.1}$$

Here, the generalized momenta

$$\boldsymbol{\Pi} = \{p_1, \ldots, p_M, J_x, J_y, J_z\}, \tag{3.2}$$

where $p_n = -i\hbar\partial/\partial\xi_n$ for $n = 1, \ldots, M$ is the momentum conjugate to the coordinate ξ_n, and J_x, J_y, J_z are components of the total angular momentum operator $\boldsymbol{J}$. The kinetic energy matrix $G_{\lambda\mu}(\boldsymbol{\xi})$ and the pseudopotential $U(\boldsymbol{\xi})$ are constructed in a recursive numerical procedure. These two quantities along with the Born-Oppenheimer potential, $V_{\mathrm{BO}}(\boldsymbol{\xi})$, are represented as series expansions with truncation order defined by the user. In most practical applications it is sufficient to truncate the kinetic and potential energy operators at 6th and 8th order, respectively.

Without detailing the working equations, which can be found in Refs. [9, 70], the quantities $G_{\lambda\mu}(\boldsymbol{\xi})$ and $U(\boldsymbol{\xi})$ depend on Cartesian and vibrational coordinate derivatives. In the original version of TROVE, finite differences are employed to generate

these derivatives but this approach can suffer from the accumulation of round-off and cancellation errors, particularly for high-order expansions. This issue was recently addressed with the implementation of a novel automatic differentiation method into TROVE [70]. Automatic differentiation is a computer algebra technique [71, 72] which enables the numerical calculation of derivatives of arbitrary order with an accuracy comparable to analytic approaches. The outcome is that rovibrational calculations show much faster convergence with respect to basis set size. Without this development, along with the implementation of curvilinear internal coordinates (discussed below), obtaining fully converged vibrational energies for the five-atom molecules considered in this thesis would have been extremely challenging.

To compute the kinetic energy operator in Eq. (3.1) it is necessary to define a molecule-fixed axis system. The optimum embedding is one which minimises rovibrational coupling and this can be achieved by satisfying the Eckart conditions [73]. The Eckart frame ensures maximum separation between rotational and vibrational motion, thus accelerating basis set convergence when computing rotation-vibration energy levels. For a molecule containing N nuclei, the translational Eckart condition can be written as

$$\sum_{A=1}^{N} m_A \boldsymbol{r}_A = 0, \tag{3.3}$$

where m_A is the mass, and $\boldsymbol{r}_A$ the instantaneous position vector of each nucleus. Finding a transformation matrix $\boldsymbol{D}$ to take the coordinates $\boldsymbol{r}_A$ into the Eckart frame, i.e. $\boldsymbol{r}'_A = \boldsymbol{D}\,\boldsymbol{r}_A$, is more complex and we must satisfy the rotational Eckart condition,

$$\sum_{A=1}^{N} m_A (\boldsymbol{r}'_A \times \boldsymbol{a}_A) = 0. \tag{3.4}$$

Here $\boldsymbol{a}_A$ is the equilibrium position vector of each nucleus in a conveniently chosen reference frame such as the principal axes system (PAS) frame [9, 70, 74]. It is not actually possible to obtain an analytic solution to the Eckart equations for a general polyatomic molecule and numerical methods have to be used. Several schemes exist to do this [75–80] and a new approach has also been implemented in

TROVE [70]. Note that for non-rigid molecules it is also necessary to satisfy the Sayvetz condition [81] which is a large amplitude analogue to Eq. (3.4).

In principle any choice of vibrational coordinates $\boldsymbol{\xi} = \{\xi_1, \xi_2, \ldots, \xi_M\}$ can be implemented in TROVE provided they are physically reasonable. In practical calculations however, I have only ever employed two types of coordinates. The first are linearized coordinates. These are selected linear combinations of Cartesian displacements of the nuclei from their equilibrium positions in the molecule-fixed xyz axis system. Further details on how these are constructed can be found in Refs. [9, 82]. The second are curvilinear internal coordinates, i.e. displacements of bond lengths, bond angles, dihedral angles from their respective equilibrium values. These were recently implemented in TROVE [70] and their use can greatly improve basis set convergence of rovibrational calculations.

The vibrational basis set in TROVE is constructed using a multi-step contraction scheme, the size of which is controlled by the polyad number

$$P = \sum_{k=1}^{M} a_k n_k \leq P_{\max}, \tag{3.5}$$

and this does not exceed a predefined maximum value $P_{\max}$. The polyad coefficient $a_k = \omega_k / \min(\omega_1 \ldots \omega_M)$ where ω_k denotes the harmonic frequency of the kth mode. This truncation scheme comes from the observation that rotation-vibration energy levels tend to appear in clusters, known as polyads. The quantum numbers n_k for $k = 1, \ldots, M$ correspond to primitive basis functions ϕ_{n_k}. These can be simple analytic Morse-oscillator or harmonic-oscillator eigenfunctions, or they can be obtained numerically by solving a one-dimensional Schrödinger equation for the desired vibrational mode by means of the Numerov-Cooley method [83, 84].

The vibrational basis set is built up in stages and utilizes products of the functions ϕ_{n_k}. Initially, reduced symmetry sub-spaces are set up by coupling equivalent modes and solving the reduced-mode Schrödinger equations; for example all stretching degrees of freedom are treated together. The resulting eigenfunctions are then combined and used as basis functions to solve the full-dimensional problem. These

final $J = 0$ eigenfunctions form the vibrational basis set. Multiplication with symmetrized rigid-rotor eigenfunctions $|J, K, m, \tau_{\rm rot}\rangle$ produces the final symmetrized basis set for use in $J > 0$ calculations. Here, the quantum number K is the projection (in units of $\hbar$) of J on to the molecule-fixed z-axis, whilst $\tau_{\rm rot}$ determines the rotational parity as $(-1)^{\tau_{\rm rot}}$.

During its construction the basis set is symmetry-adapted which allows the Hamiltonian matrix to be factorized into smaller symmetry blocks. Each block corresponds to an irreducible representation of the molecular symmetry group [82] of the molecule being considered. This is particularly useful when handling the large matrices associated with variational calculations as each sub-block can be diagonalized separately. The resulting energy levels are also automatically symmetry labelled which is extremely helpful for computing spectra. Symmetry imposes additional selection rules and the intensity of a transition will depend on its nuclear spin statistical weight $g_{\rm ns}$. The value of $g_{\rm ns}$ is determined by the irreducible representations of the states involved. Note that TROVE automatically assigns quantum numbers to the eigenvalues and corresponding eigenvectors by analysing the contribution of the basis functions. To be of spectroscopic use it is always necessary to map the vibrational quantum numbers n_k to the normal mode quantum numbers v_k commonly used.

For all calculations TROVE requires as input a PES and DMS. As discussed in Chapter 2 these surfaces are generated on extensive grids of nuclear geometries using sophisticated electronic structure methods. Once a suitable analytic representation has been determined for the PES and DMS, for example a polynomial expansion, the respective functions must be implemented in TROVE. Each molecular structure, e.g. $\mathrm{XY_4}$-type molecules, will have its own module containing all the necessary subroutines and coordinate transformations to construct the analytic form of the PES and DMS. This is the only molecule-specific part of TROVE which otherwise is general in its approach.

3.2.2 Potential energy surface refinement

To approach a level of accuracy competitive with experiment in rovibrational calculations the PES has to be empirically refined. By adjusting the parameters of the analytic representation of the PES, the computed theoretical energies can be fitted to high-resolution experimental data. The resulting "spectroscopic" PES is far more reliable than a purely empirical PES as regions not sampled by experiment can be reliably extrapolated.

In TROVE, empirical refinement is done using an efficient least-squares fitting procedure [85]. Assuming the *ab initio* PES, V, is a reasonable representation the effect of the refinement can be treated as a perturbation ΔV, i.e. $V' = V + \Delta V$ where V' is the refined PES. The correction ΔV is expanded in terms of the vibrational coordinates $\boldsymbol{\xi} = \{\xi_1, \xi_2, \ldots, \xi_M\}$ according to the formula,

$$\Delta V = \sum_{ijk\ldots} \Delta \mathrm{f}_{ijk\ldots} \left\{ \xi_1^i \xi_2^j \xi_3^k \ldots \right\}^A , \tag{3.6}$$

where the coefficients $\Delta \mathrm{f}_{ijk\ldots}$ are corrections to the original PES expansion parameters $\mathrm{f}_{ijk\ldots}$. The expansion terms $\left\{ \xi_1^i \xi_2^j \xi_3^k \ldots \right\}^A$ are symmetrized combinations of the vibrational coordinates $\boldsymbol{\xi} = \{\xi_1, \xi_2, \ldots, \xi_M\}$ and transform according to the totally symmetric representation A of the molecular symmetry group [82].

The new perturbed Hamiltonian, $H' = T + V' = H + \Delta V$, is then diagonalized using a basis set of eigenfunctions from the initial unperturbed Hamiltonian eigenvalue problem. Each iteration utilizes the previous "unperturbed" basis set in this way until a PES of desirable quality is reached. To ensure the consistency of the refined surface the expansion parameters $\mathrm{f}_{ijk\ldots}$ are simultaneously fitted to both the experimental data and the original *ab initio* dataset [86]. This stops any unrealistic distortion of the PES in regions not sampled by experiment. It also means each expansion parameter can be adjusted irrespective of the amount or coverage of the experimental energies used for the refinement.

A practical PES refinement needs vibrational ($J = 0$) and rovibrational ($J > 0$)

term values in the fitting dataset. It is recommended that only measurements carried out with an accuracy of $0.02\,\mathrm{cm}^{-1}$ or better should be included [52]. Incorporating as many J values as possible improves extrapolation to higher rotational excitations. It is worth noting that rigorously refining all parameters of the PES is a computationally intensive task and may not always be necessary. High quality spectroscopic PESs can be obtained by only treating certain expansion coefficients, for example up to quartic expansion parameters only.

3.2.3 Line strengths and intensities

The ability to compute accurate transition intensities is a major strength of TROVE and this gives the variational approach incredible predictive power. After establishing a suitable analytic representation for the dipole moment $\boldsymbol{\mu}$, it is relatively straightforward to generate transition intensities given a set of rovibrational wavefunctions.

Experimental conditions such as temperature and pressure will influence the intensity of an electric dipole transition but the most significant factor is the line strength $S(f \leftarrow i)$. This intrinsic molecular quantity is defined in a space-fixed XYZ axis system as

$$S(f \leftarrow i) = g_{\mathrm{ns}} \sum_{m_i, m_f} \sum_{A=X,Y,Z} \left| \langle \Phi_{\mathrm{rv}}^{(f)} | \bar{\mu}_A | \Phi_{\mathrm{rv}}^{(i)} \rangle \right|^2, \tag{3.7}$$

where g_{ns} is the nuclear spin statistical weight, $\Phi_{\mathrm{rv}}^{(i)}$ and $\Phi_{\mathrm{rv}}^{(f)}$ are the initial and final state rovibrational wavefunctions respectively, and $\bar{\mu}_A$ is the electronically averaged DMS along the space-fixed axis $A = X, Y, Z$. The summation over the quantum numbers m_i and m_f, which correspond to the projection of the total angular momentum on to the Z axis in the initial and final state respectively, is to account for degeneracy in the absence of an external electric field. Note that we have neglected hyperfine structure (splitting of energy levels due to nuclear spin) and disregarded electronic transitions as we are working in the electronic ground state only.

Using the line strength we can determine the Einstein A coefficient,

$$A_{if} = \frac{64\pi^4}{3h(4\pi\epsilon_0)} \frac{\nu_{if}^3}{(2J_f+1)} S(f \leftarrow i), \tag{3.8}$$

of a transition with wavenumber ν_{if} (in cm^{-1}). Here, J_f is the rotational quantum number of the final state and h is the Planck constant. The Einstein A coefficient gives the probability of spontaneous emission from state i to f. Once known it is possible to simulate intensities. For example, the absolute absorption intensity can be found using the expression,

$$I(f \leftarrow i) = \frac{A_{if}}{8\pi c} g_{\text{ns}} (2J_f+1) \frac{\exp\left(-E_i/kT\right)}{Q(T)\ \nu_{if}^2} \left[1 - \exp\left(-\frac{hc\nu_{if}}{kT}\right)\right], \tag{3.9}$$

where the initial state has energy E_i, k is the Boltzmann constant, T is the absolute temperature, c is the speed of light and $Q(T)$ the partition function for a given temperature.

Considering the computational aspects of the calculation, TROVE uses an optimized two-step strategy [61] to determine the matrix elements $\langle \Phi_{\text{rv}}^{(f)} | \bar{\mu}_A | \Phi_{\text{rv}}^{(i)} \rangle$ needed for $S(f \leftarrow i)$. This reduces computational time by roughly an order of magnitude compared to calculating the matrix elements in one-step. Further savings are introduced through the use of pre-screening of the expansion coefficients associated with the symmetrized basis set [87]. Only coefficients above a certain threshold value, e.g. 10^{-16}, will lead to $\langle \Phi_{\text{rv}}^{(f)} | \bar{\mu}_A | \Phi_{\text{rv}}^{(i)} \rangle$ being evaluated. On the practical side, calculations can be run in batches by only considering transitions between $J \rightarrow J$ and $J \rightarrow J+1$. This is the smallest grouping of J permitted by selection rules. The use of a symmetrized basis set, whilst crucial for intensity calculations through the nuclear spin statistical weights, also means transitions can be run independently according to symmetry. These two measures make the construction of huge line lists far more manageable both computationally and in terms of data handling.

As discussed in Sec. 3.2.1, separation between rotational and vibrational motion is achieved through the Eckart conditions where a suitable molecule-fixed embedding

is set up in which the rovibrational wavefunctions are defined. It is therefore necessary to evaluate $S(f \leftarrow i)$ in the molecule-fixed frame. This is done by transforming the space-fixed dipole moment components $\bar{\mu}_A$ $(A = X, Y, Z)$ to dipole moment components $\bar{\mu}_\alpha$ $(\alpha = x, y, z)$ in the molecule-fixed axis system. Detailed expressions for this procedure can be found in Refs. [87, 88], whilst a slightly modified approach using automatic differentiation has recently been implemented [70].

Another quantity of interest which can be computed using TROVE is the vibrational transition moment between two states, defined as

$$\mu_{if} = \sqrt{\sum_{\alpha=x,y,z} |\langle \Phi^{(f)}_{\rm vib} | \bar{\mu}_\alpha | \Phi^{(i)}_{\rm vib} \rangle|^2}, \tag{3.10}$$

where $|\Phi^{(i)}_{\rm vib}\rangle$ and $|\Phi^{(f)}_{\rm vib}\rangle$ are the initial and final state vibrational eigenfunctions respectively, and $\bar{\mu}_\alpha$ is the electronically averaged dipole moment function along the molecule-fixed axis $\alpha = x, y, z$. Transition moments offer a cheap and reliable way to evaluate the quality of a DMS against experiment, provided experimental values are available. The additional computational effort required is small and can be carried out after the initial $J = 0$ energy level calculation.

3.3 Simulating rotation-vibration spectra

After running extensive rovibrational calculations in TROVE, energy levels and Einstein A coefficients are extracted and then processed using an in-house code developed by the ExoMol group to generate synthetic rotation-vibration spectra. Different line profiles, spectral resolutions and temperatures can then be applied which is particular useful for comparing against different experimental setups. Whilst some experimental work and spectroscopic databases such as HITRAN [89] provide absolute line intensities for measured transitions, it is more common to encounter spectral lines which have a definite profile.

For an isolated spectral transition the line profile can be attributed to physical

factors. Each line possesses an intrinsic natural line width which is a consequence of the uncertainty principle. This dictates that any measurement of energy and time must satisfy $\Delta E \Delta t \geq \hbar/2$, where ΔE is the uncertainty in energy, Δt is the lifetime of the state and $\hbar$ is the reduced Planck constant. Longer lived states will have a narrower line width. This contribution can often be ignored however, as the effects of collisional broadening and thermal (Doppler) broadening tend to dominate the line shape.

Collisions between molecules in a gas reduce the lifetime of an excited state resulting in line broadening since the line width $\Gamma \sim 1/\Delta t$. For environments with high pressure there are more collisions and this effect is amplified. The most suitable shape function to model collisional broadening is a homogeneous Lorentzian profile,

$$f_L(\nu) = \frac{\gamma/4\pi^2}{(\nu - \nu_0)^2 + (\gamma/4\pi)^2}, \tag{3.11}$$

where γ is the half-width at half-maximum (HWHM), ν is the frequency and ν_0 the line-centre frequency.

Another source of broadening is the thermal translational motion of molecules and the well-known Doppler effect. Radiation emitted from a molecule in motion will be Doppler shifted by an amount dependent on the component of velocity in the line of sight. The cumulative effect of a large number of molecules moving in different directions and at different speeds is the inhomogeneous broadening of spectral lines. This is well represented by a Gaussian profile,

$$f_G(\nu) = \frac{1}{\sqrt{\pi}\Delta\nu_D} \exp\left(-\left(\frac{\nu - \nu_0}{\Delta\nu_D}\right)^2\right), \tag{3.12}$$

where the Doppler width

$$\Delta\nu_D = \frac{\nu_0}{c}\sqrt{\frac{2kT}{m}}, \tag{3.13}$$

and the HWHM $\gamma = \Delta\nu_D\sqrt{\ln(2)}$. Here, c is the speed of light, k is the Boltzmann constant, T is the temperature and m is the molecular mass. In Fig. 3.1 is a plotted Gaussian and Lorentzian line profile to illustrate the difference. Lorentzian profiles

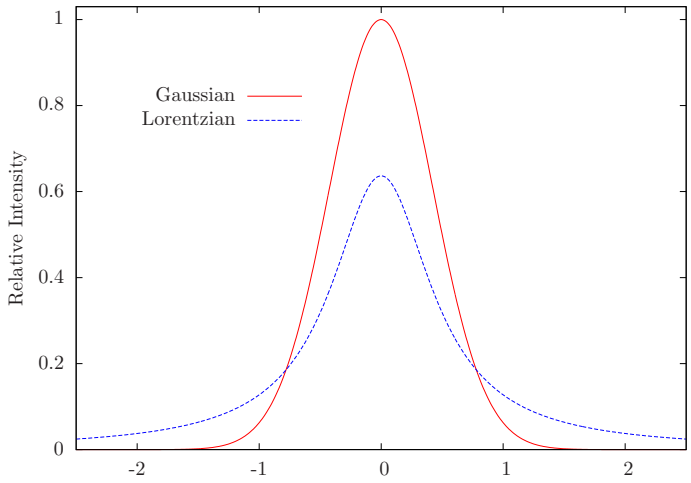

Figure 3.1: Comparison of a Gaussian and Lorentzian line profile with HWHM = 0.5.

show extended wings and tail off at a slower rate, whilst a Gaussian falls off fairly rapidly away from the line centre.

The Voigt profile, which is a convolution of a Lorentzian and Gaussian line profile, is routinely employed in high-resolution spectroscopic studies. Although it is able to model both thermal and collisional contributions, it cannot provide a wholly accurate representation of the spectral line shape [90]. Recently, a task group was set up to identify a more reliable reference line profile and the recommendation was a seven parameter Hartmann-Tran profile [91]. This line shape has yet to be implemented in the in-house code developed by the ExoMol group used to generate synthetic spectra but will no doubt be adopted in the future.

3.4 Chapter summary

The methodology for obtaining an accurate solution to the nuclear motion problem for a general polyatomic molecule has been discussed. High-accuracy work demands that a variational approach is employed and in calculations I have used the computer program TROVE. The flexibility of TROVE is achieved by constructing a rovibrational Hamiltonian in product form as a power series expansion in terms of

user defined internal coordinates. An optimum molecule-fixed coordinate system is defined by satisfying the Eckart conditions, which minimises the coupling between rotational and vibrational motion. The rovibrational Hamiltonian can then be diagonalized in a symmetry-adapted basis set. This is vital for intensity calculations and also eases the computational strain associated with generating comprehensive line lists.

The ability to empirically refine the PES without substantial deviation from the original *ab initio* surface should eliminate possible spurious results caused by the refinement. An improved PES not only yields more accurate rotation-vibration energy levels but also better wavefunctions, which in turn produces more reliable intensities. Before intensities can be simulated the line strength must be computed for every transition, from which Einstein A coefficients can be determined. This requires a well-defined DMS. Once Einstein A coefficients and rotation-vibration energy levels have been extracted, intensities can be generated with different line profiles, temperatures and spectral resolutions. This is where the predictive power of the variational approach is realised.

The material presented in this and the previous chapter can now be applied in practical calculations on different four- and five-atom molecular systems. This will undoubtedly provide a better understanding of the background theoretical concepts. As we have seen, accurate solution of the molecular Schrödinger equation relies on a range of approximations. It is important then to evaluate different aspects of the calculation process such as the electronic structure methods, analytic representation of the PES and DMS, size of the vibrational basis set, and so on, by comparing with experiment and other theoretical work. The theoretical model is unlikely to be accurate in all regions of the spectrum, however, provided there is some knowledge of the limitations this should not be an issue. Future work can then compare and judge their results accordingly.

4 Methyl chloride (CH_3Cl)

4.1 Introduction

Methyl chloride has been proposed as an observable biosignature gas in the search for life outside the Solar System [92]. A model of different hypothetical Earth-like planets orbiting a range of M stars predicted that a higher concentration of CH_3Cl would exist than on Earth, and with stronger spectral features. Seager et al. have since gone on to classify CH_3Cl as a Type III biomarker — a molecule produced from a secondary metabolic process — and estimated the required concentration needed for a realistic detection in a generalized oxidized atmosphere [93], and for an exoplanet with a thin H_2 rich atmosphere and a habitable surface temperature [94]. The infrared spectrum of CH_3Cl has received increased interest as a result.

A highly accurate and comprehensive line list is lacking for methyl chloride, with varying coverage in the spectroscopic databases [89, 95–97]. The HITRAN database [89] has the most detailed coverage with over 212 000 lines for the two main isotopologues, $^{12}CH_3{}^{35}Cl$ and $^{12}CH_3{}^{37}Cl$ (henceforth labelled as $CH_3{}^{35}Cl$ and $CH_3{}^{37}Cl$). This includes rovibrational transitions up to $J = 82$ and covers the 0–3200 cm^{-1} region. However, there are deficiencies and we will see in Sec. 4.5.5 that HITRAN is missing a band around 2880 cm^{-1}. Some line positions and intensities are also from theoretical predictions using a fairly old, empirically refined anharmonic force field [98]. Given the numerous high-resolution studies since then, notably in the 3.4 μm region [99] (included in HITRAN2012), and in the 6.9 and 7.4 μm regions [100, 101], improvements can be expected in the coverage of CH_3Cl. Another valuable resource is the PNNL spectral library [95] which covers the 600–6500 cm^{-1} region at a resolution of around 0.06 cm^{-1} for temperatures of 5, 25 and 50 °C. Other databases such as GEISA [96] include CH_3Cl but the datasets are not as extensive,

whilst the JPL [97] catalog has been incorporated into HITRAN.

Due to its prominent role in depletion of the ozone layer, levels of methyl chloride are being closely monitored by satellite missions such as the Atmospheric Chemistry Experiment [102–105] and the Microwave Limb Sounder [106]. The huge number of recent spectroscopic studies [99–101, 103–128], particularly those on line shapes and broadening coefficients which are needed for a realistic modelling of atmospheric spectra, confirm its importance as a terrestrial molecule. The 3.4 μm region is particularly relevant for atmospheric remote sensing due to a relatively transparent window and strong spectral features of the ν_1 band of CH_3Cl. A high-resolution study of the ν_1, ν_4 and $3\nu_6$ bands in this region produced a line list for the range 2920–3100 cm^{-1} [99]. The 6.9 μm region has seen line positions, intensities, and self-broadening coefficients determined for more than 900 rovibrational transitions of the ν_5 band [100], with this work later extended to incorporate the ν_2 band [101]. Nikitin et al. have also measured, modelled and assigned over 20 000 transitions for each isotopologue in the region 0–2600 cm^{-1} [120–123]. An effective Hamiltonian model adapted to the polyad structure of methyl chloride reproduced observed transitions involving the ground state and 13 excited vibrational states with an overall standard deviation of 0.0003 cm^{-1}.

On the theoretical side there has been a consistent effort over the years to characterize the spectrum of CH_3Cl. Much attention has been given to a description of harmonic [129–136] and anharmonic [98, 137–142] force fields, both empirically and using *ab initio* methods. The latest work by Black and Law [136] employed spectroscopic data from ten isotopomers of methyl chloride to produce an empirical harmonic force field incorporating the most up to date treatment of anharmonic corrections. These were largely based on a complete set of empirical anharmonicity constants derived from a joint local mode and normal mode analysis of 66 vibrational energy levels in the 700–16 500 cm^{-1} region [141], and follow-up work in a similar vein by Law [143].

From a purely *ab initio* standpoint, Nikitin [144] has computed global nine-

dimensional PESs for vibrational energy level calculations, considering both $CH_3{}^{35}Cl$ and $CH_3{}^{37}Cl$ in the region 0–3500 cm^{-1}. Using fourth-order Møller-Plesset perturbation theory MP4 and a correlation-consistent quadruple-zeta basis set, as well as coupled cluster theory CCSD(T) with a triple-zeta basis set, a combined total of 7241 points with energies up to $hc \cdot 40\,000\,cm^{-1}$ were employed to generate and fit the PESs (h is the Planck constant and c is the speed of light). Vibrational energies were calculated variationally using a finite basis representation and an exact kinetic energy operator, reproducing the fundamental term values with a root-mean-square error of 1.97 and 1.71 cm^{-1} for $CH_3{}^{35}Cl$ and $CH_3{}^{37}Cl$, respectively. Calculations of dipole moment derivatives and infrared intensities have been reported [98, 128, 132, 134, 145–149]. However, I am unaware of any global DMS which could be used for intensity simulations of the rotation-vibration spectrum of CH_3Cl.

In this chapter I apply the techniques discussed in Chapters 2 and 3 to investigate the rotation-vibration spectrum of methyl chloride. State-of-the-art electronic structure calculations are employed to construct nine-dimensional potential energy and dipole moment surfaces applicable for the two main isotopologues of methyl chloride, $CH_3{}^{35}Cl$ and $CH_3{}^{37}Cl$. As discussed in Chapter 2, to produce a highly accurate *ab initio* PES this requires inclusion of the leading HL corrections and extrapolation of the one-particle basis set to the CBS limit. For the DMS these contributions are not as significant. A symmetrized molecular bond (SMB) representation for XY_3Z-type molecules has been implemented in TROVE [9] to represent the PES and DMS analytically. The quality of the respective surfaces can then be assessed by variational calculations of the rovibrational spectrum.

The chapter is structured as follows: In Sec. 4.2 the *ab initio* calculations and analytic representation of the PES are detailed. Similarly, in Sec. 4.3 the electronic structure calculations and analytic representation of the DMS are described. Details of the variational calculations are given in Sec. 4.4. In Sec. 4.5, the combined effect of the HL corrections and CBS extrapolation on the vibrational term values and

equilibrium geometry is assessed. The DMS is evaluated using a range of experimental measurements with comparisons against the HITRAN and PNNL spectroscopic databases. Results include vibrational transition moments, absolute line intensities of the ν_1, ν_4, ν_5 and $3\nu_6$ bands, and an overview of the rotation-vibration spectrum for states up to $J = 85$ in the 0–6500 cm^{-1} frequency range. We summarise and discuss future work in Sec. 4.6.

4.2 Potential energy surface

4.2.1 Electronic structure calculations

We take a focal-point approach [150] to represent the total electronic energy,

$$E_{\mathrm{tot}} = E_{\mathrm{CBS}} + \Delta E_{\mathrm{CV}} + \Delta E_{\mathrm{HO}} + \Delta E_{\mathrm{SR}} + \Delta E_{\mathrm{DBOC}}, \tag{4.1}$$

which allows for greater control over the PES. To compute E_{CBS}, I employed the explicitly correlated F12 coupled cluster method CCSD(T)-F12b [25] (for a detailed review of this method see Refs. [24, 27]) in conjunction with the F12-optimized correlation consistent polarized valence basis sets, cc-pVTZ-F12 and cc-pVQZ-F12 [36], in the frozen core approximation. The diagonal fixed amplitude ansatz 3C(FIX) [18], and a Slater geminal exponent value of $\beta = 1.0\, a_0^{-1}$ as recommended by Hill et al. [46] were used. To evaluate the many electron integrals in F12 theory, additional auxiliary basis sets (ABS) are required. For the resolution of the identity (RI) basis, and the two density fitting (DF) basis sets, I utilized the corresponding OptRI [40], cc-pV5Z/JKFIT [41], and aug-cc-pwV5Z/MP2FIT [42] ABS, respectively. All calculations were carried out using MOLPRO2012 [151] unless stated otherwise.

To extrapolate to the CBS limit I used the parameterized two-point formula proposed by Hill et al. [46],

$$E^C_{\mathrm{CBS}} = (E_{n+1} - E_n)F^C_{n+1} + E_n, \tag{4.2}$$

which was introduced earlier in Sec. 2.3.3 (see Eq. (2.18)). The coefficients F_{n+1}^{C} are specific to the CCSD − F12b and (T) components of the total CCSD(T)-F12b energy and I used values of $F^{\mathrm{CCSD-F12b}} = 1.363388$ and $F^{(\mathrm{T})} = 1.769474$ as recommended in Ref. [46]. No extrapolation was applied to the Hartree-Fock (HF) energy, rather the HF+CABS (complementary auxiliary basis set) singles correction [25] calculated in the larger basis set was used.

The energy correction from CV electron correlation ΔE_{CV} was calculated at the CCSD(T)-F12b level of theory with the F12-optimized correlation consistent core-valence basis set cc-pCVQZ-F12 [37]. The same ansatz and ABS as in the frozen core approximation computations were used, however, I set $\beta = 1.5\, a_0^{-1}$. All-electron calculations kept the $(1s)$ orbital of Cl frozen with all other electrons correlated due to the inability of the basis set to adequately describe this orbital.

Core-valence and higher-order electron correlation often contribute to the electronic energy with opposing signs and should thus be considered jointly. I used the hierarchy of coupled cluster methods to estimate the HO correction as $\Delta E_{\mathrm{HO}} = \Delta E_{\mathrm{T}} + \Delta E_{(\mathrm{Q})}$, including the full triples contribution $\Delta E_{\mathrm{T}} = \left[E_{\mathrm{CCSDT}} - E_{\mathrm{CCSD(T)}}\right]$, and the perturbative quadruples contribution $\Delta E_{(\mathrm{Q})} = \left[E_{\mathrm{CCSDT(Q)}} - E_{\mathrm{CCSDT}}\right]$. Calculations were carried out in the frozen core approximation at the CCSD(T), CCSDT and CCSDT(Q) levels of theory using the general coupled cluster approach [152, 153] as implemented in the MRCC code [154] interfaced to CFOUR [155]. For the full triples and the perturbative quadruples calculations, I employed the augmented correlation consistent triple zeta basis set, aug-cc-pVTZ(+d for Cl) [30–32, 34], and the double zeta basis set, aug-cc-pVDZ(+d for Cl), respectively. Note that for HO coupled cluster corrections, it is possible to use successively smaller basis sets at each step up in excitation level due to faster convergence [49].

In exploratory calculations of the PES, the contributions from the full quadruples $\left[E_{\mathrm{CCSDTQ}} - E_{\mathrm{CCSDT(Q)}}\right]$ and perturbative pentuples $\left[E_{\mathrm{CCSDTQ(P)}} - E_{\mathrm{CCSDTQ}}\right]$ were found to largely cancel each other out. Thus, to reduce the computational expense only ΔE_{T} and $\Delta E_{(\mathrm{Q})}$ were deemed necessary for an adequate representation of HO

electron correlation.

Scalar relativistic effects ΔE_{SR} were included through the one-electron mass velocity and Darwin terms (MVD1) from the Breit-Pauli Hamiltonian in first-order perturbation theory [53]. Calculations were performed with all electrons correlated (except for the $(1s)$ of Cl) at the CCSD(T)/aug-cc-pCVTZ(+d for Cl) [33, 35] level of theory using the MVD1 approach [156] implemented in CFOUR. The contribution from the two-electron Darwin term is expected to be small enough to be neglected [157].

The diagonal Born-Oppenheimer correction ΔE_{DBOC} was computed again with the $(1s)$ orbital of Cl frozen and all other electrons correlated. Calculations employed the CCSD method [158] as implemented in CFOUR with the aug-cc-pCVTZ(+d for Cl) basis set. The DBOC is the contribution from the nuclear kinetic energy operator acting on the ground state electronic wavefunction. It is mass dependent, so separate contributions were generated for $CH_3{}^{35}Cl$ and $CH_3{}^{37}Cl$.

The spin-orbit interaction was not considered as it can be safely neglected in spectroscopic calculations on light closed-shell molecules [56]. A simple estimate of the Lamb shift was also calculated from the MVD1 contribution [159], but its effect on the vibrational energy levels was negligible. The differing levels of theory and basis set size reflect the fact that different HL energy corrections converge at different rates.

Grid points were generated using a random energy-weighted sampling algorithm of Monte Carlo type (provided by Dr Andrey Yachmenev) in terms of nine internal coordinates: the C–Cl bond length r_0; three C–H bond lengths r_1, r_2 and r_3; three $\angle(\mathrm{H}_i\mathrm{CCl})$ interbond angles β_1, β_2 and β_3; and two dihedral angles τ_{12} and τ_{13} between adjacent planes containing $\mathrm{H}_i\mathrm{CCl}$ and $\mathrm{H}_j\mathrm{CCl}$ (see Figure 4.1). This led to a global grid of 44 820 geometries with energies up to $hc \cdot 50\,000\,\mathrm{cm}^{-1}$, which included geometries in the range $1.3 \leq r_0 \leq 2.95\,\text{Å}$, $0.7 \leq r_i \leq 2.45\,\text{Å}$, $65 \leq \beta_i \leq 165°$ for $i = 1, 2, 3$ and $55 \leq \tau_{jk} \leq 185°$ with $jk = 12, 13$. To ensure an adequate description of the equilibrium region, around 1000 carefully chosen low-energy points were also

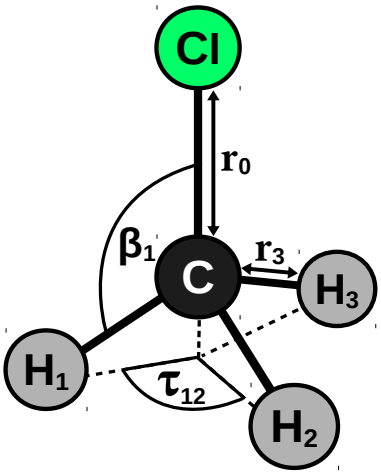

Figure 4.1: Definition of internal coordinates used for CH_3Cl.

incorporated into the data set. At each grid point the computed coupled cluster energies were extrapolated to the CBS limit using Eq. (4.2).

The HL energy corrections are generally small in magnitude and vary in a smooth manner [60], displaying a straightforward polynomial-type dependence as can be seen in Figures 4.2 and 4.3. For each of the HL terms, a reduced grid was designed to obtain a satisfactory description of the correction with minimum computational effort. Reduced grids of 9377, 3526, 12 296 and 3679 points with energies up to $hc \cdot 50\,000\,\mathrm{cm}^{-1}$ were used for the CV, HO, SR and DBOC corrections, respectively.

4.2.2 Analytic representation

Methyl chloride is a prolate symmetric top molecule of the $\boldsymbol{C}_{3v}(\mathrm{M})$ symmetry group [82]. Of the six symmetry operations $\{E, (123), (132), (12)^*, (23)^*, (13)^*\}$ which make up $\boldsymbol{C}_{3v}(\mathrm{M})$, the cyclic permutation (123) replaces nucleus 1 with nucleus 2, nucleus 2 with nucleus 3, and nucleus 3 with nucleus 1. The permutation-inversion operation $(12)^*$ interchanges nuclei 1 and 2 and inverts all particles (including electrons) in the molecular centre of mass. The identity operation E leaves the molecule unchanged.

To represent the PES analytically, an on-the-fly symmetrization procedure has been implemented. Generating a PES on-the-fly is advantageous when it comes to variational calculations as its implementation requires only a short amount of

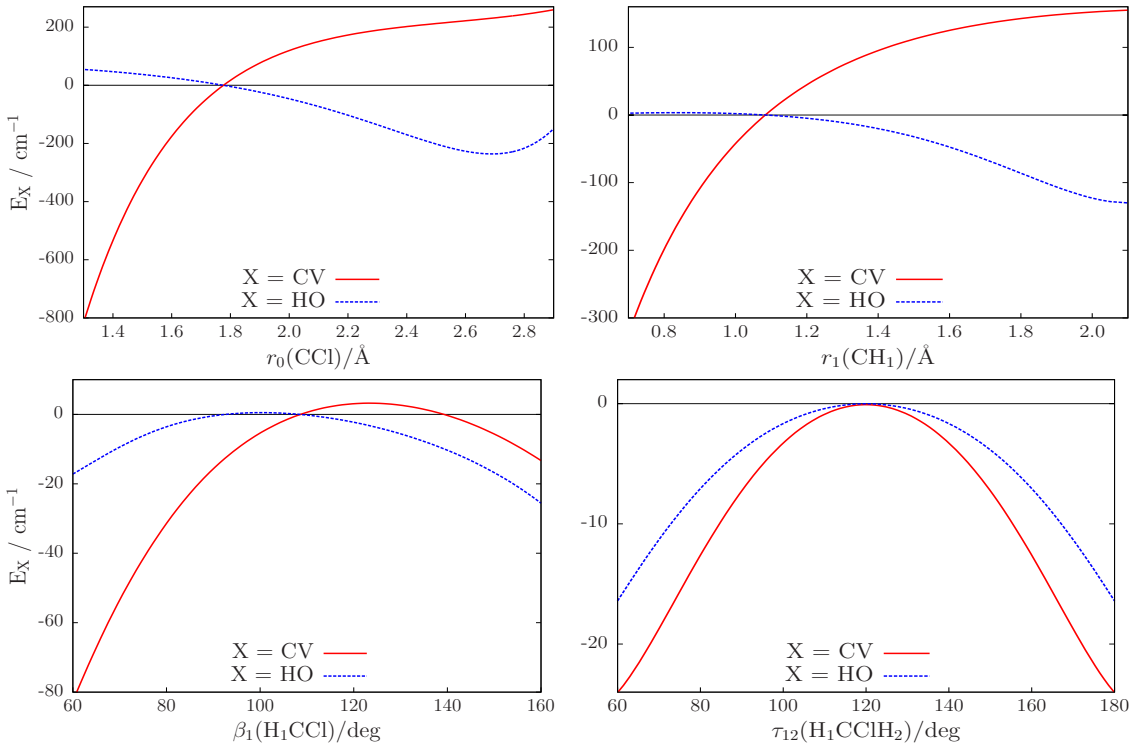

Figure 4.2: One-dimensional cuts of the core-valence (CV) and higher-order (HO) corrections with all other coordinates held at their equilibrium values.

code. Alternatively, one can derive the full analytic expression for the potential and incorporate this into the nuclear motion computations, but this method can be cumbersome.

We first introduce the coordinates

$$\xi_1 = 1 - \exp\left(-a(r_0 - r_0^{\mathrm{eq}})\right), \tag{4.3}$$

$$\xi_j = 1 - \exp\left(-b(r_i - r_1^{\mathrm{eq}})\right) \; ; \;\; j = 2, 3, 4 \, , \;\; i = j - 1, \tag{4.4}$$

where $a = 1.65\,\text{Å}^{-1}$ for the C–Cl internal coordinate r_0, and $b = 1.75\,\text{Å}^{-1}$ for the three C–H internal coordinates r_1, r_2 and r_3. For the angular terms

$$\xi_k = (\beta_i - \beta^{\mathrm{eq}}) \; ; \;\; k = 5, 6, 7 \, , \;\; i = k - 4, \tag{4.5}$$

$$\xi_8 = \frac{1}{\sqrt{6}} \left(2\tau_{23} - \tau_{13} - \tau_{12}\right), \tag{4.6}$$

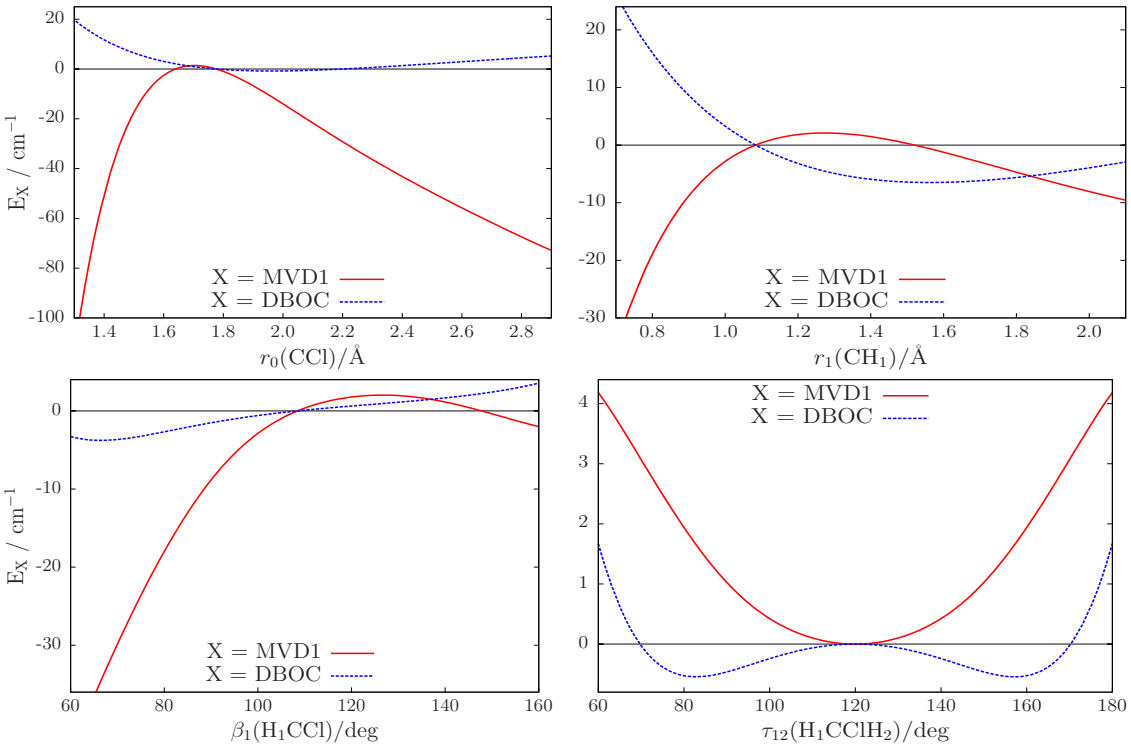

Figure 4.3: One-dimensional cuts of the scalar relativistic (MVD1) and diagonal Born-Oppenheimer (DBOC) corrections with all other coordinates held at their equilibrium values.

$$\xi_9 = \frac{1}{\sqrt{2}}\left(\tau_{13} - \tau_{12}\right). \tag{4.7}$$

Here $\tau_{23} = 2\pi - \tau_{12} - \tau_{13}$, and r_0^{eq}, r_1^{eq} and β^{eq} are the reference equilibrium structural parameters of CH_3Cl.

Taking an initial potential term of the form

$$V_{ijk\ldots}^{\text{initial}} = \xi_1^i \xi_2^j \xi_3^k \xi_4^l \xi_5^m \xi_6^n \xi_7^p \xi_8^q \xi_9^r, \tag{4.8}$$

with maximum expansion order $i+j+k+l+m+n+p+q+r = 6$, each symmetry operation of $\boldsymbol{C}_{3\text{v}}(\text{M})$ is independently applied to $V_{ijk\ldots}^{\text{initial}}$, i.e.

$$V_{ijk\ldots}^{\mathbf{X}} = \mathbf{X}\, V_{ijk\ldots}^{\text{initial}} = \mathbf{X}\left(\xi_1^i \xi_2^j \xi_3^k \xi_4^l \xi_5^m \xi_6^n \xi_7^p \xi_8^q \xi_9^r\right), \tag{4.9}$$

where $\mathbf{X} = \{E, (123), (132), (12)^*, (23)^*, (13)^*\}$, to create six new terms. The results

are summed up to produce a final term,

$$V_{ijk\ldots}^{\text{final}} = V_{ijk\ldots}^{E} + V_{ijk\ldots}^{(123)} + V_{ijk\ldots}^{(132)} + V_{ijk\ldots}^{(12)^*} + V_{ijk\ldots}^{(23)^*} + V_{ijk\ldots}^{(13)^*}, \tag{4.10}$$

which is itself subjected to the six $\boldsymbol{C}_{3\text{v}}(\text{M})$ symmetry operations to check its invariance. The total potential function is then given by the expression

$$V_{\text{total}}(\xi_1, \xi_2, \xi_3, \xi_4, \xi_5, \xi_6, \xi_7, \xi_8, \xi_9) = \sum_{ijk\ldots} \text{f}_{ijk\ldots} V_{ijk\ldots}^{\text{final}}, \tag{4.11}$$

where $\text{f}_{ijk\ldots}$ are the corresponding expansion coefficients, determined through a least-squares fitting to the *ab initio* data. Weight factors of the form suggested by Partridge and Schwenke [160],

$$w_i = \left(\frac{\tanh\left[-0.0006 \times (\tilde{E}_i - 15\,000)\right] + 1.002002002}{2.002002002} \right) \times \frac{1}{N\tilde{E}_i^{(w)}}, \tag{4.12}$$

were used in the fitting, with $\tilde{E}_i^{(w)} = \max(\tilde{E}_i, 10\,000)$ where $\tilde{E}_i$ is the potential energy at the ith geometry above equilibrium and the normalization constant $N = 0.0001$ (all values in cm^{-1}). In the fitting, energies below $15\,000\,\text{cm}^{-1}$ are favoured by the weight factors. For geometries where $r_0 \geq 2.35\,\text{Å}$ and $r_i \geq 2.00\,\text{Å}$ for $i = 1, 2, 3$, the weights were reduced by several orders of magnitude. At such large stretch coordinates, the coupled cluster method is known to become unreliable, as indicated by a T1 diagnostic value > 0.02 [161]. Although energies at these points may not be wholly accurate, they are still useful and ensure that the PES maintains a reasonable shape towards dissociation.

The same form of potential function, Eq. (4.11), and the same procedure, Eqs. (4.8) to (4.10), was used to fit the higher-level correction surfaces. The stretching coordinates however were replaced with linear expansion variables; $\xi_1 = (r_0 - r_0^{\text{eq}})$ and $\xi_j = (r_i - r_1^{\text{eq}})$ where $j = 2, 3, 4$ and $i = j - 1$. The angular terms, Eqs. (4.5) to (4.7), remained the same as before. Each HL correction was fitted independently and the parameters r_0^{eq}, r_1^{eq} and β^{eq} were optimized for each surface. The four HL

corrections were applied at each of the 44 820 grid points, either from a directly calculated value at that geometry, or by interpolation using the corresponding analytic representation. Two final data sets were produced, one for each isotopologue of CH_3Cl, the only difference being the contribution from the DBOC.

Two independent fits were carried out and in each instance I could usefully vary 414 expansion parameters to give a weighted root-mean-square (rms) error of $0.82\,\mathrm{cm}^{-1}$ for energies up to $50\,000\,\mathrm{cm}^{-1}$. The fit employed Watson's robust fitting scheme [162], the idea of which is to reduce the weight of outliers and lessen their influence in determining the final set of parameters. The Watson scheme improves the fit at energies below $10\,000\,\mathrm{cm}^{-1}$ which is preferable for our purposes. When comparing the expansion parameters for $CH_3{}^{35}Cl$ and $CH_3{}^{37}Cl$, only very slight differences were observed in the determined values. We refer to these two PESs as CBS-35$^{\mathrm{HL}}$ and CBS-37$^{\mathrm{HL}}$ in subsequent calculations. The CBS-35$^{\mathrm{HL}}$ and CBS-37$^{\mathrm{HL}}$ expansion parameter sets along with a FORTRAN routine to construct the PESs are provided in the supplementary material of Ref. [163].

To assess the combined effect of the HL corrections and CBS extrapolation on the vibrational energy levels and equilibrium geometry of CH_3Cl, I fitted a reference PES to the raw CCSD(T)-F12b/cc-pVQZ-F12 energies. Again I used Watson's robust fitting scheme and 414 parameters to give a weighted rms error of $0.82\,\mathrm{cm}^{-1}$ for energies up to $50\,000\,\mathrm{cm}^{-1}$. We refer to this PES as VQZ-F12 in subsequent calculations. Note that the CBS-(35/37)$^{\mathrm{HL}}$ and VQZ-F12 PESs are composed of slightly different parameters.

The choice of reference equilibrium structural parameters in the PES expansion is to some extent arbitrary due to the inclusion of linear expansion terms in the parameter set. For this reason, values of $r_0^{\mathrm{eq}} = 1.7775\,\text{Å}$, $r_1^{\mathrm{eq}} = 1.0837\,\text{Å}$, and $\beta^{\mathrm{eq}} = 108.445°$, used for the CBS-35$^{\mathrm{HL}}$ PES, were also employed for the CBS-37$^{\mathrm{HL}}$ and VQZ-F12 PESs. Note that these are not the actual equilibrium parameters which define the minimum of the PES, they are simply parameters of a function. The true equilibrium values will be determined and discussed in Sec. 4.5.2.

4.3 Dipole moment surface

4.3.1 Electronic structure calculations

As shown in Eq. (2.1), the first derivative of the electronic energy with respect to external electric field strength defines the electric dipole moment of a molecule. Working in a Cartesian laboratory-fixed XYZ coordinate system with origin at the C nucleus, an external electric field with components ± 0.005 a.u. was applied along each axis and the respective dipole moment component μ_A for $A = X, Y, Z$ determined using finite differences as given by Eq. (2.2). Calculations were carried out at the CCSD(T) level of theory with the augmented correlation consistent quadruple zeta basis set, aug-cc-pVQZ(+d for Cl) [30–32, 34], in the frozen core approximation. The DMS was evaluated on the same nine-dimensional grid as the PES (44,820 points with energies up to $hc \cdot 50\,000\,\mathrm{cm}^{-1}$). MOLPRO2012 [151] was used for all calculations.

4.3.2 Analytic representation

Before fitting an analytic expression to the *ab initio* data it is necessary to establish a suitable molecule-fixed xyz coordinate system. The symmetrized molecular bond (SMB) representation has been successfully applied to molecules of $\boldsymbol{C}_{3\mathrm{v}}$(M) symmetry [61, 66] and this approach is employed for the present work.

We first define unit vectors along each of the four bonds of CH_3Cl,

$$\mathbf{e}_i = \frac{\mathbf{r}_i - \mathbf{r}_\mathrm{C}}{|\mathbf{r}_i - \mathbf{r}_\mathrm{C}|}\,; \quad i = 0, 1, 2, 3, \tag{4.13}$$

where $\mathbf{r}_\mathrm{C}$ is the position vector of the C nucleus, $\mathbf{r}_0$ the Cl nucleus, and $\mathbf{r}_1$, $\mathbf{r}_2$ and $\mathbf{r}_3$ the respective H atoms. The *ab initio* dipole moment vector $\boldsymbol{\mu}$ is projected onto the molecular bonds and can be described by molecule-fixed xyz dipole moment

components,

$$\mu_x = \frac{1}{\sqrt{6}} \left(2(\boldsymbol{\mu} \cdot \mathbf{e}_1) - (\boldsymbol{\mu} \cdot \mathbf{e}_2) - (\boldsymbol{\mu} \cdot \mathbf{e}_3)\right), \tag{4.14}$$

$$\mu_y = \frac{1}{\sqrt{2}} \left((\boldsymbol{\mu} \cdot \mathbf{e}_2) - (\boldsymbol{\mu} \cdot \mathbf{e}_3)\right), \tag{4.15}$$

$$\mu_z = \boldsymbol{\mu} \cdot \mathbf{e}_0. \tag{4.16}$$

Symmetry-adapted combinations have been formed for μ_x and μ_y and these transform according to E symmetry, while the μ_z component is of A_1 symmetry. The advantage of the SMB representation is that the unit vectors $\mathbf{e}_i$ used to define μ for any instantaneous positions of the nuclei are related to the internal coordinates only.

To construct the three dipole surfaces corresponding to the components given in Eqs. (4.14) to (4.16), a numerical, on-the-fly symmetrization procedure has been implemented. This is similar to the approach employed for the PES detailed in Sec. 4.2.2. However, because $\boldsymbol{\mu}$ is a vector quantity we have to consider the transformation properties of the dipole moment components themselves. For μ_z, which points along the C–Cl bond, the process is trivial owing to its A_1 symmetry and invariance to the $\boldsymbol{C}_{3\mathrm{v}}$(M) symmetry operations. Building an analytic expression follows the same steps as in the case of the PES. For the two E symmetry components, μ_x and μ_y, the construction is more subtle and they must be treated together.

We consider an initial (reference) term in the dipole expansion belonging to μ_x,

$$\begin{pmatrix} \mu_x \\ \mu_y \end{pmatrix} = \begin{pmatrix} \mu^{\mathrm{initial}}_{x,ijk\ldots} \\ 0 \end{pmatrix}, \tag{4.17}$$

where

$$\mu^{\mathrm{initial}}_{x,ijk\ldots} = \left(\xi_1^i \xi_2^j \xi_3^k \xi_4^l \xi_5^m \xi_6^n \xi_7^p \xi_8^q \xi_9^r\right). \tag{4.18}$$

This term has maximum expansion order $i+j+k+l+m+n+p+q+r = 6$, and is expressed in terms of nine coordinates. Linear expansion variables are utilized for

the stretches,

$$\xi_1 = \left(r_0 - r_0^{\text{ref}}\right), \tag{4.19}$$

$$\xi_j = \left(r_i - r_1^{\text{ref}}\right) \; ; \;\; j = 2, 3, 4 \, , \;\; i = j - 1, \tag{4.20}$$

whilst the angular terms are the same as those defined in Eqs. (4.5) to (4.7). For the reference structural parameters $r_0^{\text{ref}} = 1.7550\,\text{Å}$, $r_1^{\text{ref}} = 1.0415\,\text{Å}$ and $\beta^{\text{ref}} = 108.414°$ and these values were optimized during the fitting of the DMS.

The action of a $\boldsymbol{C}_{3\text{v}}$(M) symmetry operation $\mathbf{X} = \{E, (123), (132), (12)^*, (23)^*, (13)^*\}$ on Eq. (4.18) will (i) permute the expansion indices $ijk\ldots$, to $i'j'k'\ldots$ to produce a new expansion term and (ii) permute the unit vectors $\mathbf{e}_i$ for $i = 1, 2, 3$. Using the projection operator technique [82], this latter contribution is projected onto the $\mathbf{e}_x$ and $\mathbf{e}_y$ molecule-fixed vectors and added to the respective dipole moment components. The resulting components, μ'_x and μ'_y, reduce to

$$\begin{pmatrix} \mu'_x \\ \mu'_y \end{pmatrix} = \begin{pmatrix} C_1 \mu^{\mathbf{X}}_{x,ijk\ldots} \\ C_2 \mu^{\mathbf{X}}_{x,ijk\ldots} \end{pmatrix}, \tag{4.21}$$

where C_1 and C_2 are constants associated with the acting $\boldsymbol{C}_{3\text{v}}$(M) symmetry operation, and $\mu^{\mathbf{X}}_{x,ijk\ldots}$ is the new expansion term connected to Eq. (4.18) by the symmetry operation $\mathbf{X}$. Note that a contribution arises in μ'_y ($C_2 \neq 0$) due to the projection operator acting on the two-component quantity (μ_x, μ_y).

The steps are repeated for each symmetry operation of $\boldsymbol{C}_{3\text{v}}$(M) and the results summed to produce a final dipole term (ignoring constants),

$$\mu^{\text{final}}_{x,ijk\ldots} = \mu^{E}_{x,ijk\ldots} + \mu^{(123)}_{x,ijk\ldots} + \mu^{(132)}_{x,ijk\ldots} + \mu^{(12)^*}_{x,ijk\ldots} + \mu^{(23)^*}_{x,ijk\ldots} + \mu^{(13)^*}_{x,ijk\ldots}, \tag{4.22}$$

which is best understood as a sum of symmetrized combinations of different permutations of coordinates ξ_i. Likewise, a similar expression contributes to μ_y. Although we have only considered an initial term belonging to μ_x, the same idea applies to ini-

tial terms belonging to μ_y. Incorporating μ_z into the procedure is straightforward, thus enabling the simultaneous construction of all three DMSs of CH_3Cl. Each surface is represented by the analytic expression

$$\mu_\alpha^{\text{total}}(\xi_1,\xi_2,\xi_3,\xi_4,\xi_5,\xi_6,\xi_7,\xi_8,\xi_9) = \sum_{ijk\ldots} F_{ijk\ldots}^{(\alpha)} \mu_{\alpha,ijk\ldots}^{\text{final}}, \tag{4.23}$$

where some of the expansion coefficients $F_{ijk\ldots}^{(\alpha)}$ are shared between the x and y components.

The coefficients $F_{ijk\ldots}^{(\alpha)}$ for $\alpha = x, y, z$ were determined in a least squares fitting to the *ab initio* data. Similar to the PES, I utilized Watson's robust fitting scheme [162] and weight factors of the form given in Eq. (4.12). That is, energies below $15\,000\,\text{cm}^{-1}$ were favoured in the fit. Again for very large stretch distances the weights were decreased by several orders of magnitude.

The three dipole surfaces for μ_x, μ_y and μ_z employed sixth order expansions and used 175, 163 and 235 parameters, respectively. A combined weighted root-mean-square (rms) error of $9 \times 10^{-5}\,\text{D}$ was obtained for the fitting. Incorporating the analytic representation into variational nuclear motion calculations is relatively straightforward and the implementation requires only a small amount of code. The dipole expansion parameters along with a FORTRAN routine to construct the DMS are provided in the supplementary material of Ref. [164].

4.4 Variational calculations

For the present study the functionality of TROVE was extended to handle molecules of the form XY_3Z. As discussed in Sec. 3.2.1, this involves implementing all the necessary subroutines and coordinate transformations to construct the analytic representations of the PES and DMS described in Sec. 4.2 and Sec. 4.3, respectively. This was the only necessary extension of TROVE.

An automatic differentiation method [70] was used to construct the rovibrational Hamiltonian numerically. The Hamiltonian itself was represented as a power series

expansion around the equilibrium geometry in terms of nine vibrational coordinates. The coordinates used are identical to those given in Eqs. (4.3) to (4.7), except for the kinetic energy operator where linear expansion variables replace the Morse oscillator functions for the stretching modes. In all calculations the kinetic and potential energy operators were truncated at 6th and 8th order, respectively. This level of truncation is adequate for our purposes (see Ref. [9] and [70] for a discussion of the associated errors of such a scheme). Atomic mass values were employed throughout.

The polyad number (see Eq. 3.5) for CH_3Cl is defined as

$$P = n_1 + 2(n_2 + n_3 + n_4) + n_5 + n_6 + n_7 + n_8 + n_9 \leq P_{\max}, \tag{4.24}$$

and this does not exceed a predefined maximum value $P_{\max}$. Here, the quantum numbers n_k for $k = 1, \ldots, 9$ correspond to primitive basis functions ϕ_{n_k} for each vibrational mode. The symmetrized rovibrational basis set was constructed in the steps detailed in Sec. 3.2.1. We will see in Sec. 4.5 that different sized basis sets had to be utilized in this work and this reflects the computational demands of variational calculations of rovibrational spectra.

TROVE automatically assigns quantum numbers to the eigenvalues and corresponding eigenvectors by analysing the contribution of the basis functions. We therefore map the vibrational quantum numbers n_k to the normal mode quantum numbers v_k. For CH_3Cl, vibrational states are labelled as $\mathrm{v}_1\nu_1+\mathrm{v}_2\nu_2+\mathrm{v}_3\nu_3+\mathrm{v}_4\nu_4+\mathrm{v}_5\nu_5+\mathrm{v}_6\nu_6$ where v_i counts the level of excitation.

The normal modes of methyl chloride are of A_1 or E symmetry. The three non-degenerate modes have A_1 symmetry; the symmetric CH_3 stretching mode ν_1 (2967.77/2967.75 cm^{-1}), the symmetric CH_3 deformation mode ν_2 (1354.88/1354.69 cm^{-1}) and the C–Cl stretching mode ν_3 (732.84/727.03 cm^{-1}). Whilst the three degenerate modes have E symmetry; the CH_3 stretching mode $\nu_4^{\ell_4}$ (3039.26/3039.63 cm^{-1}), the CH_3 deformation mode $\nu_5^{\ell_5}$ (1452.18/1452.16 cm^{-1}) and the CH_3 rocking mode $\nu_6^{\ell_6}$ (1018.07/1017.68 cm^{-1}). The values in parentheses are the experimentally determined fundamental frequencies for $CH_3{}^{35}Cl/CH_3{}^{37}Cl$ [99, 123]. The additional

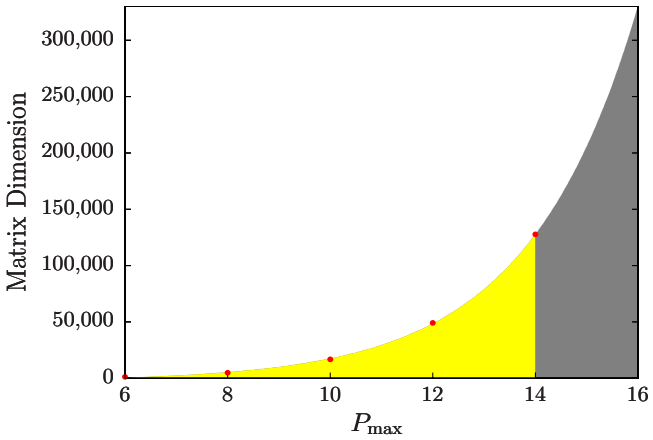

Figure 4.4: Size of the $J = 0$ Hamiltonian matrix with respect to the polyad truncation number $P_{\max}$. Computations were only possible up to $P_{\max} = 14$.

vibrational angular momentum quantum numbers ℓ_4, ℓ_5 and ℓ_6 are there to resolve the degeneracy of their respective modes.

4.4.1 Extrapolation to the complete vibrational basis set limit

Fully converged energies in variational calculations are usually obtained with the use of an extended basis set. I have only been able to compute $J = 0$ vibrational energies up to a polyad truncation number of $P_{\max} = 14$ for CH_3Cl. As shown in Figure 4.4, this requires the diagonalization of a Hamiltonian matrix of dimension close to 128 000, which in turn equals the number of primitive basis functions generated. The extension to $P_{\max} = 16$ using TROVE would be an arduous computational task.

One means of achieving converged vibrational energy levels without having to diagonalize increasingly large matrices is the use of a complete vibrational basis set (CVBS) extrapolation [59]. In analogy to the common basis set extrapolation techniques of electronic structure theory [165, 166], the same principles can be applied to TROVE calculations with respect to $P_{\max}$. We adopt the exponential decay expression

$$E_i(P_{\max}) = E_i^{\mathrm{CVBS}} + A_i \exp(-\lambda_i P_{\max}), \tag{4.25}$$

where E_i is the energy of the ith level, E_i^{CVBS} is the respective energy at the CVBS

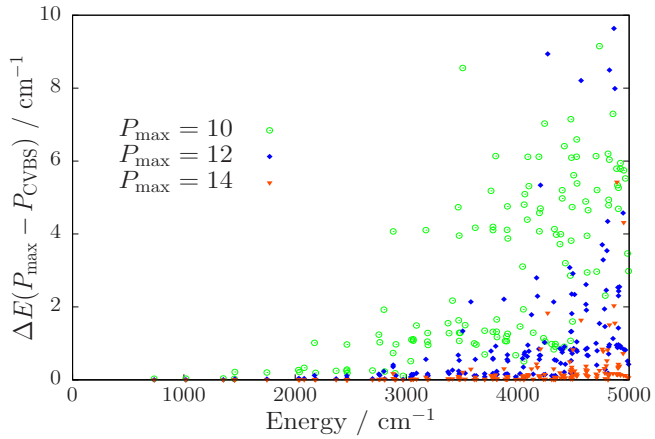

Figure 4.5: Convergence of vibrational term values of $CH_3{}^{35}Cl$ up to 5000 cm^{-1} with respect to $P_{\max} = P_{\mathrm{CVBS}}$. For illustrative purposes we restrict the range of $\Delta E(P_{\max} - P_{\mathrm{CVBS}})$ to 10 cm^{-1}.

limit, A_i is a fitting parameter, and λ_i can be found from

$$\lambda_i = -\frac{1}{2} \ln \left(\frac{E_i(P_{\max} + 2) - E_i(P_{\max})}{E_i(P_{\max}) - E_i(P_{\max} - 2)} \right). \tag{4.26}$$

Values of $P_{\max} = \{10, 12, 14\}$ were employed for a CVBS extrapolation of all vibrational term values up to 5000 cm^{-1}, and for selected higher energies to compare with experiment. This was done for the CBS-35$^{\mathrm{HL}}$, CBS-37$^{\mathrm{HL}}$, and VQZ-F12 PESs. In Figure 4.5, the convergence of the vibrational energy levels up to 5000 cm^{-1} for the CBS-35$^{\mathrm{HL}}$ PES can be seen with respect to the final E_i^{CVBS} extrapolated values. Below 4000 cm^{-1} the computed $P_{\max} = 14$ term values are already reasonably well converged. Only five levels in this range possess a residual $\Delta E(P_{\max} - P_{\mathrm{CVBS}})$ larger than 0.1 cm^{-1}, none of which is greater than 0.3 cm^{-1}. As expected, levels involving highly excited modes benefit the most from extrapolation as these converge at a much slower rate.

The limiting factor of a CVBS extrapolation is the correct identification of the energy levels at each step up in basis set size. TROVE automatically assigns quantum numbers to the eigenvalues and corresponding eigenvectors by analysing the contribution of the basis functions. Due to the increased density of states above 5000 cm^{-1} for higher values of $P_{\max}$, it quickly becomes difficult to consistently

identify and match levels, except for highly excited individual modes.

4.5 Results

4.5.1 Vibrational $J = 0$ energies

The calculated $J = 0$ energy levels for $CH_3{}^{35}Cl$ using the CBS-35^{HL} and VQZ-F12 PESs are listed in Table 4.1. We compare against all available experimental data taken from Refs. [99, 123, 141, 143]. A small number of levels from Refs. [141] and [143] have not been included as I was unable to confidently identify the corresponding values in TROVE.

Table 4.1: Comparison of calculated and experimental $J = 0$ vibrational term values (in cm^{-1}) for $CH_3{}^{35}Cl$. The zero-point energy was computed to be 8219.661 cm^{-1} at the CVBS limit.

Mode	Sym.	VQZ-F12 (A)	CBS-35^{HL} (B)	Experiment	Obs−calc (A)	Obs−calc (B)	Ref.
ν_3	A_1	734.37	733.22	732.8422	-1.53	-0.38	[123]
ν_6	E	1018.16	1018.05	1018.0709	-0.09	0.02	[123]
ν_2	A_1	1355.11	1355.01	1354.8811	-0.23	-0.13	[123]
ν_5	E	1451.57	1452.56	1452.1784	0.61	-0.38	[123]
$2\nu_3$	A_1	1459.94	1457.54	1456.7626	-3.18	-0.78	[123]
$\nu_3 + \nu_6$	E	1747.10	1745.78	1745.3711	-1.73	-0.41	[123]
$2\nu_6$	A_1	2029.67	2029.46	2029.3753	-0.29	-0.09	[123]
$2\nu_6$	E	2038.58	2038.37	2038.3262	-0.25	-0.04	[123]
$\nu_2 + \nu_3$	A_1	2082.35	2080.98	2080.5357	-1.82	-0.45	[123]
$3\nu_3$	A_1	2176.84	2173.09	2171.8875	-4.95	-1.20	[123]
$\nu_3 + \nu_5$	E	2183.51	2183.30	2182.5717	-0.94	-0.73	[123]
$\nu_2 + \nu_6$	E	2368.08	2367.90	2367.7222	-0.35	-0.18	[123]
$\nu_5 + \nu_6$	E	2461.19	2461.98	2461.6482	0.46	-0.33	[123]
$2\nu_3 + \nu_6$	E	2467.19	2464.65	2463.8182	-3.37	-0.83	[123]
$\nu_5 + \nu_6$	A_1	2464.50	2465.28	2464.9025	0.40	-0.38	[123]
$\nu_5 + \nu_6$	A_2	2466.85	2467.85	2467.6694	0.82	-0.18	[123]
$2\nu_2$	A_1	2694.69	2694.61	2693.0	-1.69	-1.61	[141]
$\nu_3 + 2\nu_6$	A_1	2753.23	2751.74	2751.18	-2.05	-0.56	[141]
$\nu_2 + 2\nu_3$	A_1	2800.39	2797.64	2796.81	-3.58	-0.83	[141]
$\nu_2 + \nu_5$	E	2803.10	2803.96	2803.26	0.16	-0.70	[141]
$4\nu_3$	A_1	2885.23	2880.47	2878	-7.23	-2.47	[141]

(*Continued*)

Mode	Sym.	VQZ-F12 (A)	CBS-35^{HL} (B)	Experiment	Obs−calc (A)	Obs−calc (B)	Ref.
$2\nu_5$	A_1	2877.75	2879.31	2879.25	1.50	-0.06	[141]
$2\nu_5$	E	2896.27	2898.22	2895.566	-0.71	-2.65	[99]
$2\nu_3+\nu_5$	E	2906.64	2905.14	2907.903	1.26	2.77	[99]
ν_1	A_1	2965.78	2969.16	2967.7691	1.99	-1.39	[99]
ν_4	E	3035.50	3038.19	3039.2635	3.76	1.07	[99]
$3\nu_6$	E	3045.08	3045.76	3042.8944	-2.18	-2.87	[99]
$3\nu_6$	A_1	3060.95	3060.62	3060.0064	-0.95	-0.62	[99]
$\nu_2+2\nu_6$	A_1	3373.81	3373.57	3373.5	-0.31	-0.07	[141]
$2\nu_2+\nu_3$	A_1	3415.53	3414.02	3413.0	-2.53	-1.02	[141]
$\nu_3+2\nu_5$	A_1	3607.98	3608.77	3607.70	-0.28	-1.07	[141]
$\nu_1+\nu_3$	A_1	3700.18	3702.43	3700.67	0.49	-1.76	[141]
$2\nu_2+\nu_6$	E	3702.92	3702.80	3702.69	-0.23	-0.11	[141]
$\nu_3+3\nu_6$	E	3760.53	3759.07	3756.6	-3.93	-2.47	[141]
$\nu_3+\nu_4$	E	3773.98	3776.04	3773.52	-0.46	-2.52	[141]
$2\nu_5+\nu_6$	E	3884.88	3886.75	3886.05	1.17	-0.70	[141]
$\nu_1+\nu_6$	E	3977.68	3980.97	3979.66	1.98	-1.31	[141]
$\nu_4+\nu_6$	E	4047.37	4049.83	4051.22	3.85	1.39	[141]
$2\nu_2+\nu_5$	E	4137.96	4138.86	4138.29	0.33	-0.57	[141]
$\nu_2+2\nu_5$	A_1	4229.37	4231.18	4230.34	0.97	-0.84	[141]
$\nu_2+3\nu_6$	E	4378.39	4379.54	4380.52	2.13	0.98	[141]
$\nu_2+\nu_4$	E	4384.03	4385.90	4382.64	-1.39	-3.26	[141]
$\nu_1+\nu_5$	E	4412.81	4416.81	4415.4	2.59	-1.41	[143]
$\nu_1+2\nu_6$	A_1	4982.68	4985.90	4984.0	1.32	-1.90	[141]
$\nu_1+2\nu_2$	A_1	5655.67	5658.93	5657.0	1.33	-1.93	[141]
$2\nu_2+\nu_4$	E	5708.85[a]	5711.12[a]	5713	4.15	1.88	[143]
$\nu_1+\nu_4$	E	5870.30	5875.98	5873.8	3.50	-2.18	[143]
$2\nu_1$	A_1	5875.28	5881.04	5878	2.72	-3.04	[143]
$\nu_4+2\nu_5$	E	5918.20[a]	5923.37[a]	5923.4	5.20	0.03	[143]
$2\nu_4$	A_1	6011.38	6018.47	6015.3	3.92	-3.17	[141]
$2\nu_1+\nu_5$	E	7303.96	7311.08	7313.2	9.24	2.12	[141]
$2\nu_4+\nu_5$	E	7437.80	7445.86	7443.2	5.40	-2.66	[141]
$2\nu_4+2\nu_5$	A_1	8870.15	8877.25	8874.3	4.15	-2.95	[141]
$3\nu_4$	A_1	9069.53	9079.28	9076.9	7.37	-2.38	[141]

[a] $P_{\max}=14$ value.

The CBS-35^{HL} PES reproduces the six fundamental term values with a root-mean-square (rms) error of 0.75 cm^{-1} and a mean-absolute-deviation (mad) of 0.56 cm^{-1}. This is a considerable improvement over the results of the VQZ-F12 PES,

which reproduces the fundamentals with a rms error of $1.86\,\mathrm{cm}^{-1}$ and a mad of $1.37\,\mathrm{cm}^{-1}$. Inspection of all computed $CH_3{}^{35}Cl$ energy levels shows that on the whole, the CBS-35$^{\mathrm{HL}}$ PES is more reliable. This is gratifying as the effort required to generate the CBS-35$^{\mathrm{HL}}$ PES is far greater than that of the VQZ-F12 PES. Unlike other instances [60], the VQZ-F12 results do not benefit from an extensive cancellation of errors. Note that the PES reported in Ref. [144], which did not treat any additional HL energy corrections, produces results with errors similar to those of the VQZ-F12 PES.

The accuracy achieved at lower energies with the CBS-35$^{\mathrm{HL}}$ PES is quite remarkable, with residuals larger than $2\,\mathrm{cm}^{-1}$ starting to appear around $3000\,\mathrm{cm}^{-1}$. This is a notoriously difficult region of CH_3Cl with strong resonances, but the experimental values we compare against are from a recent high-resolution study and should thus be trustworthy [99]. However, we will discuss this point further in Sec. 4.6 when discussing empirical refinement of the CBS-35$^{\mathrm{HL}}$ PES.

In the comparison against values reported in Duncan and Law [141], and subsequently used in Law [143], I exercise minor caution. The $2\nu_5(E)$ and $2\nu_3 + \nu_5(E)$ levels presented in Duncan and Law [141] are lower by around 3 and $5\,\mathrm{cm}^{-1}$, respectively, when compared with new values determined in Bray et al. [99]. However, the agreement for the ν_1, ν_4 and $3\nu_6(E)$ levels is excellent. The residual for the $2\nu_2$ level seems large given the residual for the ν_2 term value, and I suspect that the experimental value is incorrect. At higher energies the quality of the CBS-35$^{\mathrm{HL}}$ PES does not appear to deteriorate significantly.

For $CH_3{}^{37}Cl$, the $J = 0$ term values calculated from the CBS-37$^{\mathrm{HL}}$ PES are compared with all available experimental data in Table 4.2. The CBS-37$^{\mathrm{HL}}$ PES reproduces the six fundamental term values with a rms error of $1.00\,\mathrm{cm}^{-1}$ and a mad of $0.70\,\mathrm{cm}^{-1}$. The reduction in accuracy when compared to the CBS-35$^{\mathrm{HL}}$ PES is primarily due to the ν_4 mode, whose residual has gone from $1.07\,\mathrm{cm}^{-1}$ for $CH_3{}^{35}Cl$ to $1.92\,\mathrm{cm}^{-1}$ for $CH_3{}^{37}Cl$. The accuracy of the $3\nu_6(E)$ level has also declined, but for energies leading up to $3000\,\mathrm{cm}^{-1}$ the agreement with experiment is excellent.

Despite being unable to compare against higher energies I expect the CBS-37$^{\mathrm{HL}}$ PES to perform as well as its ^{35}Cl counterpart.

Table 4.2: Comparison of calculated and experimental $J = 0$ vibrational term values (in cm^{-1}) for $CH_3{}^{37}Cl$. The zero-point energy was computed to be 8216.197 cm^{-1} at the CVBS limit.

Mode	Sym.	CBS-37$^{\mathrm{HL}}$	Experiment[a]	Obs−calc
ν_3	A_1	727.40	727.0295	-0.37
ν_6	E	1017.66	1017.6824	0.02
ν_2	A_1	1354.82	1354.6908	-0.13
$2\nu_3$	A_1	1446.12	1445.3509	-0.77
ν_5	E	1452.53	1452.1552	-0.38
$\nu_3 + \nu_6$	E	1739.64	1739.2357	-0.41
$2\nu_6$	A_1	2028.68	2028.5929	-0.09
$2\nu_6$	E	2037.59	2037.5552	-0.04
$\nu_2 + \nu_3$	A_1	2074.90	2074.4526	-0.45
$3\nu_3$	A_1	2156.31	2155.1179	-1.19
$\nu_3 + \nu_5$	E	2177.47	2176.7504	-0.72
$\nu_2 + \nu_6$	E	2367.32	2367.1394	-0.18
$2\nu_3 + \nu_6$	E	2452.76	2451.9048	-0.85
$\nu_5 + \nu_6$	E	2461.78	2461.4849	-0.29
$\nu_5 + \nu_6$	A_1	2464.85	2464.4690	-0.38
$\nu_5 + \nu_6$	A_2	2467.43	2467.2469	-0.18
$\nu_2 + \nu_5$	E	2803.73	2803.2[b]	-0.53
$2\nu_5$	A_1	2879.81	2879.0[b]	-0.81
$2\nu_3 + \nu_5$	E	2893.71	2893.7394[c]	0.03
$2\nu_5$	E	2898.19	2895.449[c]	-2.74
ν_1	A_1	2969.14	2967.7469[c]	-1.39
ν_4	E	3037.71	3039.6311[c]	1.92
$3\nu_6$	E	3044.97	3041.2568[c]	-3.72
$3\nu_6$	A_1	3059.47	3058.6913[c]	-0.78

[a] Values from Ref. [123] unless stated otherwise. [b] Ref. [167]. [c] Ref. [99].

I have not computed term values for $CH_3{}^{37}Cl$ using the VQZ-F12 PES but I expect errors similar to those reported for $CH_3{}^{35}Cl$. It is evident that for methyl chloride, the inclusion of additional HL corrections and a CBS extrapolation in the PES lead to considerable improvements in computed $J = 0$ energies. The CBS-35$^{\mathrm{HL}}$ and CBS-37$^{\mathrm{HL}}$ PESs are recommended for future use. Note that I have been able to

Table 4.3: Equilibrium structural parameters of CH_3Cl

	r(C–Cl)/Å	r(C–H)/Å	β(HCCl)/deg
CBS-(35/37) [HL]	1.7777	1.0834	108.38
VQZ-F12	1.7805	1.0849	108.39
Ref. [169] [a]	1.7768	1.0842	108.72
Ref. [171] [b]	1.7772	1.0838	108.45

[a] Value determined from empirical data and CCSD(T) calculations.

[b] CCSD(T)(*fc*)/cc-pV(Q,5)Z + MP2(*ae*)/cc-pwCVQZ - MP2(*fc*)/cc-pwCVQZ.

identify and assign over 100 new energy levels for both $CH_3{}^{35}Cl$ and $CH_3{}^{37}Cl$ which are given in Appendix A.

4.5.2 Equilibrium geometry and pure rotational energies

The equilibrium geometry of methyl chloride determined empirically by Jensen et al. [168] is often utilized as a reference for other studies. However, the reliability of the axial rotational constants used in their analysis has been questioned [169]. The C–H bond length reported in Jensen et al. [168] also appears too large to be consistent with *ab initio* calculations, and also with the isolated C–H bond stretching frequency [170]. A combined empirical and *ab initio* structure was later determined based on $^{12}CH_3{}^{35}Cl$, $^{12}CH_3{}^{37}Cl$, $^{12}CD_3{}^{35}Cl$ and $^{12}CD_3{}^{37}Cl$ experimental data [169] We compare against this as well as another high-level *ab initio* study [171].

The equilibrium structural parameters calculated from the CBS-(35/37) [HL] PES and the VQZ-F12 PES are listed in Table 4.3. The CBS-(35/37) [HL] bond lengths are shorter than the VQZ-F12 values, which is to be expected due to the inclusion of CV electron correlation [172]. There is good agreement with the values from Refs. [169] and [171]. The largest discrepancy concerns the bond angle determined in Ref. [169] which is around 0.3 degrees larger than all *ab initio* computed values.

For further validation I studied the pure rotational spectrum as rotational energies are highly dependent on the molecular geometry through the moments of inertia. In Table 4.4, the calculated $J \leq 5$ rotational energies in the ground vibrational state

for $CH_3{}^{35}Cl$ using the CBS-35^{HL} PES are presented. The computed values reproduce the experimental levels with a rms error of 0.0018 cm^{-1}. The CBS-(35/37)^{HL} *ab initio* structural parameters reported in Table 4.3 can thus be regarded as reliable, and I expect the true equilibrium geometry of methyl chloride to be close to these values.

Table 4.4: Comparison of calculated and experimental $J \leq 5$ pure rotational term values (in cm^{-1}) for $CH_3{}^{35}Cl$. The observed ground state energy levels are from Ref. [122].

J	K	Sym.	Experiment	CBS-35^{HL}	Obs−calc
0	0	A_1	0.0000	0.0000	0.0000
1	0	A_2	0.8868	0.8868	0.0000
1	1	E	5.6486	5.6489	-0.0003
2	0	A_1	2.6604	2.6603	0.0001
2	1	E	7.4222	7.4223	-0.0001
2	2	E	21.7067	21.7075	-0.0008
3	0	A_2	5.3208	5.3205	0.0003
3	1	E	10.0825	10.0826	-0.0001
3	2	E	24.3668	24.3676	-0.0008
3	3	A_1	48.1707	48.1727	-0.0020
3	3	A_2	48.1707	48.1727	-0.0020
4	0	A_1	8.8678	8.8675	0.0003
4	1	E	13.6295	13.6294	0.0001
4	2	E	27.9137	27.9143	-0.0006
4	3	A_1	51.7173	51.7191	-0.0018
4	3	A_2	51.7173	51.7191	-0.0018
4	4	E	85.0354	85.0389	-0.0035
5	0	A_2	13.3015	13.3010	0.0005
5	1	E	18.0632	18.0629	0.0003
5	2	E	32.3472	32.3476	-0.0004
5	3	A_1	56.1505	56.1521	-0.0016
5	3	A_2	56.1505	56.1521	-0.0016
5	4	E	89.4681	89.4714	-0.0033
5	5	E	132.2931	132.2985	-0.0054

4.5.3 Vibrational transition moments

As an initial test of the DMS I computed vibrational transition moments, introduced in Eq. (3.10). Transition moments have been determined experimentally for the six fundamental modes of $CH_3{}^{35}Cl$ and these are listed in Table 4.5 along with the computed values. Calculations employed a polyad truncation number of $P_{\max} = 12$, which is sufficient for converging μ_{if}. Overall the agreement is encouraging and it indicates that the DMS should be reliable for intensity simulations of the fundamental bands.

Table 4.5: Calculated vibrational transition moments (in Debye) and frequencies (in cm^{-1}) from the vibrational ground state for $CH_3{}^{35}Cl$ and $CH_3{}^{37}Cl$.

Mode	Sym.	Experiment[a]	Calculated	μ_{if}^{calc}	μ_{if}^{exp}	Ref.
				$CH_3{}^{35}Cl$		
ν_1	A_1	2967.77	2969.16	0.05296	0.053[b]	Elkins et al. [173]
ν_2	A_1	1354.88	1355.01	0.05260	0.05006(1)[c]	Blanquet et al. [174]
ν_3	A_1	732.84	733.22	0.11468	0.1121(8)	Dang-Nhu et al. [175]
ν_4	E	3039.26	3038.19	0.03108	0.033[d]	Elkins et al. [173]
ν_5	E	1452.18	1452.56	0.05451	0.0527(7)	Cappellani et al. [176]
ν_6	E	1018.07	1018.05	0.03707	0.0388[e]	Blanquet et al. [177]
				$CH_3{}^{37}Cl$		
ν_1	A_1	2967.75	2969.14	0.05296	–	–
ν_2	A_1	1354.69	1354.82	0.05275	–	–
ν_3	A_1	727.03	727.40	0.11416	–	–
ν_4	E	3039.63	3037.71	0.02939	–	–
ν_5	E	1452.16	1452.53	0.05449	–	–
ν_6	E	1017.68	1017.66	0.03724	–	–

[a] From Bray et al. [99] and Nikitin et al. [123]. [b] From Papoušek et al. [148] but derived from band strength measurement of $S_{\text{v}} = 84.3 \pm 3.3\,\text{cm}^{-2}\,\text{atm}^{-1}$ at 296 K [173]. [c] Value of $\mu_{\nu_2}^{\text{exp}} = 0.0473(7)$ D determined in Cappellani et al. [176]. [d] From Papoušek et al. [148] but derived from band strength measurement of $S_{\text{v}} = 33.6 \pm 1.4\,\text{cm}^{-2}\,\text{atm}^{-1}$at 296 K [173]. [e] From Papoušek et al. [148] but derived from band strength measurement of $S_{\text{v}} = 15.1 \pm 1.6\,\text{cm}^{-2}\,\text{atm}^{-1}$at 296 K [177].

For $CH_3{}^{37}Cl$, band strength measurements of the ν_3 [178] and ν_6 [179] bands have been carried out but only minor differences were observed compared to $CH_3{}^{35}Cl$ [175, 177]. Likewise, as seen in Table 4.5 the computed transition moments for the fundamentals only marginally differ compared to $CH_3{}^{35}Cl$. It seems the intensity vari-

ation from isotopic substitution in methyl chloride is relatively small and in some instances almost negligible. A list of computed transitions moments from the vibrational ground state for 79 levels up to $4200\,\mathrm{cm}^{-1}$ is given in Appendix A. Note that for the equilibrium dipole moment of methyl chloride I calculate $\mu = 1.8909\,\mathrm{D}$ which is close to the experimental value of $\mu = 1.8959(15)\,\mathrm{D}$ [180].

4.5.4 Absolute line intensities of the ν_1, ν_4, ν_5 and $3\nu_6$ bands

Intensities of the six fundamental bands of CH_3Cl have all been measured at some stage [99–101, 173–179, 181–187]. Notably, absolute line intensities were determined for the ν_1, ν_4 and $3\nu_6$ bands around the $3.4\,\mu$m region [99] (included in HITRAN2012), and for the ν_5 band in the $6.9\,\mu$m region [100]. To assess the DMS we compare against these works for both isotopologues up to $J = 15$. Calculating higher rotational excitation is computationally demanding (rovibrational matrices scale linearly with J) so we set $P_{\max} = 10$, which is sufficient for reliable intensities. A study on the five-atom molecule SiH_4, which will be discussed in detail in Chapter 5, displayed similar convergence properties with respect to $P_{\max}$. Line intensities of the ν_3 band were computed with $P_{\max} = 10$ and possesed an estimated convergence error of 1% or less for transitions up to $J = 16$. Note that because the two *ab initio* PESs used in this study, CBS-35$^{\mathrm{HL}}$ and CBS-37$^{\mathrm{HL}}$, can at best only be considered accurate to about $\pm 1\,\mathrm{cm}^{-1}$, for illustrative purposes I have shifted computed line positions to better match experiment in the following comparisons.

Absolute absorption intensities have been simulated at room temperature ($T = 296\,\mathrm{K}$) using Eq. (3.9). The nuclear spin statistical weights of CH_3Cl are $g_{\mathrm{ns}} = \{16, 16, 16\}$ for states of symmetry $\{A_1, A_2, E\}$, respectively. These values have been calculated using the method detailed in Jensen and Bunker [188]. For the partition function I used values of $Q(T) = 57,915.728$ and $58,833.711$ for $CH_3{}^{35}Cl$ and $CH_3{}^{37}Cl$, respectively [89]. Note that to ensure a correct comparison with the experimental studies of Bray et al. [99] and Barbouchi Ramchani et al. [100], the intensities of overlapping A_1 and A_2 spectral lines (listed as being of A symmetry)

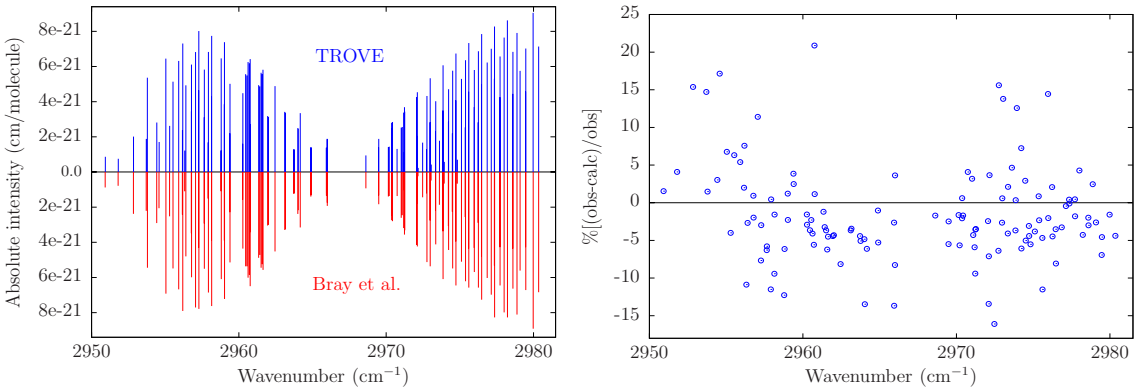

Figure 4.6: Absolute line intensities of the ν_1 band for transitions up to $J = 15$ (left) and the corresponding residuals $\left(\% \left[\frac{\text{obs}-\text{calc}}{\text{obs}}\right]\right)$ (right) when compared with measurements from Bray et al. [99]. Transitions for both $CH_3{}^{35}Cl$ and $CH_3{}^{37}Cl$ are shown and the intensities have not been scaled to natural abundance. For illustrative purposes TROVE line positions have been shifted by $-1.35\,\text{cm}^{-1}$.

must be halved.

In Fig. 4.6, absolute line intensities for 126 transitions of the ν_1 band and their corresponding residuals $\left(\% \left[\frac{\text{obs}-\text{calc}}{\text{obs}}\right]\right)$ compared to measurements from Bray et al. [99] are plotted. The majority of computed intensities, although tending to be marginally stronger, are within the experimental accuracy of 10% or better [189]. Calculated line positions had on average a residual error of $\Delta_{\text{obs}-\text{calc}} = -1.35\,\text{cm}^{-1}$ and this has been corrected for in Fig. 4.6. Similarly, computed intensities of the ν_4 band shown in Fig. 4.7 are largely within experimental uncertainty. Here, line positions possessed a residual error of $\Delta_{\text{obs}-\text{calc}} = -1.42\,\text{cm}^{-1}$.

Line intensities of the $3\nu_6$ band are shown in Fig. 4.8. Excited modes are harder to converge and the size of the vibrational basis set at $P_{\text{max}} = 10$ means the respective rovibrational energy levels have a convergence error of $1.0\,\text{cm}^{-1}$ for low J values (compared to errors of ≈ 0.1, 0.5 and $0.03\,\text{cm}^{-1}$ for the ν_1, ν_4 and ν_5 bands, respectively). The effect is that computed line intensities will have an uncertainty of around 5%. Even so, the agreement for the 16 lines from Bray et al. [99] is good. Note that line positions displayed a residual error of $\Delta_{\text{obs}-\text{calc}} = -1.23\,\text{cm}^{-1}$.

A high-resolution study of the ν_5 band measured absolute line intensities with an

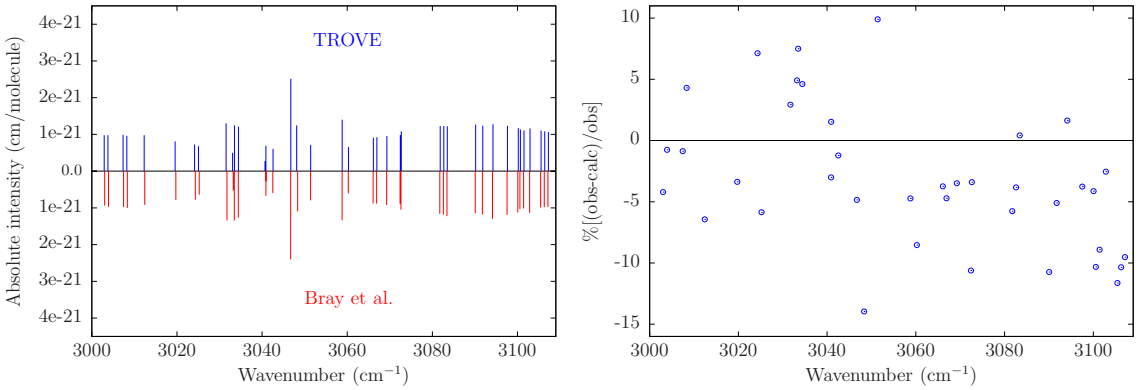

Figure 4.7: Absolute line intensities of the ν_4 band for transitions up to $J = 15$ (left) and the corresponding residuals $\left(\% \left[\frac{\text{obs}-\text{calc}}{\text{obs}}\right]\right)$ (right) when compared with measurements from Bray et al. [99]. Transitions for both $CH_3{}^{35}Cl$ and $CH_3{}^{37}Cl$ are shown and the intensities have not been scaled to natural abundance. For illustrative purposes TROVE line positions have been shifted by $-1.42\,\text{cm}^{-1}$.

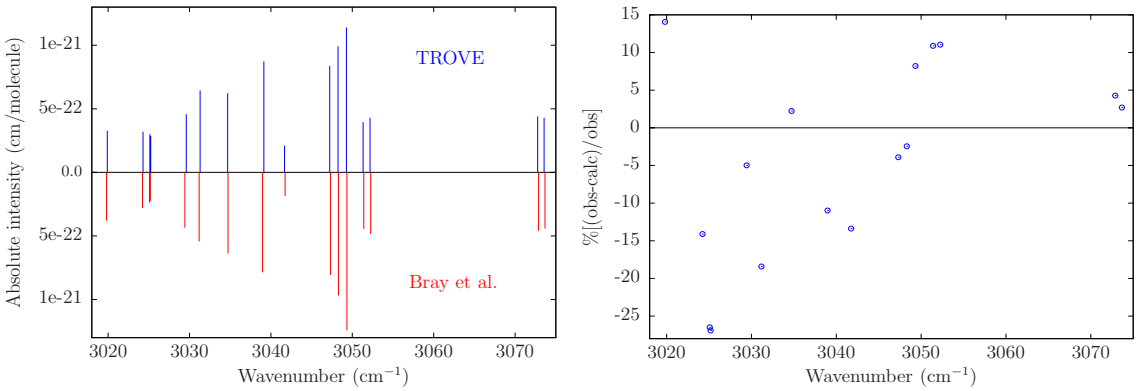

Figure 4.8: Absolute line intensities of the $3\nu_6$ band for transitions up to $J = 15$ (left) and the corresponding residuals $\left(\% \left[\frac{\text{obs}-\text{calc}}{\text{obs}}\right]\right)$ (right) when compared with measurements from Bray et al. [99]. Transitions for both $CH_3{}^{35}Cl$ and $CH_3{}^{37}Cl$ are shown and the intensities have not been scaled to natural abundance. For illustrative purposes TROVE line positions have been shifted by $-1.23\,\text{cm}^{-1}$.

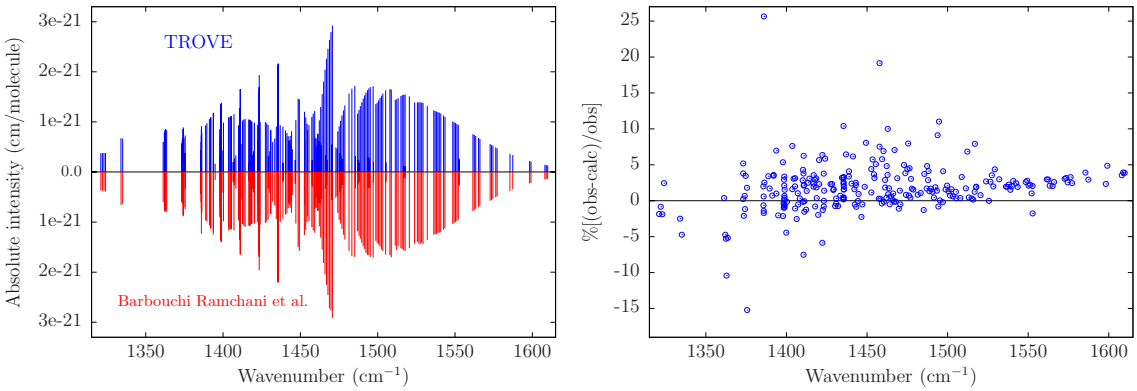

Figure 4.9: Absolute line intensities of the ν_5 band for transitions up to $J = 15$ (left) and the corresponding residuals $\left(\% \left[\frac{\text{obs}-\text{calc}}{\text{obs}}\right]\right)$ (right) when compared with measurements from Barbouchi Ramchani et al. [100]. Transitions for both $CH_3{}^{35}Cl$ and $CH_3{}^{37}Cl$ are shown and the intensities have not been scaled to natural abundance. For illustrative purposes TROVE line positions have been shifted by $-0.40\,\text{cm}^{-1}$.

experimental accuracy of 5% or less, and line positions with an average estimated accuracy between 10^{-3} to $10^{-4}\,\text{cm}^{-1}$. As shown in Fig. 4.9 a significant number of computed line intensities are within experimental uncertainty and agreement for the 256 transitions up to $J = 15$ is excellent. Here calculated line positions had a residual error of $\Delta_{\text{obs}-\text{calc}} = -0.40\,\text{cm}^{-1}$.

4.5.5 Overview of rotation-vibration line list

The HITRAN database contains over 212 000 lines for CH_3Cl and considers transitions up to $J = 82$. To compute such highly excited rovibrational energy levels it has been necessary to again reduce the size of the vibrational basis set. Calculations were carried out with $P_{\text{max}} = 8$ and an upper energy level cut-off of $8000\,\text{cm}^{-1}$. Subsequent transitions and intensities were computed for a $6300\,\text{cm}^{-1}$ frequency window with a lower state energy threshold of $4400\,\text{cm}^{-1}$. Information has undoubtedly been lost by introducing these thresholds but the values were carefully chosen to keep this to a minimum. Such restrictions also allow the straightforward calculation of high J values in a timely manner on compute nodes with 64 GB of RAM. Note that for pure rotational transitions in HITRAN the hyperfine structure has been resolved [190].

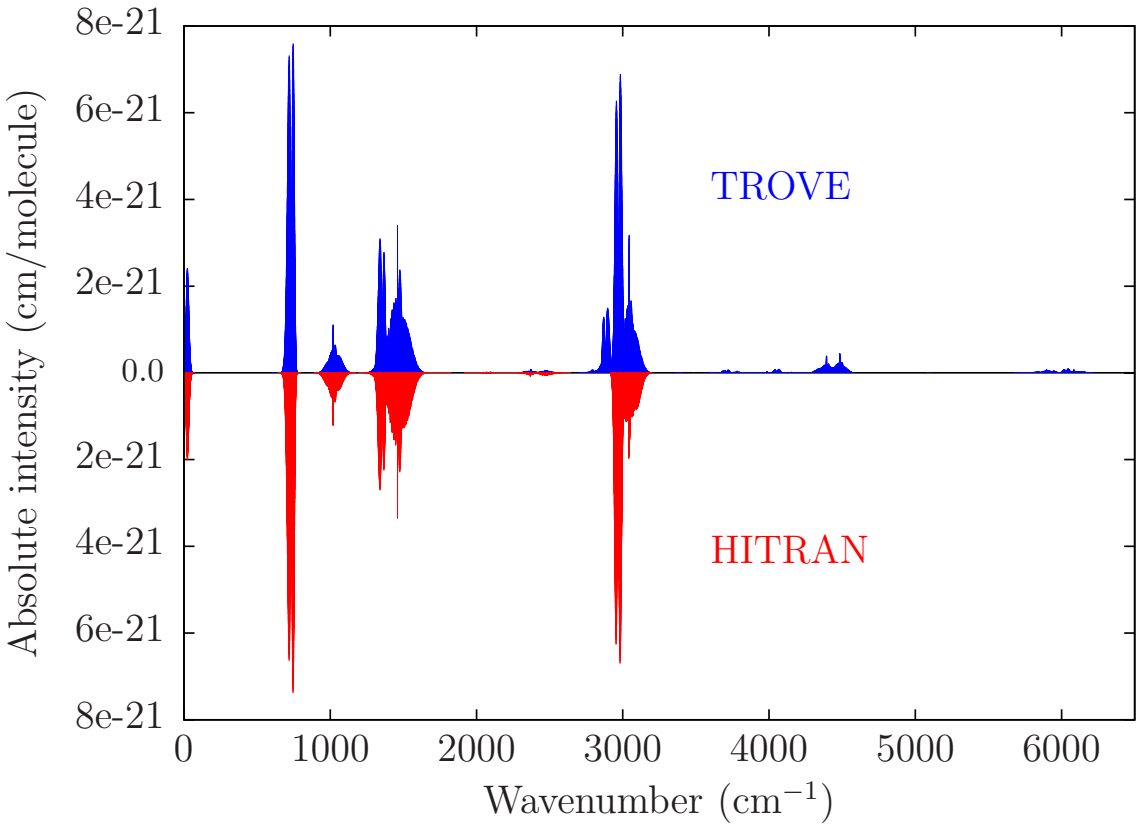

Figure 4.10: Overview of methyl chloride rotation-vibration line list up to $J = 85$ compared with all transitions in the HITRAN database [89]. Computed intensities have been scaled to natural abundance.

Therefore, in order to have a reliable comparison for this spectral region I scaled the computed intensities by a factor of 1/2.

In Fig. 4.10, a computed line list up to $J = 85$ for both isotopologues of methyl chloride is presented. Computed intensities have been scaled to natural abundance (0.748937 for $CH_3{}^{35}Cl$ and 0.239491 for $CH_3{}^{37}Cl$) and are compared against all available lines in the HITRAN database. Overall the agreement is pleasing, particularly given the reduced size of the vibrational basis set and energy level thresholds. Up to 3200 cm^{-1} the only noticeable missing band in HITRAN appears to be the $2\nu_5$ band around 2880 cm^{-1} shown in Fig. 4.11. This is not expected to be important for atmospheric sensing.

An improved spectroscopic line list in the range 1900–2600 cm^{-1} was recently published [124] and considered transitions up to $J = 47$ with absolute line intensities

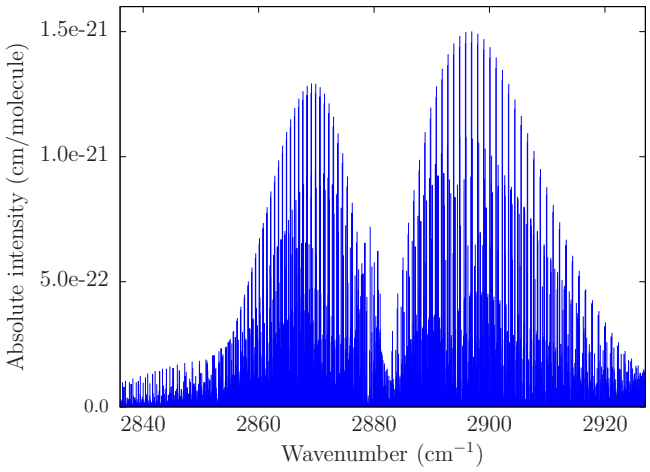

Figure 4.11: The $2\nu_5$ band of methyl chloride. Computed intensities have been scaled to natural abundance.

possessing an estimated uncertainty of 20% or less. In Fig. 4.12 a comparison of this region, which is composed of several weak bands, is shown for $CH_3{}^{35}Cl$. The DMS appears reasonable for much weaker intensities and the overall band structure in this region is well reproduced. There are some irregularities between TROVE and Nikitin et al. [124]; I expect that these are caused by the low-level nature of the TROVE calculations and also the assignment procedure in TROVE. In future work we intend to carry out a more comprehensive analysis of this region. Note that the computed TROVE line list has not been truncated at $J = 47$ for this comparison.

Whilst spectral features above $3200\,\mathrm{cm}^{-1}$ are not as prominent, there are noticeable bands between 4300–$4550\,\mathrm{cm}^{-1}$ and 5700–$6200\,\mathrm{cm}^{-1}$ as shown in Fig. 4.13. Here I have compared against the PNNL spectral library [95] (overview of entire spectrum presented in Fig. 4.14). Cross sections have been generated at a resolution of $0.06\,\mathrm{cm}^{-1}$ and fitted using a Gaussian profile with a half width at half maximum of $0.112\,\mathrm{cm}^{-1}$. This line shape provides a straightforward and reasonable comparison [191], however, I expect a Voigt profile dependent on instrumental factors would be more suitable.

Looking at Fig. 4.13 it is clear that TROVE calculations are becoming worse at higher energies and producing spurious intensities. This is to be expected given the size of the vibrational basis set and thresholds imposed in the variational cal-

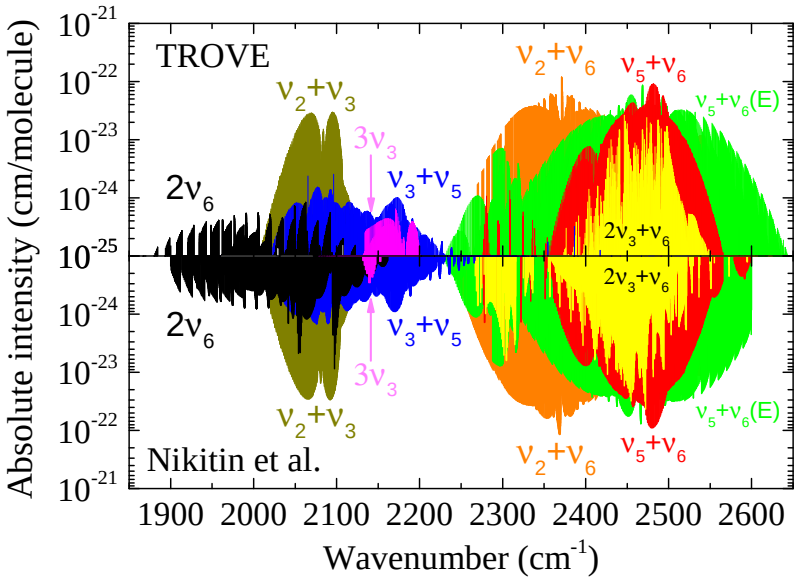

Figure 4.12: Absolute line intensities of $CH_3{}^{35}Cl$ in the range 1900–2600 cm^{-1} compared with measurements from Nikitin et al. [124]. Computed TROVE transitions are up to $J = 85$ whilst the results from Nikitin et al. [124] are up to $J = 47$. Note that a logarithmic scale has been used for the y-axis.

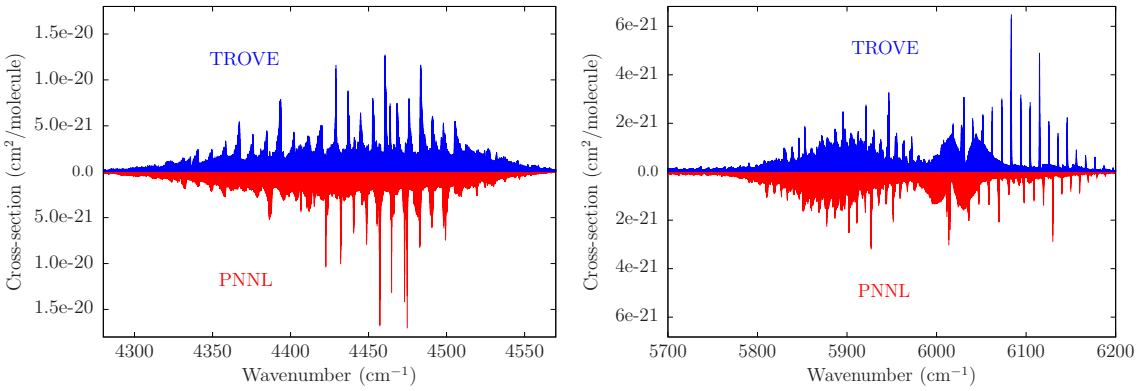

Figure 4.13: Overview of simulated rotation-vibration spectrum compared with the PNNL spectral library [95] in the 4300–4550 cm^{-1} (left) and 5700–6200 cm^{-1} (right) regions. Computed intensities have been scaled to natural abundance.

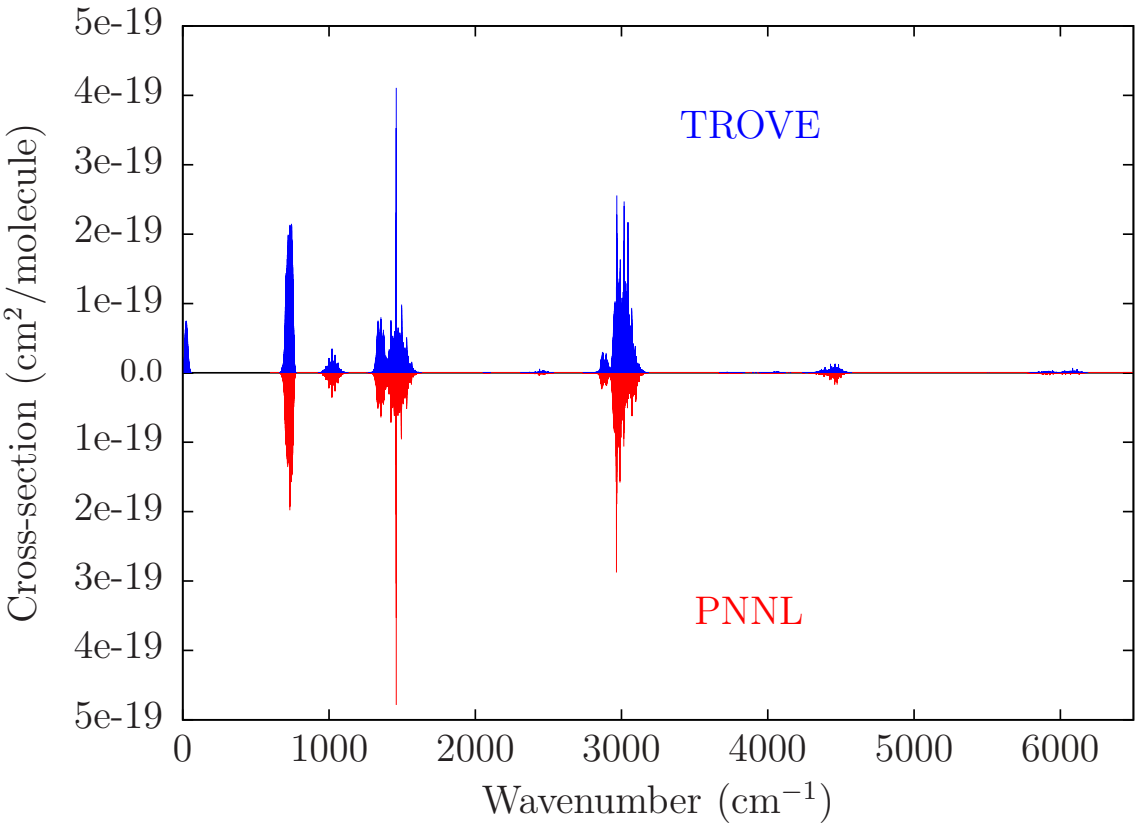

Figure 4.14: Overview of methyl chloride rotation-vibration spectrum up to $J = 85$ compared with the PNNL spectral library [95]. Computed intensities have been scaled to natural abundance.

culations. For the complete spectrum in Fig. 4.14 the agreement with PNNL is encouraging but does indicate the need for improved computations which will be discussed further in Sec. 4.6.

4.6 Chapter summary and further work

The first system we have considered in this thesis was CH_3Cl. In doing so we have seen how the methods discussed in Chapters 2 and 3 are employed in practical calculations. Methyl chloride is near the threshold of what is possible variationally and studying this five-atom molecule should highlight the challenges involved with simulating rovibrational spectra to a high degree of accuracy. Namely, the huge matrices that must be diagonalized and the sheer number of transitions that have to be considered.

Using state-of-the-art *ab initio* theory, two new nine-dimensional PESs were generated for the two main isotopologues of CH_3Cl. An analysis of the combined effect of the HL corrections and CBS extrapolation on the vibrational wavenumbers indicated that their inclusion can vastly improve computed term values. The same applies to the determination of equilibrium structural parameters. I believe that the accuracy achieved by these PESs is at the limit of what is currently possible using solely *ab initio* methods, and that it would be extremely challenging to go beyond this without empirical refinement of the respective PESs.

A new nine-dimensional DMS was computed and fitted with a symmetry-adapted analytic representation. Variational calculations of the infrared spectrum showed good agreement with a range of experimental results. Notably, computed absolute line intensities were comparable with highly accurate experimental measurements for certain fundamental bands. Considering the quality of the DMS and intensity simulations, further improvements could come from using a larger (augmented) basis set for the electronic structure calculations. However, this would be very computationally demanding and the change in predicted intensities may not necessarily reflect the computational effort.

There is still further work to be carried out regarding methyl chloride. For the requirements of high-resolution spectroscopy, the *ab initio* PESs presented here need to be refined to experiment. The resulting "spectroscopic PESs" can then be used to achieve unprecedented accuracy in the simulation of rovibrational spectra, and it is at this stage that the predictive power of the variational approach is fully realised. Empirical refinement of the PES should also produce more reliable intensities as a result of better rovibrational energy levels and associated wavefunctions.

Refinement of the CBS-35$^{\mathrm{HL}}$ PES is currently in progress. Experimental data from HITRAN [89] and Refs. [99, 122, 123, 141, 143] have been analysed to produce a set of 53 vibrational and 687 rovibrational energies up to $J = 5$. Preliminary fittings to the experimental values have yielded residual errors $\Delta_{\mathrm{obs-calc}}$ of the order $10^{-2}\,\mathrm{cm}^{-1}$ for the fundamentals. This accuracy continues for the majority of rovi-

brational energies and was obtained by adjusting only 33 expansion parameters of the CBS-35$^{\mathrm{HL}}$ PES. In carrying out initial fittings, it has become apparent that the $2\nu_5(E)$, $2\nu_3+\nu_5(E)$, $\nu_4(E)$, $3\nu_6(A_1)$ and $3\nu_6(E)$ $J=0$ "energy levels" from Bray et al. [99] cannot be reproduced with sub-wavenumber accuracy (the residual for the $2\nu_3+\nu_5(E)$ level is as large as $4\,\mathrm{cm}^{-1}$). This is despite numerous attempts to vary more expansion parameters of the CBS-35$^{\mathrm{HL}}$ PES in the fitting, or to increase the weights of the respective energy levels in the fit.

For the $\nu_4(E)$ and $3\nu_6(E)$ levels, Bray et al. [99] report band centre values at 3037.1416 and $3045.0164\,\mathrm{cm}^{-1}$, respectively. If these are substituted into the refinement, the CBS-35$^{\mathrm{HL}}$ PES is able to reproduce them with an accuracy of the order $10^{-2}\,\mathrm{cm}^{-1}$. The band centre values also agree with energy levels derived from HITRAN, which are directly involved in transitions. No such data is available for the $2\nu_5(E)$, $2\nu_3+\nu_5(E)$ and $3\nu_6(A_1)$ states and we must therefore treat these levels with extreme caution.

The other main isotopologue, $CH_3{}^{37}Cl$, will also need to be considered for any practical line list. The question here is whether or not to separately refine the CBS-37$^{\mathrm{HL}}$ PES, which is a computationally intensive task. An alternative strategy would be to use the refined CBS-35$^{\mathrm{HL}}$ PES. Strictly speaking this is incorrect, particularly because of the inclusion of the DBOC, however, calculations of $CH_3{}^{37}Cl$ term values using the *ab initio* CBS-35$^{\mathrm{HL}}$ PES showed only minor differences to the CBS-37$^{\mathrm{HL}}$ PES results. Further tests will have to be performed once the refinement for $CH_3{}^{35}Cl$ is complete.

Ultimately, I am planning to construct a comprehensive, hot line list for the ExoMol database [7, 8]. This will require improvements in the variational nuclear motion calculations, particularly regarding the size of the vibrational basis set which largely dictates the accuracy of rovibrational calculations. Work is underway to produce a compact, yet accurate, basis set to work with. This will be important as measurements of absolute line intensities of the order 10^{-26}–10^{-27} cm/molecule have been reported as high as the 11 590–11 760 cm^{-1} spectral region [127]. Presently we

are unable to accurately model such high frequencies and this is a major challenge for variational calculations on small polyatomic molecules.

5 Silane (SiH_4)

5.1 Introduction

The infrared (IR) absorption spectrum of silane (SiH_4) was first documented over eighty years ago [192, 193]. Since then numerous high-resolution spectroscopic studies of SiH_4 and its isotopomers have followed, including astronomical observation of rotation-vibration transitions around the carbon star IRC +10216 [194–196], and in the atmospheres of Jupiter [197] and Saturn [198]. Although unlikely, SiH_4 has already been considered in the context of biosignature gases on rocky exoplanets [94]. In industry, silane gas is used extensively in the semiconductor manufacturing process and for the production of solar cells.

Despite its industrial and astrophysical importance, very few rigorous theoretical studies have been carried out. Martin et al. [199] computed an accurate quartic force field for silane based on CCSD(T) calculations using the correlation consistent quadruple zeta basis set, cc-pVQZ [30], plus an additional high-exponent d-function [200] (denoted as cc-pVQZ+1 in Ref. [199]). Minor empirical refinement of the four diagonal quadratic constants produced a force field of spectroscopic quality ($\pm 1\,\mathrm{cm}^{-1}$ when reproducing the fundamental frequencies) applicable for several isotopomers of silane.

The resultant force field was subsequently used to calculate vibrational energy levels of SiH_4, SiH_3D, $SiHD_3$, and SiH_2D_2 by means of canonical Van-Vleck perturbation theory (CVPT) [201]. When compared to results of a variational four-dimensional stretch model, full-dimensional CVPT calculations were necessary to accurately describe certain stretch levels as they incorporated the effects of Fermi resonance. The importance of treating Fermi interactions to compute vibrational energies of silane was also highlighted previously using an algebraic approach [202].

The use of stretch-only models has generally been successful in describing stretching overtones [203–206] and corresponding band intensities [204, 207–210] however. This is because of the pronounced local mode behaviour of silane, the effects of which have been documented experimentally in a series of papers by Zhu et al. [211–215]. It is only at higher energies (above $12\,000\,\mathrm{cm}^{-1}$) that the rotational structure of the $|6000\rangle$ and $|7000\rangle$ stretch eigenstates can no longer be analysed in a local mode description due to vibrational resonances [216]. For intensity calculations, even a small treatment of bending motion can improve the description of intensities compared to stretch-only models [217] (an overview of previously computed *ab initio* DMSs for silane can be found in Ref. [11]).

At present there is no coverage of SiH_4 in several of the popular spectroscopic databases [89, 97, 218, 219]. The PNNL spectral library [95] is an exception and covers the range of 600 to $6500\,\mathrm{cm}^{-1}$ at a resolution of around $0.06\,\mathrm{cm}^{-1}$ for temperatures of 5, 25, and 50 °C. The Spherical Top Data System [220] (STDS) is another valuable resource for spectral information on silane. However, a significant portion of the measured transitions and intensities are from unpublished work which makes it hard to verify the methods used and subsequently the reliability of the data.

In this chapter we construct new nine-dimensional potential energy and dipole moment surfaces for silane. This is again carried out using high-level *ab initio* theory. In Chapter 4 we saw the importance of treating HL corrections and working at the CBS limit. Here we still include the leading HL contributions and extrapolate to the CBS limit, however, a slightly different approach is employed for SiH_4 to reduce the time associated with constructing a high-accuracy *ab initio* PES. After fitting the PES and DMS with suitable analytic representations, the surfaces are rigorously tested by means of variational calculations of the infrared spectrum. From a practical perspective, XY_4-type molecules have already been implemented in TROVE, notably for the construction of the 10to10 methane line list [5, 68, 221]. Simulating the spectrum of SiH_4 should therefore be a smoother process than it was for CH_3Cl.

The chapter is structured as follows: In Sec. 5.2 the *ab initio* calculations and

analytic representation of the PES are presented. Similarly, in Sec. 5.3 the electronic structure calculations and analytic representation of the DMS are detailed. Pure rotational energies, the equilibrium Si–H bond length, vibrational $J = 0$ energy levels, absolute line intensities of the ν_3 band, and an overview of the rovibrational spectrum up to $J = 20$ are calculated and compared against available experimental data in Sec. 5.4. We offer concluding remarks and discuss further work in Sec. 5.5.

5.2 Potential energy surface

5.2.1 Electronic structure calculations

Focal-point analysis [150] is used to represent the total electronic energy as

$$E_{\text{tot}} = E_{\text{CBS}} + \Delta E_{\text{SR}} + \Delta E_{\text{CV}} + \Delta E_{\text{HO}}. \tag{5.1}$$

The energy at the CBS limit E_{CBS} was computed using the explicitly correlated F12 coupled cluster method CCSD(T)-F12b [25] with the F12-optimized correlation consistent polarized valence basis sets, cc-pVTZ-F12 and cc-pVQZ-F12 [36]. Calculations were carried out in the frozen core approximation and used the diagonal fixed amplitude ansatz 3C(FIX) [18] with a Slater geminal exponent value of $\beta = 1.0\, a_0^{-1}$ [46]. For the RI basis and the two DF basis sets, I employed the corresponding OptRI [40], cc-pV5Z/JKFIT [41], and aug-cc-pwCV5Z/MP2FIT [42] ABS, respectively. All calculations were carried out with MOLPRO2012 [151] unless stated otherwise.

The two-point formula, Eq. (4.2), was used to extrapolate to the CBS limit. For the coefficients F_{n+1}^{C} I employed values of $F^{\text{CCSD-F12b}} = 1.363388$ and $F^{(\text{T})} = 1.769474$ as recommended in Hill et al. [46]. The HF energy was not extrapolated. Instead the HF+CABS singles correction [25] calculated in the larger basis set was used.

The SR correction ΔE_{SR} was computed using the second-order Douglas-Kroll-

Hess approach [54, 55] at the CCSD(T)/cc-pVQZ-DK [222] level of theory in the frozen core approximation. The spin-orbit interaction was not considered as for light, closed-shell molecules it can be safely ignored in spectroscopic calculations [56].

The CV electron correlation correction ΔE_{CV} was calculated at the CCSD(T)-F12b level of theory in conjunction with the F12-optimized correlation consistent core-valence basis set cc-pCVTZ-F12 [37]. The same ansatz and ABS as in the frozen core approximation computations were used, however I set $\beta = 1.4\, a_0^{-1}$. The $(1s)$ orbital of Si was frozen for all-electron calculations.

To estimate the HO correction ΔE_{HO} I used the hierarchy of coupled cluster methods such that $\Delta E_{\mathrm{HO}} = \Delta E_{\mathrm{T}} + \Delta E_{(\mathrm{Q})}$. Here the full triples contribution is $\Delta E_{\mathrm{T}} = \left[E_{\mathrm{CCSDT}} - E_{\mathrm{CCSD(T)}}\right]$, and the perturbative quadruples contribution is $\Delta E_{(\mathrm{Q})} = \left[E_{\mathrm{CCSDT(Q)}} - E_{\mathrm{CCSDT}}\right]$. Calculations were carried out in the frozen core approximation at the CCSD(T), CCSDT, and CCSDT(Q) levels of theory using the general coupled cluster approach [152, 153] as implemented in the MRCC code [154] interfaced to CFOUR [155]. The full triples computation utilized the correlation consistent triple zeta basis set, cc-pVTZ(+d for Si) [30–32, 34], whilst the perturbative quadruples computation employed the double zeta basis set, cc-pVDZ(+d for Si).

The contribution from the DBOC was computed with all electrons correlated (bar the $(1s)$ orbital of Si) using the CCSD method [158] as implemented in CFOUR with the aug-cc-pCVDZ basis set. A preliminary analysis of the DBOC on the vibrational energy levels showed no improvement overall when compared against experimental values. Given that inclusion of the DBOC means the PES becomes applicable only for $^{28}SiH_4$ and no other isotopologues, the correction was not included.

In generating a high-level *ab initio* PES for silane I have opted for a more pragmatic approach. Obtaining tightly converged energies with respect to basis set size for the HL corrections is less important, particularly for the CV and HO contributions which are computationally more demanding. Since the CV and HO corrections usually enter the electronic energy with opposing sign, I have calculated them to-

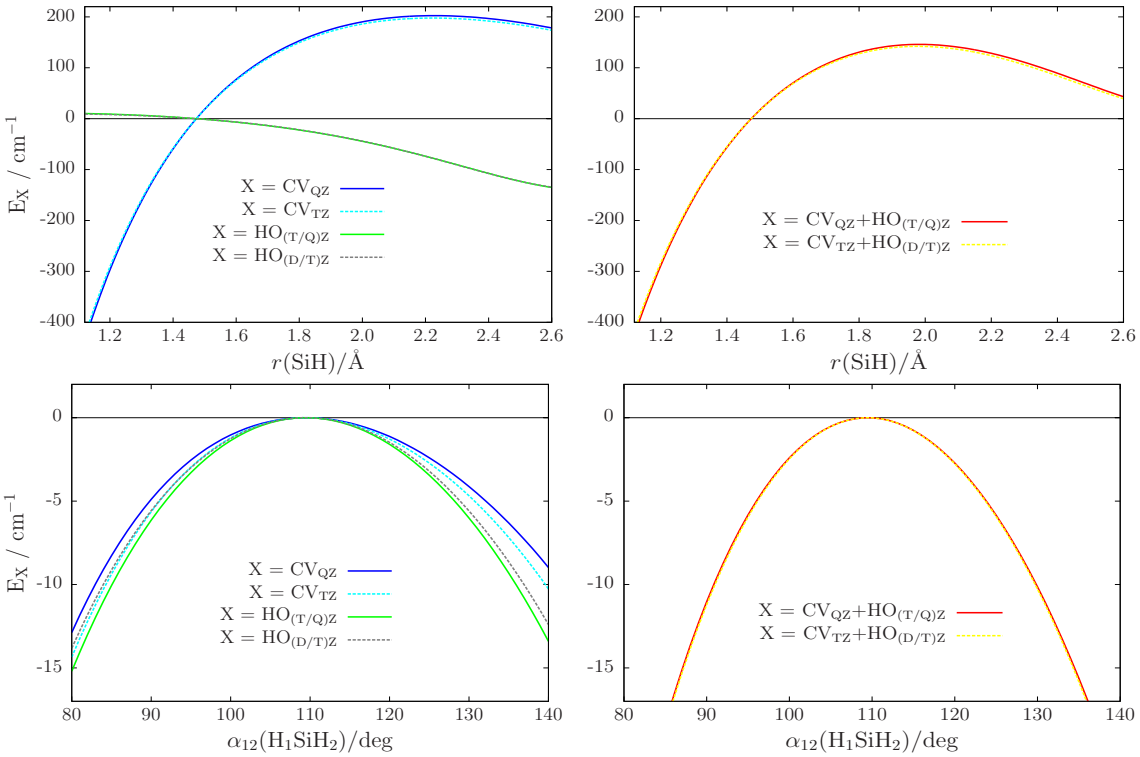

Figure 5.1: One-dimensional cuts of the CV, HO, and CV+HO corrections for different sizes of basis set. For CV the subscript TZ(QZ) refers to calculations with the cc-pCVTZ-F12(cc-pCVQZ-F12) basis set. For HO the subscript (D/T)Z refers to calculations with the cc-pVDZ and cc-pVTZ basis sets for the perturbative quadruples and full triples, respectively. Likewise the (T/Q)Z subscript corresponds to the cc-pVTZ and cc-pVQZ basis sets.

gether utilizing smaller basis sets. Although independently the separate corrections are not fully converged, this error is compensated for when considering their sum. This is illustrated through one-dimensional cuts of the PES in Fig. 5.1, most noticeably in the bending cut.

The global grid was built in terms of nine internal coordinates; four Si–H bond lengths r_1, r_2, r_3, r_4, and five $\angle$(H$_j$–Si–H$_k$) interbond angles α_{12}, α_{13}, α_{14}, α_{23}, and α_{24}, where j and k label the respective hydrogen atoms. The Si–H stretch distances ranged from $0.98 \leq r_i \leq 2.95\,\text{Å}$ for $i = 1, 2, 3, 4$ whilst bending angles varied from $40 \leq \alpha_{jk} \leq 140°$ where $jk = 12, 13, 14, 23, 24$. All terms in Eq. (5.1) were calculated on a grid of 84 002 geometries with energies up to $hc \cdot 50\,000\,\text{cm}^{-1}$ (h is the Planck

constant and c is the speed of light). At every grid point the coupled cluster energy was extrapolated to the CBS limit, and each HL correction was calculated and added to the total electronic energy.

The HL corrections have been computed at each grid point which is in fact time-effective at the levels of theory chosen for the electronic structure calculations. The alternative is to design reduced grids for each correction, fit a corresponding analytic representation and apply the resulting form to the global grid of geometries by interpolation as was done for CH_3Cl (see also Ref. [60] for an example of this strategy). Although this alternative is computationally less intensive, achieving a satisfactory description of each HL correction requires careful consideration and may not be trivial; any such problems are avoided in our present approach.

5.2.2 Analytic representation

The analytic representation chosen for the present study has previously been used for methane [5, 68, 221]. For the stretch coordinates,

$$\xi_i = 1 - \exp\left(-a(r_i - r^{\text{ref}})\right) \; ; \;\; i = 1, 2, 3, 4, \tag{5.2}$$

where $a = 1.47\,\text{Å}^{-1}$ and the reference equilibrium structural parameter $r^{\text{ref}} = 1.4741\,\text{Å}$ (value discussed in Sec. 5.4.1). The angular terms are given as symmetrized combinations of interbond angles,

$$\xi_5 = \frac{1}{\sqrt{12}}\left(2\alpha_{12} - \alpha_{13} - \alpha_{14} - \alpha_{23} - \alpha_{24} + 2\alpha_{34}\right), \tag{5.3}$$

$$\xi_6 = \frac{1}{2}\left(\alpha_{13} - \alpha_{14} - \alpha_{23} + \alpha_{24}\right), \tag{5.4}$$

$$\xi_7 = \frac{1}{\sqrt{2}}\left(\alpha_{24} - \alpha_{13}\right), \tag{5.5}$$

$$\xi_8 = \frac{1}{\sqrt{2}}\left(\alpha_{23} - \alpha_{14}\right), \tag{5.6}$$

$$\xi_9 = \frac{1}{\sqrt{2}}\left(\alpha_{34} - \alpha_{12}\right). \tag{5.7}$$

The potential function (maximum expansion order of $i+j+k+l+m+n+p+q+r = 6$),

$$V(\xi_1, \xi_2, \xi_3, \xi_4, \xi_5, \xi_6, \xi_7, \xi_8, \xi_9) = \sum_{ijk\ldots} \mathrm{f}_{ijk\ldots} V_{ijk\ldots}, \tag{5.8}$$

contains the terms

$$V_{ijk\ldots} = \{\xi_1^i \xi_2^j \xi_3^k \xi_4^l \xi_5^m \xi_6^n \xi_7^p \xi_8^q \xi_9^r\}^{\boldsymbol{T}_\mathrm{d}(\mathrm{M})}, \tag{5.9}$$

which are symmetrized combinations of different permutations of the coordinates ξ_i, and transform according to the A_1 representation of the $\boldsymbol{T}_\mathrm{d}(\mathrm{M})$ molecular symmetry group [82]. They are found by solving an over-determined system of linear equations in terms of the nine coordinates given above. A total of 287 symmetrically unique terms were derived up to sixth order of which only 104 were employed for the final PES. The corresponding expansion parameters $\mathrm{f}_{ijk\ldots}$ were determined from a least-squares fitting to the *ab initio* data. The same Partridge and Schwenke [160] weighting function, Eq. (4.12), was employed with $\tilde{E}_i^{(w)} = \max(\tilde{E}_i, 10\,000)$ and $N = 0.0001$ (all values in cm^{-1}). The final fitted PES required 106 expansion parameters ($104 + r_\mathrm{ref} + a$) and employed Watson's robust fitting scheme [162], which reduces the weights of outliers and improves the fit at lower energies. A weighted root-mean-square (rms) error of $1.77\,\mathrm{cm}^{-1}$ was obtained for energies up to $hc \cdot 50\,000\,\mathrm{cm}^{-1}$.

Note that geometries with $r_i \geq 2.30\,\text{Å}$ for $i = 1, 2, 3, 4$ possessed a T1 diagnostic value > 0.02 [161], and so the corresponding weights were reduced by several orders of magnitude. Although the coupled cluster method is not completely accurate at these points, by including them the PES maintains a reasonable shape towards dissociation. In subsequent calculations we refer to this PES as CBS-F12$^{\mathrm{HL}}$. The CBS-F12$^{\mathrm{HL}}$ expansion parameter set is provided in the supplementary material of Ref. [223] along with a FORTRAN routine to construct the PES.

5.3 Dipole moment surface

5.3.1 Electronic structure calculations

For each of the X, Y, and Z Cartesian coordinate axes with origin at the Si nucleus, an external electric field with components ± 0.005 a.u. was applied and the dipole moment components μ_X, μ_Y, and μ_Z computed by means of the central finite difference scheme. Calculations were carried out at the CCSD(T)/aug-cc-pVTZ(+d for Si) level of theory in the frozen core approximation using MOLPRO2012. The same nine-dimensional grid as used for the PES with energies up to $hc \cdot 50\,000\,\mathrm{cm}^{-1}$ was employed.

5.3.2 Analytic representation

To represent the DMS analytically it is necessary to transform to a suitable molecule-fixed xyz coordinate system. For the present study we utilize the symmetrized molecular bond (SMB) representation for XY_4 molecules [68]. We first define unit vectors along the four Si–H bonds,

$$\mathbf{e}_i = \frac{\mathbf{r}_i - \mathbf{r}_0}{|\mathbf{r}_i - \mathbf{r}_0|}\,; \quad i = 1, 2, 3, 4, \tag{5.10}$$

where $\mathbf{r}_0$ is the position vector of the Si nucleus, and $\mathbf{r}_i$ is that of the respective H_i atom. Three symmetrically independent reference vectors which span the F_2 representation are formed,

$$\mathbf{n}_1 = \frac{1}{2}\left(\mathbf{e}_1 - \mathbf{e}_2 + \mathbf{e}_3 - \mathbf{e}_4\right), \tag{5.11}$$

$$\mathbf{n}_2 = \frac{1}{2}\left(\mathbf{e}_1 - \mathbf{e}_2 - \mathbf{e}_3 + \mathbf{e}_4\right), \tag{5.12}$$

$$\mathbf{n}_3 = \frac{1}{2}\left(\mathbf{e}_1 + \mathbf{e}_2 - \mathbf{e}_3 - \mathbf{e}_4\right). \tag{5.13}$$

Using these the *ab initio* dipole moment vector $\boldsymbol{\mu}$ can be expressed as

$$\boldsymbol{\mu} = \mu_x \mathbf{n}_1 + \mu_y \mathbf{n}_2 + \mu_z \mathbf{n}_3. \tag{5.14}$$

Here μ_α ($\alpha = x, y, z$) are the dipole moment functions (also of F_2 symmetry) which take the form

$$\mu_\alpha(\xi_1, \xi_2, \xi_3, \xi_4, \xi_5, \xi_6, \xi_7, \xi_8, \xi_9) = \sum_{ijk\ldots} F^{(\alpha)}_{ijk\ldots} \mu^{F_2}_{\alpha,ijk\ldots}. \tag{5.15}$$

The expansion terms

$$\mu^{F_2}_{\alpha,ijk\ldots} = \{\xi_1^i \xi_2^j \xi_3^k \xi_4^l \xi_5^m \xi_6^n \xi_7^p \xi_8^q \xi_9^r\}^{F_{2\alpha}}, \tag{5.16}$$

are symmetrized combinations of different permutations of coordinates ξ_i, and span the $F_{2\alpha}$ representation of the $\boldsymbol{T}_\mathrm{d}$(M) molecular symmetry group (see Ref. [68] for more detail). A sixth order expansion was employed in terms of the coordinates,

$$\xi_i = (r_i - r^\mathrm{ref}) \exp\left(-\beta(r_i - r^\mathrm{ref})^2\right) \; ; \;\; i = 1, 2, 3, 4, \tag{5.17}$$

for the stretches, with the same angular coordinates as before (Eqs. (5.3) to (5.7)). The factor $\exp\left(-\beta(r_i - r^\mathrm{ref})^2\right)$ prevents the expansion from diverging at large values of r_i. The DMS fitting employed the parameters $r^\mathrm{ref} = 1.5355\,\text{Å}$ and $\beta = 1.0\,\text{Å}^{-2}$.

The expansion coefficients $F^{(\alpha)}_{ijk\ldots}$ for all three components $\alpha = x, y, z$ were determined simultaneously through a least squares fitting to the *ab initio* data. Again weight factors of the form given in Eq. (4.12) were used which favor energies below $hc \cdot 15\,000\,\mathrm{cm}^{-1}$. The fitting required 283 parameters and reproduced the *ab initio* data with a weighted rms error of 0.001 D for energies up to $hc \cdot 50\,000\,\mathrm{cm}^{-1}$. The expansion parameter set for the DMS is provided in the supplementary material of Ref. [223] along with a FORTRAN routine to construct the corresponding analytic representation.

5.4 Results

5.4.1 Equilibrium bond length and pure rotational energies

Since rotational energies depend on the molecular geometry through the moments of inertia, I first refine the Si–H reference equilibrium structural parameter r^{ref} before proceeding to extensive rovibrational energy level calculations. Thereby, the accuracy of the computed intra-band rotational wavenumbers can be significantly improved [61, 224].

Two iterations of a nonlinear least-squares fit to the experimental $J \leq 6$ rotational energies from the STDS [220] produced a refined parameter of $r^{\text{ref}} = 1.4741\,\text{Å}$. However, due to the inclusion of a linear expansion term in the parameter set of the potential, this value does not define the minimum of the PES. The true equilibrium bond length was determined to be $r^{\text{eq}} = 1.4737\,\text{Å}$. This is in good agreement with the experimental estimate of $r(\text{Si–H}) = 1.4741\,\text{Å}$ [225], and an *ab initio* value of $r(\text{Si–H}) = 1.4742\,\text{Å}$ calculated at the all electron CCSD(T)/cc-pCVQZ level of theory [172]. Note that before the refinement the original *ab initio* bond length of the CBS-F12$^{\text{HL}}$ PES was $r^{\text{eq}}_{ab\ initio} = 1.4735\,\text{Å}$.

The computed pure rotational energies are listed in Table 5.1. The details of the calculations will be discussed in Sec. 5.4.2. As can be seen, the agreement with experiment is excellent and energy levels up to $J \leq 6$ are reproduced with a rms error of $0.00005\,\text{cm}^{-1}$. I therefore expect the true Si–H equilibrium bond length to be very close to the value $r^{\text{eq}} = 1.4737\,\text{Å}$.

5.4.2 Vibrational $J = 0$ energies

In variational calculations the rovibrational Hamiltonian was represented as a power series expansion around the equilibrium geometry in terms of the coordinates given in Eqs. (5.2) to (5.7). However, for the kinetic energy operator linear displacement variables $(r_i - r^{\text{ref}})$ were used for the stretching coordinates. The Hamiltonian

Table 5.1: Comparison of calculated and experimental $J \leq 6$ pure rotational term values (in cm^{-1}) for $^{28}SiH_4$. The observed ground state energy levels are from Ref. [220].

J	K	Sym.	Experiment	Calculated	Obs−calc
0	0	A_1	0.00000	0.00000	0.00000
1	1	F_1	5.71801	5.71800	0.00001
2	2	E	17.15306	17.15302	0.00004
2	1	F_2	17.15321	17.15317	0.00004
3	2	A_2	34.30453	34.30448	0.00005
3	3	F_1	34.30319	34.30313	0.00006
3	1	F_2	34.30379	34.30373	0.00006
4	0	A_1	57.16474	57.16467	0.00007
4	2	E	57.16653	57.16647	0.00006
4	1	F_1	57.16578	57.16572	0.00006
4	3	F_2	57.16877	57.16872	0.00005
5	2	E	85.74233	85.74231	0.00002
5	1	F_1	85.73510	85.73504	0.00006
5	3	F_1	85.74330	85.74328	0.00002
5	5	F_2	85.73711	85.73707	0.00004
6	4	A_1	120.02574	120.02581	-0.00007
6	2	A_2	120.01143	120.01144	-0.00001
6	6	E	120.00784	120.00784	0.00000
6	3	F_1	120.02350	120.02356	-0.00006
6	1	F_2	120.00873	120.00874	-0.00001
6	5	F_2	120.02097	120.02102	-0.00005

was constructed numerically using an automatic differentiation method [70], with the kinetic and potential energy operators truncated at 6th and 8th order, respectively. The vibrational basis set was generated using a multi-step contraction scheme. For SiH_4 the polyad number

$$P = 2(n_1 + n_2 + n_3 + n_4) + n_5 + n_6 + n_7 + n_8 + n_9 \leq P_{\max}, \tag{5.18}$$

and for $J = 0$ vibrational energy level calculations I set $P_{\max} = 14$. Note that atomic mass values were employed in the subsequent TROVE calculations.

The normal modes of silane are classified by the symmetry species, A_1, E, and F_2.

Of A_1 symmetry is the non-degenerate symmetric stretching mode ν_1 (2186.87 cm^{-1}). The doubly degenerate antisymmetric bending mode ν_2 (970.93 cm^{-1}) has E symmetry. Whilst of F_2 symmetry are the triply degenerate modes; the antisymmetric stretching mode ν_3 (2189.19 cm^{-1}), and the antisymmetric bending mode ν_4 (913.47 cm^{-1}). The values in parentheses are the experimentally determined values from Ref. [220]. To be of spectroscopic use we map the vibrational quantum numbers n_k of TROVE to the normal mode quantum numbers v_k commonly used. For SiH_4 the vibrational states are labelled as $\mathrm{v}_1\nu_1 + \mathrm{v}_2\nu_2 + \mathrm{v}_3\nu_3 + \mathrm{v}_4\nu_4$ where v_i counts the level of excitation.

In Table 5.2 the computed vibrational energies using the CBS-F12$^{\mathrm{HL}}$ PES are listed against all available experimental data up to 8500 cm^{-1}. The four fundamental frequencies are all reproduced with sub-wavenumber accuracy, resulting in an overall rms error of 0.63 cm^{-1} and a mean-absolute-deviation (mad) of 0.57 cm^{-1}. Altogether the 49 experimental levels are reproduced with a rms error of 1.33 cm^{-1} and mad of 1.07 cm^{-1}. Note that energies are converged to 0.01 cm^{-1} or better (the majority are converged to orders of magnitude lower), except for the two levels at 8347.86 cm^{-1} which are converged to within 0.02 cm^{-1}. This was confirmed by performing a complete vibrational basis set extrapolation with values of $P_{\max} = \{10, 12, 14\}$.

Table 5.2: Comparison of calculated and experimental $J = 0$ vibrational term values (in cm^{-1}) for $^{28}SiH_4$. The zero-point energy was computed to be 6847.084 cm^{-1}.

Mode	Sym.	Experiment	Calculated	Obs−calc	Ref.
ν_4	F_2	913.47	912.85	0.62	[220]
ν_2	E	970.93	970.14	0.79	[220]
$2\nu_4$	A_1	1811.80	1810.90	0.90	[220]
$2\nu_4$	F_2	1824.19	1823.15	1.04	[220]
$2\nu_4$	E	1827.81	1827.00	0.81	[220]
$\nu_2 + \nu_4$	F_2	1881.96	1880.87	1.09	[220]
$\nu_2 + \nu_4$	F_1	1887.10	1885.36	1.74	[220]
$2\nu_2$	A_1	1937.50	1935.84	1.66	[220]

(*Continued*)

Mode	Sym.	Experiment	Calculated	Obs−calc	Ref.
$2\nu_2$	E	1942.77	1941.29	1.48	[220]
ν_1	A_1	2186.87	2187.63	-0.76	[220]
ν_3	F_2	2189.19	2189.32	-0.13	[220]
$3\nu_4$	F_2	2713.07	2712.16	0.91	[220]
$3\nu_4$	A_1	2731.17	2729.97	1.20	[220]
$3\nu_4$	F_1	2735.42	2734.26	1.16	[220]
$3\nu_4$	F_2	2739.35	2738.48	0.87	[220]
$\nu_2 + 2\nu_4$	E	2780.47	2779.32	1.15	[220]
$\nu_2 + 2\nu_4$	F_1	2793.32	2791.84	1.48	[220]
$\nu_2 + 2\nu_4$	A_1	2795.11	2793.94	1.17	[220]
$\nu_2 + 2\nu_4$	F_2	2797.41	2795.53	1.88	[220]
$\nu_2 + 2\nu_4$	E	2800.20	2798.25	1.95	[220]
$\nu_2 + 2\nu_4$	A_2	2803.95	2801.56	2.39	[220]
$2\nu_2 + \nu_4$	F_2	2848.26	2846.60	1.66	[220]
$2\nu_2 + \nu_4$	F_1	2856.43	2854.36	2.07	[220]
$2\nu_2 + \nu_4$	F_2	2859.74	2857.18	2.56	[220]
$3\nu_2$	E	2904.99	2902.60	2.39	[220]
$3\nu_2$	A_1	2915.40	2913.34	2.06	[220]
$3\nu_2$	A_2	2915.48	2913.44	2.04	[220]
$\nu_3 + \nu_4$	F_1	3094.81	3094.35	0.46	[201] [a]
$\nu_1 + \nu_4$	F_2	3095.26	3095.10	0.16	[201] [a]
$\nu_3 + \nu_4$	E	3095.86	3095.52	0.34	[201] [a]
$\nu_3 + \nu_4$	F_2	3098.02	3097.60	0.42	[201] [a]
$\nu_3 + \nu_4$	A_1	3099.48	3098.73	0.75	[201] [a]
$\nu_2 + \nu_3$	F_2	3152.59	3152.92	-0.33	[201] [a]
$\nu_2 + \nu_3$	F_1	3153.08	3152.17	0.91	[201] [a]
$\nu_1 + \nu_2$	E	3153.60	3152.12	1.48	[201] [a]
$2\nu_3$	A_1	4308.87	4308.96	-0.09	[216] [b]
$\nu_1 + \nu_3$	F_2	4309.35	4309.89	-0.54	[214]
$2\nu_1$	A_1	4374.56	4375.92	-1.36	[205] [c]
$2\nu_3$	E	4378.40	4380.23	-1.83	[220]
$2\nu_3$	F_2	4380.28	4378.73	1.55	[205] [c]
$\nu_1 + 2\nu_3$	A_1	6362.05	6362.88	-0.83	[216] [d]

(*Continued*)

Mode	Sym.	Experiment	Calculated	Obs−calc	Ref.
$3\nu_3$	F_2	6362.05	6362.97	-0.92	[216] [d]
$3\nu_1$	A_1	6496.13	6498.19	-2.06	[205] [c]
$2\nu_1 + \nu_3$	F_2	6497.45	6498.48	-1.03	[215]
$\nu_1 + 2\nu_3$	E	6500.30	6500.58	-0.28	[205] [c]
$3\nu_3$	F_2	6500.60	6500.71	-0.11	[205] [c]
$3\nu_3$	F_1	6502.88	6502.94	-0.06	[205] [c]
$\nu_1 + 3\nu_3$	A_1	8347.86	8349.38	-1.52	[216] [d]
$\nu_1 + 3\nu_3$	F_2	8347.86	8349.39	-1.53	[216] [d]

[a] Originally attributed to Ref. [220], but unable to confirm value independently. [b] Originally attributed to Ref. [214]. [c] Originally attributed to Ref. [226]. [d] Originally attributed to Refs. [211–213].

Of the 35 term values up to 3153.60 cm^{-1}, the energy of 32 levels is underestimated by the CBS-F12$^{\mathrm{HL}}$ PES. This can be explained by the residual errors of the ν_2 and ν_4 fundamentals, which largely dictates the accuracy of the subsequent combination bands and overtones. Above 3153.60 cm^{-1} computed energy levels are consistently higher than experiment which is a result of overestimating the ν_1 and ν_3 fundamentals. Despite this, the performance of the CBS-F12$^{\mathrm{HL}}$ PES is extremely encouraging.

Experimental values for stretching overtones above 8500 cm^{-1} are available [212, 216, 227]. However, the corresponding values in TROVE are harder to identify given the increased density of states at higher energies. Highly excited modes also show slower convergence with respect to vibrational basis set size. Thus, to obtain reasonably well converged energies would require calculations with $P_{\mathrm{max}} = 16$ or greater, which is currently unachievable with the computational resources available to us.

As an aside in Table 5.3 we show the effect of the empirical refinement of the equilibrium geometry on the fundamental frequencies. Results computed using the

ab initio bond length (overall rms error of $0.57\,\mathrm{cm}^{-1}$) are marginally better which is to be expected. In the refined geometry PES the shape of the original *ab initio* PES has been altered by shifting its minimum, resulting in a poorer representation of vibrational energies. For spectral analysis an improved description of rotational structure is more desirable however, as vibrational band position can be easily corrected at a later stage [61].

Table 5.3: Comparison of the computed fundamental term values (in cm^{-1}) with the refined (ref) and *ab initio* (*ai*) equilibrium geometry.

Mode	Sym.	Experiment[a]	ref eq. (A)	*ai* eq. (B)	Obs-calc (A)	Obs-calc (B)
ν_1	A_1	2186.87	2187.63	2187.63	-0.76	-0.76
ν_2	E	970.93	970.14	970.26	0.79	0.67
ν_3	F_2	2189.19	2189.32	2189.31	-0.13	-0.12
ν_4	F_2	913.47	912.85	912.97	0.62	0.50

[a] See Table 5.2 for experimental references.

5.4.3 Vibrational transition moments

In Table 5.4, computed vibrational transition moments, Eq. (3.10), from the vibrational ground state are listed. Calculations used the CBS-F12$^{\mathrm{HL}}$ PES and a polyad number of $P_{\max} = 12$ which ensured converged results.

Experimentally determined transitions moments have only been derived for the ν_3 ($2189.19\,\mathrm{cm}^{-1}$) and ν_4 ($913.47\,\mathrm{cm}^{-1}$) modes. Fox and Person [228] using earlier band intensity measurements [229, 230] found $\mu_{\nu_3} = 0.139 \pm 4\%\,\mathrm{D}$ and $\mu_{\nu_4} = 0.232 \pm 7\%\,\mathrm{D}$. The reliability of the intensity data [229, 230] has however been questioned [231]. In other work, Cadot [232] determined a transition moment of $\mu_{\nu_3} = 0.1293 \pm 3\%\,\mathrm{D}$. Whilst a value of $\mu_{\nu_4} = 0.247\,\mathrm{D}$ was quoted in Ref. [195] but attributed to unpublished results.

Although the experimental situation is not entirely clear, the computed TROVE transition moments of $\mu_{\nu_3} = 0.2470\,\mathrm{D}$ and $\mu_{\nu_4} = 0.4149\,\mathrm{D}$ are notably larger than their experimental counterparts. We will show in Sec. 5.4.4 and Sec. 5.4.5 that the

Table 5.4: Calculated vibrational transition moments (in Debye) and frequencies (in cm^{-1}) from the vibrational ground state for $^{28}SiH_4$. Only levels of F_2 symmetry are accessible from the ground state in IR absorption.

Mode	Sym.	Experiment[a]	Calculated	μ_{if}
ν_4	F_2	913.47	912.85	0.4149E+0
$2\nu_4$	F_2	1824.19	1823.15	0.2500E-2
$\nu_2 + \nu_4$	F_2	1881.96	1880.87	0.2350E-1
ν_3	F_2	2189.19	2189.32	0.2470E+0
$3\nu_4$	F_2	2713.07	2712.16	0.4578E-2
$3\nu_4$	F_2	2739.35	2738.48	0.8123E-3
$\nu_2 + 2\nu_4$	F_2	2797.41	2795.53	0.1734E-2
$2\nu_2 + \nu_4$	F_2	2848.26	2846.60	0.1835E-2
$2\nu_2 + \nu_4$	F_2	2859.74	2857.18	0.9093E-4
$\nu_1 + \nu_4$	F_2	3095.26	3095.10	0.1320E-1
$\nu_3 + \nu_4$	F_2	3098.02	3097.60	0.1319E-1
$\nu_2 + \nu_3$	F_2	3152.59	3152.92	0.1050E-1
$4\nu_4$	F_2	-	3609.08	0.4741E-3
$4\nu_4$	F_2	-	3638.92	0.1892E-4
$\nu_2 + 3\nu_4$	F_2	-	3677.72	0.6075E-3
$\nu_2 + 3\nu_4$	F_2	-	3704.01	0.5424E-3
$\nu_2 + 3\nu_4$	F_2	-	3707.66	0.2098E-4
$2\nu_2 + 2\nu_4$	F_2	-	3758.50	0.1628E-3
$2\nu_2 + 2\nu_4$	F_2	-	3767.13	0.5799E-4
$3\nu_2 + \nu_4$	F_2	-	3810.86	0.2432E-3
$3\nu_2 + \nu_4$	F_2	-	3827.61	0.3848E-3
$\nu_1 + \nu_3$	F_2	4309.35	4309.89	0.1336E-1
$2\nu_3$	F_2	4380.28	4378.73	0.4262E-2
$3\nu_3$	F_2	6362.05	6362.97	0.5762E-3
$2\nu_1 + \nu_3$	F_2	6497.45	6498.48	0.5813E-3
$3\nu_3$	F_2	6500.60	6500.71	0.1517E-3
$\nu_1 + 3\nu_3$	F_2	8347.86	8349.39	0.1390E-2

[a] See Table 5.2 for experimental references.

DMS does marginally overestimate the strength of line intensities. The magnitude of this overestimation is not consistent with the discrepancy in the experimental and computed values for μ_{ν_3} and μ_{ν_4} however. Experimentally derived transition moments for the other levels of silane could help clarify previous results and assist future theoretical benchmarking.

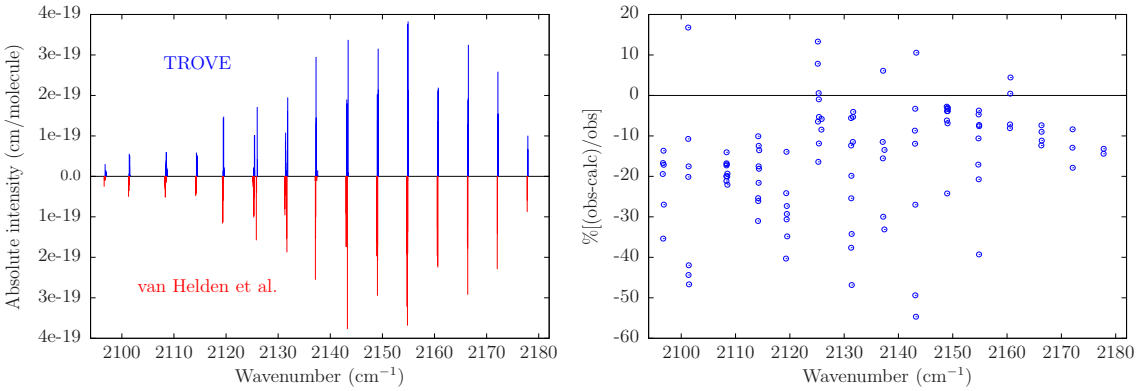

Figure 5.2: Absolute line intensities of the ν_3 band for transitions up to $J = 16$ (left) and the corresponding residuals $\left(\% \left[\frac{\text{obs}-\text{calc}}{\text{obs}}\right]\right)$ (right) when compared with measurements from van Helden et al. [237].

It is worth nothing that if we use the values from Fox and Person [228] and compare the ratio $\mu_{\nu_3}^{\text{exp}}/\mu_{\nu_4}^{\text{exp}} = 0.599$ with $\mu_{\nu_3}^{\text{TROVE}}/\mu_{\nu_4}^{\text{TROVE}} = 0.595$, there is excellent agreement which suggests the relative intensity for the two strongest bands is reasonable.

5.4.4 Absolute line intensities of the ν_3 band

Absolute absorption intensities were simulated at room temperature ($T = 296\,\text{K}$) using Eq. (3.9). For SiH_4, the nuclear spin statistical weights are $g_{\text{ns}} = \{5, 5, 2, 3, 3\}$ for states of symmetry $\{A_1, A_2, E, F_1, F_2\}$, respectively. The partition function $Q(T)$ was estimated using, $Q(T) \approx Q_{\text{rot}}(T) \times Q_{\text{vib}}(T)$. For tetrahedral molecules the rotational partition function is given as [233],

$$Q_{\text{rot}}(T) = \frac{4}{3}\pi^{1/2}\left(\frac{Bhc}{kT}\right)^{-3/2}\exp\left(\frac{Bhc}{4kT}\right), \tag{5.19}$$

where for SiH_4 I used a ground state rotational constant of $B = 2.859$, which is consistent with Refs. [234–236]. At $T = 296\,\text{K}$, $Q_{\text{rot}} = 1447.6001$, the vibrational partition function $Q_{\text{vib}} = 1.0551$ [220], resulting in $Q = 1527.3629$.

A recent high-resolution study of the ν_3 band measured the absolute line intensities of numerous P-branch transitions up to $J = 16$ at 296 K [237]. Line intensities

were recorded at a resolution of $0.0011\,\mathrm{cm}^{-1}$ and were given an estimated experimental measurement accuracy of 10%. To validate the DMS and to a lesser extent the PES, in Table 5.5 we compare frequencies and absolute line intensities of over 100 transitions from Ref. [237]. The results are also illustrated in Fig. 5.2.

Table 5.5: Comparison of calculated and observed frequencies (in cm^{-1}) and absolute line intensities (in cm/molecule) for transitions between the ν_3 and ground vibrational state. To quantify the error in the computed line intensity we use the percentage measure, %[(obs − calc)/obs].

Γ'	J'	K'	Γ''	J''	K''	ν_{obs}	ν_{calc}	$\Delta_{\mathrm{obs-calc}}$	I_{obs}	I_{calc}	$\%\left[\frac{\mathrm{obs-calc}}{\mathrm{obs}}\right]$
F_1	1	1	F_2	2	1	2177.782	2177.908	-0.126	8.784E-20	1.005E-19	-14.42
E	1	1	E	2	1	2177.793	2177.921	-0.128	5.920E-20	6.701E-20	-13.19
A_1	2	1	A_2	3	1	2172.045	2172.170	-0.125	2.290E-19	2.586E-19	-12.92
F_1	2	1	F_2	3	1	2172.072	2172.197	-0.125	1.417E-19	1.535E-19	-8.38
F_2	2	1	F_1	3	2	2172.091	2172.216	-0.125	1.315E-19	1.550E-19	-17.88
F_1	3	1	F_2	4	2	2166.306	2166.431	-0.125	1.682E-19	1.889E-19	-12.35
E	3	1	E	4	1	2166.340	2166.466	-0.126	1.212E-19	1.301E-19	-7.37
F_2	3	2	F_1	4	1	2166.357	2166.483	-0.126	1.776E-19	1.935E-19	-8.98
A_2	3	2	A_1	4	0	2166.377	2166.504	-0.127	2.923E-19	3.250E-19	-11.17
F_2	4	2	F_1	5	2	2160.524	2160.654	-0.130	1.959E-19	2.118E-19	-8.09
E	4	2	E	5	1	2160.547	2160.678	-0.131	1.270E-19	1.361E-19	-7.16
F_1	4	1	F_2	5	3	2160.591	2160.718	-0.127	2.201E-19	2.191E-19	0.44
F_2	4	1	F_1	5	1	2160.629	2160.755	-0.126	2.250E-19	2.150E-19	4.43
A_2	5	2	A_1	6	2	2154.706	2154.832	-0.126	3.217E-19	3.766E-19	-17.08
F_2	5	2	F_1	6	2	2154.738	2154.865	-0.127	1.930E-19	2.135E-19	-10.62
F_1	5	1	F_2	6	3	2154.768	2154.895	-0.127	1.852E-19	1.939E-19	-4.70
F_1	5	1	F_2	6	1	2154.780	2154.907	-0.127	1.705E-20	2.058E-20	-20.73
A_1	5	3	A_2	6	1	2154.810	2154.935	-0.125	3.688E-19	3.826E-19	-3.73
F_1	5	1	F_2	6	3	2154.844	2154.975	-0.131	1.071E-20	1.491E-20	-39.28
F_1	5	1	F_2	6	1	2154.856	2154.987	-0.131	1.901E-19	2.039E-19	-7.29
E	5	1	E	6	3	2154.862	2154.992	-0.130	1.380E-19	1.485E-19	-7.60
F_2	6	2	F_1	7	3	2148.893	2149.021	-0.128	1.970E-19	2.025E-19	-2.77
E	6	2	E	7	3	2148.926	2149.052	-0.126	1.319E-19	1.400E-19	-6.17
F_1	6	3	F_2	7	2	2148.954	2149.080	-0.126	1.639E-19	1.702E-19	-3.89
F_1	6	3	F_2	7	1	2148.976	2149.102	-0.126	3.234E-20	4.017E-20	-24.23
A_1	6	3	A_2	7	1	2149.046	2149.184	-0.138	2.950E-19	3.153E-19	-6.89
F_1	6	1	F_2	7	2	2149.052	2149.186	-0.134	2.740E-20	2.832E-20	-3.34
F_1	6	1	F_2	7	1	2149.074	2149.207	-0.133	1.714E-19	1.781E-19	-3.88
F_2	6	3	F_1	7	1	2149.082	2149.214	-0.132	2.077E-19	2.140E-19	-3.02
F_1	7	3	F_2	8	2	2143.025	2143.165	-0.140	1.747E-19	1.899E-19	-8.70

(*Continued*)

Γ'	J'	K'	Γ''	J''	K''	ν_{obs}	ν_{calc}	$\Delta_{\text{obs}-\text{calc}}$	I_{obs}	I_{calc}	$\%\left[\frac{\text{obs}-\text{calc}}{\text{obs}}\right]$
E	7	3	E	8	1	2143.056	2143.197	-0.141	9.223E-20	1.032E-19	-11.94
F_2	7	2	F_1	8	2	2143.084	2143.223	-0.139	1.740E-19	1.798E-19	-3.30
E	7	3	E	8	3	2143.104	2143.246	-0.142	1.340E-20	2.002E-20	-49.38
F_2	7	2	F_1	8	1	2143.125	2143.264	-0.139	1.201E-20	1.525E-20	-26.99
E	7	1	E	8	1	2143.228	2143.372	-0.144	6.575E-21	1.017E-20	-54.68
A_2	7	1	A_1	8	0	2143.286	2143.424	-0.138	3.771E-19	3.373E-19	10.56
F_1	8	3	F_2	9	1	2137.100	2137.240	-0.140	1.135E-20	1.265E-20	-11.48
A_1	8	3	A_2	9	3	2137.136	2137.267	-0.131	2.554E-19	2.951E-19	-15.55
F_1	8	2	F_2	9	3	2137.173	2137.301	-0.128	1.546E-19	1.452E-19	6.09
F_2	8	2	F_1	9	4	2137.198	2137.324	-0.126	1.010E-19	1.313E-19	-29.97
F_2	8	2	F_1	9	4	2137.417	2137.570	-0.153	1.122E-20	1.493E-20	-33.10
F_2	8	1	F_1	9	2	2137.426	2137.569	-0.143	3.185E-21	3.613E-21	-13.46
E	9	3	E	10	3	2131.274	2131.402	-0.128	8.116E-20	8.571E-20	-5.61
F_2	9	4	F_1	10	3	2131.298	2131.424	-0.126	9.629E-20	1.082E-19	-12.38
A_1	9	1	A_2	10	1	2131.302	2131.439	-0.137	4.663E-20	6.417E-20	-37.62
F_1	9	3	F_2	10	2	2131.315	2131.445	-0.130	5.899E-21	7.399E-21	-25.42
F_2	9	4	F_1	10	1	2131.340	2131.467	-0.127	2.822E-20	3.382E-20	-19.86
F_1	9	3	F_2	10	1	2131.381	2131.512	-0.131	1.117E-20	1.499E-20	-34.22
E	9	3	E	10	5	2131.399	2131.527	-0.128	6.337E-21	9.306E-21	-46.85
F_1	9	1	F_2	10	4	2131.594	2131.678	-0.084	6.694E-21	3.753E-21	43.93
F_2	9	3	F_1	10	3	2131.600	2131.764	-0.164	1.449E-20	1.615E-20	-11.48
A_2	9	4	A_1	10	4	2131.629	2131.796	-0.167	1.534E-19	1.616E-19	-5.31
A_1	9	3	A_2	10	1	2131.672	2131.826	-0.154	1.876E-19	1.952E-19	-4.06
F_2	10	4	F_1	11	2	2125.142	2125.281	-0.139	1.315E-20	1.212E-20	7.82
E	10	1	E	11	3	2125.162	2125.302	-0.140	2.551E-20	2.212E-20	13.30
F_2	10	4	F_1	11	4	2125.194	2125.333	-0.139	1.512E-20	1.610E-20	-6.46
E	10	1	E	11	1	2125.249	2125.389	-0.140	8.867E-21	1.032E-20	-16.41
F_2	10	4	F_1	11	2	2125.312	2125.441	-0.129	1.016E-19	1.011E-19	0.58
E	10	2	E	11	3	2125.340	2125.467	-0.127	5.186E-20	5.236E-20	-0.97
F_1	10	1	F_2	11	2	2125.348	2125.481	-0.133	1.369E-20	1.531E-20	-11.88
F_1	10	3	F_2	11	3	2125.362	2125.488	-0.126	9.684E-20	1.020E-19	-5.32
A_1	10	4	A_2	11	1	2125.809	2125.973	-0.164	1.579E-19	1.712E-19	-8.44
E	10	4	E	11	1	2125.851	2126.025	-0.174	3.963E-20	4.194E-20	-5.82
F_2	11	1	F_1	12	4	2119.300	2119.431	-0.131	9.978E-21	1.400E-20	-40.30
A_2	11	2	A_1	12	4	2119.331	2119.461	-0.130	1.160E-19	1.440E-19	-24.15
F_1	11	3	F_2	12	5	2119.389	2119.515	-0.126	6.041E-20	6.883E-20	-13.94
A_1	11	3	A_2	12	3	2119.414	2119.540	-0.126	1.131E-19	1.477E-19	-30.63
F_2	11	1	F_1	12	2	2119.440	2119.571	-0.131	1.284E-20	1.634E-20	-27.32
F_1	11	3	F_2	12	1	2119.449	2119.576	-0.127	7.866E-21	1.017E-20	-29.29
F_2	11	2	F_1	12	2	2119.508	2119.635	-0.127	1.635E-20	2.204E-20	-34.82
F_2	12	1	F_1	13	1	2114.154	2114.321	-0.167	4.479E-20	5.868E-20	-31.03

(*Continued*)

Γ'	J'	K'	Γ''	J''	K''	ν_{obs}	ν_{calc}	$\Delta_{\text{obs}-\text{calc}}$	I_{obs}	I_{calc}	% $\left[\frac{\text{obs}-\text{calc}}{\text{obs}}\right]$
E	12	5	E	13	1	2114.169	2114.352	-0.183	2.707E-20	3.394E-20	-25.38
F_1	12	1	F_2	13	1	2114.179	2114.349	-0.170	4.882E-20	5.374E-20	-10.08
F_2	12	1	F_1	13	2	2114.187	2114.373	-0.186	3.173E-20	4.001E-20	-26.09
A_1	12	1	A_2	13	5	2114.252	2114.453	-0.201	4.283E-20	5.208E-20	-21.59
F_2	12	3	F_1	13	5	2114.259	2114.457	-0.198	2.253E-20	2.647E-20	-17.51
F_1	12	4	F_2	13	1	2114.263	2114.463	-0.200	2.538E-20	2.854E-20	-12.45
A_2	12	4	A_1	13	2	2114.309	2114.506	-0.197	3.990E-20	4.713E-20	-18.13
F_2	12	3	F_1	13	2	2114.354	2114.554	-0.200	2.886E-21	3.277E-21	-13.55
E	13	2	E	14	7	2108.308	2108.486	-0.178	2.272E-20	2.725E-20	-19.96
F_1	13	1	F_2	14	1	2108.321	2108.499	-0.178	3.210E-20	3.888E-20	-21.14
A_2	13	5	A_1	14	6	2108.343	2108.545	-0.202	5.088E-20	5.941E-20	-16.77
F_1	13	2	F_2	14	2	2108.349	2108.544	-0.195	2.889E-20	3.389E-20	-17.30
A_1	13	2	A_2	14	1	2108.354	2108.535	-0.181	5.234E-20	5.969E-20	-14.04
F_2	13	2	F_1	14	3	2108.392	2108.590	-0.198	2.090E-20	2.445E-20	-17.00
F_1	13	2	F_2	14	5	2108.482	2108.694	-0.212	1.629E-20	1.955E-20	-20.03
F_2	13	3	F_1	14	1	2108.501	2108.711	-0.210	1.259E-20	1.537E-20	-22.06
E	13	4	E	14	3	2108.510	2108.721	-0.211	9.767E-21	1.165E-20	-19.31
A_1	14	3	A_2	15	5	2101.289	2101.420	-0.131	5.038E-20	5.580E-20	-10.74
F_1	14	4	F_2	15	4	2101.294	2101.420	-0.126	9.089E-21	7.565E-21	16.77
F_2	14	2	F_1	15	2	2101.310	2101.440	-0.130	5.713E-21	6.863E-21	-20.13
F_1	14	3	F_2	15	4	2101.345	2101.472	-0.127	1.368E-20	1.974E-20	-44.37
F_2	14	5	F_1	15	4	2101.369	2101.496	-0.127	2.202E-20	2.588E-20	-17.52
A_2	14	4	A_1	15	4	2101.397	2101.523	-0.126	3.615E-20	5.131E-20	-41.95
E	14	2	E	15	1	2101.445	2101.569	-0.124	2.451E-21	3.595E-21	-46.67
A_2	15	4	A_1	16	0	2096.608	2096.799	-0.191	2.530E-20	3.021E-20	-19.42
E	15	2	E	16	1	2096.658	2096.850	-0.192	9.113E-21	1.064E-20	-16.71
F_1	15	2	F_2	16	3	2096.686	2096.897	-0.211	1.131E-20	1.532E-20	-35.38
E	15	6	E	16	7	2096.743	2096.963	-0.220	8.317E-21	9.454E-21	-13.67
F_1	15	3	F_2	16	1	2096.772	2096.994	-0.222	9.262E-21	1.085E-20	-17.14
F_2	15	7	F_1	16	2	2096.802	2097.017	-0.215	9.495E-21	1.206E-20	-26.98

Due to the computational demands of calculating higher rotational excitation (rovibrational matrices scale linearly with J), calculations were performed with $P_{\max} = 10$. Convergence tests were carried out up to $J = 6$ for $P_{\max} = 12$. The corresponding transition frequencies showed a consistent correction of around $\Delta(P_{\max} = 12) = -0.00185\,\text{cm}^{-1}$. This correction was applied to all computed frequencies listed in Table 5.5. For the corresponding intensities, the $1 \leftarrow 2$ ($J' \leftarrow J''$)

transitions possessed a convergence correction of the order 10^{-24}. The magnitude of this correction showed a linear relationship with increasing J, from which I estimated that for the $15 \leftarrow 16$ transitions the correction would be of the order 10^{-22}. The respective intensities therefore have an error of at most 1%. I am confident that the results in Table 5.5 are sufficiently converged to reliably evaluate the DMS and PES.

Around one third of the calculated absolute line intensities are within the estimated experimental measurement accuracy of 10%. However, as is best seen by the residuals plotted in Fig. 5.2, nearly all of the computed line intensities are larger than the corresponding experimental values. I suspect this is due to the electronic structure calculations and the use of only a triple-zeta basis set, aug-cc-pVTZ(+d for Si), to generate the DMS. A larger (augmented) correlation consistent basis set and possibly the inclusion of additional higher-level corrections (such as those incorporated for the PES) would most likely reduce the strength of computed line intensities. Despite this, Fig. 5.2 shows that the ν_3 band is well reproduced. Computed frequencies are on average larger by 0.1–0.2 cm^{-1} across all transitions. This more or less systematic error can be attributed to the minor empirical refinement of the equilibrium Si–H bond length.

5.4.5 Overview of rotation-vibration spectrum

As a final test of the PES and DMS, in Fig. 5.3 we have simulated the rotation-vibration spectrum of $^{28}SiH_4$ for transitions up to $J = 20$ at 296 K. A polyad number of $P_{\max} = 10$ was employed. Transition frequencies and corresponding intensities were calculated for a 5000 cm^{-1} frequency window with a lower state energy threshold of 5000 cm^{-1}. A Gaussian profile with a half width at half maximum of 0.135 cm^{-1} was used to simulate the spectrum. The experimental PNNL silane spectrum [95], also shown in Fig. 5.3, is at a resolution of around 0.06 cm^{-1}. It was measured at a temperature of 25 °C with the dataset subsequently re-normalized to 22.84 °C (296 K). Note that the PNNL spectrum is of electronics grade silane

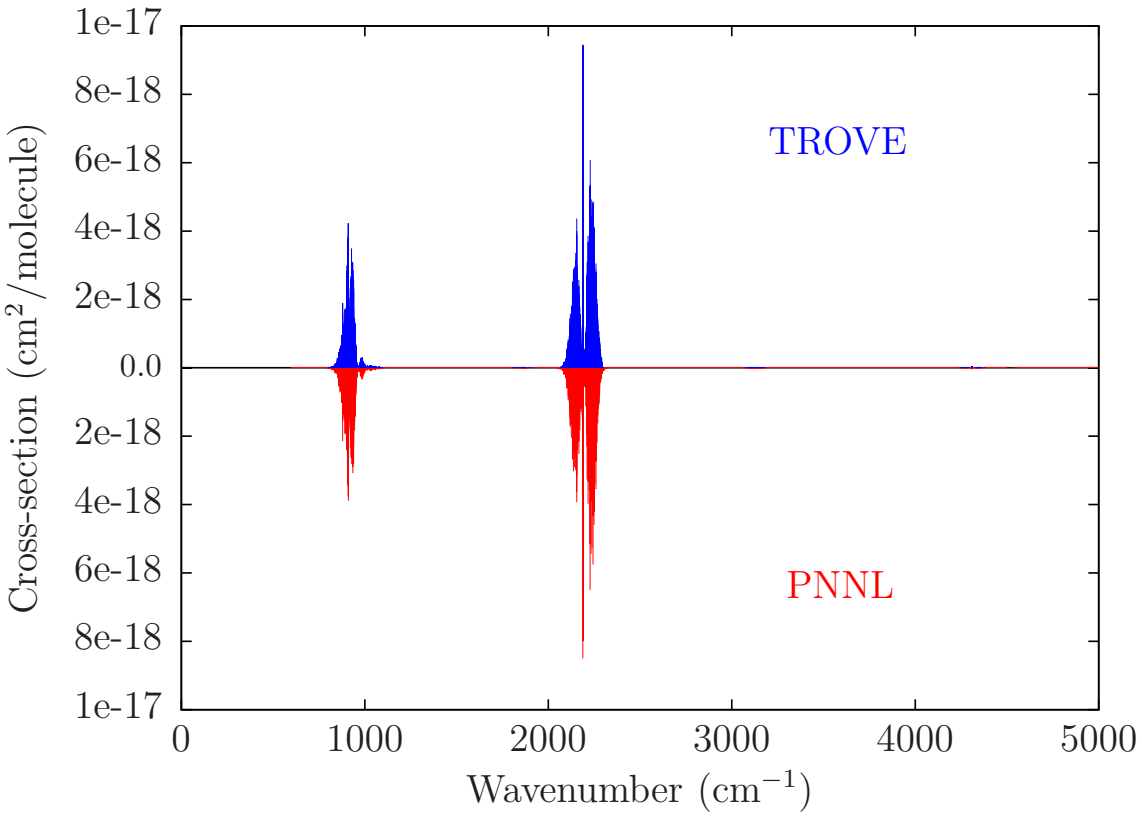

Figure 5.3: Overview of simulated $^{28}SiH_4$ rotation-vibration spectrum up to $J = 20$. Note that the experimental PNNL spectrum [95] is composed of $^{28}SiH_4$ (92.2%), $^{29}SiH_4$ (4.7%), and $^{30}SiH_4$ (3.1%) (see text).

gas which is composed of $^{28}SiH_4$ (92.2%), $^{29}SiH_4$ (4.7%), and $^{30}SiH_4$ (3.1%). I have therefore scaled the TROVE computed $^{28}SiH_4$ cross-sections by 0.922 to provide a reliable comparison.

The computed TROVE intensities are marginally stronger but overall there is good agreement with the experimental PNNL results. Even with $P_{\max} = 10$, which does not give fully converged transition frequencies, both band shape and position appear reliable. Of course there are shortcomings in the simulations which we will now discuss.

Some of the band structure is undoubtedly lost as we have not considered $^{29}SiH_4$ or $^{30}SiH_4$, and by only computing transitions up to $J = 20$ the spectrum is unlikely to be complete at room temperature. There may also be minor errors arising from the use of a Gaussian profile to model the line shape. More desirable would be to

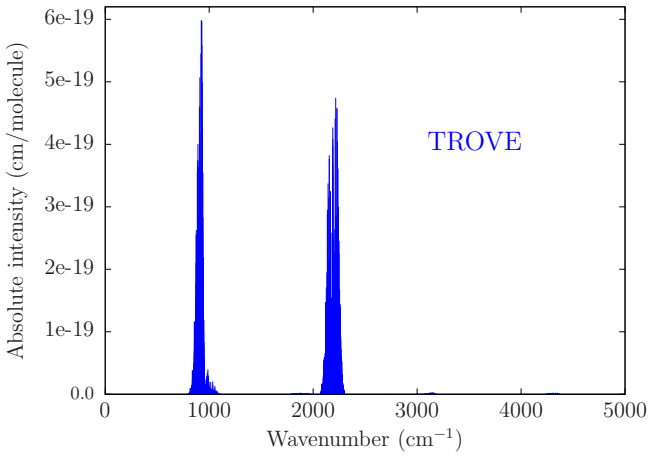

Figure 5.4: Overview of absolute line intensities of $^{28}SiH_4$ up to $J = 20$.

fit a Voigt profile which incorporates instrumental factors. The largest source of error, as discussed before, is likely to be the electronic structure calculations. For the purposes of modelling exoplanet atmospheres however, I expect that the level of theory employed to compute the DMS is sufficient. The features of the SiH_4 spectrum are clear and identifiable as seen in Fig. 5.3.

Note that in Fig. 5.3, the ν_3 (2189.19 cm^{-1}) band is stronger than the ν_4 (913.47 cm^{-1}) band. This is contrast to the vibrational transition moments where $\mu_{\nu_4} > \mu_{\nu_3}$. If, however, we plot absolute line intensities up to $J = 20$ as shown in Fig. 5.4, the ν_4 band is indeed stronger than the ν_3 band. The behaviour displayed in Fig. 5.3 is caused by the use of a line profile to model the spectrum.

5.5 Chapter summary and further work

In the previous chapter I wanted to push the *ab initio* limit for CH_3Cl and this was reflected in the electronic structure calculations. For SiH_4, a more pragmatic approach has been taken. This was guided by the following considerations: (i) incorporating the leading HL corrections and an extrapolation to the CBS limit can significantly improve the quality of the PES, (ii) I expect the PES will be empirically refined, therefore generating an *ab initio* PES which has the 'correct' shape should be sufficient and computing tightly converged energies with respect to basis set size for the HL corrections is not as important, and (iii) to treat more molecular species,

the ExoMol database would benefit from a fast and reliable approach.

In this chapter I have generated new nine-dimensional potential energy and dipole moment surfaces for silane. The quality of the PES is reflected by the achievement of sub-wavenumber accuracy for all four fundamental frequencies. Combination and overtone bands are also consistently reproduced which confirms that the level of *ab initio* theory used to generate the PES is adequate. Minor empirical refinement of the equilibrium geometry of SiH_4 produced an Si–H bond length in excellent agreement with previous experimental and theoretical results. The rotational structure of vibrational bands was improved as a result of the refinement. Absolute line intensities were marginally overestimated and I suspect this behaviour can be resolved by using a larger (augmented) basis set for the electronic structure calculations when computing the DMS. Overall however, band shape and structure across the spectrum display good agreement with experiment and I thus recommend the PES and DMS for future use.

To achieve sub-wavenumber accuracy for all rovibrational energy levels a rigorous empirical refinement of the PES is necessary. Work is currently underway in this direction before a comprehensive line list applicable for elevated temperatures is generated. Refinement of the CBS-F12$^{\mathrm{HL}}$ PES has highlighted the difficulty in obtaining reliable experimental data for SiH_4. The STDS [220] contains rovibrational energy levels with adequate quantum number labelling. However, the energy levels are from an effective Hamiltonian model based on four sources of experimental work, two published [238, 239] and two unpublished. This makes it difficult to assess the reliability of the data and how much it can be trusted in the refinement. Despite this, because the *ab initio* PES is reliable I can depend on it more and ensure that the refined PES does not deviate too far away from the original *ab initio* surface. This is one of the strengths of quantum chemical methods and generating a robust *ab initio* PES.

6 Methane (CH_4)

6.1 Introduction

In the last two chapters I have constructed highly accurate *ab initio* PESs for CH_3Cl and SiH_4. In doing so, a pragmatic approach towards the electronic structure calculations has been developed. We now turn our attention to methane. As a key atmospheric molecule, the infrared spectrum of CH_4 has been the subject of numerous studies. Its complex polyad structure is beginning to be explored in greater detail at higher energies [240–265], and there is strong motivation to continue working towards the visible region to aid the study of exoplanets [266]. Variational calculations from first principles were recently used in conjunction with an experimental line list [267] to assign a significant number of vibrational band centres in the icosad range (6300–7900 cm^{-1}) [264]. This kind of analysis could prove extremely useful for more congested regions and its success depends on having a reliable PES to work with.

A number of accurate PESs for CH_4 have been reported in the literature [5, 68, 268–279]. These include purely *ab initio* surfaces [268, 272–275, 278, 279], and those which are based on *ab initio* calculations but have subsequently been refined to experiment [5, 68, 269–271, 276, 277]. The most rigorous *ab initio* treatment to date was by Schwenke [273] who accounted for several HL contributions. Corrections to the FCI limit, CV electron correlation, SR effects, the Lamb shift, the DBOC, non-adiabatic corrections, as well as extrapolation of the basis set to the CBS limit, were all treated at some level. Whilst low-lying states of $^{12}CH_4$ were reproduced with sub-wavenumber accuracy, the description of the stretching fundamentals, ν_1 and ν_3, was relatively poor in comparison and the errors in vibrational energies gradually increased after 3000 cm^{-1}.

A comprehensive methane line list, 10to10 [5], was produced as part of the ExoMol project and this represented a significant step forward in the variational treatment of five-atom molecules. The 10to10 line list has facilitated the detection of CH_4 in brown dwarfs [5], T dwarfs [280], and the hot Jupiter exoplanet HD 189733b [221]. Since its construction a number of high resolution spectroscopic measurements on methane above the tetradecad region (above 6300 cm^{-1}) have been reported [259–264]. There have also been key developments [70] in the nuclear motion code TROVE [9] which considerably improve basis set convergence; a major bottleneck in the past. Given the demand for comprehensive methane data at higher energies and the knowledge acquired from the 10to10 line list, it seems natural to begin working on a more extensive and accurate treatment of CH_4.

The chapter is structured as follows: In Sec. 6.2 the electronic structure calculations and analytic representation of the PES are presented. The variational nuclear motion computations used to validate the PES are described in Sec 6.3. In Sec. 6.4, vibrational $J = 0$ energy levels for $^{12}CH_4$, the equilibrium C–H bond length, and pure rotational energies up to $J = 10$ are calculated and compared with available experimental results. We conclude and discuss future work in Sec. 6.5.

6.2 Potential energy surface

6.2.1 Electronic structure calculations

The approach employed for the electronic structure calculations is almost identical to that of SiH_4. We want to generate a PES which possesses the 'correct' shape and computing tightly converged energies with respect to basis set size for the HL contributions is less important. The methods and basis sets have therefore been chosen to strike a balance between accuracy and computational cost.

Utilizing focal-point analysis [150] the total electronic energy is written as

$$E_{\text{tot}} = E_{\text{CBS}} + \Delta E_{\text{CV}} + \Delta E_{\text{HO}} + \Delta E_{\text{SR}} + \Delta E_{\text{DBOC}}. \tag{6.1}$$

The energy at the CBS limit E_{CBS} was computed using the explicitly correlated F12 coupled cluster method CCSD(T)-F12b [25] in conjunction with the F12-optimized cc-pVTZ-F12 and cc-pVQZ-F12 [36] correlation consistent polarized valence basis sets. The frozen core approximation was employed and calculations used the diagonal fixed amplitude ansatz 3C(FIX) [18] with a Slater geminal exponent value of $\beta = 1.0\, a_0^{-1}$ [46]. For the ABS, the OptRI [40], cc-pV5Z/JKFIT [41] and aug-cc-pwCV5Z/MP2FIT [42] were used for the RI basis and the two DF basis sets, respectively. Calculations were carried out with MOLPRO2012 [151] unless stated otherwise. To extrapolate to the CBS limit I used Eq. (4.2). No extrapolation was applied to the HF energy, rather the HF+CABS singles correction [25] calculated in the larger basis set was used.

The contribution from CV electron correlation ΔE_{CV} was computed at the CCSD(T)-F12b level of theory with the F12-optimized correlation consistent core-valence basis set cc-pCVTZ-F12 [37]. Calculations employed the same ansatz and ABS as used for E_{CBS}, however, the Slater geminal exponent was changed to $\beta = 1.4\, a_0^{-1}$.

HO correlation effects were accounted for using the hierarchy of coupled cluster methods such that $\Delta E_{\mathrm{HO}} = \Delta E_{\mathrm{T}} + \Delta E_{(\mathrm{Q})}$. Here, the full triples contribution is $\Delta E_{\mathrm{T}} = \left[E_{\mathrm{CCSDT}} - E_{\mathrm{CCSD(T)}}\right]$, and the perturbative quadruples contribution is $\Delta E_{(\mathrm{Q})} = \left[E_{\mathrm{CCSDT(Q)}} - E_{\mathrm{CCSDT}}\right]$. Calculations were performed in the frozen core approximation at the CCSD(T), CCSDT, and CCSDT(Q) levels of theory using the general coupled cluster approach [152, 153] as implemented in the MRCC code [154] interfaced to CFOUR [155]. The correlation consistent triple zeta basis set, cc-pVTZ [30], was utilized for the full triples contribution, whilst the perturbative quadruples employed the double zeta basis set, cc-pVDZ.

The SR correction ΔE_{SR} was calculated with the second-order Douglas-Kroll-Hess approach [54, 55] at the CCSD(T)/cc-pVQZ-DK [222] level of theory in the frozen core approximation. For light, closed-shell molecules the spin-orbit interaction can be neglected in spectroscopic calculations [56].

The DBOC ΔE_{DBOC} was computed with all electrons correlated using the CCSD method [158] implemented in CFOUR with the aug-cc-pCVDZ basis set. The DBOC has a noticeable effect on vibrational term values of methane [273] but because it is mass dependent its inclusion means the PES is only applicable for $^{12}CH_4$.

All terms in Eq. (6.1) were calculated on a grid of 97 721 geometries with energies up to $hc \cdot 50\,000\,\mathrm{cm}^{-1}$ (h is the Planck constant and c is the speed of light). The global grid was built in terms of nine internal coordinates; four C–H bond lengths r_1, r_2, r_3, r_4, and five $\angle(\mathrm{H}_j\text{–C–H}_k)$ interbond angles α_{12}, α_{13}, α_{14}, α_{23}, and α_{24}, where j and k label the respective hydrogen atoms. The C–H stretch distances ranged from $0.71 \leq r_i \leq 2.60\,\text{Å}$ for $i = 1, 2, 3, 4$ whilst bending angles varied from $40 \leq \alpha_{jk} \leq 140^\circ$ where $jk = 12, 13, 14, 23, 24$.

Although it is computationally demanding to calculate the HL corrections at every grid point, it is actually time-effective given the system size, levels of theory and basis sets used. Timing data is shown in Table 6.1 and we see it takes just over 15 minutes to compute all the contributions in Eq. (6.1) at the equilibrium geometry. Naturally this time will increase as we stretch and bend the molecule due to slower energy convergence, with calculations needing at most 2–3 times longer for highly distorted geometries.

Table 6.1: Wall clock times (seconds) for the different contributions to the potential energy surface. Calculations were performed on a single core of an Intel Xeon E5-2690 v2 3.0 GHz processor. Timings shown have been averaged over 10 runs for one point at the equilibrium geometry.

Contribution	No. of calculations required per point	Time
E_{CBS}	2	296
ΔE_{CV}	2	107
ΔE_{HO}	3	234
ΔE_{SR}	2	189
ΔE_{DBOC}	1	87
E_{tot}	10	913

Alternatively, one can compute each HL correction on a reduced grid, fit a suitable analytic representation to the data and then interpolate to other points on the global grid as was done for CH_3Cl in Chapter 4. For more demanding systems this approach can significantly reduce computational time, however, obtaining an adequate description of each HL correction requires careful consideration and may not be straightforward. These issues are avoided in the present approach.

6.2.2 Analytic representation

The XY_4 symmetrized analytic representation employed here is the same as that used in the previous chapter for the PES of SiH_4. I therefore summarise only the key aspects relevant for CH_4 and refer the reader back to Sec. 5.2.2 for more details.

The stretch coordinates were described by Morse oscillator functions, Eq. (5.2), with values of $a = 1.845\,\text{Å}^{-1}$ and $r_{\text{ref}} = 1.08594\,\text{Å}$ (value discussed in Sec. 6.4.2). Symmetrized combinations of interbond angles, Eqs. (5.3) to (5.7), represented the angular terms. A sixth order expansion was used for the potential function, Eq. (5.8), and this was determined in a least-squares fitting to the *ab initio* data. Weight factors of the form given in Eq. (4.12) were used and this favoured energies below $15\,000\,\text{cm}^{-1}$. To further improve the description at lower energies and reduce the weights of outliers I employed Watson's robust fitting scheme [162]. The final PES was fitted with a weighted root-mean-square (rms) error of $1.08\,\text{cm}^{-1}$ for energies up to $hc \cdot 50\,000\,\text{cm}^{-1}$ and required 112 expansion parameters ($110 + r_{\text{ref}} + a$). For geometries where $r_i \geq 1.80\,\text{Å}$ for $i = 1, 2, 3, 4$, the respective weights were dropped by several orders of magnitude. In subsequent calculations we refer to this PES as CBS-F12$^{\text{HL}}$. The CBS-F12$^{\text{HL}}$ expansion parameter set is provided in the supplementary material of Ref. [281] along with a FORTRAN routine to construct the PES.

6.3 Variational calculations

The rovibrational Hamiltonian was represented as a power series expansion around the equilibrium geometry in terms of the nine coordinates given in Eqs. (5.2)

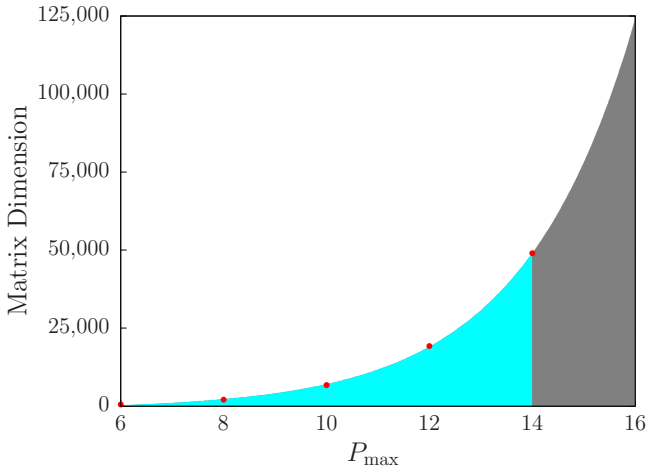

Figure 6.1: Size of the $J=0$ Hamiltonian matrix with respect to the polyad truncation number $P_{\max}$. Calculations have not been possible above $P_{\max} = 14$.

to (5.7). However, for the kinetic energy operator linear displacement variables $(r_i - r_{\text{ref}})$ were used for the stretching coordinates. The Hamiltonian was constructed numerically using an automatic differentiation method [70] with the kinetic and potential energy operators truncated at 6th and 8th order, respectively. Atomic mass values were used throughout.

The definition of the polyad number for CH_4 is the same as SiH_4, that is

$$P = 2(n_1 + n_2 + n_3 + n_4) + n_5 + n_6 + n_7 + n_8 + n_9 \leq P_{\max}, \tag{6.2}$$

and this does not exceed a predefined maximum value $P_{\max}$. As shown in Fig. 6.1, the size of the Hamiltonian matrix grows exponentially with respect to $P_{\max}$ and calculations above $P_{\max} = 14$ have not been possible with the resources available to us. Here the quantum numbers n_k for $k = 1, \ldots, 9$ relate to primitive basis functions ϕ_{n_k}, which are obtained by solving a one-dimensional Schrödinger equation for each kth vibrational mode using the Numerov-Cooley method [83, 84]. Multiplication with symmetrized rigid-rotor eigenfunctions $|J, \Gamma_{\text{rot}}, n\rangle$ gives the final basis set for use in $J > 0$ calculations. The label Γ_{rot} is the rotational symmetry and n is a multiplicity index used to count states within a given J (see Boudon et al. [242]).

In TROVE, eigenvalues and the respective eigenfunctions are assigned with quan-

tum numbers based on the contribution of the basis functions ϕ_{n_k}. To be of spectroscopic use we map these to the normal mode quantum numbers v_k commonly used. For CH_4, vibrational states are labelled as $\mathrm{v}_1\nu_1 + \mathrm{v}_2\nu_2^{L_2} + \mathrm{v}_3\nu_3^{L_3} + \mathrm{v}_4\nu_4^{L_4}$ where v_i counts the level of excitation. The additional quantum numbers L_i are the absolute values of the vibrational angular momentum quantum numbers ℓ_i, which are needed to resolve the degeneracy of their respective modes (see Yurchenko and Tennyson [5] for further details). The non-degenerate symmetric stretching mode ν_1 ($2916.48\,\mathrm{cm}^{-1}$) is of A_1 symmetry. The doubly degenerate antisymmetric bending mode ν_2 ($1533.33\,\mathrm{cm}^{-1}$) has E symmetry. Whilst of F_2 symmetry are the triply degenerate modes; the antisymmetric stretching mode ν_3 ($3019.49\,\mathrm{cm}^{-1}$), and the antisymmetric bending mode ν_4 ($1310.76\,\mathrm{cm}^{-1}$). The values in parentheses are the experimentally determined values [244].

6.4 Results

6.4.1 Vibrational $J=0$ energy levels

A reliable assessment of the CBS-F12$^{\mathrm{HL}}$ PES is only possible with converged vibrational term values. Calculations with $P_{\max} = 14$ are sufficient for converging low-lying states but this gradually deteriorates as we go up in energy. A way of overcoming this problem, as was done for CH_3Cl in Sec. 4.4.1, is to employ a complete vibrational basis set (CVBS) extrapolation [59]. Again I used the exponential decay expression given in Eq. (4.25) with values of $P_{\max} = \{10, 12, 14\}$.

Briefly commenting on the accuracy of the CVBS extrapolation itself, similar to electronic structure theory the use of larger basis sets is always preferable for the extrapolation. Highly excited modes benefit the most as convergence is much slower, however, at higher energies the increased density of states makes it harder to consistently identify and match energy levels for different values of $P_{\max}$. To ensure a reliable extrapolation I have also found that the quantity λ_i defined in Eq. (4.26) should satisfy $\lambda_i \geq 0.5$.

In the following comparisons I have collected, to the best of my knowledge, all $J = 0$ energies that have been accurately determined from experiment (see Manca Tanner and Quack [282] for a discussion of the experimental uncertainties associated with methane spectra). Although very minor discrepancies occasionally occur between different studies, the majority of vibrational term values up to the tetradecad region (up to 6300 cm^{-1}) are fairly well established. Progress is being made in the icosad range (6300–7900 cm^{-1}) and a large number of levels have recently been assigned [263, 264] using the WKLMC line list [267]. At even higher energies several vibrational band centres have been measured and assigned by means of an assignment of their P(1) transitions up to about 11 300 cm^{-1} [259].

Computed vibrational energy levels for $^{12}CH_4$ up to the tetradecad region are listed in Table 6.2. The four fundamentals are reproduced with a rms error of 0.70 cm^{-1} and a mean-absolute-deviation (mad) of 0.64 cm^{-1}. Around 70% of the 89 term values are calculated within spectroscopic accuracy (better than $\pm 1\,\mathrm{cm}^{-1}$) and this does not include the $4\nu_4$ levels computed at $P_{\max} = 14$, which are not fully converged.

Table 6.2: Comparison of calculated and experimental $J = 0$ vibrational term values (in cm^{-1}) up to the tetradecad region for $^{12}CH_4$. The zero-point energy was computed to be 9708.846 cm^{-1} at the CVBS limit.

Mode	Sym.	Experiment	Calculated	Obs−calc	Ref.
ν_4^1	F_2	1310.76	1310.24	0.52	[244]
ν_2^1	E	1533.33	1533.04	0.29	[244]
$2\nu_4^0$	A_1	2587.04	2585.74	1.30	[244]
$2\nu_4^2$	F_2	2614.26	2613.04	1.22	[244]
$2\nu_4^2$	E	2624.62	2624.08	0.54	[244]
$\nu_2^1 + \nu_4^1$	F_2	2830.32	2829.71	0.61	[244]
$\nu_2^1 + \nu_4^1$	F_1	2846.07	2845.44	0.63	[244]
ν_1	A_1	2916.48	2917.16	-0.68	[244]
ν_3^1	F_2	3019.49	3020.57	-1.08	[244]
$2\nu_2^0$	A_1	3063.65	3063.04	0.61	[244]

(*Continued*)

Mode	Sym.	Experiment	Calculated	Obs−calc	Ref.
$2\nu_2^2$	E	3065.14	3064.53	0.61	[244]
$3\nu_4^1$	F_2	3870.49	3869.18	1.31	[244]
$3\nu_4^1$	A_1	3909.20	3907.11	2.09	[244]
$3\nu_4^3$	F_1	3920.50	3919.01	1.49	[257]
$3\nu_4^3$	F_2	3930.92	3930.00	0.92	[244]
$\nu_2^1 + 2\nu_4^0$	E	4101.39	4100.52	0.87	[244]
$\nu_2^1 + 2\nu_4^2$	F_1	4128.77	4127.77	1.00	[257]
$\nu_2^1 + 2\nu_4^2$	A_1	4132.88	4132.21	0.67	[257]
$\nu_2^1 + 2\nu_4^2$	F_2	4142.86	4142.03	0.83	[257]
$\nu_2^1 + 2\nu_4^2$	E	4151.20	4150.62	0.58	[257]
$\nu_2^1 + 2\nu_4^2$	A_2	4161.84	4161.00	0.84	[257]
$\nu_1 + \nu_4^1$	F_2	4223.46	4223.62	-0.16	[244]
$\nu_3^1 + \nu_4^1$	F_2	4319.21	4319.37	-0.16	[244]
$\nu_3^1 + \nu_4^1$	E	4322.18	4323.38	-1.20	[244]
$\nu_3^1 + \nu_4^1$	F_1	4322.58	4323.53	-0.95	[257]
$\nu_3^1 + \nu_4^1$	A_1	4322.72	4323.01	-0.29	[257]
$2\nu_2^0 + \nu_4^1$	F_2	4348.72	4348.07	0.65	[244]
$2\nu_2^2 + \nu_4^1$	F_1	4363.62	4362.86	0.76	[257]
$2\nu_2^2 + \nu_4^1$	F_2	4378.94	4378.30	0.64	[257]
$\nu_1 + \nu_2^1$	E	4435.13	4435.25	-0.12	[257]
$\nu_2^1 + \nu_3^1$	F_1	4537.55	4538.13	-0.58	[244]
$\nu_2^1 + \nu_3^1$	F_2	4543.76	4544.36	-0.60	[244]
$3\nu_2^1$	E	4592.03	4591.08	0.95	[244]
$3\nu_2^3$	A_2	4595.28	4594.40	0.88	[257]
$3\nu_2^3$	A_1	4595.52	4594.49	1.03	[257]
$4\nu_4^0$	A_1	5121.77	5121.51[a]	0.26	[265]
$4\nu_4^2$	F_2	5143.36	5143.07[a]	0.29	[257]
$4\nu_4^2$	E	5167.20	5167.15[a]	0.05	[257]
$4\nu_4^4$	F_2	5210.74	5209.06[a]	1.68	[257]
$4\nu_4^4$	E	5228.74	5227.45[a]	1.29	[257]
$4\nu_4^4$	F_1	5230.59	5229.46[a]	1.13	[265]
$4\nu_4^4$	A_1	5240.46	5239.76[a]	0.70	[265]

(*Continued*)

Mode	Sym.	Experiment	Calculated	Obs−calc	Ref.
$\nu_2^1 + 3\nu_4^1$	F_2	5370.48	5369.79	0.69	[265]
$\nu_2^1 + 3\nu_4^1$	F_1	5389.74	5388.96	0.78	[265]
$\nu_2^1 + 3\nu_4^1$	E	5424.80	5423.39	1.41	[265]
$\nu_2^1 + 3\nu_4^3$	F_2	5429.86	5428.85	1.01	[265]
$\nu_2^1 + 3\nu_4^3$	F_1	5437.28	5436.38	0.90	[265]
$\nu_2^1 + 3\nu_4^3$	F_2	5444.80	5444.07	0.73	[257]
$\nu_2^1 + 3\nu_4^3$	F_1	5462.91	5461.86	1.05	[265]
$\nu_1 + 2\nu_4^0$	A_1	5492.90	5492.32	0.58	[265]
$\nu_3^1 + 2\nu_4^0$	F_2	5587.97	5587.97	0.00	[257]
$\nu_3^1 + 2\nu_4^2$	A_1	5604.47	5604.51	-0.04	[257]
$2\nu_2^0 + 2\nu_4^0$	A_1	5613.88	5612.61	1.27	[265] [b]
$2\nu_2^2 + 2\nu_4^0$	E	5614.58	5613.15	1.43	[265]
$\nu_3^1 + 2\nu_4^2$	F_1	5615.37	5615.75	-0.38	[265]
$\nu_3^1 + 2\nu_4^2$	F_2	5616.02	5615.46	0.56	[265]
$\nu_3^1 + 2\nu_4^2$	E	5618.23	5618.85	-0.62	[265]
$\nu_3^1 + 2\nu_4^2$	F_1	5626.10	5626.96	-0.86	[265]
$\nu_3^1 + 2\nu_4^2$	F_2	5627.35	5628.29	-0.94	[265]
$2\nu_2^0 + 2\nu_4^2$	F_2	5641.88	5641.63	0.25	[265]
$2\nu_2^2 + 2\nu_4^2$	E	5654.47	5653.58	0.89	[265]
$2\nu_2^2 + 2\nu_4^2$	F_1	5655.76	5655.28	0.48	[257]
$2\nu_2^2 + 2\nu_4^2$	A_2	5664.08	5663.38	0.70	[265]
$2\nu_2^0 + 2\nu_4^2$	F_2	5668.33	5668.25	0.08	[265]
$2\nu_2^2 + 2\nu_4^2$	A_1	5681.26	5681.25	0.01	[265]
$2\nu_2^0 + 2\nu_4^2$	E	5691.10	5690.32	0.78	[265]
$2\nu_1$	A_1	5790.25	5792.08	-1.83	[283]
$\nu_2^1 + \nu_3^1 + \nu_4^1$	F_2	5823.10	5823.65	-0.55	[257]
$\nu_2^1 + \nu_3^1 + \nu_4^1$	F_1	5825.43	5825.59	-0.16	[265]
$\nu_2^1 + \nu_3^1 + \nu_4^1$	E	5832.02	5832.60	-0.58	[257]
$\nu_2^1 + \nu_3^1 + \nu_4^1$	A_1	5834.82	5835.64	-0.82	[257]
$\nu_2^1 + \nu_3^1 + \nu_4^1$	E	5842.57	5843.12	-0.55	[265]
$\nu_2^1 + \nu_3^1 + \nu_4^1$	A_2	5843.19	5843.83	-0.64	[265]
$\nu_2^1 + \nu_3^1 + \nu_4^1$	F_2	5844.03	5844.28	-0.25	[257]

(*Continued*)

Mode	Sym.	Experiment	Calculated	Obs−calc	Ref.
$\nu_2^1+\nu_3^1+\nu_4^1$	F_1	5847.39	5847.66	-0.27	[265]
$\nu_1+\nu_3^1$	F_2	5861.49	5861.90	-0.41	[257]
$3\nu_2^1+\nu_4^1$	F_2	5867.52	5868.09	-0.57	[265]
$3\nu_2^3+\nu_4^1$	F_1	5879.80	5878.97	0.83	[265]
$3\nu_2^3+\nu_4^1$	F_2	5894.34	5893.51	0.83	[265]
$3\nu_2^1+\nu_4^1$	F_1	5908.74	5908.52	0.22	[265]
$\nu_1+2\nu_2^2$	E	5952.44	5952.00	0.44	[257]
$2\nu_3^0$	A_1	5968.15	5969.12	-0.97	[284]
$2\nu_3^2$	F_2	6004.62	6006.54	-1.92	[257]
$2\nu_3^2$	E	6043.82	6046.12	-2.30	[257]
$2\nu_2^0+\nu_3^1$	F_2	6054.61	6054.74	-0.13	[257]
$2\nu_2^2+\nu_3^1$	F_1	6060.62	6060.67	-0.05	[257]
$2\nu_2^2+\nu_3^1$	F_2	6065.59	6065.48	0.11	[257]
$4\nu_2^2$	E	6118.95	6117.21	1.74	[265]
$4\nu_2^4$	E	6124.12	6122.77	1.35	[265]

[a] $P_{\max}=14$ value. [b] Assigned as $\nu_3+2\nu_4$ in TROVE.

Six energy levels in the tetradecad region have not been included in Table 6.2 because their experimental uncertainty could be as large as $5\,\mathrm{cm}^{-1}$ (see Nikitin et al. [257]). Instead they are listed in Table 6.3 alongside computed values from the CBS-F12$^{\mathrm{HL}}$ PES, the empirically refined PES of Wang and Carrington [277] (denoted as WC), and the empirically adjusted PES of Nikitin et al. [276] (denoted as NRT). The three PESs show consistent agreement with each other, notably for the $\nu_1+2\nu_2^0(A_1)$ and $4\nu_2^0(A_1)$ levels where the residual errors, $\Delta E(\mathrm{obs}-\mathrm{calc})$, compared to Nikitin et al. [257] are the largest. This would suggest that the effective Hamiltonian model used in Nikitin et al. [257] and subsequently updated by Amyay et al. [265] may need further refinement in the tetradecad region.

For the icosad region and above, shown in Table 6.4 and Table 6.5, spectroscopic

Table 6.3: Six $J=0$ vibrational term values (in cm^{-1}) in the tetradecad region which have a large experimental uncertainty (see text). Comparisons are given with the CBS-F12$^{\mathrm{HL}}$ PES (this work), the empirically refined PES of Wang and Carrington [277] (denoted as WC), and the empirically adjusted PES of Nikitin et al. [276] (denoted as NRT).

Mode	Sym.	Experiment [257]	CBS-F12$^{\mathrm{HL}}$	WC	NRT
$\nu_1+2\nu_4^2$	F_2	5519.88	5520.95	5522.32	5522.66
$\nu_1+2\nu_4^2$	E	5536.23	5533.62	5534.54	5534.20
$\nu_1+\nu_2^1+\nu_4^1$	F_2	5728.58	5726.71	5727.50	5727.72
$\nu_1+\nu_2^1+\nu_4^1$	F_1	5745.90	5744.72	5745.78	5745.31
$\nu_1+2\nu_2^0$	A_1	5945.81	5940.11	5939.90	5939.96
$4\nu_2^0$	A_1	6122.13	6115.42	6116.74	6117.75

accuracy is again achieved for around 70% of the 134 term values considered. Here I have separated the computed energies into two separate tables based on the accuracy of the corresponding values from experiment, which are predominantly from Refs. [252, 263, 264]. The values in Table 6.4 have an experimental accuracy of $0.0015\,\mathrm{cm}^{-1}$ (the $\nu_2^1+2\nu_3^2$ level from Hippler and Quack [240] has an uncertainty of $0.0010\,\mathrm{cm}^{-1}$). In Table 6.5, energies have an accuracy of 0.1–$0.4\,\mathrm{cm}^{-1}$, except for the vibrational band centres from Ulenikov et al. [259] which have a reported experimental uncertainty of around $0.001\,\mathrm{cm}^{-1}$ (a result of the direct method used). However, the $\nu_1+\nu_3^1+\nu_4^1(F_2)$ level from Ulenikov et al. [259] shows a discrepancy of $1.41\,\mathrm{cm}^{-1}$ compared to the recent value published by Rey et al. [264].

Three term values from Ulenikov et al. [259] above $10\,000\,\mathrm{cm}^{-1}$ could not be confidently identified in TROVE. The increased density of states and approximate TROVE labelling scheme can make it difficult to unambiguously discern certain levels. Regardless, from Table 6.4 and Table 6.5 it is evident that the CBS-F12$^{\mathrm{HL}}$ PES provides a reliable description at higher energies and there does not appear to be any significant deterioration in accuracy (see Fig. 6.2 for an overview of the residual errors for all term values). This will be important for investigating methane

spectra up to the 14 000 cm^{-1} region, which is a key motivation for the present work.

Table 6.4: Comparison of calculated and experimental $J=0$ vibrational term values (in cm^{-1}) for $^{12}CH_4$ in the icosad region (see text for a discussion of the experimental uncertainties). The zero-point energy was computed to be 9708.846 cm^{-1} at the CVBS limit.

Mode	Sym.	Experiment	Calculated	Obs−calc	Ref.
$5\nu_4^1$	F_2	6450.06	6449.72	0.34	[252]
$5\nu_4^5$	F_2	6507.55	6505.66	1.89	[252]
$5\nu_4^5$	F_2	6539.18	6538.17	1.01	[252]
$\nu_2^1+4\nu_4^2$	F_2	6657.09	6657.88 [a]	-0.79	[263]
$\nu_2^1+4\nu_4^4$	F_2	6717.99	6715.72	2.27	[264]
$\nu_2^1+4\nu_4^4$	F_2	6733.11	6731.87	1.24	[264]
$\nu_1+3\nu_4^1$	F_2	6769.19	6769.51	-0.32	[264]
$\nu_1+3\nu_4^3$	F_2	6833.19	6833.46	-0.27	[264]
$\nu_3^1+3\nu_4^1$	F_2	6858.71	6858.84	-0.13	[264]
$2\nu_2^0+3\nu_4^1$	F_2	6869.79	6869.70	0.09	[264]
$\nu_3^1+3\nu_4^3$	F_2	6897.38	6896.88	0.50	[264]
$\nu_3^1+3\nu_4^1$	F_2	6910.38	6910.46	-0.08	[264]
$\nu_3^1+3\nu_4^1$	F_2	6924.97	6925.69	-0.72	[264]
$2\nu_2^2+3\nu_4^3$	F_2	6940.05	6939.69	0.36	[263]
$2\nu_2^2+3\nu_4^3$	F_2	6992.58	6992.15	0.43	[264]
$\nu_1+\nu_2^1+2\nu_4^2$	F_2	7035.18	7035.07	0.11	[264]
$2\nu_1+\nu_4^1$	F_2	7085.64	7086.77	-1.13	[264]
$\nu_2^1+\nu_3^1+2\nu_4^0$	F_2	7097.92	7098.61	-0.69	[264] [b]
$\nu_2^1+\nu_3^1+2\nu_4^2$	F_2	7116.39	7117.01	-0.62	[264]
$\nu_2^1+\nu_3^1+2\nu_4^2$	F_2	7131.14	7131.56	-0.42	[264]
$\nu_1+\nu_3^1+\nu_4^1$	F_2	7158.13	7159.05	-0.92	[264] [c]
$3\nu_2^3+2\nu_4^2$	F_2	7168.42	7168.23	0.19	[264]
$\nu_1+2\nu_2^2+\nu_4^1$	F_2	7225.43	7225.49	-0.06	[264]
$2\nu_3^0+\nu_4^1$	F_2	7250.54	7251.24	-0.70	[264]
$\nu_1+2\nu_2^0+\nu_4^1$	F_2	7269.44	7269.68	-0.24	[264]
$2\nu_3^2+\nu_4^1$	F_2	7299.44	7300.72	-1.28	[264]
$2\nu_2^0+\nu_3^1+\nu_4^1$	F_2	7331.05	7331.69	-0.64	[264]

(*Continued*)

Mode	Sym.	Experiment	Calculated	Obs−calc	Ref.
$2\nu_2^2+\nu_3^1+\nu_4^1$	F_2	7346.01	7346.10	-0.10	[264]
$2\nu_2^2+\nu_3^1+\nu_4^1$	F_2	7365.40	7365.35	0.05	[264]
$\nu_1+\nu_2^1+\nu_3^1$	F_2	7374.25	7374.42	-0.17	[264]
$4\nu_2^2+\nu_4^1$	F_2	7384.11	7384.03	0.08	[264]
$\nu_2^1+2\nu_3^2$	F_2	7510.34	7511.56	-1.22	[240]
$3\nu_2^1+\nu_3^1$	F_2	7575.86	7575.43	0.43	[264]
$3\nu_2^3+\nu_3^1$	F_2	7584.51	7583.50	1.01	[264]

[a] $P_{\max}=14$ value. [b] Assigned as $2\nu_1+\nu_4$ in TROVE. [c] Value of 7156.72 cm^{-1} reported by Ulenikov et al. [259].

Table 6.5: Comparison of calculated and experimental $J=0$ vibrational term values (in cm^{-1}) for $^{12}CH_4$ in the icosad region and above (see text for a discussion of the experimental uncertainties). The zero-point energy was computed to be 9708.846 cm^{-1} at the CVBS limit.

Mode	Sym.	Experiment	Calculated	Obs−calc	Ref.
$5\nu_4^5$	F_2	6377.53	6381.09 [a]	-3.56	[252]
$5\nu_4^1$	A_1	6405.89	6410.06 [a]	-4.17	[264]
$5\nu_4^3$	F_1	6429.20	6428.63	0.57	[264]
$5\nu_4^3$	E	6507.37	6505.12	2.25	[264]
$5\nu_4^5$	F_1	6529.74	6528.34	1.40	[264]
$\nu_2^1+4\nu_4^0$	E	6617.50	6615.81	1.69	[264]
$\nu_2^1+4\nu_4^2$	F_1	6638.52	6636.01	2.51	[264]
$\nu_2^1+4\nu_4^2$	A_1	6655.88	6655.99	-0.11	[264]
$\nu_2^1+4\nu_4^2$	E	6680.93	6680.84	0.09	[263]
$\nu_2^1+4\nu_4^4$	A_2	6682.82	6681.55	1.27	[264]
$\nu_2^1+4\nu_4^4$	F_1	6722.00	6719.33	2.67	[264]
$\nu_2^1+4\nu_4^4$	E	6729.60	6728.27	1.33	[263]
$\nu_2^1+4\nu_4^4$	A_1	6737.79	6737.18	0.61	[264]

(*Continued*)

Mode	Sym.	Experiment	Calculated	Obs−calc	Ref.
$\nu_2^1 + 4\nu_4^2$	A_2	6746.23	6745.40	0.83	[264]
$\nu_2^1 + 4\nu_4^4$	F_1	6755.38	6754.15	1.23	[264]
$\nu_2^1 + 4\nu_4^4$	E	6766.23	6765.13	1.10	[263]
$\nu_1 + 3\nu_4^1$	A_1	6809.40	6808.77	0.63	[264]
$\nu_1 + 3\nu_4^3$	F_1	6822.30	6821.92	0.38	[264]
$\nu_3^1 + 3\nu_4^1$	E	6862.74	6863.53	-0.79	[264]
$\nu_3^1 + 3\nu_4^1$	F_1	6862.85	6863.20	-0.35	[263]
$\nu_3^1 + 3\nu_4^1$	A_1	6863.10	6864.32	-1.22	[264]
$2\nu_2^2 + 3\nu_4^1$	F_1	6889.68	6889.53	0.15	[264]
$2\nu_2^2 + 3\nu_4^3$	F_2	6905.60	6905.65	-0.05	[264]
$\nu_3^1 + 3\nu_4^3$	E	6908.80	6908.84	-0.04	[264]
$\nu_3^1 + 3\nu_4^3$	F_1	6915.18	6915.22	-0.04	[264]
$\nu_3^1 + 3\nu_4^3$	A_2	6918.55	6918.95	-0.40	[264]
$\nu_3^1 + 3\nu_4^3$	F_1	6921.58	6921.75	-0.17	[264]
$\nu_3^1 + 3\nu_4^3$	A_1	6922.07	6923.24	-1.17	[264]
$\nu_3^1 + 3\nu_4^3$	E	6925.67	6927.00	-1.33	[264]
$2\nu_2^2 + 3\nu_4^1$	E	6938.40	6937.71	0.69	[264]
$2\nu_2^0 + 3\nu_4^1$	A_1	6940.10	6939.47	0.63	[264]
$2\nu_2^0 + 3\nu_4^3$	F_1	6945.16	6944.87	0.29	[263]
$2\nu_2^2 + 3\nu_4^3$	F_1	6949.70	6949.57	0.13	[264]
$2\nu_2^0 + 3\nu_4^3$	F_2	6962.42	6962.61	-0.19	[264]
$\nu_1 + \nu_2^1 + 2\nu_4^0$	E	6990.01	6990.06	-0.05	[264]
$\nu_1 + \nu_2^1 + 2\nu_4^2$	F_1	7020.43	7020.19	0.24	[264]
$\nu_1 + \nu_2^1 + 2\nu_4^2$	A_1	7024.03	7024.05	-0.02	[264]
$\nu_1 + \nu_2^1 + 2\nu_4^2$	E	7045.69	7045.89	-0.20	[264]
$\nu_1 + \nu_2^0 + 2\nu_4^2$	A_2	7056.56	7056.50	0.06	[264]
$\nu_2^1 + \nu_3^1 + 2\nu_4^0$	F_1	7085.73	7085.45	0.28	[264]
$\nu_2^1 + \nu_3^1 + 2\nu_4^0$	E	7107.28	7107.39	-0.11	[264]
$\nu_2^1 + \nu_3^1 + 2\nu_4^2$	A_2	7114.54	7114.43	0.11	[264]
$3\nu_2^1 + 2\nu_4^0$	E	7118.40	7118.32	0.08	[264]
$3\nu_2^3 + 2\nu_4^0$	A_1	7120.74	7120.58	0.16	[264]
$\nu_2^1 + \nu_3^1 + 2\nu_4^2$	F_2	7121.90	7122.10	-0.20	[264]

(*Continued*)

Mode	Sym.	Experiment	Calculated	Obs−calc	Ref.
$\nu_2^1+\nu_3^1+2\nu_4^2$	F_1	7130.90	7131.40	-0.50	[264]
$\nu_2^1+\nu_3^1+2\nu_4^2$	A_1	7132.50	7132.71	-0.21	[264]
$3\nu_2^3+2\nu_4^0$	A_2	7133.69	7133.51	0.18	[264]
$\nu_2^1+\nu_3^1+2\nu_4^2$	E	7134.00	7134.10	-0.10	[264]
$\nu_2^1+\nu_3^1+2\nu_4^2$	F_1	7139.23	7140.33	-1.10	[264]
$\nu_2^1+\nu_3^1+2\nu_4^2$	F_2	7141.50	7142.22	-0.72	[264]
$\nu_2^1+\nu_3^1+2\nu_4^2$	F_1	7151.02	7151.08	-0.06	[264]
$3\nu_2^1+2\nu_4^2$	F_1	7153.84	7153.86	-0.02	[264]
$\nu_1+\nu_3^1+\nu_4^1$	A_1	7157.16	7158.06	-0.90	[264]
$\nu_1+\nu_3^1+\nu_4^1$	E	7164.60	7165.63	-1.03	[264]
$\nu_1+\nu_3^1+\nu_4^1$	F_1	7165.60	7167.95	-2.35	[264]
$3\nu_2^3+2\nu_4^2$	E	7168.00	7168.62	-0.62	[264] [b]
$3\nu_2^1+2\nu_4^2$	A_1	7176.10	7176.09	0.01	[264]
$3\nu_2^3+2\nu_4^2$	F_1	7180.00	7180.01	-0.01	[264]
$3\nu_2^1+2\nu_4^2$	F_2	7191.05	7191.12	-0.07	[264]
$3\nu_2^3+2\nu_4^2$	E	7191.85	7191.45	0.40	[264]
$3\nu_2^1+2\nu_4^2$	E	7217.40	7217.22	0.18	[264]
$3\nu_2^1+2\nu_4^2$	A_2	7221.10	7220.74	0.36	[264]
$\nu_1+2\nu_2^2+\nu_4^1$	F_1	7246.01	7245.65	0.36	[264]
$2\nu_1+\nu_2^1$	E	7295.20	7296.34	-1.14	[264]
$2\nu_3^2+\nu_4^1$	E	7295.50	7298.40	-2.90	[264]
$2\nu_3^2+\nu_4^1$	F_1	7295.80	7297.66	-1.86	[264]
$2\nu_3^2+\nu_4^1$	A_1	7299.45	7300.32	-0.87	[264]
$2\nu_2^2+\nu_3^1+\nu_4^1$	F_1	7326.25	7326.94	-0.69	[264]
$2\nu_3^2+\nu_4^1$	F_2	7337.55	7339.75	-2.20	[264]
$2\nu_3^2+\nu_4^1$	F_1	7338.16	7340.03	-1.87	[264]
$2\nu_2^0+\nu_3^1+\nu_4^1$	A_1	7341.60	7341.87	-0.27	[264]
$2\nu_2^2+\nu_3^1+\nu_4^1$	E	7342.10	7342.38	-0.28	[264]
$2\nu_2^2+\nu_3^1+\nu_4^1$	F_1	7346.46	7346.66	-0.20	[264]
$2\nu_2^2+\nu_3^1+\nu_4^1$	A_2	7348.85	7349.29	-0.44	[264]
$2\nu_2^2+\nu_3^1+\nu_4^1$	E	7352.20	7352.48	-0.28	[264]
$2\nu_2^2+\nu_3^1+\nu_4^1$	A_1	7360.80	7361.31	-0.51	[264]

(*Continued*)

Mode	Sym.	Experiment	Calculated	Obs−calc	Ref.
$2\nu_2^0+\nu_3^1+\nu_4^1$	F_1	7368.88	7368.97	-0.09	[264]
$\nu_1+\nu_2^1+\nu_3^1$	F_1	7373.16	7373.97	-0.81	[264]
$4\nu_2^2+\nu_4^1$	F_1	7394.20	7393.64	0.56	[264]
$4\nu_2^4+\nu_4^1$	F_2	7408.20	7407.40	0.80	[264]
$4\nu_2^4+\nu_4^1$	F_1	7422.30	7421.35	0.95	[264]
$4\nu_2^2+\nu_4^1$	F_2	7436.30	7435.90	0.40	[264]
$\nu_1+3\nu_2^1$	E	7447.52	7447.83	-0.31	[264]
$\nu_1+3\nu_2^3$	A_2	7468.21	7467.33	0.88	[264]
$\nu_1+3\nu_2^3$	A_1	7468.50	7467.42	1.08	[264]
$\nu_2^1+2\nu_3^0$	E	7483.67	7483.79	-0.12	[264]
$\nu_2^1+2\nu_3^2$	F_1	7512.26	7513.39	-1.13	[264]
$\nu_2^1+2\nu_3^2$	E	7552.23	7553.79	-1.56	[264]
$\nu_2^1+2\nu_3^2$	A_1	7559.00	7560.60	-1.60	[264]
$3\nu_2^1+\nu_3^1$	F_1	7569.51	7569.25	0.26	[264]
$3\nu_2^3+\nu_3^1$	F_1	7580.90	7580.36	0.54	[264]
$2\nu_1+2\nu_4^2$	F_2	8388.00	8384.52	3.48	[259]
$\nu_1+\nu_3^1+2\nu_4^2$	F_2	8421.00	8422.37	-1.37	[259]
$\nu_1+2\nu_3^2$	F_2	8618.67	8613.92	4.75	[259]
$2\nu_1+\nu_3$	F_2	8808.95	8812.01 [a,c]	-3.06	[259]
$3\nu_3^1$	F_2	8907.30	8909.59	-2.29	[259]
$3\nu_3^3$	F_2	9045.96	9048.87	-2.91	[259]
$\nu_1+2\nu_3^0+\nu_4^1$	F_2	9888.47	9892.46 [a]	-3.99	[259]
$\nu_1+\nu_2+2\nu_3$	F_2	10115.67	[d]	–	[259]
$3\nu_3+\nu_4$	F_2	10265.59	[d]	–	[259]
$2\nu_1+\nu_2+\nu_3$	F_2	10302.17	[d]	–	[259]
$\nu_1+3\nu_3$	F_2	11276.31	11277.96 [c]	-1.65	[259]

[a] $P_{\max}=14$ value. [b] Assigned as $\nu_1+\nu_3+\nu_4$ in TROVE. [c] Unable to identify vibrational angular momentum quantum numbers. [d] Unable to identify energy level in TROVE.

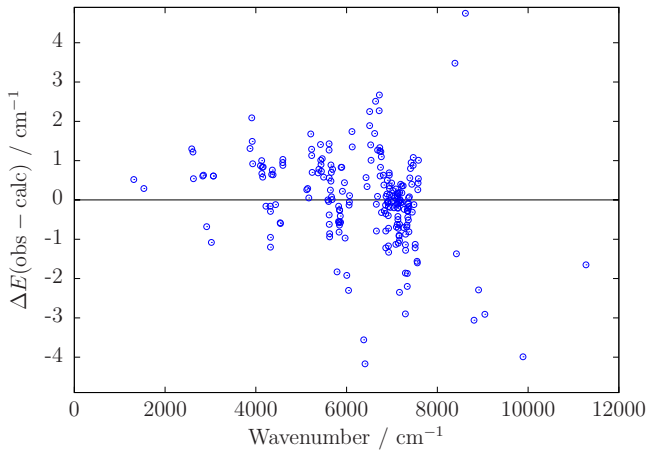

Figure 6.2: Residual errors ΔE(obs − calc) for all computed term values of $^{12}CH_4$ (see Tables 6.2, 6.4 and 6.5).

Table 6.6: Equilibrium C–H bond length of methane

r(C–H) / Å	Ref.	Approach
1.08601	This work	Purely *ab initio* PES
1.08598	This work	Refined geometry PES
1.08601(4)	[276]	Empirically adjusted PES
1.08609	[277]	Empirically refined PES
1.08595(30)	[285]	Combined experimental and *ab initio* analysis
1.086(2)	[286]	Quantum Monte Carlo calculations
1.0847	[244]	Effective Hamiltonian model
1.08553(4)	[265]	Effective Hamiltonian model

6.4.2 Equilibrium geometry and pure rotational energies

The value of r_{ref} used in Eq. (5.2) does not define the minimum of the PES because a linear expansion term has been included in the parameter set. The true equilibrium C–H bond length determined from the CBS-F12$^{\text{HL}}$ PES is listed in Table 6.6. It is in excellent agreement with previous values which is gratifying as it has been calculated in a purely *ab initio* fashion.

However, it is more informative to look at pure rotational energies as these are highly dependent on the molecular geometry through the moments of inertia. In Table 6.7, computed rotational energy levels up to $J = 10$ are compared against ex-

perimental values listed in Nikitin et al. [276] (originally attributed to the spherical top data system [220], which contains measurements from Oldani et al. [287]). Calculations were carried out with $P_{\max} = 12$ which is sufficient for converging ground state rotational energies.

Table 6.7: Comparison of calculated and experimental $J \leq 10$ pure rotational energy levels (in cm^{-1}) for $^{12}CH_4$. The experimental ground state values are from Nikitin et al. [276] but are originally attributed to the spherical top data system [220]. Computed values correspond to the *ab initio* geometry (A) and the empirically refined geometry (B) (see text).

J	K	Sym.	Experiment	Calc. (A)	Calc. (B)	Obs−calc (A)	Obs−calc (B)
0	0	A_1	0.00000	0.00000	0.00000	0.00000	0.00000
1	1	F_1	10.48165	10.48105	10.48164	0.00060	0.00001
2	1	F_2	31.44239	31.44061	31.44235	0.00178	0.00004
2	2	E	31.44212	31.44034	31.44209	0.00178	0.00003
3	1	F_2	62.87684	62.87329	62.87678	0.00355	0.00006
3	2	A_2	62.87817	62.87462	62.87811	0.00355	0.00006
3	3	F_1	62.87578	62.87222	62.87571	0.00356	0.00007
4	0	A_1	104.77284	104.76692	104.77274	0.00592	0.00010
4	1	F_1	104.77470	104.76879	104.77460	0.00591	0.00010
4	2	E	104.77603	104.77012	104.77594	0.00591	0.00009
4	3	F_2	104.78001	104.77411	104.77993	0.00590	0.00008
5	1	F_1	157.12434	157.11548	157.12420	0.00886	0.00014
5	2	E	157.13719	157.12837	157.13709	0.00882	0.00010
5	3	F_1	157.13892	157.13010	157.13882	0.00882	0.00010
5	5	F_2	157.12793	157.11908	157.12780	0.00885	0.00013
6	1	F_2	219.91505	219.90268	219.91487	0.01237	0.00018
6	2	A_2	219.91985	219.90750	219.91969	0.01235	0.00016
6	3	F_1	219.94126	219.92897	219.94117	0.01229	0.00009
6	4	A_1	219.94523	219.93295	219.94515	0.01228	0.00008
6	5	F_2	219.93677	219.92446	219.93666	0.01231	0.00011
6	6	E	219.91346	219.90109	219.91328	0.01237	0.00018
7	1	F_1	293.12299	293.10652	293.12277	0.01647	0.00022
7	1	F_2	293.12655	293.11010	293.12634	0.01645	0.00021
7	2	A_2	293.15420	293.13783	293.15408	0.01637	0.00012
7	3	F_2	293.16457	293.14823	293.16448	0.01634	0.00009

(*Continued*)

J	K	Sym.	Experiment	Calc. (A)	Calc. (B)	Obs−calc (A)	Obs−calc (B)
7	5	F_1	293.17868	293.16238	293.17864	0.01630	0.00004
7	6	E	293.17013	293.15381	293.17007	0.01632	0.00006
8	0	A_1	376.73044	376.70932	376.73019	0.02112	0.00025
8	1	F_1	376.73372	376.71261	376.73349	0.02111	0.00023
8	2	E	376.82129	376.80044	376.82133	0.02085	-0.00004
8	3	F_1	376.80478	376.78388	376.80476	0.02090	0.00002
8	3	F_2	376.82627	376.80544	376.82632	0.02083	-0.00005
8	5	F_2	376.78587	376.76492	376.78581	0.02095	0.00006
8	6	E	376.73565	376.71454	376.73541	0.02111	0.00024
9	1	F_1	470.71696	470.69064	470.71670	0.02632	0.00026
9	1	F_2	470.72034	470.69403	470.72009	0.02631	0.00025
9	2	E	470.79897	470.77290	470.79898	0.02607	-0.00001
9	3	F_1	470.80528	470.77923	470.80531	0.02605	-0.00003
9	4	A_1	470.83096	470.80498	470.83106	0.02598	-0.00010
9	5	F_2	470.86506	470.83918	470.86528	0.02588	-0.00022
9	6	A_2	470.87292	470.84707	470.87315	0.02585	-0.00023
9	7	F_1	470.85500	470.82910	470.85517	0.02590	-0.00017
10	1	F_1	575.18430	575.15264	575.18447	0.03166	-0.00017
10	1	F_2	575.05266	575.02059	575.05242	0.03207	0.00024
10	2	A_2	575.05567	575.02361	575.05544	0.03206	0.00023
10	3	F_2	575.17008	575.13837	575.17019	0.03171	-0.00011
10	5	F_1	575.25978	575.22834	575.26020	0.03144	-0.00042
10	6	E	575.27192	575.24050	575.27236	0.03142	-0.00044
10	7	F_2	575.28542	575.25405	575.28589	0.03137	-0.00047
10	8	A_1	575.22292	575.19137	575.22321	0.03155	-0.00029
10	10	E	575.05127	575.01920	575.05101	0.03207	0.00026

The CBS-F12$^{\mathrm{HL}}$ PES consistently underestimates ground state rotational energy levels and the residual error increases systematically by about $0.00060\,\mathrm{cm}^{-1}$ at each step up in J. Overall, the 51 energies are reproduced with a rms error of $0.02008\,\mathrm{cm}^{-1}$. This is around two orders of magnitude larger than the empirically adjusted PES of Nikitin et al. [276] which yields an identical value of r(C–H)= 1.08601 Å for the C–H bond length but a rms error of $0.00029\,\mathrm{cm}^{-1}$.

To help explain this discrepancy it is relatively straightforward to improve the

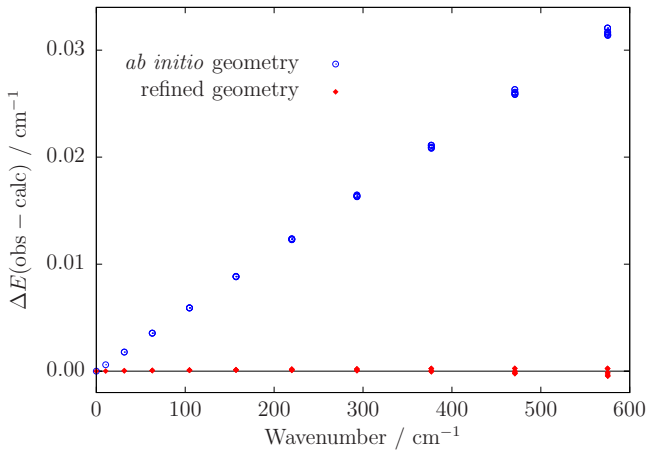

Figure 6.3: Residual errors $\Delta E(\text{obs} - \text{calc})$ for computed pure rotational energies using the *ab initio* and empirically refined equilibrium geometry (see Table 6.7).

CBS-F12$^{\text{HL}}$ results by refining the equilibrium geometry. This is done through a nonlinear least-squares fitting to the experimental energy levels and can improve the accuracy of computed intra-band rotational wavenumbers as we saw for SiH_4 in Chapter 5. After two iterations refining the parameter r_{ref}, the experimental energy levels up to $J = 10$ are reproduced with a rms error of $0.00018\,\text{cm}^{-1}$ (see Table 6.7 and Fig. 6.3) and this corresponds to a bond length of $r(\text{C–H}) = 1.08598\,\text{Å}$ (also given in Table 6.6). This value is within the uncertainty of the bond length from Nikitin et al. [276] and is remarkably close to the original *ab initio* result. However, I have refrained from adopting the new equilibrium geometry for the CBS-F12$^{\text{HL}}$ PES as it leads to a poorer description of vibrational energies (see Table 5.3 in Sec. 5.4.2), which were the main focus of this work.

6.5 Chapter summary and further work

In this chapter the knowledge acquired from treating CH_3Cl and SiH_4 has been used to construct and test a new nine-dimensional PES for methane. The CBS-F12$^{\text{HL}}$ PES is one of the most accurate *ab initio* surfaces to date. This is confirmed by the achievement of sub-wavenumber accuracy for a considerable number of vibrational energy levels including those at higher energies. The computed *ab initio* equilibrium C–H bond length displayed excellent agreement with previous values,

however, systematic errors arose in calculated pure rotational energies of $^{12}CH_4$. These errors were significantly reduced by adjusting the equilibrium geometry of the CBS-F12^{HL} PES. The resultant bond length was remarkably close to the original *ab initio* value and still consistent with prior studies.

Despite the advances in electronic structure theory the best *ab initio* PES is rarely accurate enough for the requirements of high-resolution spectroscopy and empirical refinement is a necessary step. Although computationally intensive, refinement can produce orders-of-magnitude improvements in the accuracy of computed rovibrational energy levels. It is natural then to question the benefit of using sophisticated methods with large basis sets to generate the original *ab initio* surface. Whilst a better *ab initio* PES will lead to a superior refinement, at some stage the gain in accuracy when simulating rovibrational spectra will not correlate with the computational cost of improving the underlying *ab initio* surface. For this reason I believe that more sophisticated electronic structure calculations to improve the CBS-F12^{HL} PES are not worthwhile at the present time. The CBS-F12^{HL} PES is currently being refined by other members of the ExoMol project before work on a new methane line list begins.

I have computed a new DMS for methane at the CCSD(T)/aug-cc-pVQZ level of theory but because this surface has not undergone rigorous testing yet, I did not discuss its construction in this chapter. A preliminary plot of computed absolute line intensities at room temperature (296 K) using the new DMS is shown in Fig. 6.4. Calculations were carried out with a medium-sized rovibrational basis set ($P_{\max} = 10$) and include transitions up to $J = 10$. In Fig. 6.4, intensities have been simulated using a DMS calculated at the CCSD(T)-F12/cc-pVTZ-F12 level of theory [68], which was utilized for the 10to10 methane linelist [5]. Whilst there are subtle differences between the two plots, notably around 8000 cm^{-1} and above, it is difficult to know which DMS would be more reliable at higher frequencies. A comparison with experiment of absolute line intensities using both DMSs is necessary before deciding on which one to use for a new line list.

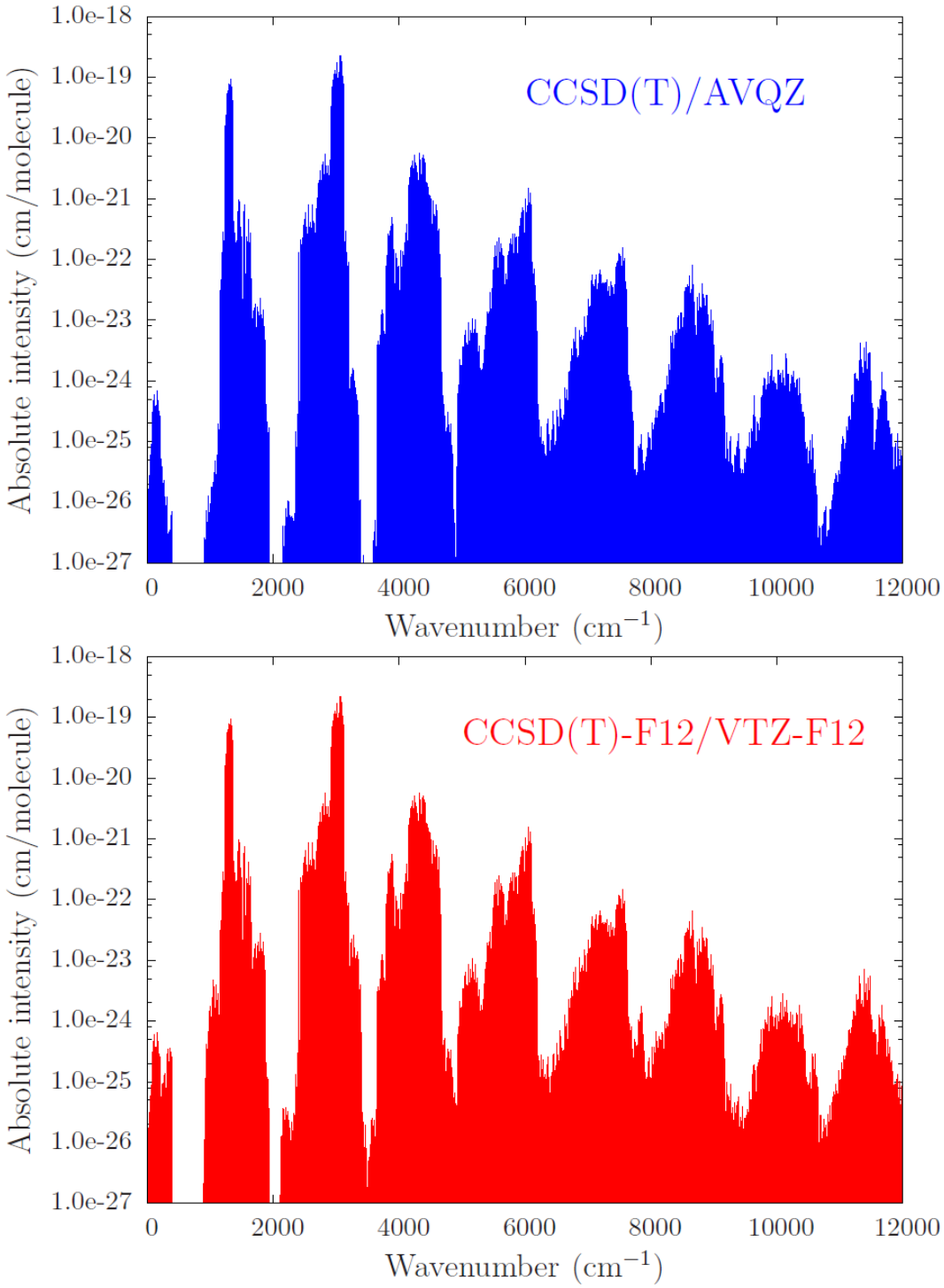

Figure 6.4: Comparison of absolute line intensities computed using two different DMSs for $^{12}CH_4$ up to $J = 10$. The two DMSs utilized were calculated at the CCSD(T)/aug-cc-pVQZ (top panel) and CCSD(T)-F12/cc-pVTZ-F12 [68] (bottom panel) levels of theory.

7 Mass sensitivity of rotation-vibration energy levels of XY_3-type molecules

7.1 Introduction

Molecules are an attractive testing ground for probing two particular dimensionless fundamental constants. Electronic transitions are sensitive to the fine structure constant α, whilst vibration, rotation and inversion transitions are sensitive to the proton-to-electron mass ratio $\mu = m_p/m_e$. If any variation did exist it would manifest as observable shifts in the transition frequencies of certain molecular species. Such shifts can be detected by high-precision laboratory experiments over short time scales (years), or from astronomical observation of spectral lines at high redshift. The idea that the fundamental constants of nature may be understood within the framework of a deeper cosmological theory dates back to Dirac [288]. As of yet there is no theoretical justification for the values they assume, or even if they have always had the same values that we measure today.

Research in the field has become more active after claims of a temporal variation in the fine structure constant, where observations of atomic absorption spectra of distant quasars suggested that α was smaller in the past [289]. A few years later, measurements of H_2 spectra indicated that the proton-to-electron mass ratio was larger by 0.002% up to twelve billion years ago [290]. Numerous studies have followed and these have all produced null results (see Ref. [291] for a detailed review). Any cosmological variation in the fundamental constants would require new physics beyond the Standard Model and as such, results are received with caution and must

be confirmed, or refuted, with independent studies on different atomic and molecular absorbers.

This leads naturally to the question of which molecular systems are most suitable. From an experimental perspective, measurements in the laboratory provide greater control over systematic effects and any gas of molecules can be utilized. However, this provides only a local constraint on a drifting constant and it could be argued that even a null result would be limited to the age of the Solar System (around 4.6 billion years) and that a variation of μ could have occurred at earlier stages in the evolution of the Universe. More desirable are molecular systems which are astronomically relevant because observation at different redshifts presents the opportunity to look back to much earlier times in the Universe. Detection in a wide variety of cosmological settings also lends itself to searches for possible spatial variations of μ.

The most important criterion is that the molecule must possess transitions which are noticeably shifted by a change in the respective constant, as not all of them are. Since we are dealing with rotation-vibration spectroscopy, in this chapter we focus on transitions sensitive to a variation in the proton-to-electron mass ratio. It is possible to quantify the sensitivity of a transition through the calculation of sensitivity coefficients. We will discuss the most common methods used to do this in Sec. 7.2 before introducing a new variational approach. This approach will then be employed to investigate ammonia and hydronium in Sec. 7.3 and 7.4, respectively. In Sec. 7.5 the contents of this chapter are summarised.

7.2 Calculating sensitivity coefficients

The sensitivity coefficient $T_{u,l}$, defined as

$$T_{u,l} = \frac{\mu}{E_u - E_l}\Big(\frac{\mathrm{d}E_u}{\mathrm{d}\mu} - \frac{\mathrm{d}E_l}{\mathrm{d}\mu}\Big), \tag{7.1}$$

where E_u and E_l refer to the energy of the upper and lower state, respectively, allows one to quantify the effect that a possible variation of μ would have for a given transition. The larger the magnitude of $T_{u,l}$, the more favourable a transition is to test for a drifting μ. The resulting sensitivities can then be used to determine the induced frequency shift of a probed transition, given by the expression

$$\frac{\Delta\nu}{\nu_0} = T_{u,l}\frac{\Delta\mu}{\mu_0}, \tag{7.2}$$

where $\Delta\nu = \nu_{\text{obs}} - \nu_0$ is the change in the frequency, and $\Delta\mu = \mu_{\text{obs}} - \mu_0$ is the change in μ, both with respect to their present day values ν_0 and μ_0.

Various methods have been utilized to compute sensitivity coefficients for a range of molecular systems. We will briefly discuss the most common before introducing a new variational approach.

7.2.1 Semi-classical WKB approximation

To determine sensitivity coefficients for inversion or tunnelling frequencies, the semi-classical Wentzel-Kramers-Brillouin (WKB) approximation has been applied to astronomically important molecules such as NH_3 [292], H_3O^+ [293], and H_2O_2 [294]. A general relationship of the form,

$$T_{\text{inv}} \approx \frac{1+S}{2}\frac{SE_0}{2(\Delta U - E_0)}, \tag{7.3}$$

where S is the action over the classically forbidden region, E_0 the ground state vibrational energy and ΔU the barrier height, was derived to predict sensitivities. The dependence on μ enters through the action S.

This approach is limited in accuracy however, providing only a semi-quantitative estimate for sensitivity coefficients. More reliable methods, for example a one-dimensional inversion Hamiltonian model [292, 293], are often used alongside the semi-classical WKB approximation to confirm results. The method is also limited to inversion or tunnelling modes only, and for coupled motion more rigorous ap-

proaches are necessary.

7.2.2 Effective Hamiltonian models

An effective Hamiltonian is one that describes only a portion of the eigenvalue spectrum of the true Hamiltonian. They are used throughout spectroscopy and provide a way of condensing detailed experimental spectra into a manageable number of parameters. The form they assume will depend on the system and region of the spectrum being studied, but they are always much easier to handle and interpret compared to the true Hamiltonian.

The most common approach to computing sensitivity coefficients for a molecule makes use of an effective Hamiltonian model, and determining how the parameters of this model depend on μ [293, 295–300]. By establishing scaling relations for the parameters, one essentially knows how each energy level depends on μ. This information can be used in Eq. (7.1) to calculate sensitivity coefficients for transitions of interest.

This method was successfully applied to methanol [295, 296], and led to numerous astronomical measurements to determine a constraint on the proton-to-electron mass ratio [296, 297, 301–304]. So far the most robust constraint was determined from methanol absorption spectra observed in the lensing galaxy PKS1830−211 [304]. The three measured transitions possessed sensitivity coefficients ranging from $T = -1.0$ to -7.4, and produced a constraint of $\dot{\mu}/\mu < 2 \times 10^{-17}\,\mathrm{yr}^{-1}$ assuming a linear rate of change. This translates to no change in μ over the past ≈ 7.5 billion years. Note that this bound is in agreement with the best laboratory constraint to date, which measured optical transitions in $^{171}\mathrm{Yb}^{+}$ ions to derive $\dot{\mu}/\mu = (0.2 \pm 1.1) \times 10^{-16}\,\mathrm{yr}^{-1}$ [305], again assuming a linear rate of change.

A disadvantage of the effective Hamiltonian approach is that it is restricted to only part of the spectrum. It is usually not possible to confidently extrapolate to other regions. The accuracy of the resultant sensitivity coefficients is also limited by the methods used to establish the scaling of the parameters of the model with μ. The

procedure used to find the μ-dependence can differ depending on the parameter, with some determined from experimental information and others by purely theoretical means.

7.2.3 Non-rigid inverter theory

The non-rigid inverter (NRI) theory for XY_3 pyramidal molecules was pioneered by Špirko [306, 307]. It is an example of an effective Hamiltonian model which uses perturbation theory to solve the Schrödinger equation to obtain rotation-vibration energy levels. The approach employs a flexible 'non-rigid' reference configuration which follows a large-amplitude motion (e.g. for NH_3 this is the inversion 'umbrella-flipping' motion). Vibrations of the molecule are then treated as small-amplitude displacements from the reference configuration. This concept was first introduced for triatomic molecules in the influential work of Hougen, Bunker, and Johns (HBJ) [308]. The choice of molecular coordinates is such that it enables maximum separation of the different types of molecular motion, facilitating solution of the Schrödinger equation.

Sensitivity coefficients for vibration-rotation-inversion transitions of $^{14}NH_3$ were computed using the NRI theory [309]. Notably, a set of several "forbidden" $\Delta k = \pm 3$ transitions between the rotation-inversion energy levels in the ν_2 vibrational state were proposed as a promising tool to probe a possible space-time variation of μ. One particular transition between the $|-, J = 3, K = 3, v_2 = 1\rangle$ and $|+, J = 3, K = 0, v_2 = 1\rangle$ roinversional states, where $-$ and $+$ refer to antisymmetric and symmetric respectively, possessed an extremely large sensitivity of $T = -853.1$. This was lower than a previous 'Born-Oppenheimer' estimate of $T = -938$ [310] and reflects the improvement in methodology. However, theoretical calculations of the sensitivities using perturbation theory may not be entirely robust since the numerator and denominator in Eq. (7.1) contain differences of large numbers.

7.2.4 Variational approach

Here we propose a robust and accurate variational approach which offers a new way to compute sensitivity coefficients. The key assumption is that all baryonic matter may be treated equally [311], and so μ is assumed to be proportional to the molecular mass. This assumption has previously been employed in the effective Hamiltonian and NRI methods discussed in Sec. 7.2.2 and Sec. 7.2.3, respectively.

It is sufficient then to perform a series of calculations employing suitably scaled values for the masses of the atoms. We choose the scaling coefficient $f_m = \{0.9996, 0.9998, 1.0000, 1.0002, 1.0004\}$ such that the scaled mass, $m' = f_m \times m$. The mass dependency of any energy level can be found by using finite differences for (a) the $f_m = \{0.9998, 1.0002\}$, and (b) the $f_m = \{0.9996, 1.0004\}$ calculated energies. Both (a) and (b) should yield identical results, with the latter values used to verify the former. Numerical values for the derivatives $\mathrm{d}E/\mathrm{d}\mu$ are easily determined and then used in Eq. (7.1), along with accurate values for the transition frequencies, to calculate sensitivity coefficients. Calculations with $f_m = 1.0000$ provide theoretical frequency data and Einstein A coefficients.

The variational approach is powerful in that it allows a comprehensive treatment of a molecule to be undertaken. All possible transitions and their mass dependence can be calculated. This permits a simple exploration of the sensitivities for any molecule, provided the necessary steps have been taken to perform accurate variational calculations in the first place. Along with sensitivity coefficients, reliable theoretical transition frequencies can be generated if no experimental data is available, and for all selected transitions Einstein A coefficients can be calculated to guide future observations.

7.3 Ammonia (NH_3)

The so-called ammonia method [292], which was adapted from van Veldhoven et al. [312], relies on inversion transitions in the vibrational ground state of $^{14}NH_3$.

Constraints on a temporal variation of μ have been determined using this method from measurements of the object B0218+357 at redshift $z \sim 0.685$ [292, 313, 314], and of the system PKS1830−211 at $z \sim 0.886$ [315]. A major source of systematic error when using the ammonia method is the comparison with rotational lines from other molecular species, particularly molecules that are non-nitrogen-bearing (see Murphy et al. [313], Henkel et al. [315], and Kanekar [314] for a more complete discussion). The most stringent limit using ammonia [314] has since been improved upon with methanol absorption transitions measured in the gravitational lens PKS1830−211 [304].

As mentioned in Sec. 7.2.3, several "forbidden" $\Delta k = \pm 3$ transitions of $^{14}NH_3$ in the ν_2 vibrational state were investigated using the NRI theory and found to possess extremely large sensitivity coefficients [309]. The semi-classical Wentzel-Kramers-Brillouin (WKB) approximation has also been employed to obtain a general relationship to estimate the sensitivity of pure inversion frequencies in the ground vibrational state for $^{14}NH_3$ [292], $^{15}NH_3$ [316], $^{14}ND_3$ [292], and $^{15}ND_3$ [312], whilst rotation-inversion transitions have been considered for the partly deuterated species $^{14}NH_2D$ and $^{14}ND_2H$ by Kozlov et al. [317].

Because of the abundance of NH_3 throughout the Universe and the ease with which its spectrum can be observed, identifying more transitions with large sensitivities in the microwave, submillimetre or far infrared regions could lead to a much tighter constraint on μ. Several $^{14}NH_3$ rotation-inversion transitions have already been observed extraterrestrially [318–320], whilst others with notable sensitivities possess Einstein A coefficients comparable to those of the observed transitions. It is legitimate then to expect their eventual extragalactic detection, and when combined with their enhanced sensitivity, there is scope for a major improvement of the current ammonia analyses.

Rotation-inversion transitions associated with the ν_2 vibrational state can display induced frequency shifts more than one order of magnitude larger than the pure inversion transitions in the vibrational ground state, which are currently used

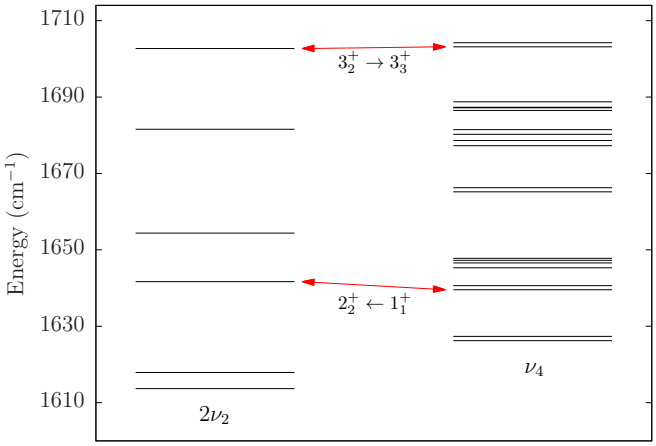

Figure 7.1: Accidental near-degeneracies between the $2\nu_2$ and ν_4 rotation-vibration energy levels of ammonia. Energy levels are labelled as $J_K^{\pm}$. For illustrative purposes only part of the rovibrational manifold is shown.

in the probing of μ both temporally [292, 313–315, 321] and spatially [322–325]. As shown in Fig. 7.1, numerous accidental near-degeneracies occur between the $2\nu_2$ and ν_4 rovibrational energy levels of ammonia. The strong Coriolis interaction between these two states [326] can give rise to highly anomalous sensitivities. Furthermore, a large number of transitions between these levels have been measured experimentally [327, 328].

Another promising anomaly exhibited by the spectra of ammonia is caused by the so-called "giant" ℓ-type doubling, which leads to a "reversal" of the inversion doublets in the $K = 1$ levels in the $+\ell$ component of the ν_4 states of $^{14}NH_3$ and $^{15}NH_3$. The inversion doublets are reversed because for $K = 1$, only one of the A_1 or A_2 sublevels is shifted by the Coriolis interactions, and only the A_2 states have non-zero spin statistical weights (see Fig. 7.2 and Špirko et al. [306]). So far these transitions have not been detected extraterrestrially. This is to be expected since the physical temperatures prevailing in the interstellar medium are too low to provide significant population of the aforementioned states. However, they could be effectively populated by exoergic chemical formation processes, resulting in the detection of highly excited states [329, 330]. Interestingly, the "highest energy" $(J, K) = (18, 18)$ line of $^{14}NH_3$ observed towards the galactic centre star forming

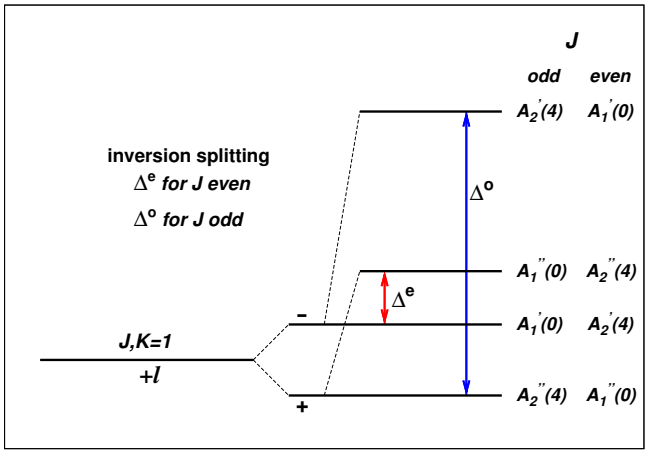

Figure 7.2: "Reversal" of the inversion doublets in the $+\ell$ component of the ν_4 level by the "giant" ℓ-type doubling effect. Values in parentheses are the spin statistical weights.

region Sgr B2, corresponds to the state lying 3130 K above the ground vibrational state [331].

Here, a comprehensive study of the mass sensitivity of the vibration-rotation-inversion transitions of $^{14}NH_3$, $^{15}NH_3$, $^{14}ND_3$, and $^{15}ND_3$ is performed. A rigorous evaluation of the sensitivity coefficients will hopefully offer new scope for the ammonia method and could potentially eliminate the systematic errors which arise from using alternative reference molecules. We also note that the transitions of the ^{15}N isotopes are optically thin and free of nuclear quadrupole structures, thus providing a simpler radiative and line-shape analysis.

7.3.1 Variational calculations

The nuclear motion program TROVE [9] has provided highly accurate theoretical frequency, intensity, and thermodynamic data for both $^{14}NH_3$ and $^{15}NH_3$ [61, 85, 332–335]. I utilized the computational setup and potential energy and dipole moment surfaces described in Yurchenko et al. [333] and Yurchenko [335], which can naturally be extended to treat $^{14}ND_3$ and $^{15}ND_3$. I provide a short summary of the

key aspects below.

The "spectroscopic" PES is based on extensive CCSD(T) calculations with extrapolation to the CBS limit [336], and was refined to experimental data up to $J \leq 8$ [85]. The *ab initio* DMS was computed at the CCSD(T)/aug-cc-pVQZ level of theory. Symmetry adapted expansions which respect $\boldsymbol{D}_{3h}(M)$ symmetry were used to represent the PES and DMS. Both surfaces have previously been used in the calculation of comprehensive line lists for $^{14}NH_3$ [333] and $^{15}NH_3$ [335]. Nuclear motion calculations were carried out with $P_{max} = 28$, and with the kinetic and potential energy operators truncated at 6th and 8th order, respectively.

As a cross-check to the variational approach, sensitivity coefficients have also been computed by Professor Vladimir Špirko using the non-rigid inverter theory [306, 307]. Note that the standard Herzberg convention [337] is used to label the vibrational states of ammonia with the normal mode quantum numbers v_1, v_2, v_3, v_4, l_3 and l_4. The ν_2 state corresponds to the singly excited inversion mode $v_2 = 1$, whilst ν_4 is the singly excited antisymmetric bending mode $v_4 = |l_4| = 1$ (see Down et al. [338] for more details).

7.3.2 Results

$^{14}NH_3$ and $^{15}NH_3$

The variationally calculated sensitivities for $^{14}NH_3$ and $^{15}NH_3$ are listed in Tables 7.1 to 7.6. The results are consistent with perturbative values obtained using the non-rigid inverter theory approach [309], and 'Born-Oppenheimer' estimates from Jansen et al. [310] (subsequently referred to as JBU). For transitions involving the ν_2 vibrational states shown in Tables 7.1, 7.2, 7.3, 7.4, the agreement is near quantitative with the exception of the "forbidden" combination difference $|-, J{=}3, K{=}3, v_2{=}1\rangle - |+, J{=}3, K{=}0, v_2 {=}1\rangle$ of $^{14}NH_3$. We expect this is due to the breakdown of the perturbational approach.

On closer inspection of Tables 7.3 and 7.4, the different sensitivities for the $|-, J{=}3, K{=}3, v_2{=}1\rangle - |+, J{=}3, K{=}0, v_2 {=}1\rangle$ resonances when going from $^{14}NH_3$ to

Table 7.1: The rotation-inversion frequencies (ν), Einstein coefficients (A), and sensitivities (T) of $^{14}NH_3$ and their $^{15}NH_3$ counterparts in the ν_2 vibrational state.

Γ'	p'	J'	K'	v_2'	Γ''	p''	J''	K''	v_2''	ν/MHz	A/s^{-1}	T
								$^{14}NH_3$				
E''	+	2	1	1	E'	−	1	1	1	140142[a]	0.1474×10^{-4}	17.24 (16.92[b])
A_2''	−	0	0	1	A_2'	+	1	0	1	466244[c]	0.1824×10^{-2}	-6.587 (-6.409)
								$^{15}NH_3$				
E''	+	2	1	1	E'	−	1	1	1	175053	0.2939×10^{-4}	13.33 (13.28)
A_2''	−	0	0	1	A_2'	+	1	0	1	430038	0.1425×10^{-2}	-6.894 (-6.908)

$^{14}NH_3$: Values in parentheses from Špirko [309], obtained using the NRI theory. [a]Astronomical observation from Mauersberger, Henkel, and Wilson [318] and Schilke et al. [319]; [b]JBU sensitivity coefficient has a value of 18.8 (see Jansen et al. [310]); [c]Astronomical observation from Schilke et al. [320]. $^{15}NH_3$: Frequencies from Urban et al. [339]; values in parentheses obtained using the NRI theory with the frequencies from Urban et al. [339].

$^{15}NH_3$ is of particular interest. A possible variation of μ requires the measurement of at least two transitions with differing sensitivities. Both isotopologues possess a large value of T and importantly they are of opposite sign, thus enabling a conclusive detection with regard to these particular transitions. An all-ammonia observation of a drifting μ would circumvent some of the intrinsic difficulties that appear when using other reference molecules [313–315], which may not necessarily reside at the same location in space.

The inversion frequencies in the ground vibrational state, shown in Table 7.5, have comparable sensitivities for both $^{14}NH_3$ and $^{15}NH_3$, and this also holds true for the rotation-inversion transitions shown in Table 7.6, demonstrating the validity of $^{15}NH_3$ as a probe of μ. The sensitivity coefficients of the ν_4 transitions shown in Table 7.7, although promising, do not acquire the impressive magnitudes of their ν_2 counterparts.

In Fig. 7.3, we have simulated the intensities at room temperature for 38 previously observed transitions between the $2\nu_2$ and ν_4 vibrational states of $^{14}NH_3$ from Ref. [327, 328] and plotted their corresponding sensitivity coefficients. The largest difference in sensitivity is $\Delta T = 59.6$, which is over nine times more sensitive than the ΔT of the methanol lines used to establish the most robust constraint to

Table 7.2: The wavenumbers (ν), wavelengths (λ), Einstein coefficients (A), and sensitivities (T) for transitions between the ground and ν_2 vibrational state of $^{14}NH_3$ and their $^{15}NH_3$ counterparts.

Γ'	p'	J'	K'	v_2'	Γ''	p''	J''	K''	v_2''	ν/cm^{-1}	$\lambda/\mu\text{m}$	A/s^{-1}	T
									$^{14}NH_3$				
A_2'	+	6	6	1	A_2''	−	6	6	0	927.3230	10.7837	$0.1316\times10^{+2}$	-0.367 (-0.356)
E'	+	2	2	1	E''	−	2	2	0	931.3333	10.7373	$0.1030\times10^{+2}$	-0.371 (-0.366)
E''	+	2	1	1	E'	−	1	1	0	971.8821	10.2893	$0.5238\times10^{+1}$	-0.399 (-0.394)
E''	+	1	1	1	E'	−	2	1	0	891.8820	11.2122	$0.6795\times10^{+1}$	-0.344 (-0.339)
A_2'	+	1	0	1	A_2''	−	2	0	0	892.1567	11.2088	$0.9054\times10^{+1}$	-0.344 (-0.339)
A_2''	+	3	3	1	A_2'	−	3	3	0	930.7571	10.7439	$0.1158\times10^{+2}$	-0.370 (-0.366)
									$^{15}NH_3$				
A_2'	+	6	6	1	A_2''	−	6	6	0	923.4541	10.8289	$0.1290\times10^{+2}$	-0.365 (-0.365)
E'	+	2	2	1	E''	−	2	2	0	927.4034	10.7828	$0.1010\times10^{+2}$	-0.373 (-0.373)
E''	+	2	1	1	E'	−	1	1	0	967.8597	10.3321	$0.5133\times10^{+1}$	-0.400 (-0.400)
E''	+	1	1	1	E'	−	2	1	0	888.0413	11.2607	$0.6664\times10^{+1}$	-0.345 (-0.345)
A_2'	+	1	0	1	A_2''	−	2	0	0	888.3174	11.2572	$0.8878\times10^{+1}$	-0.346 (-0.346)
A_2''	+	3	3	1	A_2'	−	3	3	0	926.8378	10.7894	$0.1135\times10^{+2}$	-0.372 (-0.372)

$^{14}NH_3$: Wavenumbers from Urban et al. [340]; Astronomical observations reported in Betz et al. [341] and Evans et al. [342]; values in parentheses from Špirko [309], obtained using the NRI theory. $^{15}NH_3$: Wavenumbers provided by Fusina et al. [343]; values in parentheses obtained using the NRI theory with the frequencies from Fusina et al. [343].

date [304], and over seventeen times larger than the ΔT of the transitions utilized in the ammonia method [292]. As well as being consistently large, the mixture of positive and negative sensitivities is highly beneficial for detecting a change in μ as transitions are shifted in opposing directions. From Fig. 7.3, one could imagine scanning this frequency window at two separate instances in time to produce a displaced spectrum if any variation of μ had occurred. In addition to the frequencies of Ref. [327, 328], there are 153 transitions with similar Einstein A coefficients and sensitivities from $T = -32.40$ to 17.27 in the frequency range 100 to 900 GHz. I provide comprehensive tables of all investigated transitions in Appendix B.

The accuracy of the calculated sensitivity coefficients will depend on the experimental frequencies and the computed TROVE numerical derivatives. For the $2\nu_2 \leftrightarrow \nu_4$ transitions it has been possible to investigate this further. A recent analysis of 56 sources of high-resolution $^{14}NH_3$ spectra utilizing the MARVEL procedure determined 4961 rovibrational energy levels of experimental quality, all labelled us-

Table 7.3: The vibration-rotation-inversion transitions of $^{14}NH_3$ associated with the $|-, J, K{=}3, v_2{=}1\rangle - |+, J, K{=}0, v_2 = 1\rangle$ resonances.

Γ'	p'	J'	K'	v_2'	Γ''	p''	J''	K''	v_2''	ν/MHz	A/s^{-1}	T	Ref.
A_2'	−	3	3	1	A_2''	+	3	3	0	29000313.7	$0.1176\times10^{+2}$	-0.484 (-0.484)	[344]
A_2'	+	3	0	1	A_2''	+	3	3	0	28997430.0	0.2025×10^{0}	-0.405 (-0.405)	[344]
	−	3	3	1		+	3	0	1	2883.7		-790.6 (-1001[a])	[344]
A_2'	−	3	3	1	A_2''	−	2	0	1	772594.9	0.6018×10^{-4}	-0.868 (-0.868)	[345]
A_2'	+	3	0	1	A_2''	−	2	0	1	769710.2	0.3471×10^{-2}	2.090 (2.089)	[345]
	−	3	3	1		+	3	0	1	2884.7		-790.3 (-1001)	[345]
A_2'	−	3	3	1	A_2''	+	3	3	1	1073050.7	0.1634×10^{-1}	-3.350 (-3.353)	[345]
A_2'	+	3	0	1	A_2''	+	3	3	1	1070166.6	0.2765×10^{-3}	-1.228 (-1.229)	[345]
	−	3	3	1		+	3	0	1	2884.1		-790.5 (-1001)	[345]
A_2'	−	5	3	1	A_2''	+	5	3	0	28971340.5	$0.4692\times10^{+1}$	-0.484 (-0.484)	[340]
A_2'	+	5	0	1	A_2''	+	5	3	0	29050552.5	0.2147×10^{-2}	-0.408 (-0.408)	[340]
	−	5	3	1		+	5	0	1	79212.0		27.38 (27.35)	[340]
A_2'	−	5	3	1	A_2''	+	5	3	1	979649.1	0.5141×10^{-2}	-3.425 (-3.427)	[340]
A_2'	+	5	0	1	A_2''	+	5	3	1	1058861.1	0.3714×10^{-5}	-1.120 (-1.120)	[340]
	−	5	3	1		+	5	0	1	79212.0		27.38 (27.35)	[340]
A_2'	−	5	3	1	A_2''	−	4	0	1	1956241.1	0.4129×10^{-4}	-0.988 (-0.988)	[340]
A_2'	+	5	0	1	A_2''	−	4	0	1	2035453.1	0.7023×10^{-1}	0.116 (0.116)	[340]
	−	5	3	1		+	5	0	1	79212.0		27.38 (29.35)	[340]
A_2'	−	7	3	1	A_2''	+	7	3	0	28934099.5	$0.2399\times10^{+1}$	-0.480 (-0.480)	[340]
A_2'	+	7	0	1	A_2''	+	7	3	0	29118808.5	0.1095×10^{-3}	-0.416 (-0.416)	[340]
	−	7	3	1		+	7	0	1	184709.0		9.561(9.582)	[340]
A_2'	−	9	3	1	A_2''	+	9	3	0	28892089.9	$0.1444\times10^{+1}$	-0.475 (-0.475)	[340]
A_2'	+	9	0	1	A_2''	+	9	3	0	29194454.6	0.1029×10^{-3}	-0.425 (-0.425)	[340]
	−	9	3	1		+	9	0	1	302364.7		4.350 (4.363)	[340]

Values in parentheses obtained using the NRI theory with the calculated TROVE frequencies. [a]JBU sensitivity coefficient reaches a value of -938 (see Jansen et al. [310]).

Table 7.4: The vibration-rotation-inversion transitions $^{15}NH_3$ associated with the $|-, J, K{=}3, v_2{=}1\rangle - |+, J, K{=}0, v_2 {=}1\rangle$ resonances.

Γ'	p'	J'	K'	v_2'	Γ''	p''	J''	K''	v_2''	ν/MHz	A/s^{-1}	T	Ref.
A_2'	$-$	3	3	1	A_2''	$+$	3	3	0	28843885.0	$0.1171\times10^{+2}$	-0.486 (-0.486)	[343]
A_2'	$+$	3	0	1	A_2''	$+$	3	3	0	28872669.9	0.2187×10^{-2}	-0.403 (-0.403)	[343]
	$-$	3	3	1		$+$	3	0	1	28784.9		82.96 (81.69)	[343]
A_2'	$-$	3	3	1	A_2''	$-$	2	0	1	774222.8	0.7160×10^{-6}	-0.999 (-0.999)	[339]
A_2'	$+$	3	0	1	A_2''	$-$	2	0	1	802986.7	0.4035×10^{-2}	2.011 (2.010)	[339]
	$-$	3	3	1		$+$	3	0	1	28763.9		83.02 (81.69)	[339]
A_2'	$-$	3	3	1	A_2''	$+$	3	3	1	1035207.4	0.1491×10^{-1}	-3.473 (-3.476)	[339]
A_2'	s	3	0	1	A_2''	$+$	3	3	1	1063971.3	0.3245×10^{-5}	-1.228 (-1.135)	[339]
	$-$	3	3	1		$+$	3	0	1	28763.9		83.02 (81.69)	[339]
A_2'	$-$	5	3	1	A_2''	$+$	5	3	0	28817906.5	$0.4598\times10^{+1}$	-0.483 (-0.483)	[343]
A_2'	$+$	5	0	1	A_2''	$+$	5	3	0	28927141.3	0.7768×10^{-3}	-0.409 (-0.409)	[343]
	$-$	5	3	1		$+$	5	0	1	109234.8		19.02 (19.02)	[343]
A_2'	$-$	5	3	1	A_2''	$+$	5	3	1	943226.9	0.4588×10^{-2}	-3.453 (-3.455)	[339]
A_2'	$+$	5	0	1	A_2''	$+$	5	3	1	1052459.7	0.1548×10^{-5}	-1.120 (-1.121)	[339]
	$-$	5	3	1		$+$	5	0	1	109232.8		19.04 (19.02)	[339]
A_2'	$-$	5	3	1	A_2''	$-$	4	0	1	1955711.7	0.1882×10^{-4}	-0.988 (-0.988)	[339]
A_2'	$+$	5	0	1	A_2''	$-$	4	0	1	2064944.5	0.7369×10^{-1}	0.071 (0.071)	[339]
	$-$	5	3	1		$+$	5	0	1	109232.8		19.05 (19.02)	[339]
A_2'	$-$	7	3	1	A_2''	$+$	7	3	0	28784706.6	$0.2399\times10^{+1}$	-0.479 (-0.479)	[343]
A_2'	$+$	7	0	1	A_2''	$+$	7	3	0	28997286.1	0.1095×10^{-3}	-0.418 (-0.418)	[343]
	$-$	7	3	1		$+$	7	0	1	212579.5		7.898 (7.073)	[343]
A_2'	$-$	9	3	1	A_2''	$+$	9	3	0	28747714.9	$0.1444\times10^{+1}$	-0.479 (-0.475)	[343]
A_2'	$+$	9	0	1	A_2''	$+$	9	3	0	29075088.5	0.1029×10^{-3}	-0.418 (-0.427)	[343]
	$-$	9	3	1		$+$	9	0	1	327373.6		3.782 (3.782)	[343]

Values in parentheses obtained using the NRI theory with the calculated TROVE frequencies.

Table 7.5: Inversion frequencies (ν), Einstein coefficients (A), and sensitivities (T) of $^{14}NH_3$ and their $^{15}NH_3$ counterparts in the ground vibrational state.

J	K	ν/MHz	A/s^{-1}	T	J	K	ν/MHz	A/s^{-1}	T
				$^{14}NH_3$					
1	1	23694.3	0.1657×10^{-6}	-4.310 (-4.365)	4	3	22688.3	0.1311×10^{-6}	-4.289 (-4.514)
2	1	23098.8	0.5123×10^{-7}	-4.297 (-4.413)	4	4	24139.4	0.2797×10^{-6}	-4.317 (-4.471)
2	2	23722.5	0.2216×10^{-6}	-4.311 (-4.385)	5	1	19838.3	0.6540×10^{-8}	-4.220 (-4.700)
3	2	22834.2	0.9902×10^{-7}	-4.288 (-4.464)	5	2	20371.5	0.2828×10^{-7}	-4.231 (-4.546)
3	3	23870.1	0.2538×10^{-6}	-4.312 (-4.419)	5	3	21285.3	0.7239×10^{-7}	-4.257 (-4.634)
4	1	21134.3	0.1182×10^{-7}	-4.249 (-4.568)	5	4	22653.0	0.1546×10^{-6}	-4.282 (-4.592)
4	2	21703.4	0.5114×10^{-7}	-4.262 (-4.545)	5	5	24533.0	0.3053×10^{-6}	-4.327 (-4.509)
				$^{15}NH_3$					
1	1	22624.9	0.1464×10^{-6}	-4.352 (-4.333)	4	3	21637.9	0.1149×10^{-6}	-4.330 (-4.309)
2	1	22044.2	0.4521×10^{-7}	-4.341 (-4.321)	4	4	23046.0	0.2469×10^{-6}	-4.360 (-4.341)
2	2	22649.8	0.1958×10^{-6}	-4.349 (-4.330)	5	1	18871.5	0.5729×10^{-8}	-4.264 (-4.239)
3	2	21783.9	0.8730×10^{-7}	-4.333 (-4.312)	5	2	19387.4	0.2480×10^{-7}	-4.278 (-4.254)
3	3	22789.4	0.2241×10^{-6}	-4.356 (-4.337)	5	3	20272.1	0.6358×10^{-7}	-4.299 (-4.276)
4	1	20131.4	0.1039×10^{-7}	-4.293 (-4.270)	5	4	21597.9	0.1360×10^{-6}	-4.330 (-4.309)
4	2	20682.8	0.4498×10^{-7}	-4.306 (-4.284)	5	5	23422.0	0.2695×10^{-6}	-4.366 (-4.347)

$^{14}NH_3$: Frequencies from Lovas et al. [346]; values in parentheses from Špirko [309], obtained using the NRI theory. $^{15}NH_3$: Frequencies from Urban et al. [339]; values in parentheses obtained using the NRI theory with the frequencies from Urban et al. [339].

Table 7.6: The rotation-inversion frequencies (ν), Einstein coefficients (A), and sensitivities (T) of $^{14}NH_3$ and their $^{15}NH_3$ counterparts in the ground vibrational state.

Γ'	p'	J'	K'	v_2'	Γ''	p''	J''	K''	v_2''	ν/MHz	A/s^{-1}	T
							$^{14}NH_3$					
A_2'	+	1	0	0	A_2''	−	0	0	0	572498	0.1561×10^{-2}	-0.860 (-0.862)
A_2''	−	2	0	0	A_2'	+	1	0	0	1214859	0.1791×10^{-1}	-1.060 (-1.063)
E'	−	2	1	0	E''	+	1	1	0	1215245	0.1344×10^{-1}	-1.061 (-1.064)
							$^{15}NH_3$					
A_2'	+	1	0	0	A_2''	−	0	0	0	572112	0.1557×10^{-2}	-0.865 (-0.866)
A_2''	−	2	0	0	A_2'	+	1	0	0	1210889	0.1774×10^{-1}	-1.058 (-1.058)
E'	−	2	1	0	E''	+	1	1	0	1211277	0.1331×10^{-1}	-1.059 (-1.059)

$^{14}NH_3$: Frequencies from Persson et al. [347]; values given in parentheses from Špirko [309], obtained using the NRI theory. $^{15}NH_3$: Frequencies from Urban et al. [339]; values in parentheses obtained using the NRI with the frequencies from Urban et al. [339].

Table 7.7: Inversion frequencies (ν), Einstein coefficients (A), and sensitivities (T) of $^{14}NH_3$ and $^{15}NH_3$ in the ν_4 vibrational state.

J	K	ℓ	ν/MHz	A/s^{-1}	T	J	K	ℓ	ν/MHz	A/s^{-1}	T
					$^{14}NH_3$						
1	1	-1	32400	0.4243×10^{-6}	-4.268	4	3	1	57132	0.1968×10^{-5}	1.561
1	1	1	57843	0.2411×10^{-5}	-2.234	4	2	-1	47526	0.5467×10^{-6}	-1.550
2	2	-1	32111	0.5514×10^{-6}	-4.250	4	2	1	46515	0.4020×10^{-6}	-0.247
2	2	1	40189	0.1056×10^{-5}	-2.381	4	1	-1	57681	0.2548×10^{-6}	-0.220
2	1	-1	36797	0.2085×10^{-6}	-3.133	4	1	1	145888[a]	0.3787×10^{-5}	-0.962
2	1	1	20655	0.3743×10^{-7}	2.720	5	5	-1	32037	0.6848×10^{-6}	-4.264
3	3	-1	31893	0.6081×10^{-6}	-4.259	5	5	1	68699	0.6198×10^{-5}	4.672
3	3	1	46679	0.1863×10^{-5}	-0.667	5	4	-1	39071	0.8020×10^{-6}	-2.832
3	2	-1	37500	0.4424×10^{-6}	-2.961	5	4	1	73534	0.4807×10^{-5}	4.480
3	2	1	44963	0.6906×10^{-6}	-1.023	5	3	-1	48346	0.8610×10^{-6}	-1.506
3	1	-1	44755	0.1908×10^{-6}	-1.687	5	3	1	64906	0.1799×10^{-5}	3.044
3	1	1	177783[a]	0.1087×10^{-4}	-0.482	5	2	-1	58699	0.6967×10^{-6}	-0.181
4	4	-1	31884	0.6482×10^{-6}	-4.258	5	2	1	44876	0.2025×10^{-6}	0.239
4	4	1	55765	0.3325×10^{-5}	1.668	5	1	1	78141[a]	0.4324×10^{-6}	0.990
4	3	-1	38460	0.6451×10^{-6}	-2.855	5	1	-1	380542[a]	0.4015×10^{-4}	-0.178
					$^{15}NH_3$						
1	1	-1	31108	0.3758×10^{-6}	-4.291	4	3	1	51989	0.1501×10^{-5}	0.684
1	1	1	55582	0.2142×10^{-5}	-2.410	4	2	-1	44599	0.4524×10^{-6}	-1.765
2	2	-1	30825	0.4880×10^{-6}	-4.271	4	2	1	43225	0.3278×10^{-6}	-0.728
2	2	1	37900	0.8883×10^{-6}	-2.722	4	1	-1	53406	0.2029×10^{-6}	-0.558
2	1	-1	34950	0.1788×10^{-6}	-3.273	4	1	1	146961[a]	0.3870×10^{-5}	-0.983
2	1	1	21904	0.4450×10^{-7}	2.351	5	5	-1	30732	0.6050×10^{-6}	-4.280
3	3	-1	30606	0.5377×10^{-6}	-4.281	5	5	1	61128[a]	0.4341×10^{-5}	2.771
3	3	1	43275	0.1492×10^{-5}	-1.358	5	4	-1	37071	0.6856×10^{-6}	-2.937
3	2	-1	35551	0.3772×10^{-6}	-3.082	5	4	1	65945[a]	0.3431×10^{-5}	3.150
3	2	1	41928	0.5649×10^{-6}	-1.494	5	3	-1	45373	0.7129×10^{-6}	-1.689
3	1	-1	41947	0.1574×10^{-6}	-1.941	5	3	1	59236[a]	0.1351×10^{-5}	2.151
3	1	1	171460[a]	0.9842×10^{-5}	-0.731	5	2	-1	54322	0.5536×10^{-6}	-0.440
4	4	-1	30591	0.5729×10^{-6}	-4.281	5	2	1	42037[a]	0.1659×10^{-6}	-0.242
4	4	1	50530	0.2502×10^{-5}	0.452	5	1	-1	71752[a]	0.3362×10^{-6}	0.639
4	3	-1	36472	0.5506×10^{-6}	-2.978	5	1	1	369287[a]	0.3728×10^{-4}	-0.379

Frequencies from Cohen and Poynter [348] and Cohen [349]; [a]TROVE calculated value.

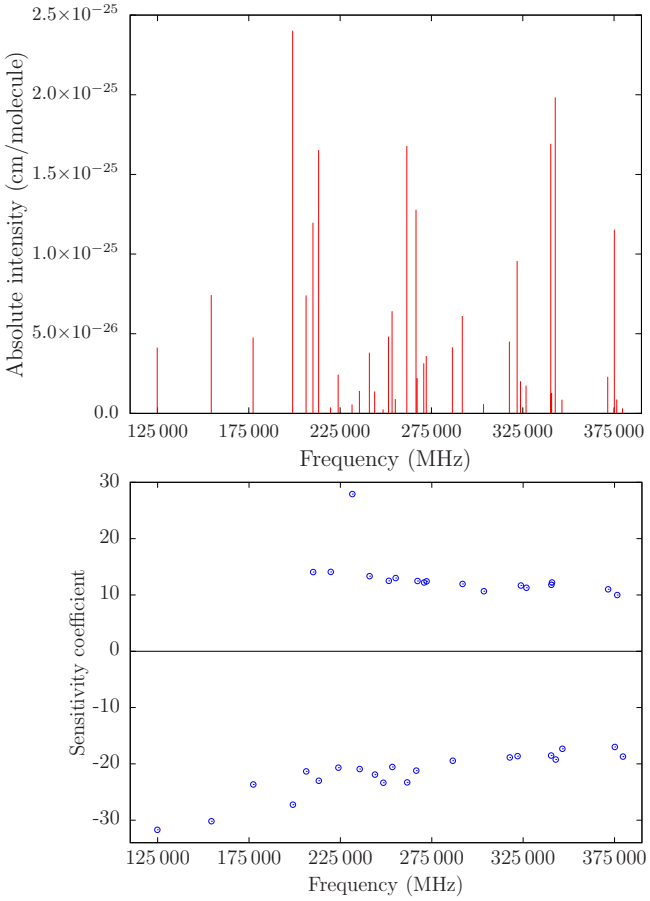

Figure 7.3: Observed frequencies [327, 328] and simulated intensities at temperature $T = 296\,\mathrm{K}$ (top panel) with the corresponding sensitivities (bottom panel) for transitions between the $2\nu_2$ and ν_4 vibrational states of $^{14}NH_3$.

ing a consistent set of quantum numbers [350]. The MARVEL analysis offers a rigorous evaluation of high-resolution $^{14}NH_3$ spectra. The $2\nu_2$ energy levels have an average error of $0.0027\,\mathrm{cm}^{-1}$ for the 251 levels up to $J = 15$, whilst a similar uncertainty of $0.0026\,\mathrm{cm}^{-1}$ is given for the 495 ν_4 energies. As such, the error on the predicted sensitivities is significantly reduced by replacing the computed TROVE energy levels with the corresponding MARVEL values in Eq. (7.1).

This is not to say that the TROVE frequencies are unreliable. As part of the MARVEL procedure the derived experimental energy levels are checked against theoretical predictions using the same PES and computational setup [333] as utilized for the present study. If sensitivity coefficients are calculated for the 38 transitions shown in Fig. 7.3 without replacing the energies, the TROVE sensitivities differ on average by 2.5% to the MARVEL substituted sensitivities, the largest difference being 5.5%. Likewise for the additional 153 transitions with similar Einstein A coefficients provided in Appendix B, the TROVE sensitivities deviate on average by 2.1%. Such small differences reflect the quality of the underlying PES.

However, the variational approach cannot account exactly for all near-degeneracies in the $2\nu_2$ and ν_4 rovibrational manifold. A striking example of this is for the extremely weak $5_3^+(\nu_4) \leftarrow 5_2^+(2\nu_2)$ transition. Here, states are labelled as $J_K^{\pm}$ where J is the rotational quantum number, K is the projection onto the molecule-fixed z axis, and $\pm$ denotes the parity of the state. A computed frequency of $\nu_{\mathrm{calc}} = 3540.5\,\mathrm{MHz}$ has a sensitivity of $T_{\mathrm{calc}} = -1843.25$, already the largest known sensitivity coefficient for ammonia. Replacing with MARVEL energy levels gives $\nu_{\mathrm{exp}} = 389.9\,\mathrm{MHz}$ and $T_{\mathrm{exp}} = -16,737.52$. The dramatic increase in magnitude occurs because of the inverse dependence on transition frequency (see Eq. (7.1)) and illustrates the huge enhancement that can happen between close-lying energy levels. Given the difference in predicted sensitivities one could question whether the computed numerical derivatives are still reliable. The change in frequency is just over $3000\,\mathrm{MHz}$ ($\approx 0.1\,\mathrm{cm}^{-1}$) so one would expect that they are reasonable. The difficulty is that quantifying the uncertainty of the numerical derivatives is

not as straightforward because there are no analogous highly accurate experimental quantities.

To investigate the error of the computed derivatives, new sensitivity coefficients were calculated using a purely *ab initio* PES [336]. One can hope to establish a relationship between the difference in $\nu = E_u - E_l$, with the difference in the quantity $\mathrm{d}E_u/\mathrm{d}\mu - \mathrm{d}E_l/\mathrm{d}\mu$, by comparing values computed using this and the empirically refined PESs. Whilst no clear general correspondence between the uncertainty on these two quantities emerges, for near-coinciding energy levels separated by $1\,\mathrm{cm}^{-1}$ or less, the percentage difference in $\mathrm{d}E_u/\mathrm{d}\mu - \mathrm{d}E_l/\mathrm{d}\mu$ is always smaller than the percentage difference in ν. This ranges from 3–4 times smaller to several orders of magnitude smaller and suggests that for extremely close-lying energy levels, the underlying numerical derivatives are relatively stable. Thus, the huge amplification in sensitivity is a result of replacing the theoretical frequencies with experimental values.

For the transitions shown in Fig. 7.3 and those with similar Einstein A coefficients, there is consistent agreement between the TROVE and MARVEL substituted sensitivities and errors in the computed derivatives will be negligible. When the two predictions differ significantly, which occurs for a number of weaker transitions with very large sensitivities ranging from $T = -712.84$ to 509.21 (see Appendix B), I am confident that the MARVEL substituted sensitivity coefficients are reliable. In all instances the residual between experiment and computed transition frequency never exceeds $1\,\mathrm{cm}^{-1}$ (regarded as spectroscopic accuracy).

$^{14}\mathbf{ND_3}$ and $^{15}\mathbf{ND_3}$

Because of the substantial difference in size of the inversion splittings, the mass sensitivities of the $^{14}ND_3$ and $^{15}ND_3$ transitions exhibit centrifugal distortion and Coriolis interaction dependence significantly different from that of $^{14}NH_3$ and $^{15}NH_3$ (see Fig. 7.4 and Tables 7.8, 7.9, 7.10, 7.11, 7.12). However, as only a small fraction of the total presence of ammonia in the interstellar medium is heavy ammonia, a

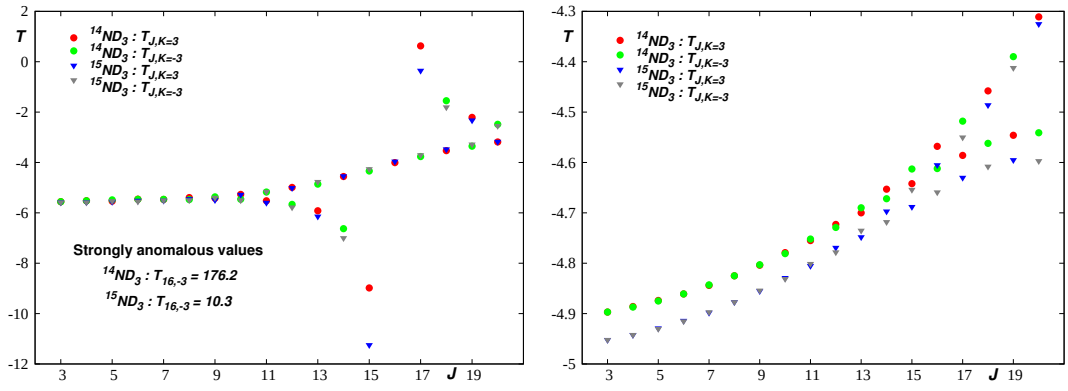

Figure 7.4: The sensitivities (T) of the inversion transitions of the ($J, K = \pm 3$) rotational states of $^{14}ND_3$ and $^{15}ND_3$ in the ground (left panel) and ν_2 (right panel) vibrational states.

detection of "higher energy" transitions is rather unlikely. The deuterated ammonia isotopomers, along with $^{14}NH_3$ and $^{15}NH_3$, are still suitable targets for terrestrial studies, such as those reported by van Veldhoven et al. [312], Bethlem et al. [316], and Quintero-Pérez et al. [351].

7.3.3 Outlook

It is expected that any variation in the fundamental constants will be confirmed, or refuted, over a series of independent measurements on a variety of molecular absorbers. As a relevant astrophysical molecule, and with certain inversion frequencies already detected extraterrestrially [357–359], $^{15}NH_3$ has potential to aid this search along with the already established probes of $^{14}NH_3$. Notably the $^{14}NH_3$ astronomically observed $2_1^+ \leftarrow 1_1^-$ and $0_0^- \leftarrow 1_0^+$ transitions in the ν_2 state [318, 320] possessed values of $T = 17.24$ and $T = -6.59$, respectively. For the deuterated species $^{14}ND_3$ and $^{15}ND_3$, it is expected that their use will be restricted to precision measurements in the laboratory, despite possessing larger sensitivity coefficients for the pure inversion frequencies in the ground vibrational state.

The $2\nu_2 \leftrightarrow \nu_4$ transitions of $^{14}NH_3$ showed consistently large sensitivities but are perhaps more likely to be detected in terrestrial studies given that the rovibrational

Table 7.8: Inversion frequencies (ν), Einstein coefficients (A), and sensitivities (T) of $^{14}ND_3$ and $^{15}ND_3$ in the ground vibrational state.

J	K	ν/MHz	A/s^{-1}	T	J	K	ν/MHz	A/s^{-1}	T
				$^{14}ND_3$					
1	1	1589.006	0.5764×10^{-10}	-5.541 (-5.528)	4	3	1558.600	0.4897×10^{-10}	-5.533 (-5.520)
2	1	1568.357	0.1849×10^{-10}	-5.556 (-5.542)	4	-3	1558.178	0.4893×10^{-10}	-5.534 (-5.521)
2	2	1591.695	0.7721×10^{-10}	-5.543 (-5.530)	4	4	1612.997	0.9623×10^{-10}	-5.536 (-5.525)
3	1	1537.915	0.8725×10^{-11}	-5.526 (-5.511)	5	1	1450.435[a]	0.2937×10^{-11}	-5.511 (-5.493)
3	2	1560.774	0.3644×10^{-10}	-5.537 (-5.523)	5	2	1471.785	0.1226×10^{-10}	-5.504 (-5.487)
3	3	1599.645	0.8810×10^{-10}	-5.571 (-5.559)	5	3	1507.525	0.2960×10^{-10}	-5.553 (-5.537)
3	-3	1599.704	0.8811×10^{-10}	-5.571 (-5.559)	5	-3	1509.218	0.2969×10^{-10}	-5.499 (-5.484)
4	1	1498.270	0.4848×10^{-11}	-5.503 (-5.487)	5	4	1561.146	0.5827×10^{-10}	-5.524 (-5.511)
4	2	1520.537	0.2025×10^{-10}	-5.493 (-5.478)	5	5	1631.784	0.1036×10^{-9}	-5.561 (-5.551)
				$^{15}ND_3$					
1	1	1430.340	0.4227×10^{-10}	-5.600 (-5.577)	4	3	1401.312	0.3578×10^{-10}	-5.600 (-5.577)
2	1	1410.980	0.1354×10^{-10}	-5.613 (-5.589)	4	-3	1400.878	0.3575×10^{-10}	-5.602 (-5.578)
2	2	1432.641	0.5661×10^{-10}	-5.604 (-5.581)	4	2	1366.027	0.1476×10^{-10}	-5.586 (-5.561)
3	1	1382.510	0.5374×10^{-11}	-5.585 (-5.560)	5	1	1300.841[a]	0.2130×10^{-11}	-5.562 (-5.534)
3	2	1403.684	0.2665×10^{-10}	-5.566 (-5.542)	5	2	1320.460[a]	0.8907×10^{-11}	-5.575 (-5.547)
3	3	1439.719	0.5458×10^{-10}	-5.601 (-5.579)	5	3	1353.451	0.2153×10^{-10}	-5.585 (-5.559)
3	-3	1439.783	0.6459×10^{-10}	-5.601 (-5.579)	5	-3	1355.161	0.2162×10^{-10}	-5.551 (-5.526)
4	1	1345.533[a]	0.3530×10^{-11}	-5.564 (-5.538)	5	4	1403.179	0.4254×10^{-10}	-5.606 (-5.583)
4	2	1366.027	0.1476×10^{-10}	-5.586 (-5.561)	5	5	1468.666	0.7595×10^{-10}	-5.639 (-5.619)

Unless stated otherwise, $^{14}ND_3$ and $^{15}ND_3$ frequencies from Fusina and Murzin [352] and Fusina et al. [353], respectively; values in parentheses obtained using the NRI theory with the calculated TROVE frequencies; the $K = -3$ values refer to transitions between levels with spin statistical weight = 10 (A_1', A_1'' species), the $K = 3$ values refer to transitions between levels with spin statistical weight = 1 (A_2', A_2'') species); [a]Urban et al. [354].

Table 7.9: The rotation-inversion frequencies (ν), Einstein coefficients (A), and sensitivities (T) of $^{14}ND_3$ and $^{15}ND_3$ in the ground vibrational state.

Γ'	p'	J'	K'	v_2'	Γ''	p''	J''	K''	v_2''	ν/MHz	A/s^{-1}	T
							$^{14}ND_3$					
A_1''	$-$	1	0	0	A_1'	$+$	0	0	0	309909[a]	0.2530×10^{-3}	-1.022
A_2''	$-$	2	0	0	A_2'	$+$	1	0	0	618075[a]	0.2409×10^{-2}	-1.009
E'	$-$	2	1	0	E''	$+$	1	1	0	618124[a]	0.1807×10^{-2}	-1.009
A_2'	$+$	1	0	0	A_2''	$-$	0	0	0	306737[a]	0.2450×10^{-3}	-0.973
A_1'	$+$	2	0	0	A_1''	$-$	1	0	0	614933[a]	0.2371×10^{-2}	-0.985
E''	$+$	2	1	0	E'	$-$	1	1	0	614968[a]	0.1778×10^{-2}	-0.985
A_1''	$-$	3	0	0	A_1'	$+$	2	0	0	925947	0.8681×10^{-2}	-1.005
E'	$-$	3	1	0	E''	$+$	2	1	0	926018	0.7717×10^{-2}	-1.005
E''	$-$	3	2	0	E'	$+$	2	2	0	926228	0.4824×10^{-2}	-1.005
A_2'	$+$	3	0	0	A_2''	$-$	2	0	0	922857	0.8591×10^{-2}	-0.989
E''	$+$	3	1	0	E'	$-$	2	1	0	922911	0.7637×10^{-2}	-0.989
E'	$+$	3	2	0	E''	$-$	2	2	0	923076	0.4773×10^{-2}	-0.999
							$^{15}ND_3$					
A_1''	$-$	1	0	0	A_1'	$+$	0	0	0	308606[a]	0.2499×10^{-3}	-1.020
A_2''	$-$	2	0	0	A_2'	$+$	1	0	0	615628[a]	0.2381×10^{-2}	-1.008
E'	$-$	2	1	0	E''	$+$	1	1	0	615677[a]	0.1785×10^{-2}	-1.009
A_2'	$+$	1	0	0	A_2''	$-$	0	0	0	305750[a]	0.2427×10^{-3}	-0.975
A_1'	$+$	2	0	0	A_1''	$-$	1	0	0	612801[a]	0.2346×10^{-2}	-0.987
E''	$+$	2	1	0	E'	$-$	1	1	0	612836[a]	0.1760×10^{-2}	-0.987
A_1''	$-$	3	0	0	A_1'	$+$	2	0	0	922356	0.8582×10^{-2}	-1.004
E'	$-$	3	1	0	E''	$+$	2	1	0	922426	0.7628×10^{-2}	-1.004
E''	$-$	3	2	0	E'	$+$	2	2	0	922636	0.4768×10^{-2}	-1.004
A_2'	$+$	3	0	0	A_2''	$-$	2	0	0	919577	0.8501×10^{-2}	-0.990
E''	$+$	3	1	0	E'	$-$	2	1	0	919632	0.7556×10^{-2}	-0.990
E'	$+$	3	2	0	E''	$-$	2	2	0	919800	0.4723×10^{-2}	-0.990

Unless stated otherwise, frequencies from [354]; [a]Helminger and Gordy [355] and Helminger et al. [356].

Table 7.10: The rotation-inversion frequencies (ν), Einstein coefficients (A), and sensitivities (T) of $^{14}ND_3$ in the ν_2 vibrational state.

Γ'	p'	J'	K'	v_2'	Γ''	p''	J''	K''	v_2''	ν/MHz	A/s^{-1}	T
							$^{14}ND_3$					
A_1''	$-$	1	0	1	A_1'	$+$	0	0	1	412847	0.4983×10^{-3}	-2.030
A_2''	$-$	2	0	1	A_2'	$+$	1	0	1	718585	0.3131×10^{-2}	-1.585
E'	$-$	2	1	1	E''	$+$	1	1	1	719092	0.2352×10^{-2}	-1.588
A_2'	$+$	1	0	1	A_2''	$-$	0	0	1	200763	0.5423×10^{-4}	1.119
A_1'	$+$	2	0	1	A_1''	$-$	1	0	1	508364	0.1082×10^{-2}	-0.170
E''	$+$	2	1	1	E'	$-$	1	1	1	507940	0.8088×10^{-3}	-0.166
A_1''	$-$	3	0	1	A_1'	$+$	2	0	1	1023449	0.9673×10^{-2}	-1.404
E'	$-$	3	1	1	E''	$+$	2	1	1	1023971	0.8608×10^{-2}	-1.405
E''	$-$	3	2	1	E'	$+$	2	2	1	1025546	0.5399×10^{-2}	-1.411
A_2'	$+$	3	0	1	A_2''	$-$	2	0	1	816294	0.4830×10^{-2}	-0.491
E''	$+$	3	1	1	E'	$-$	2	1	1	815898	0.4286×10^{-2}	-0.488
E'	$+$	3	2	1	E''	$-$	2	2	1	814696	0.2663×10^{-2}	-0.480
A_2''	$-$	4	0	1	A_2'	$+$	3	0	1	1327334	0.2188×10^{-1}	-1.304
E'	$-$	4	1	1	E''	$+$	3	1	1	1327865	0.2053×10^{-1}	-1.305
E''	$-$	4	2	1	E'	$+$	3	2	1	1329473	0.1647×10^{-1}	-1.309
A_2'	$-$	4	3	1	A_2''	$+$	3	3	1	1332194	0.9646×10^{-2}	-1.317
A_1'	$-$	4	-3	1	A_1''	$+$	3	-3	1	1332194	0.9646×10^{-2}	-1.317
A_1'	$+$	4	0	1	A_1''	$-$	3	0	1	1124392	0.1315×10^{-1}	-0.637
E''	$+$	4	1	1	E'	$-$	3	1	1	1124025	0.1231×10^{-1}	-0.636
E'	$+$	4	2	1	E''	$-$	3	2	1	1122914	0.9805×10^{-2}	-0.630
A_2''	$+$	4	3	1	A_2'	$-$	3	3	1	1121023	0.5679×10^{-2}	-0.621
A_1''	$+$	4	-3	1	A_1'	$-$	3	-3	1	1121023	0.5679×10^{-2}	-0.621
A_1''	$-$	5	0	1	A_1'	$+$	4	0	1	1630141	0.4149×10^{-1}	-1.239
E'	$-$	5	1	1	E''	$+$	4	1	1	1630681	0.3986×10^{-1}	-1.240
E''	$-$	5	2	1	E'	$+$	4	2	1	1632314	0.3494×10^{-1}	-1.243
A_2'	$-$	5	3	1	A_2''	$+$	4	3	1	1635074	0.2671×10^{-1}	-1.249
A_1'	$-$	5	-3	1	A_1''	$+$	4	-3	1	1635075	0.2671×10^{-1}	-1.249
E''	$-$	5	4	1	E'	$+$	4	4	1	1639027	0.1509×10^{-1}	-1.258
A_2'	$+$	5	0	1	A_2''	$-$	4	0	1	1432485	0.2790×10^{-1}	-0.722
E''	$+$	5	1	1	E'	$-$	4	1	1	1432151	0.2676×10^{-1}	-0.721
E'	$+$	5	2	1	E''	$-$	4	2	1	1431137	0.2333×10^{-1}	-0.717
A_2''	$+$	5	3	1	A_2'	$-$	4	3	1	1429410	0.1768×10^{-1}	-0.710
A_1''	$+$	5	-3	1	A_1'	$-$	4	-3	1	1429409	0.1768×10^{-1}	-0.710
E'	$+$	5	4	1	E''	$-$	4	4	1	1426908	0.9864×10^{-2}	-0.700

Frequencies from Urban et al. [354].

Table 7.11: The rotation-inversion frequencies (ν), Einstein coefficients (A), and sensitivities (T) of $^{15}ND_3$ in the ν_2 vibrational state.

Γ'	p'	J'	K'	v_2'	Γ''	p''	J''	K''	v_2''	ν/MHz	A/s^{-1}	T
							$^{15}ND_3$					
A_1''	$-$	1	0	1	A_1'	$+$	0	0	1	402779	0.4636×10^{-3}	-1.979
A_2''	$-$	2	0	1	A_2'	$+$	1	0	1	707552	0.2995×10^{-2}	-1.551
E'	$-$	2	1	1	E''	$+$	1	1	1	708033	0.2250×10^{-2}	-1.554
A_2'	$+$	1	0	1	A_2''	$-$	0	0	1	208813	0.6139×10^{-4}	0.891
A_1'	$+$	2	0	1	A_1''	$-$	1	0	1	515358	0.1131×10^{-2}	-0.241
E''	$+$	2	1	1	E'	$-$	1	1	1	514961	0.8458×10^{-3}	-0.237

Frequencies from Urban et al. [354].

states involved lie above 1600 cm^{-1}. Astronomical detection is not impossible however. The energy levels of the $(J, K) = (18, 18)$ inversion transition in the ground vibrational state of $^{14}NH_3$ reside at 2176.93 and 2178.47 cm^{-1}, respectively, and this line was observed towards the galactic centre star forming region Sgr B2 [331]. A number of $2\nu_2 \leftrightarrow \nu_4$ transitions which possess sizeable Einstein A coefficients and involve energy levels lower than the $(J, K) = (18, 18)$ energies are listed in Table 7.13. Such highly excited states could effectively be populated by exoergic chemical formation processes [330].

There are now novel techniques to produce ultracold polyatomic molecules [360], which have rich spectra well suited for testing fundamental physics. Already experiments which decelerate, cool and trap ammonia molecules are being developed to probe a temporal variation of μ [312, 316, 351, 361, 362]. In Table 7.14, several highly sensitive $2\nu_2 \leftrightarrow \nu_4$ transitions of $^{14}NH_3$ are listed, which despite being around two orders of magnitude weaker than the lowest intensity lines displayed in Fig. 7.3, could possibly be detected in such high-precision studies.

If the transitions in Table 7.14 are too weak to be detected directly, the use of combination differences involving infrared transitions from the ground vibrational state to the $2\nu_2$ and ν_4 vibrational states should be considered. This technique would apply to any two levels provided transitions from a common ground state

Table 7.12: The wavenumbers (ν), wavelengths (λ), Einstein coefficients (A), and sensitivities (T) for transitions between the ground and ν_2 vibrational state of $^{14}ND_3$ and $^{15}ND_3$.

Γ'	p'	J'	K'	v_2'	Γ''	p''	J''	K''	v_2''	ν/cm^{-1}	$\lambda/\mu\mathrm{m}$	A/s^{-1}	T
									$^{14}ND_3$				
A_1''	−	1	0	1	A_1'	+	0	0	0	759.3704	13.1688	$0.1955\times10^{+1}$	-0.475
A_2''	−	2	0	1	A_2'	+	1	0	0	769.5283	12.9950	$0.2444\times10^{+1}$	-0.482
E'	−	2	1	1	E''	+	1	1	0	769.5306	12.9949	$0.1834\times10^{+1}$	-0.482
A_2'	+	1	0	1	A_2''	−	0	0	0	755.7906	13.2312	$0.1948\times10^{+1}$	-0.454
A_1'	+	2	0	1	A_1''	−	1	0	0	765.9901	13.0550	$0.2434\times10^{+1}$	-0.461
E''	+	2	1	1	E'	−	1	1	0	765.9767	13.0552	$0.1827\times10^{+1}$	-0.461
E'	−	1	1	1	E''	+	1	1	0	749.0866	13.3496	$0.2810\times10^{+1}$	-0.468
E'	−	2	1	1	E''	+	2	1	0	748.9645	13.3518	0.9344×10^{0}	-0.468
E''	−	2	2	1	E'	+	2	2	0	748.9671	13.3517	$0.3744\times10^{+1}$	-0.468
E''	+	1	1	1	E'	−	1	1	0	745.4912	13.4140	$0.2798\times10^{+1}$	-0.446
E''	+	2	1	1	E'	−	2	1	0	745.4112	13.4154	0.9305×10^{0}	-0.446
E'	+	2	2	1	E''	−	2	2	0	745.3664	13.4162	$0.3729\times10^{+1}$	-0.446
A_2''	−	0	0	1	A_2'	+	1	0	0	738.8622	13.5343	$0.5381\times10^{+1}$	-0.461
A_1''	−	1	0	1	A_1'	+	2	0	0	728.5209	13.7264	$0.3427\times10^{+1}$	-0.453
E'	−	1	1	1	E''	+	2	1	0	728.5205	13.7264	$0.2572\times10^{+1}$	-0.453
A_1'	+	0	0	1	A_1''	−	1	0	0	735.2618	13.6006	$0.5358\times10^{+1}$	-0.439
A_2'	+	1	0	1	A_2''	−	2	0	0	724.9421	13.7942	$0.3412\times10^{+1}$	-0.431
E''	+	1	1	1	E'	−	2	1	0	724.9258	13.7945	$0.2560\times10^{+1}$	-0.431
									$^{15}ND_3$				
A_1''	−	1	0	1	A_1'	+	0	0	0	752.9702	13.2807	$0.1888\times10^{+1}$	-0.475
A_2''	−	2	0	1	A_2'	+	1	0	0	763.1000	13.1044	$0.2359\times10^{+1}$	-0.482
E'	−	2	1	1	E''	+	1	1	0	763.0998	13.1044	$0.1770\times10^{+1}$	-0.482
A_2'	+	1	0	1	A_2''	−	0	0	0	749.6973	13.3387	$0.1881\times10^{+1}$	-0.455
A_1'	+	2	0	1	A_1''	−	1	0	0	759.8667	13.1602	$0.2351\times10^{+1}$	-0.463
E''	+	2	1	1	E'	−	1	1	0	759.8517	13.1605	$0.1764\times10^{+1}$	-0.462
E'	−	1	1	1	E''	+	1	1	0	742.7222	13.4640	$0.2713\times10^{+1}$	-0.468
E'	−	2	1	1	E''	+	2	1	0	742.6101	13.4660	0.9023×10^{0}	-0.468
E''	−	2	2	1	E'	+	2	2	0	742.6053	13.4661	$0.3616\times10^{+1}$	-0.468
E''	+	1	1	1	E'	−	1	1	0	739.4346	13.5238	$0.2702\times10^{+1}$	-0.448
E''	+	2	1	1	E'	−	2	1	0	739.3626	13.5252	0.8988×10^{0}	-0.448
E'	+	2	2	1	E''	−	2	2	0	739.3131	13.5261	$0.3602\times10^{+1}$	-0.447
A_2''	−	0	0	1	A_2'	+	1	0	0	732.5333	13.6513	$0.5197\times10^{+1}$	-0.461
A_1''	−	1	0	1	A_1'	+	2	0	0	722.2354	13.8459	$0.3311\times10^{+1}$	-0.452
E'	−	1	1	1	E''	+	2	1	0	722.2324	13.8460	$0.2484\times10^{+1}$	-0.453
A_1'	+	0	0	1	A_1''	−	1	0	0	729.2409	13.7129	$0.5176\times10^{+1}$	-0.440
A_2'	+	1	0	1	A_2''	−	2	0	0	718.9634	13.9089	$0.3296\times10^{+1}$	-0.432
E''	+	1	1	1	E'	−	2	1	0	718.9456	13.9093	$0.2474\times10^{+1}$	-0.432

Wavenumbers from Urban et al. [354].

Table 7.13: Astronomically relevant transitions between the $2\nu_2$ and ν_4 vibrational states of NH_3.

$\nu' \leftarrow \nu''$	$J_K^{\pm\prime} \leftarrow J_K^{\pm\prime\prime}$	$\nu_{\rm exp}$/MHz	A/s^{-1}	T
$\nu_4 \leftarrow 2\nu_2$	$0_0^+ \leftarrow 1_1^+$	379 596.5	4.703×10^{-6}	-18.70
$\nu_4 \leftarrow 2\nu_2$	$1_1^+ \leftarrow 1_0^+$	824 624.2	6.427×10^{-5}	-9.13
$2\nu_2 \leftarrow \nu_4$	$2_1^+ \leftarrow 1_0^+$	231 528.2	1.180×10^{-6}	27.91
$\nu_4 \leftarrow 2\nu_2$	$2_2^+ \leftarrow 2_1^+$	687 852.5	6.318×10^{-5}	-10.70
$2\nu_2 \leftarrow \nu_4$	$3_3^+ \leftarrow 2_2^+$	489 672.2	4.360×10^{-6}	12.72
$\nu_4 \leftarrow 2\nu_2$	$3_3^+ \leftarrow 3_2^+$	557 275.3	7.623×10^{-5}	-12.87
$2\nu_2 \leftarrow \nu_4$	$3_2^+ \leftarrow 2_1^+$	672 644.4	3.223×10^{-5}	8.89
$\nu_4 \leftarrow 2\nu_2$	$3_2^+ \leftarrow 3_1^+$	679 163.4	6.964×10^{-5}	-10.79
$\nu_4 \leftarrow 2\nu_2$	$3_1^+ \leftarrow 3_0^+$	774 889.5	4.660×10^{-5}	-9.59
$2\nu_2 \leftarrow \nu_4$	$3_1^+ \leftarrow 2_0^+$	842 667.6	1.210×10^{-4}	6.91
$\nu_4 \leftarrow 2\nu_2$	$4_4^+ \leftarrow 4_3^+$	441 874.1	7.796×10^{-5}	-15.68
$\nu_4 \leftarrow 2\nu_2$	$4_3^+ \leftarrow 4_2^+$	548 781.8	9.102×10^{-5}	-12.94
$\nu_4 \leftarrow 2\nu_2$	$4_2^+ \leftarrow 4_1^+$	657 787.0	6.078×10^{-5}	-11.07
$\nu_4 \leftarrow 2\nu_2$	$5_5^+ \leftarrow 5_4^+$	342 797.1	7.054×10^{-5}	-19.22
$\nu_4 \leftarrow 2\nu_2$	$5_4^+ \leftarrow 5_3^+$	434 941.1	9.782×10^{-5}	-15.59
$\nu_4 \leftarrow 2\nu_2$	$5_3^+ \leftarrow 5_2^+$	527 333.3	8.219×10^{-5}	-13.31
$\nu_4 \leftarrow 2\nu_2$	$5_2^+ \leftarrow 5_1^+$	618 776.8	4.583×10^{-5}	-11.66
$\nu_4 \leftarrow 2\nu_2$	$5_1^+ \leftarrow 5_0^+$	672 376.5	2.542×10^{-5}	-10.86
$\nu_4 \leftarrow 2\nu_2$	$6_6^+ \leftarrow 6_5^+$	261 535.4	5.745×10^{-5}	-23.29
$\nu_4 \leftarrow 2\nu_2$	$6_5^+ \leftarrow 6_4^+$	340 322.9	9.137×10^{-5}	-18.52
$\nu_4 \leftarrow 2\nu_2$	$6_4^+ \leftarrow 6_3^+$	413 748.1	9.006×10^{-5}	-15.98
$\nu_4 \leftarrow 2\nu_2$	$6_3^+ \leftarrow 6_2^+$	488 661.3	6.308×10^{-5}	-14.12
$\nu_4 \leftarrow 2\nu_2$	$6_2^+ \leftarrow 6_1^+$	559 214.0	3.027×10^{-5}	-12.73
$\nu_4 \leftarrow 2\nu_2$	$7_7^+ \leftarrow 7_6^+$	198 997.4	4.284×10^{-5}	-27.24
$\nu_4 \leftarrow 2\nu_2$	$7_6^+ \leftarrow 7_5^+$	266 541.0	7.700×10^{-5}	-21.20
$\nu_4 \leftarrow 2\nu_2$	$7_5^+ \leftarrow 7_4^+$	321 935.0	8.437×10^{-5}	-18.62
$\nu_4 \leftarrow 2\nu_2$	$7_4^+ \leftarrow 7_3^+$	375 174.5	6.887×10^{-5}	-16.99
$\nu_4 \leftarrow 2\nu_2$	$7_3^+ \leftarrow 7_2^+$	430 468.6	4.113×10^{-5}	-15.29
$\nu_4 \leftarrow 2\nu_2$	$8_8^+ \leftarrow 8_7^+$	154 415.5	3.036×10^{-5}	-30.19

For symmetry of transitions see comprehensive tables in Appendix B. Experimental frequencies from Ref. [327, 328] or obtained using energy levels from the MARVEL analysis [350].

Table 7.14: Highly sensitive weak transitions between the $2\nu_2$ and ν_4 vibrational states of $^{14}NH_3$.

$\nu' \leftarrow \nu''$	$J_K^{\pm\prime} \leftarrow J_K^{\pm\prime\prime}$	$\nu_{\rm exp}$/MHz	A/s^{-1}	T
$2\nu_2 \leftarrow \nu_4$	$2_2^+ \leftarrow 1_1^+$	61 712.7	1.042×10^{-8}	107.95
$\nu_4 \leftarrow 2\nu_2$	$7_3^- \leftarrow 7_1^+$	110 957.2	9.461×10^{-8}	-54.08
$\nu_4 \leftarrow 2\nu_2$	$10_2^+ \leftarrow 10_1^+$	123 427.8	4.745×10^{-7}	-44.11
$\nu_4 \leftarrow 2\nu_2$	$6_3^- \leftarrow 6_1^+$	169 341.3	2.539×10^{-8}	-37.57

All transitions are of symmetry $E' \leftarrow E''$. Experimental frequencies have been obtained using energy levels from the MARVEL analysis [350].

level can be identified, or for a situation such as that depicted in Fig. 7.5. Infrared transitions to the respective levels of the $2_2^+(2\nu_2) \leftarrow 1_1^+(\nu_4)$ transition (sensitivity of $T = 107.95$) have been measured experimentally [328], whilst the corresponding ground state pure inversion frequency is well known [346]. Combination differences could be utilized to determine a possible shift in these energy levels provided the sensitivities of the three involved transitions are also known. The large number of potential combination differences prohibits us from carrying out a rigorous evaluation of all possible transitions. However, if particular combination differences could be readily measured in the future, it would be straightforward to compute the required sensitivity coefficients.

7.4 Hydronium (H_3O^+)

The hydronium cation (H_3O^+) is one of the key molecular ions for inferring properties of the interstellar medium, particularly for constraining the cosmic-ray ionization rate of atomic and molecular hydrogen (see Indriolo et al. [363] and references therein). Knowledge of such parameters is of astrophysical importance, and as a result, H_3O^+ is one of the most searched for galactic and extragalactic interstellar molecules [330, 364–375]. Since H_3O^+ formation requires the presence of H_2O, and the chemical relation between H_3O^+ and H_2O is well-understood, H_3O^+ can serve as an excellent proxy for H_2O, which is often hard to observe directly [376].

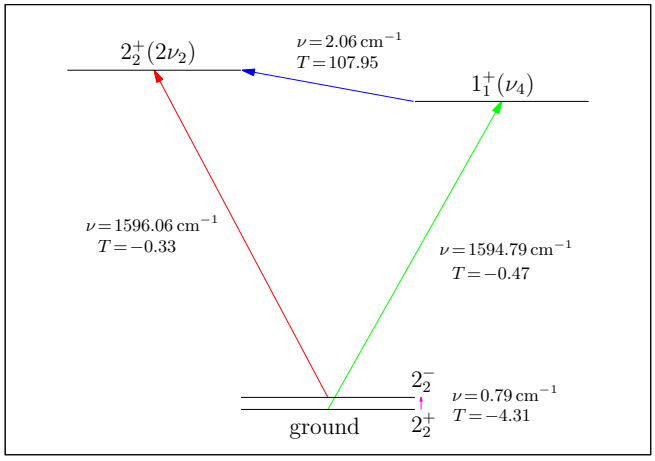

Figure 7.5: Use of combination differences involving infrared transitions from the ground vibrational state to the $2\nu_2$ and ν_4 vibrational states of ammonia. Energy levels are labelled as $J_K^{\pm}$.

Similar to the ammonia molecule, H_3O^+ has several far infrared and submillimetre transitions that are particularly sensitive to the proton-to-electron mass ratio μ [293, 377]. The most robust constraint on a variable μ was determined using methanol absorption lines with sensitivities differing by $\Delta T = 6.4$ [304]. In principle then, hydronium is capable of being used exclusively to constrain a possible variation in the proton-to-electron mass ratio, thus avoiding certain systematic errors which arise when using transitions from different molecular species [292, 313–315].

A small number of pure inversion and rotation-inversion transitions in the ground vibrational state of H_3O^+ were originally investigated by Kozlov and Levshakov [377]. However, the calculated sensitivity coefficients were overestimated and new values have been computed for H_3O^+, along with the isotopologues H_2DO^+, HD_2O^+, and D_3O^+ [293]. Given the astronomical relevance of H_3O^+, and a good representative set of accurate experimental data [378–383], it seems worthwhile to carry out a comprehensive study of hydronium, $H_3{}^{16}O^+$ (also referred to as H_3O^+), and its two symmetric top isotopologues, $H_3{}^{18}O^+$ and $D_3{}^{16}O^+$. Like NH_3 [309, 310, 384], there is a possibility to find transitions with strongly anomalous sensitivities caused by the $\Delta k = \pm 3$ interactions (see Papoušek et al. [385]), which have not yet been considered.

7.4.1 Variational calculations

To compute rotation-vibration transitions and corresponding intensities, TROVE requires as input a PES and DMS. For the present work I utilized a new *ab initio* PES and DMS. A detailed description of these will be reported elsewhere (Polyansky & Ovsyannikov (in preparation)). Here we provide only a brief description of the respective surfaces.

The PES was computed at the all-electron multireference configuration interaction (MRCI) level of theory using the core-valence-weighted basis sets, aug-cc-pwCVQZ and aug-cc-pwCV5Z. A two-point formula was applied to extrapolate the electronic energy to the CBS limit. Additional complete-active-space and relativistic corrections were also incorporated into the PES. For the DMS, the MRCI/aug-cc-pwCV5Z level of theory was used, which is known to produce reliable line intensities [386]. The same symmetry adapted expansion as used for the ammonia PES and DMS (see Refs. [61, 85]) was employed to represent the *ab initio* data. Although reliable PESs exist for hydronium [387–390], using these would require implementing the corresponding analytic form to be compatible with TROVE.

Variational calculations used a polyad number of $P_{\max} = 28$, with truncation of the kinetic and potential energy operators at 6th and 8th order, respectively. Note that atomic mass values were used to determine the mass sensitivity of the energy levels, however for theoretical frequency data and Einstein A coefficients I used nuclear mass values. This was done because the PES was optimized using nuclear mass values.

Again to demonstrate that the variational calculations are robust, sensitivity coefficients have been computed by Professor Vladimir Špirko using the NRI theory approach [307]. The NRI potential energy function for hydronium [391] was upgraded by fitting to a much broader set of experimental data.

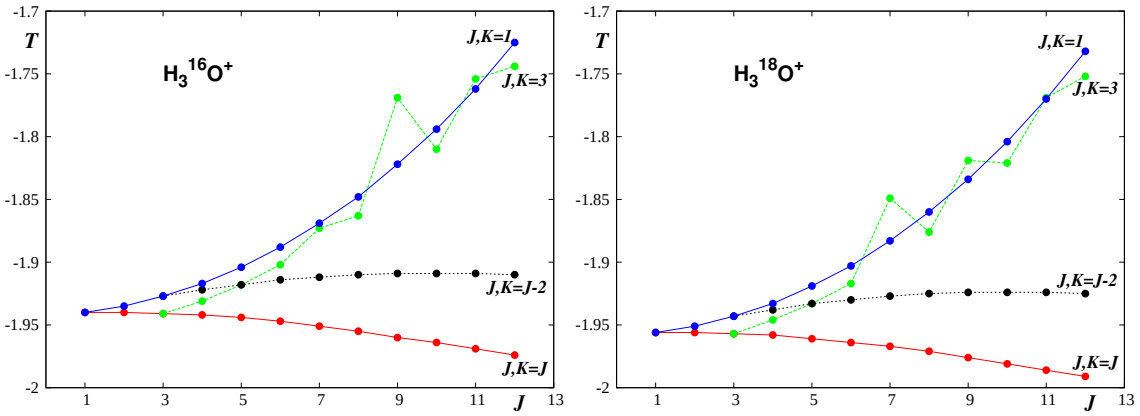

Figure 7.6: Rotational dependence of the sensitivities (T) of the inversion transitions in the ground vibrational states of $H_3{}^{16}O^+$ and $H_3{}^{18}O^+$.

7.4.2 Results

The results are illustrated in Figures 7.6 to 7.9, with detailed tables given in Appendix C. In Fig. 7.6 the rotational dependence of the sensitivities for the inversion transitions in the ground vibrational state of $H_3{}^{16}O^+$ and $H_3{}^{18}O^+$ is shown. The non-smooth behaviour of the $(J, K=3)$ transitions is caused by the $\Delta k = \pm 3$ interactions (for details see Belov et al. [345]). For $D_3{}^{16}O^+$ the sensitivities display a very similar, albeit smoother trend.

More encouraging are the low J rotation-inversion transitions displayed in Fig. 7.7, of which a large number have been observed experimentally in both laboratory [381, 383], and astronomical [366, 367, 369, 370, 375] environments. The appearance of both positive and negative sensitivities is beneficial to constrain a possible variation in the proton-to-electron mass ratio. The effective Hamiltonian model used by Kozlov et al. [293] (KPR in Fig. 7.7), which does not account for all centrifugal corrections, shows consistent agreement with both the non-rigid inverter theory (NRI), and variational (TROVE) results. Thus the strongly anomalous sensitivity coefficients of the $1^-_{1,1} \leftarrow 2^+_{2,1}$ and $1^-_{1,0} \leftarrow 2^+_{2,0}$ transitions of H_2DO^+, and the $1^-_{0,1} \leftarrow 1^+_{1,1}$ transition of HD_2O^+, proposed by Kozlov et al. [293] have real promise. The close agreement also confirms that the *ab initio* theory used in the present study is adequate. As discussed by Kozlov et al. [293], the results of Kozlov and Levshakov

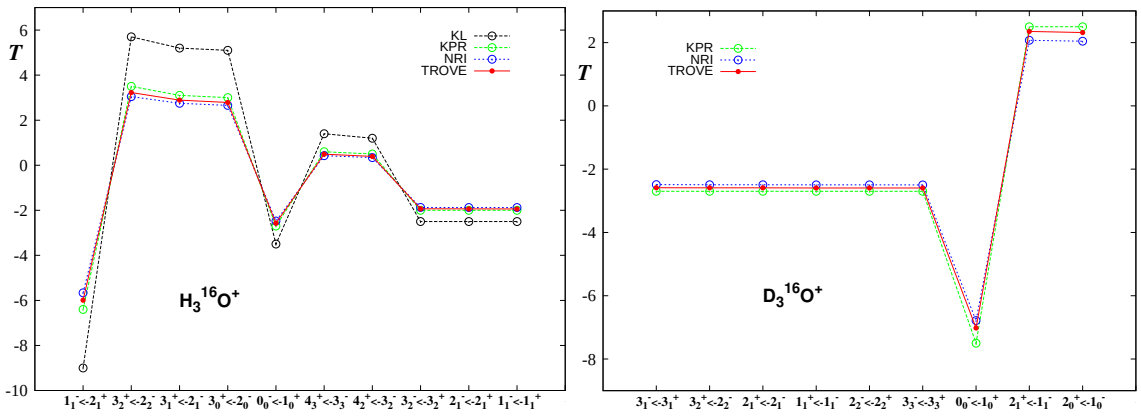

Figure 7.7: State dependence of the calculated sensitivities (T) of the rotation-inversion transitions in the ground vibrational states of $H_3{}^{16}O^+$ and $D_3{}^{16}O^+$. KL: calculated in Kozlov and Levshakov [377]; KPR: calculated in Kozlov et al. [293]; NRI: calculated using the non-rigid inverter theory (this study); TROVE: calculated variationally (this study). States are labelled as $J_K^{\pm}$ on the x-axis.

[377] (KL in Fig. 7.7) overestimate the $H_3{}^{16}O^+$ sensitivities and should not be used in future studies.

The $\Delta k = \pm 3$ interactions give rise to several "forbidden" rovibrational combination differences of the ν_3 band (see Fig. 7.8). The most sensitive of these are presented in Fig. 7.9. Notably the $7_3^- \leftarrow 7_0^+$ and $9_3^- \leftarrow 9_0^+$ combination differences, for which a number of the corresponding transitions have been observed experimentally [378], have theoretically derived values of $T = -15.416$ and 10.518, respectively. The difference, $\Delta T = 25.934$, is comparable to the most stringent limit on μ obtained using methanol, which utilized transitions with $\Delta T = 31.8$ [302]. However, it should be noted that this constraint was deemed unreliable, and subsequently replaced by a more robust value which employed methanol transitions with $\Delta T = 6.4$ [304]. Despite available experimental data [380], the $D_3{}^{16}O^+$ counterparts of these combination differences do not appear to be of any real use, with sensitivities around $T = -1.006$ (see Appendix C for more detail).

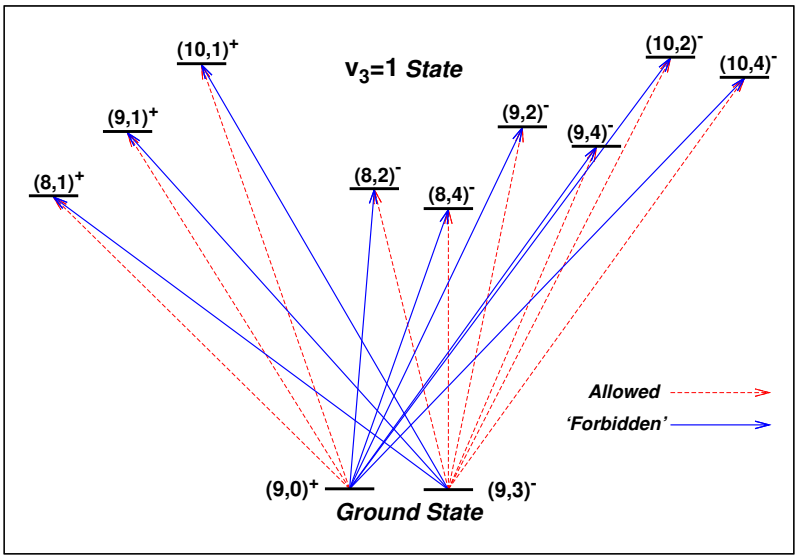

Figure 7.8: The $|J=9, K=0, v_2=0^+\rangle - |J=9, K=3, v_2=0^-\rangle$ combination differences of the ν_3 band of H_3O^+.

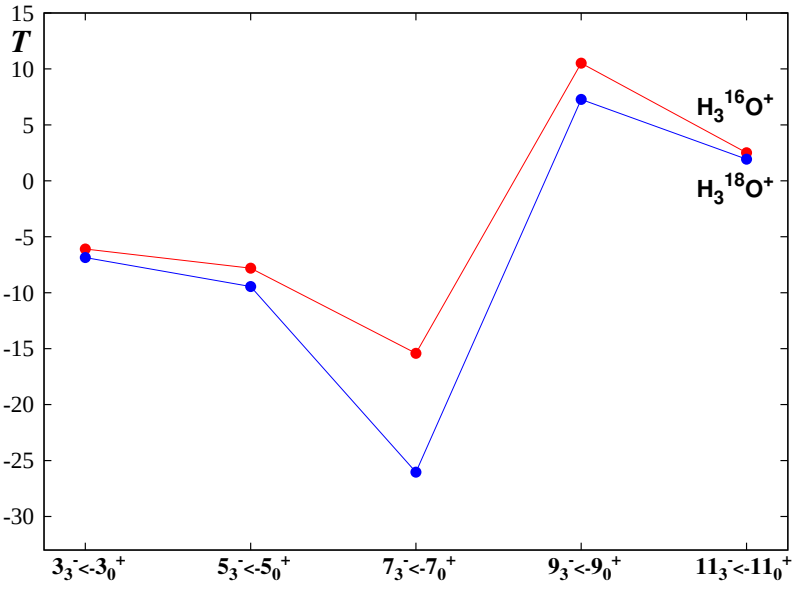

Figure 7.9: The sensitivities (T) of the most sensitive $|J, K=0, v_2=0^+\rangle - |J, K=3, v_2=0^-\rangle$ ($J=3,5,7,9,11$) combination differences of $H_3{}^{16}O^+$ and $H_3{}^{18}O^+$. States are labelled as $J_K^{\pm}$ on the x-axis.

7.5 Chapter summary

The challenge of computing sensitivity coefficients is largely one of establishing the μ-dependence of energy levels. The assumption that all baryonic matter can be treated equally, i.e. any variation in the neutron-to-electron mass ratio would be the same as in the proton-to-electron mass ratio, leads to the statement that μ is directly proportional to atomic mass. The problem translates then to finding the mass dependence of rovibrational energies.

After discussing the most common methods for computing sensitivity coefficients, a new, variational approach was presented. It was based on running a series of calculations using scaled values for the masses of the atoms and then extracting the mass dependence of the energy levels using finite differences. Frequency data and Einstein A coefficients could be computed, along with the mass dependence, for all investigated transitions. This is a major advantage which could help future laboratory and astronomical studies to measure transitions which possess sizeable sensitivities. With this approach it is possible to consider any transition without loss of accuracy, and in principle any molecule can be investigated. However, to do so the necessary steps to perform variational calculations must be in place. This requires reliable potential energy and dipole moment surfaces, and a working implementation of the molecule in a nuclear motion code.

Given the past success of the ammonia method to constrain a possible variation in the proton-to-electron mass ratio, a comprehensive study of the vibration-rotation-inversion transitions of all stable, symmetric top isotopomers of ammonia was performed. The calculated sensitivity coefficients provide perspectives for the further development of the ammonia method. Given the astrophysical importance of NH_3, the sensitivities presented here confirm that ammonia can be used exclusively to constrain a spatial or temporal variation of μ. The reliance on other reference molecular species, which is the main source of systematic error in the ammonia method, can be avoided.

We then looked at the astronomically important hydronium cation $H_3{}^{16}O^+$ and its isotopologues, $H_3{}^{18}O^+$ and $D_3{}^{16}O^+$. Most promising were the "forbidden" combination differences of the ν_3 band, since several of the corresponding transitions had already been experimentally measured. In particular, the $7_3^- \leftarrow 7_0^+$ and $9_3^- \leftarrow 9_0^+$ combination differences are separated by $\Delta T = 25.934$. This is around four times larger than the ΔT of the methanol transitions recently used to determine the most reliable constraint on a possible variation of μ.

8 Summary and outlook

This thesis has been concerned with variational calculations of rotation-vibration spectra for small polyatomic molecules of astrophysical interest. The systems considered were CH_3Cl, SiH_4, CH_4, NH_3 and H_3O^+. Sophisticated electronic structure methods were used to construct new *ab initio* potential energy and dipole moment surfaces for CH_3Cl, SiH_4 and CH_4. Apart from the DMS of CH_4, all surfaces were rigorously evaluated against a range of high-resolution spectroscopic data. Whilst the accuracy of the DMSs was sufficient for atmospheric purposes, the PESs will need to be empirically refined and this is currently in progress before hot line lists are produced. For CH_3Cl and SiH_4 I plan to cover the 0–9000 cm^{-1} range and include transitions up to $J = 85$ and $J = 50$, respectively. A new methane line list will have to go to much higher wavenumber regions, ideally to 14 000 cm^{-1}, but the exact details have not yet been decided.

Computing a complete and accurate line list for five-atom molecules is computationally challenging. Only methane, with the 10to10 line list [5], has been treated using TROVE and this required around 3 million CPU (central processing unit) hours on the Darwin and COSMOS high-performance computing clusters. A line list for nitric acid (HNO_3) applicable up to 500 K [392, 393] was produced for the ExoMol database but this was calculated using a hybrid variational-perturbation method [394]. The approach partitions the Hamiltonian matrix into separate sub-blocks based on the contribution of the matrix elements to the energy levels. The sub-blocks are treated either variationally or using perturbation theory depending on their importance. Naturally some degree of accuracy is lost but the method is promising for larger molecular systems.

A major bottleneck in rovibrational calculations is the diagonalization of huge matrices. The size of the matrix will depend on the number of basis functions so it

is desirable to use a compact basis set. A new approach which is currently being tested, and will most likely be adopted for the CH_3Cl, SiH_4 and CH_4 line lists, is to use a transition moment pruned (TM-pruned) basis set. Vibrational transition moments are relatively inexpensive to compute and can be done with a large polyad number $P_{\max}$ in TROVE. Each vibrational energy level, and therefore each $J = 0$ basis function, is assigned a transition moment which is simply the largest value computed for that state. The $J = 0$ basis set is then pruned with respect to the transition moments and energy levels with small values are removed and neglected in subsequent spectral simulations. How aggressive the pruning procedure is will depend on thresholds set by the user and it is possible to only prune after a certain energy e.g. after $8000\,\mathrm{cm}^{-1}$. The TM-pruned basis set is then multiplied in the usual manner with symmetrized rigid-rotor functions for $J > 0$ calculations.

An advantage of this approach is that the accuracy of the vibrational energies calculated with a large $P_{\max}$ is retained. Removing functions from the basis set will affect all rovibrational energy levels to some degree. However, the errors introduced by pruning the basis set, and also the convergence error associated with $P_{\max}$, can be compensated for by refining the PES with the TM-pruned basis set. The resulting 'effective' PES is only reliable for that exact computational setup. This is usually the case in theoretical line list production.

Another bottleneck arises when calculating intensities because of the sheer number of transitions which must be considered; a comprehensive five-atom molecule line list applicable for elevated temperatures will easily contain billions of lines. To speed up this process a new standalone code to work with TROVE for computing intensities, GAIN-MPI [395], was recently developed to exploit the massively parallel architecture of GPUs (graphics processing units). GAIN-MPI has been used in the production of hot line lists for PH_3 [396], H_2CO [191], and H_2O_2 [397], and significantly accelerated the calculation of intensities. Combined with the implementation of curvilinear internal coordinates and an automatic differentiation method to construct the rovibrational Hamiltonian in TROVE [70], accurately simulating

rovibrational spectra from first principles is far more manageable than when the 10to10 methane line list was produced.

Discussing now the work concerning a possible variation of the proton-to-electron mass ratio μ, existing potential energy and dipole moment surfaces were used to uncover highly sensitive and potentially observable transitions in NH_3 and H_3O^+. The variational approach was robust and new spectral lines could be investigated without loss of accuracy; something not usually possible with effective Hamiltonian models. Given that the ExoMol database is actively expanding and including notable astrophysical molecules, there is an opportunity to probe new systems and transitions. As demonstrated in this thesis, a lot of effort goes into constructing reliable PESs and DMSs to work with. Furthermore, optimizing the nuclear motion calculations is not always straightforward and it can take some time to do so.

Several nuclear motion codes are used within the ExoMol project (discussed further in Ref. [69]) such as Duo [398] for diatomics, DVR3D [399] for triatomics, and TROVE [9] for polyatomics. With each program are tailored input files for a variety of different molecules. Sensitivity coefficients are fairly trivial to compute and require a series of calculations with different values for the mass of the molecule. Whilst there are no strict criteria for which molecular systems are best for probing μ, molecules which can be observed in different astrophysical environments at different red shifts are highly favourable. This is why the observation of H_2 spectra has been so successful and it can be said that if μ had changed, it is by less than 0.0005% in the past (10–12.4) $\times 10^9$ years [291].

The future of variational calculations of rotation-vibration spectra will be concerned with larger molecules. The ExoMol project is actively working on hydrocarbons such as ethylene (C_2H_4) and ethane (C_2H_6) but these are challenging systems. The so-called curse of dimensionality, the exponential scaling of matrix size with the number of atoms, will only partially be addressed as computing power increases. Instead, efficient techniques will have to be developed in areas such as vibrational basis set pruning and exploiting matrix sparsity to make the problem tractable.

Finally, an issue we have not discussed is the huge amount of data associated with a line list and how best to store it. The ExoMol data structure (see Tennyson et al. [8]) was designed to be as concise as possible. Even so, storing a line list takes up a sizeable amount of computer memory and for larger systems the demands will only grow. In a line list a significant number of computed transitions have relatively weak intensities. These are important as they contribute to opacity in astronomical spectra but are unlikely to be observed directly due to the resolution of spectroscopic observations. There should therefore be a more compact way of representing weak lines. One suggestion is to separate the wavenumber range of the line list into bins, e.g. $10^{-3}\,\mathrm{cm}^{-1}$, and for each bin sum the intensities of the weak lines. Stronger lines above a certain intensity threshold remain so that band structure is preserved but the size of the line list is reduced. Techniques such as these will undoubtedly emerge in the future.

References

[1] M. Born and W. Heisenberg, "Zur quantentheorie der molekeln," Ann. Phys. (Berlin) **74**, 1 (1924).

[2] M. Born and R. Oppenheimer, "Zur quantentheorie der molekeln," Ann. Phys. (Berlin) **84**, 457 (1927).

[3] M. Born and K. Huang, *Dynamical Theory of Crystal Lattices* (Clarendon Press, Oxford, 1954).

[4] P. R. Bunker, C. J. McLarnon, and R. E. Moss, "Application of the effective vibration-rotation Hamiltonian to H_2 and D_2," Mol. Phys. **33**, 425 (1977).

[5] S. N. Yurchenko and J. Tennyson, "ExoMol line lists - IV. The rotation-vibration spectrum of methane up to 1500 K," Mon. Not. R. Astron. Soc. **440**, 1649 (2014).

[6] L. S. Rothman, I. E. Gordon, R. J. Barber, H. Dothe, R. R. Gamache, A. Goldman, V. I. Perevalov, S. A. Tashkun, and J. Tennyson, "HITEMP, the high-temperature molecular spectroscopic database," J. Quant. Spectrosc. Radiat. Transf. **111**, 2139 (2010).

[7] J. Tennyson and S. N. Yurchenko, "ExoMol: molecular line lists for exoplanet and other atmospheres," Mon. Not. R. Astron. Soc. **425**, 21 (2012).

[8] J. Tennyson, S. N. Yurchenko, A. F. Al-Refaie, E. J. Barton, K. L. Chubb, P. A. Coles, S. Diamantopoulou, M. N. Gorman, C. Hill, A. Z. Lam, et al., "The ExoMol database: molecular line lists for exoplanet and other hot atmospheres," J. Mol. Spectrosc. **327**, 73 (2016).

[9] S. N. Yurchenko, W. Thiel, and P. Jensen, "Theoretical ROVibrational Energies (TROVE): A robust numerical approach to the calculation of rovibrational energies for polyatomic molecules," J. Mol. Spectrosc. **245**, 126 (2007).

[10] R. I. Ovsyannikov, W. Thiel, S. N. Yurchenko, M. Carvajal, and P. Jensen, "PH_3 revisited: Theoretical transition moments for the vibrational transitions below 7000 cm^{-1}," J. Mol. Spectrosc. **252**, 121 (2008).

[11] S. N. Yurchenko, in *Chemical Modelling: Volume 10* (The Royal Society of Chemistry, 2014), vol. 10, pp. 183–228, ISBN 978-1-84973-586-5, URL `http://dx.doi.org/10.1039/9781849737241-00183`.

[12] R. J. Bartlett and M. Musial, "Coupled-cluster theory in quantum chemistry," Rev. Mod. Phys. **79**, 291 (2007).

[13] C. Riplinger, B. Sandhoefer, A. Hansen, and F. Neese, "Natural triple excitations in local coupled cluster calculations with pair natural orbitals," J. Chem. Phys. **139**, 134101 (2013).

[14] R. J. Bartlett and G. D. Purvis, "Many-body perturbation theory, coupled-pair many-electron theory, and the importance of quadruple excitations for the correlation problem," Int. J. Quantum Chem. **14**, 561 (1978).

[15] J. A. Pople, J. S. Binkley, and R. Seeger, "Theoretical models incorporating electron correlation," Int. J. Quantum Chem. Symp. **10**, 1 (1976).

[16] E. A. Hylleraas, "Neue berechnung der energie des heliums im grundzustande, sowie des tiefsten terms von ortho-helium," Z. Phys. **54**, 347 (1929).

[17] T. Helgaker, W. Klopper, and D. P. Tew, "Quantitative quantum chemistry," Mol. Phys. **106**, 2107 (2008).

[18] S. Ten-No, "Initiation of explicitly correlated Slater-type geminal theory," Chem. Phys. Lett. **398**, 56 (2004).

[19] E. F. Valeev, "Combining explicitly correlated R12 and Gaussian geminal electronic structure theories," J. Chem. Phys. **125**, 244106 (2006).

[20] W. Kutzelnigg, "r_{12}-Dependent terms in the wave function as closed sums of partial wave amplitudes for large l," Theor. Chim. Acta **68**, 445 (1985).

[21] E. F. Valeev, "Improving on the resolution of the identity in linear R12 *ab initio* theories," Chem. Phys. Lett. **395**, 190 (2004).

[22] F. R. Manby, "Density fitting in second-order linear-r_{12} Møller-Plesset perturbation theory," J. Chem. Phys. **119**, 4607 (2003).

[23] S. Ten-no and F. R. Manby, "Density fitting for the decomposition of three-electron integrals in explicitly correlated electronic structure theory," J. Chem. Phys. **119**, 5358 (2003).

[24] D. P. Tew, C. Hättig, R. A. Bachorz, and W. Klopper, in *Recent Progress in Coupled Cluster Methods*, edited by P. Cársky, J. Paldus, and J. Pittner (Springer, New York, 2010).

[25] T. B. Adler, G. Knizia, and H.-J. Werner, "A simple and efficient CCSD(T)-F12 approximation," J. Chem. Phys. **127**, 221106 (2007).

[26] G. Knizia, T. B. Adler, and H.-J. Werner, "Simplified CCSD(T)-F12 methods: Theory and benchmarks," J. Chem. Phys. **130**, 054104 (2009).

[27] H.-J. Werner, T. B. Adler, G. Knizia, and F. R. Manby, in *Recent Progress in Coupled Cluster Methods*, edited by P. Cársky, J. Paldus, and J. Pittner (Springer, New York, 2010).

[28] F. Jensen, "Atomic orbital basis sets," WIREs Comput. Mol. Sci. **3**, 273 (2013).

[29] J. G. Hill, "Gaussian basis sets for molecular applications," Int. J. Quantum Chem. **113**, 21 (2013).

[30] T. H. Dunning Jr., "Gaussian basis sets for use in correlated molecular calculations. 1. The atoms boron through neon and hydrogen," J. Chem. Phys. **90**, 1007 (1989).

[31] R. A. Kendall, T. H. Dunning Jr., and R. J. Harrison, "Electron affinities of the first-row atoms revisited. Systematic basis sets and wave functions," J. Chem. Phys. **96**, 6796 (1992).

[32] D. E. Woon and T. H. Dunning Jr., "Gaussian basis sets for use in correlated molecular calculations. III. The atoms aluminum through argon," J. Chem. Phys. **98**, 1358 (1993).

[33] D. E. Woon and T. H. Dunning Jr., "Gaussian basis sets for use in correlated molecular calculations. V. Core-valence basis sets for boron through neon," J. Chem. Phys. **103**, 4572 (1995).

[34] T. H. Dunning Jr., K. A. Peterson, and A. K. Wilson, "Gaussian basis sets for use in correlated molecular calculations. X. The atoms aluminum through argon revisited," J. Chem. Phys. **114**, 9244 (2001).

[35] K. A. Peterson and T. H. Dunning Jr., "Accurate correlation consistent basis sets for molecular core-valence correlation effects: The second row atoms Al–Ar, and the first row atoms B–Ne revisited," J. Chem. Phys. **117**, 10548 (2002).

[36] K. A. Peterson, T. B. Adler, and H.-J. Werner, "Systematically convergent basis sets for explicitly correlated wavefunctions: The atoms H, He, B–Ne, and Al–Ar," J. Chem. Phys. **128**, 084102 (2008).

[37] J. G. Hill, S. Mazumder, and K. A. Peterson, "Correlation consistent basis sets for molecular core-valence effects with explicitly correlated wave functions: The atoms B–Ne and Al–Ar," J. Chem. Phys. **132**, 054108 (2010).

[38] K. A. Peterson, M. K. Kesharwani, and J. M. L. Martin, "The cc-pV5Z-F12 basis set: reaching the basis set limit in explicitly correlated calculations," Mol. Phys. **113**, 1551 (2015).

[39] J. Almlöf and P. R. Taylor, "General contraction of Gaussian basis sets. I. Atomic natural orbitals for first- and second-row atoms," J. Chem. Phys. **86**, 4070 (1987).

[40] K. E. Yousaf and K. A. Peterson, "Optimized auxiliary basis sets for explicitly correlated methods," J. Chem. Phys. **129**, 184108 (2008).

[41] F. Weigend, "A fully direct RI-HF algorithm: Implementation, optimised auxiliary basis sets, demonstration of accuracy and efficiency," Phys. Chem. Chem. Phys. **4**, 4285 (2002).

[42] C. Hättig, "Optimization of auxiliary basis sets for RI-MP2 and RI-CC2 calculations: Core-valence and quintuple-zeta basis sets for H to Ar and QZVPP basis sets for Li to Kr," Phys. Chem. Chem. Phys. **7**, 59 (2005).

[43] S. Kritikou and J. G. Hill, "Auxiliary basis sets for density fitting in explicitly correlated calculations: The atoms H–Ar," J. Chem. Theory Comput. **11**, 5269 (2015).

[44] D. Feller, K. A. Peterson, and J. G. Hill, "On the effectiveness of CCSD(T) complete basis set extrapolations for atomization energies," J. Chem. Phys. **135**, 044102 (2011).

[45] D. W. Schwenke, "The extrapolation of one-electron basis sets in electronic structure calculations: How it should work and how it can be made to work," J. Chem. Phys. **122**, 014107 (2005).

[46] J. G. Hill, K. A. Peterson, G. Knizia, and H.-J. Werner, "Extrapolating MP2 and CCSD explicitly correlated correlation energies to the complete basis set limit with first and second row correlation consistent basis sets," J. Chem. Phys. **131**, 194105 (2009).

[47] D. Feller and K. A. Peterson, "An expanded calibration study of the explicitly correlated CCSD(T)-F12b method using large basis set standard CCSD(T) atomization energies," J. Chem. Phys. **139**, 084110 (2013).

[48] K. A. Peterson, D. Feller, and D. A. Dixon, "Chemical accuracy in *ab initio* thermochemistry and spectroscopy: current strategies and future challenges," Theor. Chem. Acc. **131** (2012).

[49] D. Feller, K. A. Peterson, and T. D. Crawford, "Sources of error in electronic structure calculations on small chemical systems," J. Chem. Phys. **124**, 054107 (2006).

[50] R. J. Gdanitz and R. Ahlrichs, "The averaged coupled-pair functional (ACPF): A size-extensive modification of MR CI(SD)," Chem. Phys. Lett. **143**, 413 (1988).

[51] H.-J. Werner and P. J. Knowles, "A comparison of variational and non-variational internally contracted multiconfiguration-reference configuration interaction calculations," Theor. Chim. Acta **78**, 175 (1990), ISSN 0040-5744.

[52] X. Huang, D. W. Schwenke, and T. J. Lee, "An accurate global potential energy surface, dipole moment surface, and rovibrational frequencies for NH_3," J. Chem. Phys. **129**, 214304 (2008).

[53] R. D. Cowan and D. C. Griffin, "Approximate relativistic corrections to atomic radial wave-functions," J. Opt. Soc. Am. **66**, 1010 (1976).

[54] M. Douglas and N. M. Kroll, "Quantum electrodynamical corrections to the fine structure of helium," Ann. Phys. **82**, 89 (1974).

[55] B. A. Heß, "Relativistic electronic-structure calculations employing a two-component no-pair formalism with external-field projection operators," Phys. Rev. A **33**, 3742 (1986).

[56] G. Tarczay, A. G. Császár, W. Klopper, and H. M. Quiney, "Anatomy of relativistic energy corrections in light molecular systems," Mol. Phys. **99**, 1769 (2001).

[57] O. Christiansen, "Vibrational structure theory: new vibrational wave function methods for calculation of anharmonic vibrational energies and vibrational contributions to molecular properties," Phys. Chem. Chem. Phys. **9**, 2942 (2007).

[58] O. Christiansen, "Selected new developments in vibrational structure theory: potential construction and vibrational wave function calculations," Phys. Chem. Chem. Phys. **14**, 6672 (2012).

[59] R. I. Ovsyannikov, W. Thiel, S. N. Yurchenko, M. Carvajal, and P. Jensen, "Vibrational energies of PH_3 calculated variationally at the complete basis set limit," J. Chem. Phys. **129**, 044309 (2008).

[60] A. Yachmenev, S. N. Yurchenko, T. Ribeyre, and W. Thiel, "High-level *ab initio* potential energy surfaces and vibrational energies of H_2CS," J. Chem. Phys. **135**, 074302 (2011).

[61] S. N. Yurchenko, R. J. Barber, A. Yachmenev, W. Thiel, P. Jensen, and J. Tennyson, "A variationally computed $T = 300\,\mathrm{K}$ line list for NH_3," J. Phys. Chem. A **113**, 11845 (2009).

[62] S. N. Yurchenko, A. Yachmenev, W. Thiel, O. Baum, T. F. Giesen, V. V. Melnikov, and P. Jensen, "An *ab initio* calculation of the vibrational energies and transition moments of HSOH," J. Mol. Spectrosc. **257**, 57 (2009).

[63] A. Yachmenev, S. N. Yurchenko, P. Jensen, O. Baum, T. F. Giesen, and W. Thiel, "Theoretical rotation-torsion spectra of HSOH," Phys. Chem. Chem. Phys. **12**, 8387 (2010).

[64] S. N. Yurchenko, M. Carvajal, A. Yachmenev, W. Thiel, and P. Jensen, "A theoretical-spectroscopy, *ab initio*-based study of the electronic ground state of $^{121}SbH_3$," J. Quant. Spectrosc. Radiat. Transf. **111**, 2279 (2010).

[65] A. Yachmenev, S. N. Yurchenko, P. Jensen, and W. Thiel, "A new "spectroscopic" potential energy surface for formaldehyde in its ground electronic state," J. Chem. Phys. **134**, 244307 (2011).

[66] D. S. Underwood, J. Tennyson, and S. N. Yurchenko, "An *ab initio* variationally computed room-temperature line list for $^{32}S^{16}O_3$," Phys. Chem. Chem. Phys. **15**, 10118 (2013).

[67] O. L. Polyansky, I. N. Kozin, R. I. Ovsyannikov, P. Malyszek, J. Koput, J. Tennyson, and S. N. Yurchenko, "Variational calculation of highly excited rovibrational energy levels of H_2O_2," J. Phys. Chem. A **117**, 7367 (2013).

[68] S. N. Yurchenko, J. Tennyson, R. J. Barber, and W. Thiel, "Vibrational transition moments of CH_4 from first principles," J. Mol. Spectrosc. **291**, 69 (2013).

[69] J. Tennyson and S. N. Yurchenko, "The ExoMol project: Software for computing large molecular line lists," Int. J. Quantum Chem. **117**, 92 (2017).

[70] A. Yachmenev and S. N. Yurchenko, "Automatic differentiation method for numerical construction of the rotational-vibrational Hamiltonian as a power series in the curvilinear internal coordinates using the Eckart frame," J. Chem. Phys. **143**, 014105 (2015).

[71] A. Griewank, in *Mathematical Programming*, edited by M. Iri and K. Tanabe (Kluwer Academic Publishing, Dordrecht, 1989).

[72] A. Griewank and A. Walther, *Evaluating Derivatives: Principles and Techniques of Algorithmic Differentiation* (SIAM, Philadelphia, PA, 2008), 2nd ed.

[73] C. Eckart, "Some studies concerning rotating axes and polyatomic molecules," Phys. Rev. **47**, 552 (1935).

[74] P. Jensen, "A new morse oscillator-rigid bender internal dynamics (MORBID) Hamiltonian for triatomic molecules," J. Mol. Spectrosc. **128**, 478 (1988).

[75] H. M. Pickett and H. L. Strauss, "Conformational structure, energy, and inversion rates of cyclohexane and some related oxanes," J. Am. Chem. Soc. **92**, 7281 (1970).

[76] A. Y. Dymarsky and K. N. Kudin, "Computation of the pseudorotation matrix to satisfy the Eckart axis conditions," J. Chem. Phys. **122**, 124103 (2005).

[77] S. V. Krasnoshchekov, E. V. Isayeva, and N. F. Stepanov, "Determination of the Eckart molecule-fixed frame by use of the apparatus of quaternion algebra," J. Chem. Phys. **140**, 154104 (2014).

[78] J. Pesonen, "Eckart frame vibration-rotation Hamiltonians: Contravariant metric tensor," J. Chem. Phys. **140**, 074101 (2014).

[79] V. Szalay, "Eckart-sayvetz conditions revisited," J. Chem. Phys. **140**, 234107 (2014).

[80] V. Szalay, "Understanding nuclear motions in molecules: Derivation of Eckart frame ro-vibrational Hamiltonian operators via a gateway Hamiltonian operator," J. Chem. Phys. **142**, 174107 (2015).

[81] A. Sayvetz, "The kinetic energy of polyatomic molecules," J. Chem. Phys. **7**, 383 (1939).

[82] P. R. Bunker and P. Jensen, *Molecular Symmetry and Spectroscopy* (NRC Research Press, Ottawa, 1998), 2nd ed.

[83] B. V. Noumerov, "A method of extrapolation of perturbations," Mon. Not. R. Astron. Soc. **84**, 592 (1924).

[84] J. W. Cooley, "An improved eigenvalue corrector formula for solving the Schrödinger equation for central fields," Math. Comput. **15**, 363 (1961).

[85] S. N. Yurchenko, R. J. Barber, J. Tennyson, W. Thiel, and P. Jensen, "Towards efficient refinement of molecular potential energy surfaces: Ammonia as a case study," J. Mol. Spectrosc. **268**, 123 (2011).

[86] S. N. Yurchenko, M. Carvajal, P. Jensen, F. Herregodts, and T. R. Huet, "Potential parameters of PH_3 obtained by simultaneous fitting of ab initio data and experimental vibrational band origins," Chem. Phys. **290**, 59 (2003).

[87] S. N. Yurchenko, W. Thiel, M. Carvajal, H. Lin, and P. Jensen, in *Advances in Quantum Chemistry* (2005), vol. 48 of *Advances in Quantum Chemistry*, pp. 209–238.

[88] A. Yachmenev, Thesis, Heinrich-Heine-Universität Düsseldorf, Germany, (2011).

[89] L. Rothman, I. Gordon, Y. Babikov, A. Barbe, D. C. Benner, P. Bernath, M. Birk, L. Bizzocchi, V. Boudon, L. Brown, et al., "The HITRAN2012 molecular spectroscopic database," J. Quant. Spectrosc. Radiat. Transf. **130**, 4 (2013).

[90] J.-M. Hartmann, C. Boulet, and D. Robert, *Collisional Effects on Molecular Spectra. Laboratory experiments and models, consequences for applications* (Elsevier, Amsterdam, 2008).

[91] J. Tennyson, P. F. Bernath, A. Campargue, A. G. Császár, L. Daumont, R. R. Gamache, J. T. Hodges, D. Lisak, O. V. Naumenko, L. S. Rothman, et al., "Recommended isolated-line profile for representing high-resolution spectroscopic transitions (IUPAC Technical Report)," Pure Appl. Chem. **86**, 1931 (2014).

[92] A. Segura, J. F. Kasting, V. Meadows, M. Cohen, J. Scalo, D. Crisp, R. A. H. Butler, and G. Tinetti, "Biosignatures from Earth-like planets around M dwarfs," Astrobiology **5**, 706 (2005).

[93] S. Seager, W. Bains, and R. Hu, "A biomass-based model to estimate the plausibility of exoplanet biosignature gases," Astrophys. J. **775**, 104 (2013).

[94] S. Seager, W. Bains, and R. Hu, "Biosignature gases in H_2-dominated atmospheres on rocky exoplanets," Astrophys. J. **777**, 95 (2013).

[95] S. W. Sharpe, T. J. Johnson, R. L. Sams, P. M. Chu, G. C. Rhoderick, and P. A. Johnson, "Gas-phase databases for quantitative infrared spectroscopy," Appl. Spectrosc. **58**, 1452 (2004).

[96] N. Jacquinet-Husson, R. Armante, N. A. Scott, A. Chédin, L. Crépeau, C. Boutammine, A. Bouhdaoui, C. Crevoisier, V. Capelle, C. Boonne, et al., "The 2015 edition of the GEISA spectroscopic database," J. Mol. Spectrosc. **327**, 31 (2016).

[97] H. M. Pickett, R. L. Poynter, E. A. Cohen, M. L. Delitsky, J. C. Pearson, and H. S. P. Müller, "Submillimeter, millimeter, and microwave spectral line catalog," J. Quant. Spectrosc. Radiat. Transf. **60**, 883 (1998).

[98] S. Kondo, Y. Koga, and T. Nakanaga, "Infrared intensities in methyl chloride. III. Improvement of the anharmonic force field and the analysis of the overtone and combination band intensities," Bull. Chem. Soc. Jpn. **58**, 65 (1985).

[99] C. Bray, A. Perrin, D. Jacquemart, and N. Lacome, "The ν_1, ν_4 and $3\nu_6$ bands of methyl chloride in the 3.4-μm region: Line positions and intensities," J. Quant. Spectrosc. Radiat. Transf. **112**, 2446 (2011).

[100] A. Barbouchi Ramchani, D. Jacquemart, M. Dhib, and H. Aroui, "Line positions, intensities and self-broadening coefficients for the ν_5 band of methyl chloride," J. Quant. Spectrosc. Radiat. Transf. **120**, 1 (2013).

[101] A. Barbouchi Ramchani and D. Jacquemart, "Line intensities and self-broadening coefficients for the ν_2 band of methyl chloride," J. Mol. Spectrosc. **326**, 81 (2016).

[102] P. F. Bernath, "Atmospheric chemistry experiment (ACE): Analytical chemistry from orbit," TrAC Trends Anal. Chem. **25**, 647 (2006).

[103] R. Nassar, P. F. Bernath, C. D. Boone, C. Clerbaux, P. F. Coheur, G. Dufour, L. Froidevaux, E. Mahieu, J. C. McConnell, S. D. McLeod, et al., "A global inventory of stratospheric chlorine in 2004," J. Geophys. Res.-Atmos. **111**, 13 (2006).

[104] A. T. Brown, M. P. Chipperfield, C. Boone, C. Wilson, K. A. Walker, and P. F. Bernath, "Trends in atmospheric halogen containing gases since 2004," J. Quant. Spectrosc. Radiat. Transf. **112**, 2552 (2011).

[105] A. T. Brown, C. M. Volk, M. R. Schoeberl, C. D. Boone, and P. F. Bernath, "Stratospheric lifetimes of CFC-12, CCl_4, CH_4, CH_3Cl and N_2O from measurements made by the Atmospheric Chemistry Experiment-Fourier Transform Spectrometer (ACE-FTS)," Atmos. Chem. Phys. **13**, 6921 (2013).

[106] M. L. Santee, N. J. Livesey, G. L. Manney, A. Lambert, and W. G. Read, "Methyl chloride from the Aura Microwave Limb Sounder: First global climatology and assessment of variability in the upper troposphere and stratosphere," J. Geophys. Res.-Atmos. **118**, 13532 (2013).

[107] C. Bray, H. Tran, D. Jacquemart, and N. Lacome, "Line mixing in the ^{Q}Q sub branches of the ν_1 band of methyl chloride," J. Quant. Spectrosc. Radiat. Transf. **113**, 2182 (2012).

[108] C. Bray, D. Jacquemart, J. Buldyreva, N. Lacome, and A. Perrin, "N_2 broadening coefficients of methyl chloride at room temperature," J. Quant. Spectrosc. Radiat. Transf. **113**, 1102 (2012).

[109] C. Bray, D. Jacquemart, N. Lacome, M. Guinet, A. Cuisset, S. Eliet, F. Hindle, G. Mouret, F. Rohart, and J. Buldyreva, "Analysis of self-broadened pure rotational and rovibrational lines of methyl chloride at room temperature," J. Quant. Spectrosc. Radiat. Transf. **116**, 87 (2013).

[110] C. Bray, D. Jacquemart, and N. Lacome, "Temperature dependence for self- and N_2-broadening coefficients of CH_3Cl," J. Quant. Spectrosc. Radiat. Transf. **129**, 186 (2013).

[111] M. Guinet, F. Rohart, J. Buldyreva, V. Gupta, S. Eliet, R. A. Motiyenko, L. Margulès, A. Cuisset, F. Hindle, and G. Mouret, "Experimental studies by complementary terahertz techniques and semi-classical calculations of N_2 broadening coefficients of $CH_3{}^{35}Cl$," J. Quant. Spectrosc. Radiat. Transf. **113**, 1113 (2012).

[112] J. Buldyreva, M. Guinet, S. Eliet, F. Hindle, G. Mouret, R. Bocquet, and A. Cuisset, "Theoretical and experimental studies of CH_3X-Y_2 rotational line shapes for atmospheric spectra modelling: application to room-temperature CH_3Cl-O_2," Phys. Chem. Chem. Phys. **13**, 20326 (2011).

[113] J. Buldyreva and F. Rohart, "Experimental and theoretical studies of room-temperature sub-millimetre $CH_3{}^{35}Cl$ line shapes broadened by H_2," Mol. Phys. **110**, 2043 (2012).

[114] J. Buldyreva, "Air-broadening coefficients of $CH_3{}^{35}Cl$ and $CH_3{}^{37}Cl$ rovibrational lines and their temperature dependence by a semi-classical approach," J. Quant. Spectrosc. Radiat. Transf. **130**, 315 (2013).

[115] J. Buldyreva, L. Margulès, R. A. Motiyenko, and F. Rohart, "Speed dependence of $CH_3{}^{35}Cl$-O_2 line-broadening parameters probed on rotational transitions: Measurements and semi-classical calculations," J. Quant. Spectrosc. Radiat. Transf. **130**, 304 (2013).

[116] A. Barbouchi Ramchani, D. Jacquemart, M. Dhib, and H. Aroui, "Theoretical calculation of self-broadening coefficients for the ν_5 band of methyl chloride at various temperatures," J. Quant. Spectrosc. Radiat. Transf. **134**, 1 (2014).

[117] A. B. Ramchani, D. Jacquemart, M. Dhib, and H. Aroui, "N_2 broadening coefficients of methyl chloride: Measurements at room temperature and calculations at atmospheric temperatures," J. Quant. Spectrosc. Radiat. Transf. **148**, 186 (2014).

[118] A. S. Dudaryonok, N. N. Lavrentieva, and J. V. Buldyreva, "CH_3Cl self-broadening coefficients and their temperature dependence," J. Quant. Spectrosc. Radiat. Transf. **130**, 321 (2013).

[119] A. S. Dudaryonok, N. N. Lavrentieva, J. Buldyreva, L. Margulès, R. A. Motiyenko, and F. Rohart, "Experimental studies, line-shape analysis and semi-empirical calculations of broadening coefficients for $CH_3{}^{35}Cl$–CO_2 sub-millimeter transitions," J. Quant. Spectrosc. Radiat. Transf. **145**, 50 (2014).

[120] A. Nikitin, L. Féjard, J. P. Champion, H. Bürger, M. Litz, J. M. Colmont, and B. Bakri, "New measurements and global analysis of chloromethane in the region from 0 to 1800 cm^{-1}," J. Mol. Spectrosc. **221**, 199 (2003).

[121] A. Nikitin, J. P. Champion, and H. Bürger, in *14th Symposium on High-resolution Molecular Spectroscopy* (2004), vol. 5311 of *SPIE Proceedings*, pp. 97–101.

[122] A. Nikitin and J. P. Champion, "New ground state constants of $^{12}CH_3{}^{35}Cl$ and $^{12}CH_3{}^{37}Cl$ from global polyad analysis," J. Mol. Spectrosc. **230**, 168 (2005).

[123] A. Nikitin, J. P. Champion, and H. Bürger, "Global analysis of $^{12}CH_3{}^{35}Cl$ and $^{12}CH_3{}^{37}Cl$: simultaneous fit of the lower five polyads (0–2600 cm^{-1})," J. Mol. Spectrosc. **230**, 174 (2005).

[124] A. V. Nikitin, T. A. Dmitrieva, and I. E. Gordan, "Improved spectroscopic line list of methyl chloride in the 1900–2600 cm^{-1} spectral region," J. Quant. Spectrosc. Radiat. Transf. **177**, 49 (2016).

[125] V. Gupta, F. Rohart, L. Margulès, R. A. Motiyenko, and J. Buldyreva, "Lineshapes and broadenings of rotational transitions of $CH_3{}^{35}Cl$ in collision with He, Ar and Kr," J. Quant. Spectrosc. Radiat. Transf. **161**, 85 (2015).

[126] A.-L. Sahlberg, J. Zhou, M. Aldén, and Z. S. Li, "Non-intrusive *in situ* detection of methyl chloride in hot gas flows using infrared degenerate four-wave mixing," J. Raman Spectrosc. **46**, 695 (2015).

[127] A. Lucchesini and S. Gozzini, "Diode laser spectroscopy of methyl chloride overtones at 850-860 nm," J. Quant. Spectrosc. Radiat. Transf. **168**, 170 (2016).

[128] T. J. Wallington, B. P. Pivesso, A. M. Lira, J. E. Anderson, C. J. Nielsen, N. H. Andersen, and Ø. Hodnebrog, "CH_3Cl, CH_2Cl_2, $CHCl_3$, and CCl_4: Infrared spectra, radiative efficiencies, and global warming potentials," J. Quant. Spectrosc. Radiat. Transf. **174**, 56 (2016).

[129] J. L. Duncan, A. Allan, and D. C. McKean, "^{13}C frequency shifts and general harmonic force fields of methyl chloride, bromide and iodide," Mol. Phys. **18**, 289 (1970).

[130] J. L. Duncan, D. C. McKean, and G. K. Speirs, "The infra-red spectrum of $^{13}CH_3F$ and the general harmonic force field of methyl fluoride," Mol. Phys. **24**, 553 (1972).

[131] J. L. Duncan, "The centrifugal distortion constant D_K of symmetric top molecules," J. Mol. Spectrosc. **60**, 225 (1976).

[132] K. B. Wiberg, "Infrared intensities. The methyl halides. Effect of substituents on charge distributions.," J. Am. Chem. Soc. **101**, 1718 (1979).

[133] T. B. Lakdar, E. Taillandier, and G. Berthier, "Vibrational properties of polyatomic molecules by quantum chemical methods," Mol. Phys. **39**, 881 (1980).

[134] W. Schneider and W. Thiel, "*Ab initio* calculation of harmonic force fields and vibrational spectra for the methyl, silyl, germyl, and stannyl halides," J. Chem. Phys. **86**, 923 (1987).

[135] N. J. Harris, "A systematic theoretical study of harmonic vibrational frequencies and deuterium isotope fractionation factors for small molecules," J. Phys. Chem. **99**, 14689 (1995).

[136] G. M. Black and M. M. Law, "The general harmonic force field of methyl chloride," J. Mol. Spectrosc. **205**, 280 (2001).

[137] H. B. Schlegel, S. Wolfe, and F. Bernardi, "*Ab initio* computation of force constants. V. The theoretical anharmonic force fields and vibrational frequencies of methyl fluoride and methyl chloride," J. Chem. Phys. **67**, 4194 (1977).

[138] N. Bensari-Zizi and C. Alamichel, "Anharmonic constants of methyl chloride," J. Mol. Spectrosc. **99**, 98 (1983).

[139] S. Kondo, Y. Koga, T. Nakanaga, and S. Saëki, "Calculation of the cubic symmetry force-constants of methyl-bromide and methyl-chloride," J. Mol. Spectrosc. **100**, 332 (1983).

[140] S. Kondo, Y. Koga, and T. Nakanaga, "*Ab initio* MO calculation of the anharmonic force field of methyl-fluoride and methyl-chloride," J. Chem. Phys. **81**, 1951 (1984).

[141] J. L. Duncan and M. M. Law, "A study of vibrational anharmonicity, Fermi resonance interactions, and local mode behaviour in CH_3Cl," J. Mol. Spectrosc. **140**, 13 (1990).

[142] W. Schneider and W. Thiel, "*Ab initio* calculation of anharmonic force fields for the methyl, silyl, germyl, and stannyl halides," Chem. Phys. **159**, 49 (1992).

[143] M. M. Law, "Joint local- and normal-mode studies of the overtone spectra of the methyl halides: CH_3F, CH_3Cl, CH_3Br, CD_3Br, and CH_3I," J. Chem. Phys. **111**, 10021 (1999).

[144] A. V. Nikitin, "Vibrational energy levels of methyl chloride calculated from full dimensional *ab initio* potential energy surface," J. Mol. Spectrosc. **252**, 17 (2008).

[145] S. Kondo, Y. Koga, T. Nakanaga, and S. Saëki, "Infrared intensities in methyl chloride. I. The fundamental bands," Bull. Chem. Soc. Jpn. **56**, 416 (1983).

[146] S. Kondo, Y. Koga, T. Nakanaga, and S. Saëki, "Infrared intensities in methyl chloride. II. Binary overtone and combination bands," Bull. Chem. Soc. Jpn. **57**, 16 (1984).

[147] D. P. Chong and D. Papoušek, "Electric dipole moment derivatives for PH_3, PD_3, CH_3F, CD_3F, CH_3Cl, and CD_3Cl computed by the density functional method," J. Mol. Spectrosc. **155**, 167 (1992).

[148] D. Papoušek, Z. Papouškovà, and D. P. Chong, "Density functional computations of the dipole moment derivatives for halogenated methanes," J. Phys. Chem. **99**, 15387 (1995).

[149] A. F. Jalbout, B. Trzaskowski, Y. Xia, and Y. Li, "Geometry predictions, vibrational analysis and IR intensities of XH_3Y (X=C, Si, Ge, Y=F, Cl, Br) calculated by hybrid density functional theory, MP2 and MP4 methods," Acta Chim. Slov. **54**, 769 (2007).

[150] A. G. Császár, W. D. Allen, and H. F. Schaefer III, "In pursuit of the *ab initio* limit for conformational energy prototypes," J. Chem. Phys. **108**, 9751 (1998).

[151] H.-J. Werner, P. J. Knowles, G. Knizia, F. R. Manby, and M. Schütz, "Molpro: a general-purpose quantum chemistry program package," WIREs Comput. Mol. Sci. **2**, 242 (2012).

[152] M. Kállay and J. Gauss, "Approximate treatment of higher excitations in coupled-cluster theory," J. Chem. Phys. **123**, 214105 (2005).

[153] M. Kállay and J. Gauss, "Approximate treatment of higher excitations in coupled-cluster theory. II. Extension to general single-determinant reference functions and improved approaches for the canonical Hartree-Fock case," J. Chem. Phys. **129**, 144101 (2008).

[154] MRCC, a string-based quantum chemical program suite written by M. Kállay, See also M. Kállay and P. R. Surján, J. Chem. Phys. **115**, 2945 (2001) as well as www.mrcc.hu.

[155] CFOUR, a quantum chemical program package written by J. F. Stanton, J. Gauss, M. E. Harding, and P. G. Szalay with contributions from A. A. Auer, R. J. Bartlett, U. Benedikt, C. Berger, D. E. Bernholdt, Y. J. Bomble, L. Cheng, O. Christiansen, M. Heckert, O. Heun, C. Huber, T.-C. Jagau, D. Jonsson, J. Jusélius, K. Klein, W. J. Lauderdale, D. A. Matthews, T. Metzroth, L. A. Mück, D. P. O'Neill, D. R. Price, E. Prochnow, C. Puzzarini, K. Ruud, F. Schiffmann, W. Schwalbach, S. Stopkowicz, A. Tajti, J. Vázquez, F. Wang, J. D. Watts, and the integral packages MOLECULE (J. Almlöf and P. R. Taylor), PROPS (P. R. Taylor), ABACUS (T. Helgaker, H. J. Aa. Jensen, P. Jørgensen, and J. Olsen), and ECP routines by A. V. Mitin and C. van Wüllen. For the current version, see http://www.cfour.de.

[156] W. Klopper, "Simple recipe for implementing computation of first-order relativistic corrections to electron correlation energies in framework of direct perturbation theory," J. Comput. Chem. **18**, 20 (1997).

[157] C. Michauk and J. Gauss, "Perturbative treatment of scalar-relativistic effects in coupled-cluster calculations of equilibrium geometries and harmonic vibrational frequencies using analytic second-derivative techniques," J. Chem. Phys. **127**, 044106 (2007).

[158] J. Gauss, A. Tajti, M. Kállay, J. F. Stanton, and P. G. Szalay, "Analytic calculation of the diagonal Born-Oppenheimer correction within configuration-interaction and coupled-cluster theory," J. Chem. Phys. **125**, 144111 (2006).

[159] P. Pyykkö, K. G. Dyall, A. G. Császár, G. Tarczay, O. L. Polyansky, and J. Tennyson, "Estimation of Lamb-shift effects for molecules: Application to the rotation-vibration spectra of water," Phys. Rev. A **63**, 024502 (2001).

[160] H. Partridge and D. W. Schwenke, "The determination of an accurate isotope dependent potential energy surface for water from extensive *ab initio* calculations and experimental data," J. Chem. Phys. **106**, 4618 (1997).

[161] T. J. Lee and P. R. Taylor, "A diagnostic for determining the quality of single-reference electron correlation methods," Int. J. Quantum Chem. **36**, 199 (1989).

[162] J. K. G. Watson, "Robust weighting in least-squares fits," J. Mol. Spectrosc. **219**, 326 (2003).

[163] A. Owens, S. N. Yurchenko, A. Yachmenev, J. Tennyson, and W. Thiel, "Accurate *ab initio* vibrational energies of methyl chloride," J. Chem. Phys. **142**, 244306 (2015).

[164] A. Owens, S. N. Yurchenko, A. Yachmenev, J. Tennyson, and W. Thiel, "A global *ab initio* dipole moment surface for methyl chloride," J. Quant. Spectrosc. Radiat. Transf. **184**, 100 (2016).

[165] G. A. Petersson, A. Bennett, T. G. Tensfeldt, M. A. Al-Laham, W. A. Shirley, and J. Mantzaris, "A complete basis set model chemistry. I. The total energies of closed-shell atoms and hydrides of the first-row elements," J. Chem. Phys. **89**, 2193 (1988).

[166] G. A. Petersson and M. A. Al-Laham, "A complete basis set model chemistry. II. Open-shell systems and the total energies of the first-row atoms," J. Chem. Phys. **94**, 6081 (1991).

[167] N. Bensari-Zizi, C. Alamichel, and G. Guelachvili, "Étude des bandes infrarouges en résonance $2\nu_2$, $\nu_2 + \nu_5$, $2\nu_5^0$, $2\nu_5^{\pm 2}$, $2\nu_3 + \nu_5$ et $4\nu_3$ chlorure de méthyle," Can. J. Phys. **60**, 825 (1982).

[168] P. Jensen, S. Brodersen, and G. Guelachvili, "Determination of A_0 for $CH_3{}^{35}Cl$ and $CH_3{}^{37}Cl$ from the ν_4 infrared and Raman bands," J. Mol. Spectrosc. **88**, 378 (1981).

[169] J. Demaison, G. Wlodarczak, and H. D. Rudolph, in *Advances in Molecular Structure Research, Vol 3*, edited by M. Hargittai and I. Hargittai (JAI Press, Greenwich, 1997).

[170] J. Demaison and G. Wlodarczak, "The equilibrium C–H bond-length," Struct. Chem. **5**, 57 (1994).

[171] J. Demaison, L. Margulès, and J. E. Boggs, "The equilibrium C–Cl, C–Br, and C–I bond lengths from *ab initio* calculations, microwave and infrared spectroscopies, and empirical correlations," Struct. Chem. **14**, 159 (2003).

[172] S. Coriani, D. Marchesan, J. Gauss, C. Hättig, T. Helgaker, and P. Jørgensen, "The accuracy of *ab initio* molecular geometries for systems containing second-row atoms," J. Chem. Phys. **123**, 184107 (2005).

[173] J. W. Elkins, R. H. Kagann, and R. L. Sams, "Infrared band strengths for methyl chloride in the regions of atmospheric interest," J. Mol. Spectrosc. **105**, 480 (1984).

[174] G. Blanquet, B. Lance, J. Walrand, and J. P. Bouanich, "Absolute line intensities in the ν_2 band of $^{12}CH_3{}^{35}Cl$ at 7.5 μm," J. Mol. Spectrosc. **170**, 466 (1995).

[175] M. Dang-Nhu, G. Blanquet, J. Walrand, and F. Derie, "Spectral intensities in the ν_3-band of $^{12}CH_3{}^{35}Cl$ at 13 μm," Mol. Phys. **65**, 77 (1988).

[176] F. Cappellani, G. Restelli, and G. Tarrago, "Absolute infrared intensities in the fundamentals ν_2 and ν_5 of $^{12}CH_3{}^{35}Cl$," J. Mol. Spectrosc. **146**, 326 (1991).

[177] G. Blanquet, J. Walrand, and M. Dang-Nhu, "Absolute line intensities of the ν_6 band of $CH_3{}^{35}Cl$ at 10 μm," J. Mol. Spectrosc. **159**, 156 (1993).

[178] G. Blanquet, J. Walrand, and M. Dang-Nhu, "Spectral intensities in the ν_3 band of $^{12}CH_3{}^{37}Cl$," J. Mol. Spectrosc. **133**, 471 (1989).

[179] G. Blanquet, J. Walrand, and M. Dang-Nhu, "Intensities of the ν_6 band of $^{12}CH_3{}^{37}Cl$ at 10 μm," J. Mol. Spectrosc. **162**, 513 (1993).

[180] G. Wlodarczak, B. Segard, J. Legrand, and J. Demaison, "The dipole moment of $CH_3{}^{35}Cl$," J. Mol. Spectrosc. **111**, 204 (1985).

[181] J. S. Margolis and R. A. Toth, "Absorption strength measurement of the ν_1 band of methyl chloride," J. Mol. Spectrosc. **66**, 30 (1977).

[182] J. S. Margolis, "Absorption strength of the perturbed ν_4 band of CH_3Cl," J. Mol. Spectrosc. **70**, 257 (1978).

[183] M. Dang-Nhu, M. Morillon-Chapey, G. Graner, and G. Guelachvili, "Intensities of the ν_1-bands of $^{12}CH_3{}^{35}Cl$ and $^{12}CH_3{}^{37}Cl$ near 3 μm," J. Quant. Spectrosc. Radiat. Transf. **26**, 515 (1981).

[184] J. P. Bouanich, G. Blanquet, and J. Walrand, "Diode-laser measurements of self-broadening coefficients and line strengths in the ν_3 band of $CH_3{}^{35}Cl$," J. Quant. Spectrosc. Radiat. Transf. **51**, 573 (1994).

[185] G. Blanquet, P. Coupe, J. Walrand, and J. P. Bouanich, "Determination of broadening coefficients and intensities for overlapping spectral lines with application to the $^{Q}R(3,K)$ lines in the ν_3 band of $CH_3{}^{35}Cl$," J. Quant. Spectrosc. Radiat. Transf. **51**, 671 (1994).

[186] G. Blanquet, J. Walrand, J. C. Populaire, and J. P. Bouanich, "Self-broadening coefficients and line strengths in the ν_3 band of $CH_3{}^{35}Cl$ at low temperature," J. Quant. Spectrosc. Radiat. Transf. **53**, 211 (1995).

[187] G. Blanquet, B. Lance, J. Walrand, and J. P. Bouanich, "Absolute line intensities in the ν_2 band of $^{12}CH_3{}^{35}Cl$ at 7.5 μm," Spectrochim. Acta, Part A **52**, 1033 (1996).

[188] P. Jensen and P. R. Bunker, "Nuclear spin statistical weights revisited," Mol. Phys. **97**, 821 (1999).

[189] D. Jacquemart and A. Perrin, private communication.

[190] M. Šimečkova, D. Jacquemart, L. S. Rothman, R. R. Gamache, and A. Goldman, "Einstein A-coefficients and statistical weights for molecular absorption transitions in the HITRAN database," J. Quant. Spectrosc. Radiat. Transf. **98**, 130 (2006).

[191] A. F. Al-Refaie, A. Yachmenev, J. Tennyson, and S. N. Yurchenko, "ExoMol line lists VIII: A variationally computed line list for hot formaldehyde," Mon. Not. R. Astron. Soc. **448**, 1704 (2015).

[192] W. B. Steward and H. H. Nielsen, "The infrared absorption spectrum of silane," J. Chem. Phys. **2**, 712 (1934).

[193] W. B. Steward and H. H. Nielsen, "The infrared absorption spectrum of silane," Phys. Rev. **47**, 828 (1935).

[194] D. M. Goldhaber and A. L. Betz, "Silane in IRC +10216," Astrophys. J. **279**, L55 (1984).

[195] J. J. Keady and S. T. Ridgway, "The IRC +10216 circumstellar envelope. III. Infrared molecular line-profiles," Astrophys. J. **406**, 199 (1993).

[196] J. D. Monnier, W. C. Danchi, D. S. Hale, P. G. Tuthill, and C. H. Townes, "Mid-infrared interferometry on spectral lines. III. Ammonia and silane around IRC +10216 and VY Canis Majoris," Astrophys. J. **543**, 868 (2000).

[197] R. R. Treffers, H. P. Larson, U. Fink, and T. N. Gautier, "Upper limits to trace constituents in jupiters atmosphere from an analysis of its 5-mu-m spectrum," Icarus **34**, 331 (1978).

[198] H. P. Larson, U. Fink, H. A. Smith, and D. S. Davis, "The middle-infrared spectrum of Saturn: Evidence for phosphine and upper limits to other trace atmospheric constituents," Astrophys. J. **240**, 327 (1980).

[199] J. M. L. Martin, K. K. Baldridge, and T. J. Lee, "Accurate *ab initio* anharmonic force field and heat of formation for silane," Mol. Phys. **97**, 945 (1999).

[200] J. M. L. Martin and O. Uzan, "Basis set convergence in second-row compounds. the importance of core polarization functions," Chem. Phys. Lett. **282**, 16 (1998).

[201] X. G. Wang and E. L. Sibert, "A nine-dimensional high order perturbative study of the vibration of silane and its isotopomers," J. Chem. Phys. **113**, 5384 (2000).

[202] X. W. Hou, F. Borondo, and R. M. Benito, "Algebraic calculation of vibrational energy levels for polyatomic molecules xh3 and xh4: application to ammonia and silane," Chem. Phys. Lett. **344**, 421 (2001).

[203] L. Halonen and M. S. Child, "A local mode model for tetrahedral molecules," Mol. Phys. **46**, 239 (1982).

[204] L. Halonen and M. S. Child, "Local mode vibrations in tetrahedral molecules," Comput. Phys. Commun. **51**, 173 (1988).

[205] D. Permogorov and A. Campargue, "The local mode model in silanes and germanes," Mol. Phys. **92**, 117 (1997).

[206] J. K. Xie and J. Tennyson, "Variational calculations of vibrational energy levels for XY_4 molecules 1. Stretching states," Mol. Phys. **100**, 1615 (2002).

[207] H. Lin, D. Wang, X. Y. Chen, X. G. Wang, Z. P. Zhou, and Q. S. Zhu, "Absorption intensity of stretching overtone states of silane and germane," J. Mol. Spectrosc. **192**, 249 (1998).

[208] H. Lin, L. F. Yuan, and Q. S. Zhu, "Local mode overtone intensities of SiH_4 and GeH_4 from a bond dipole model with an *ab initio* calculated dipole moment surface," Chem. Phys. Lett. **308**, 137 (1999).

[209] H. Lin, S. G. He, X. G. Wang, L. F. Yuan, H. Bürger, J. F. D'Eu, N. Reuter, and W. Thiel, "The vibrational overtones of SiH_4 isotopomers: experimental wavenumbers, assignment, *ab initio* dipole moment surfaces and intensities," Phys. Chem. Chem. Phys. **3**, 3506 (2001).

[210] S. G. He, A. W. Liu, H. Lin, S. M. Hu, J. J. Zheng, L. Y. Hao, and Q. S. Zhu, "Study of the stretching vibrational band intensities of XH_4 molecules employing four-dimensional *ab initio* (X = C and Sn) and effective (X = C and Si) dipole moment surfaces," J. Chem. Phys. **117**, 10073 (2002).

[211] Q. S. Zhu, B. S. Zhang, Y. R. Ma, and H. B. Qian, "Local-mode rotational structures in the (3000) and (5000) stretching overtone bands of silane," Chem. Phys. Lett. **164**, 596 (1989).

[212] Q. S. Zhu, B. S. Zhang, Y. R. Ma, and H. B. Qian, "The (3000), (4000) and (5000) stretching overtone bands of silane - I. The effect of local-mode vibration on rotational constants," Spectrochim. Acta A **46**, 1217 (1990).

[213] Q. S. Zhu, H. Ma, B. S. Zhang, Y. R. Ma, and H. B. Qian, "The (3000), (4000) and (5000) stretching overtone bands of silane - II. The rotational analysis in a normal-mode picture," Spectrochim. Acta A **46**, 1323 (1990).

[214] Q. S. Zhu, H. B. Qian, H. Ma, and L. Halonen, "High-resolution spectroscopic study of the (2000) stretching vibrational band and vibrational dependence of rotational constants of silane," Chem. Phys. Lett. **177**, 261 (1991).

[215] F. G. Sun, X. G. Wang, Q. S. Zhu, C. Pierre, and G. Pierre, "Coriolis interaction parameters of the $(2100, F_2)$ bands of SiH_4 and GeH_4. A test of local mode models," Chem. Phys. Lett. **239**, 373 (1995).

[216] Q. S. Zhu, A. Campargue, and F. Stoeckel, "A high-resolution spectroscopic study of SiH_4 $\nu = 6$ and 7 overtones," Spectrochim. Acta A **50**, 663 (1994).

[217] H. Lin, H. Bürger, S. G. He, L. F. Yuan, J. Breidung, and W. Thiel, "Overtones of the Si–H stretching-bending polyad in $SiHD_3$: Internal coordinate force field, *ab initio* dipole moment surfaces, and band intensities," J. Phys. Chem. A **105**, 6065 (2001).

[218] N. Jacquinet-Husson, L. Crepeau, R. Armante, C. Boutammine, A. Chédin, N. A. Scott, C. Crevoisier, V. Capelle, C. Boone, N. Poulet-Crovisier, et al., "The 2009 edition of the GEISA spectroscopic database," J. Quant. Spectrosc. Radiat. Transf. **112**, 2395 (2011).

[219] H. S. P. Müller, F. Schlöder, J. Stutzki, and G. Winnewisser, "The Cologne Database for Molecular Spectroscopy, CDMS: a useful tool for astronomers and spectroscopists," J. Mol. Struct. **742**, 215 (2005).

[220] C. Wenger and J. P. Champion, "Spherical top data system (STDS) software for the simulation of spherical top spectra," J. Quant. Spectrosc. Radiat. Transf. **59**, 471 (1998).

[221] S. N. Yurchenko, J. Tennyson, J. Bailey, M. D. J. Hollis, and G. Tinetti, "Spectrum of hot methane in astronomical objects using a comprehensive computed line list," Proc. Natl. Acad. Sci. U.S.A. **111**, 9379 (2014).

[222] W. A. de Jong, R. J. Harrison, and D. A. Dixon, "Parallel Douglas-Kroll energy and gradients in NWChem: Estimating scalar relativistic effects using Douglas-Kroll contracted basis sets," J. Chem. Phys. **114**, 48 (2001).

[223] A. Owens, S. N. Yurchenko, A. Yachmenev, and W. Thiel, "A global potential energy surface and dipole moment surface for silane," J. Chem. Phys. **143**, 244317 (2015).

[224] A. Yachmenev, I. Polyak, and W. Thiel, "Theoretical rotation-vibration spectrum of thioformaldehyde," J. Chem. Phys. **139**, 204308 (2013).

[225] K. Ohno, H. Matsuura, Y. Endo, and E. Hirota, "The microwave spectra of deuterated silanes: SiH_3D, SiH_2D_2, and $SiHD_3$," J. Mol. Spectrosc. **111**, 73 (1985).

[226] M. Chevalier, Thesis, Université de Paris Sud, France, (1988).

[227] R. A. Bernheim, F. W. Lampe, J. F. O'Keefe, and J. R. Qualey III, "Visible and near IR Si–H vibrational overtones in SiH_4," J. Chem. Phys. **80**, 5906 (1984).

[228] K. Fox and W. B. Person, "Transition moments in infrared-active fundamentals of spherical-top molecules," J. Chem. Phys. **64**, 5218 (1976).

[229] D. F. Ball and D. C. McKean, "Infrared intensities in SiH_4 and SiD_4," Spectroc. Acta **18**, 1019 (1962).

[230] I. W. Levin and W. T. King, "Infrared intensities of silane," J. Chem. Phys. **37**, 1375 (1962).

[231] A. M. Coats, D. C. McKean, and D. Steele, "Infrared intensities of ν_3 and ν_4 in SiH_4, GeH_4 and SnH_4," J. Mol. Struct. **320**, 269 (1994).

[232] J. Cadot, "Measurement of the transition dipole moment of silane $^{28}SiH_4$ by diode laser spectroscopy," J. Mol. Spectrosc. **154**, 383 (1992).

[233] K. Fox, "Rotational partition function for tetrahedral molecules," J. Quant. Spectrosc. Radiat. Transf. **10**, 1335 (1970).

[234] M. Dang-Nhu, G. Pierre, and R. Saint-Loup, "The ground-state rotational constants of silane," Mol. Phys. **28**, 447 (1974).

[235] G. Pierre, G. Guelachvili, and C. Amiot, "New determination of ground state rotational constants of silane," J. Phys. France **36**, 487 (1975).

[236] G. Pierre, A. Valentin, and L. Henry, "The basic level of silane obtained from the ν_2 and ν_4 Fourier transformation spectra studies," Can. J. Phys. **62**, 254 (1984).

[237] J. H. van Helden, D. Lopatik, A. Nave, N. Lang, P. B. Davies, and J. Röpcke, "High resolution spectroscopy of silane with an external-cavity quantum cascade laser: Absolute line strengths of the ν_3 fundamental band at 4.6 μm," J. Quant. Spectrosc. Radiat. Transf. **151**, 287 (2015).

[238] G. Pierre, A. Valentin, and L. Henry, "Étude par transformée de Fourier, du spectre, du silane dans la région de 1000 cm^{-1}. analyse de la diade ν_2 et ν_4," Can. J. Phys. **64**, 341 (1986).

[239] B. Lavorel, G. Millot, Q. L. Kou, G. Guelachvili, K. Bouzouba, P. Lepage, V. G. Tyuterev, and G. Pierre, "Study of ν_1/ν_3 interacting bands of silane: Analysis of infrared and Raman spectra," J. Mol. Spectrosc. **143**, 35 (1990).

[240] M. Hippler and M. Quack, "High-resolution Fourier transform infrared and cw-diode laser cavity ringdown spectroscopy of the $\nu_2 + 2\nu_3$ band of methane near 7510 cm^{-1} in slit jet expansions and at room temperature," J. Chem. Phys. **116**, 6045 (2002).

[241] L. R. Brown, "Empirical line parameters of methane from 1.1 to 2.1 μm," J. Quant. Spectrosc. Radiat. Transf. **96**, 251 (2005).

[242] V. Boudon, M. Rey, and M. Loëte, "The vibrational levels of methane obtained from analyses of high-resolution spectra," J. Quant. Spectrosc. Radiat. Transf. **98**, 394 (2006).

[243] S. Kassi, B. Gao, D. Romanini, and A. Campargue, "The near-infrared (1.30–1.70 μm) absorption spectrum of methane down to 77 K," Phys. Chem. Chem. Phys. **10**, 4410 (2008).

[244] S. Albert, S. Bauerecker, V. Boudon, L. R. Brown, J. P. Champion, M. Loëte, A. Nikitin, and M. Quack, "Global analysis of the high resolution infrared spectrum of methane $^{12}CH_4$ in the region from 0 to 4800 cm^{-1}," Chem. Phys. **356**, 131 (2009).

[245] S. Kassi, D. Romanini, and A. Campargue, "Mode by mode CW-CRDS at 80 K: Application to the 1.58 μm transparency window of CH_4," Chem. Phys. Lett. **477**, 17 (2009).

[246] E. Sciamma-O'Brien, S. Kassi, B. Gao, and A. Campargue, "Experimental low energy values of CH_4 transitions near 1.33 μm by absorption spectroscopy at 81 K," J. Quant. Spectrosc. Radiat. Transf. **110**, 951 (2009).

[247] O. Votava, M. Masat, P. Pracna, S. Kassi, and A. Campargue, "Accurate determination of low state rotational quantum numbers ($J < 4$) from planar-jet and liquid nitrogen cell absorption spectra of methane near 1.4 micron," Phys. Chem. Chem. Phys. **12**, 3145 (2010).

[248] A. Campargue, L. Wang, S. Kassi, M. Mašát, and O. Votava, "Temperature dependence of the absorption spectrum of CH_4 by high resolution spectroscopy at 81 K: (II) The icosad region (1.49–1.30 μm)," J. Quant. Spectrosc. Radiat. Transf. **111**, 1141 (2010).

[249] L. Wang, S. Kassi, A. W. Liu, S. M. Hu, and A. Campargue, "High sensitivity absorption spectroscopy of methane at 80 K in the 1.58 μm transparency window: Temperature dependence and importance of the CH_3D contribution," J. Mol. Spectrosc. **261**, 41 (2010).

[250] Y. Lu, D. Mondelain, S. Kassi, and A. Campargue, "The CH_3D absorption spectrum in the 1.58 μm transparency window of methane: Empirical line lists at 81 K and 294 K and temperature dependence," J. Quant. Spectrosc. Radiat. Transf. **112**, 2683 (2011).

[251] D. Mondelain, S. Kassi, L. Wang, and A. Campargue, "The 1.28 μm transparency window of methane (7541–7919 cm^{-1}): Empirical line lists and temperature dependence (80 K–300 K)," Phys. Chem. Chem. Phys. **13**, 7985 (2011).

[252] A. V. Nikitin, X. Thomas, L. Regalia, L. Daumont, P. Von der Heyden, V. G. Tyuterev, L. Wang, S. Kassi, and A. Campargue, "First assignment of the $5\nu_4$ and $\nu_2 + 4\nu_4$ band systems of $^{12}CH_4$ in the 6287–6550 cm^{-1} region," J. Quant. Spectrosc. Radiat. Transf. **112**, 28 (2011).

[253] L. Wang, S. Kassi, A. W. Liu, S. M. Hu, and A. Campargue, "The 1.58 μm transparency window of methane (6165–6750 cm^{-1}): Empirical line list and temperature dependence between 80 and 296 K," J. Quant. Spectrosc. Radiat. Transf. **112**, 937 (2011).

[254] A. Campargue, L. Wang, D. Mondelain, S. Kassi, B. Bézard, E. Lellouch, A. Coustenis, C. de Bergh, M. Hirtzig, and P. Drossart, "An empirical line list for methane in the 1.26–1.71 μm region for planetary investigations ($T = 80$–300 K). Application to Titan," Icarus **219**, 110 (2012).

[255] A. Campargue, O. Leshchishina, L. Wang, D. Mondelain, S. Kassi, and A. V. Nikitin, "Refinements of the WKMC empirical line lists (5852–7919 cm^{-1}) for methane between 80 K and 296 K," J. Quant. Spectrosc. Radiat. Transf. **113**, 1855 (2012).

[256] L. Wang, D. Mondelain, S. Kassi, and A. Campargue, "The absorption spectrum of methane at 80 and 294 K in the icosad (6717–7589 cm^{-1}): Improved

empirical line lists, isotopologue identification and temperature dependence," J. Quant. Spectrosc. Radiat. Transf. **113**, 47 (2012).

[257] A. V. Nikitin, V. Boudon, C. Wenger, S. Albert, L. R. Brown, S. Bauerecker, and M. Quack, "High resolution spectroscopy and the first global analysis of the Tetradecad region of methane $^{12}CH_4$," Phys. Chem. Chem. Phys. **15**, 10071 (2013).

[258] M. Rey, A. V. Nikitin, and V. G. Tyuterev, "First principles intensity calculations for the methane rovibrational spectra in the infrared up to 9300 cm^{-1}," Phys. Chem. Chem. Phys. **15**, 10049 (2013).

[259] O. N. Ulenikov, E. S. Bekhtereva, S. Albert, S. Bauerecker, H. M. Niederer, and M. Quack, "Survey of the high resolution infrared spectrum of methane ($^{12}CH_4$ and $^{13}CH_4$): Partial vibrational assignment extended towards 12 000 cm^{-1}," J. Chem. Phys. **141**, 234302 (2014).

[260] O. Votava, M. Masat, P. Pracna, D. Mondelain, S. Kassi, A. W. Liu, S. M. Hu, and A. Campargue, "Empirical determination of low J values of $^{13}CH_4$ transitions from jet cooled and 80 K cell spectra in the icosad region (7170–7367 cm^{-1})," J. Quant. Spectrosc. Radiat. Transf. **149**, 64 (2014).

[261] S. Beguier, S. Kassi, and A. Campargue, "An empirical line list for methane in the 1.25 μm transparency window," J. Mol. Spectrosc. **308**, 1 (2015).

[262] S. Beguier, A. W. Liu, and A. Campargue, "An empirical line list for methane near 1 μm (9028–10,435 cm^{-1})," J. Quant. Spectrosc. Radiat. Transf. **166**, 6 (2015).

[263] A. V. Nikitin, M. Rey, S. A. Tashkun, S. Kassi, D. Mondelain, A. Campargue, and V. G. Tyuterev, "Analyses and modeling of the $^{12}CH_4$ spectrum at 80 K between 6539 and 6800 cm^{-1}," J. Quant. Spectrosc. Radiat. Transf. **168**, 207 (2016).

[264] M. Rey, A. V. Nikitin, A. Campargue, S. Kassi, D. Mondelain, and V. G. Tyuterev, "*Ab initio* variational predictions for understanding highly congested spectra: rovibrational assignment of 108 new methane sub-bands in the icosad range (6280–7800 cm^{-1})," Phys. Chem. Chem. Phys. **18**, 176 (2016).

[265] B. Amyay, M. Louviot, O. Pirali, R. Georges, J. Vander Auwera, and V. Boudon, "Global analysis of the high temperature infrared emission spectrum of $^{12}CH_4$ in the dyad (ν_2/ν_4) region," J. Chem. Phys. **144**, 024312 (2016).

[266] R. E. Lupu, M. S. Marley, N. Lewis, M. Line, W. A. Traub, and K. Zahnle, "Developing atmospheric retrieval methods for direct imaging spectroscopy of gas giants in reflected light. I. Methane abundances and basic cloud properties," Astron. J. **152**, 217 (2016).

[267] A. Campargue, O. Leshchishina, L. Wang, D. Mondelain, and S. Kassi, "The WKLMC empirical line lists (5852–7919 cm^{-1}) for methane between 80 K and 296 K: "Final" lists for atmospheric and planetary applications," J. Mol. Spectrosc. **291**, 16 (2013).

[268] T. J. Lee, J. M. L. Martin, and P. R. Taylor, "An accurate *ab initio* quartic force field and vibrational frequencies for CH_4 and isotopomers," J. Chem. Phys. **102**, 254 (1995).

[269] R. Marquardt and M. Quack, "Global analytical potential hypersurfaces for large amplitude nuclear motion and reactions in methane. I. Formulation of the potentials and adjustment of parameters to *ab initio* data and experimental constraints," J. Chem. Phys. **109**, 10628 (1998).

[270] R. Marquardt and M. Quack, "Global analytical potential hypersurface for large amplitude nuclear motion and reactions in methane II. Characteristic properties of the potential and comparison to other potentials and experimental information," J. Phys. Chem. A **108**, 3166 (2004).

[271] X. G. Wang and E. L. Sibert, "A nine-dimensional perturbative treatment of the vibrations of methane and its isotopomers," J. Chem. Phys. **111**, 4510 (1999).

[272] D. W. Schwenke and H. Partridge, "Vibrational energy levels for CH_4 from an *ab initio* potential," Spectrochim. Acta, Part A **57**, 887 (2001).

[273] D. W. Schwenke, "Towards accurate *ab initio* predictions of the vibrational spectrum of methane," Spectrochim. Acta, Part A **58**, 849 (2002).

[274] C. Oyanagi, K. Yagi, T. Taketsugu, and K. Hirao, "Highly accurate potential-energy and dipole moment surfaces for vibrational state calculations of methane," J. Chem. Phys. **124**, 064311 (2006).

[275] R. Warmbier, R. Schneider, A. R. Sharma, B. J. Braams, J. M. Bowman, and P. H. Hauschildt, "*Ab initio* modeling of molecular IR spectra of astrophysical interest: application to CH_4," Astron. Astrophys. **495**, 655 (2009).

[276] A. V. Nikitin, M. Rey, and V. G. Tyuterev, "Rotational and vibrational energy levels of methane calculated from a new potential energy surface," Chem. Phys. Lett. **501**, 179 (2011).

[277] X.-G. Wang and T. Carrington, Jr., "Using experimental data and a contracted basis Lanczos method to determine an accurate methane potential energy surface from a least squares optimization," J. Chem. Phys. **141**, 154106 (2014).

[278] M. Majumder, S. E. Hegger, R. Dawes, S. Manzhos, X.-G. Wang, T. Carrington, Jr., J. Li, and H. Guo, "Explicitly correlated MRCI-F12 potential energy surfaces for methane fit with several permutation invariant schemes and full-dimensional vibrational calculations," Mol. Phys. **113**, 1823 (2015).

[279] A. V. Nikitin, M. Rey, and V. G. Tyuterev, "First fully *ab initio* potential energy surface of methane with a spectroscopic accuracy," J. Chem. Phys. **145**, 114309 (2016).

[280] J. I. Canty, P. W. Lucas, S. N. Yurchenko, J. Tennyson, S. K. Leggett, C. G. Tinney, H. R. A. Jones, B. Burningham, D. J. Pinfield, and R. L. Smart,

"Methane and ammonia in the near-infrared spectra of late-T dwarfs," Mon. Not. R. Astron. Soc. **450**, 454 (2015).

[281] A. Owens, S. N. Yurchenko, A. Yachmenev, J. Tennyson, and W. Thiel, "A highly accurate *ab initio* potential energy surface for methane," J. Chem. Phys. **145**, 104305 (2016).

[282] C. Manca Tanner and M. Quack, "Reinvestigation of the $\nu_2 + 2\nu_3$ subband in the overtone icosad of $^{12}CH_4$ using cavity ring-down (CRD) spectroscopy of a supersonic jet expansion," Mol. Phys. **110**, 2111 (2012).

[283] R. Z. Martinez, D. Bermejo, J. Santos, J.-P. Champion, and J. C. Hilico, "High resolution Raman spectroscopy from vibrationally excited states populated by a stimulated Raman process: $2\nu_1 - \nu_1$ of $^{12}CH_4$," J. Chem. Phys. **107**, 4864 (1997).

[284] R. Georges, M. Herman, J. C. Hilico, and O. Robert, "High-resolution FTIR spectroscopy using a jet: Sampling the rovibrational spectrum of $^{12}CH_4$," J. Mol. Spectrosc. **187**, 13 (1998).

[285] J. F. Stanton, "A refined estimate of the bond length of methane," Mol. Phys. **97**, 841 (1999).

[286] H. Hollenstein, R. R. Marquardt, M. Quack, and M. A. Suhm, "Dipole moment function and equilibrium structure of methane in an analytical, anharmonic nine-dimensional potential surface related to experimental rotational constants and transition moments by quantum Monte Carlo calculations," J. Chem. Phys. **101**, 3588 (1994).

[287] M. Oldani, M. Andrist, A. Bauder, and A. G. Robiette, "Pure rotational spectra of methane and methane-d_4 in the vibrational ground state observed by microwave Fourier transform spectroscopy," J. Mol. Spectrosc. **110**, 93 (1985).

[288] P. A. M. Dirac, "The cosmological constants," Nature **139**, 323 (1937).

[289] J. K. Webb, M. T. Murphy, V. V. Flambaum, V. A. Dzuba, J. D. Barrow, C. W. Churchill, J. X. Prochaska, and A. M. Wolfe, "Further evidence for cosmological evolution of the fine structure constant," Phys. Rev. Lett. **87**, 091301 (2001).

[290] E. Reinhold, R. Buning, U. Hollenstein, A. Ivanchik, P. Petitjean, and W. Ubachs, "Indication of a cosmological variation of the proton-electron mass ratio based on laboratory measurement and reanalysis of H_2 spectra," Phys. Rev. Lett. **96**, 151101 (2006).

[291] W. Ubachs, J. Bagdonaite, E. J. Salumbides, M. T. Murphy, and L. Kaper, "Search for a drifting proton-to-electron mass ratio from H_2," Rev. Mod. Phys. **88**, 021003 (2016).

[292] V. V. Flambaum and M. G. Kozlov, "Limit on the cosmological variation of m_p/m_e from the inversion spectrum of ammonia," Phys. Rev. Lett. **98**, 240801 (2007).

[293] M. G. Kozlov, S. G. Porsev, and D. Reimers, "Sensitivity of the isotopologues of hydronium to variation of the electron-to-proton mass ratio," Phys. Rev. A **83**, 052123 (2011).

[294] M. G. Kozlov, "Sensitivity of microwave transitions in H_2O_2 to variation of the electron-to-proton mass ratio," Phys. Rev. A **84**, 042120 (2011).

[295] P. Jansen, I. Kleiner, L.-H. Xu, W. Ubachs, and H. L. Bethlem, "Sensitivity of transitions in internal rotor molecules to a possible variation of the proton-to-electron mass ratio," Phys. Rev. A **84**, 062505 (2011).

[296] P. Jansen, L.-H. Xu, I. Kleiner, W. Ubachs, and H. L. Bethlem, "Methanol as a sensitive probe for spatial and temporal variations of the proton-to-electron mass ratio," Phys. Rev. Lett. **106**, 100801 (2011).

[297] S. A. Levshakov, M. G. Kozlov, and D. Reimers, "Methanol as a tracer of fundamental constants," Astrophys. J. **738**, 26 (2011).

[298] V. V. Ilyushin, P. Jansen, M. G. Kozlov, S. A. Levshakov, I. Kleiner, W. Ubachs, and H. L. Bethlem, "Sensitivity to a possible variation of the proton-to-electron mass ratio of torsion-wagging-rotation transitions in methylamine CH_3NH_2," Phys. Rev. A **85**, 032505 (2012).

[299] V. V. Ilyushin, "Sensitivity to a possible variation of the proton-to-electron mass ratio of torsion-rotation transitions in acetone $(CH_3)_2CO$," J. Mol. Spectrosc. **300**, 86 (2014).

[300] A. V. Viatkina and M. G. Kozlov, "Sensitivity of tunneling-rotational transitions in ethylene glycol to variation of electron-to-proton mass ratio," J. Mol. Spectrosc. **300**, 94 (2014).

[301] J. Bagdonaite, P. Jansen, C. Henkel, H. L. Bethlem, K. M. Menten, and W. Ubachs, "A stringent limit on a drifting proton-to-electron mass ratio from alcohol in the early universe," Science **339**, 46 (2013).

[302] J. Bagdonaite, M. Daprà, P. Jansen, H. L. Bethlem, W. Ubachs, S. Muller, C. Henkel, and K. M. Menten, "Robust constraint on a drifting proton-to-electron mass ratio at $z = 0.89$ from methanol observation at three radio telescopes," Phys. Rev. Lett. **111**, 231101 (2013).

[303] R. I. Thompson, "A new substantive proton to electron mass ratio constraint on rolling scalar field cosmologies," Mon. Not. R. Astron. Soc. **431**, 2576 (2013).

[304] N. Kanekar, W. Ubachs, K. M. Menten, J. Bagdonaite, A. Brunthaler, C. Henkel, S. Muller, H. L. Bethlem, and M. Daprà, "Constraints on changes in the proton-electron mass ratio using methanol lines," Mon. Not. R. Astron. Soc. **448**, L104 (2015).

[305] R. M. Godun, P. B. R. Nisbet-Jones, J. M. Jones, S. A. King, L. A. M. Johnson, H. S. Margolis, K. Szymaniec, S. N. Lea, K. Bongs, and P. Gill, "Frequency ratio of two optical clock transitions in $^{171}Yb^+$ and constraints on the time variation of fundamental constants," Phys. Rev. Lett. **113**, 210801 (2014).

[306] V. Špirko, J. M. R. Stone, and D. Papoušek, "Vibration-inversion-rotation spectra of ammonia: Centrifugal distortion, Coriolis interactions, and force field in $^{14}NH_3$, $^{15}NH_3$, $^{14}ND_3$, and $^{14}NT_3$," J. Mol. Spectrosc. **60**, 159 (1976).

[307] V. Špirko, "Vibrational anharmonicity and the inversion potential function of NH_3," J. Mol. Spectrosc. **101**, 30 (1983).

[308] J. T. Hougen, P. R. Bunker, and J. W. C. Johns, "The vibration-rotation problem in triatomic molecules allowing for a large-amplitude bending vibration," J. Mol. Spectrosc. **34**, 136 (1970).

[309] V. Špirko, "Highly sensitive ammonia probes of a variable proton-to-electron mass ratio," J. Phys. Chem. Lett. **5**, 919 (2014).

[310] P. Jansen, H. L. Bethlem, and W. Ubachs, "Perspective: Tipping the scales: Search for drifting constants from molecular spectra," J. Chem. Phys. **140**, 010901 (2014).

[311] T. Dent, "Composition-dependent long range forces from varying m_p/m_e," J. Cosmol. Astropart. Phys. **0701**, 013 (2007).

[312] J. van Veldhoven, J. Küpper, H. L. Bethlem, B. Sartakov, A. J. A. van Roij, and G. Meijer, "Decelerated molecular beams for high-resolution spectroscopy - The hyperfine structure of $^{15}ND_3$," Eur. Phys. J. D **31**, 337 (2004).

[313] M. T. Murphy, V. V. Flambaum, S. Muller, and C. Henkel, "Strong limit on a variable proton-to-electron mass ratio from molecules in the distant Universe," Science **320**, 1611 (2008).

[314] N. Kanekar, "Constraining changes in the proton-electron mass ratio with inversion and rotational lines," Astrophys. J. Lett. **728**, L12 (2011).

[315] C. Henkel, K. M. Menten, M. T. Murphy, N. Jethava, V. V. Flambaum, J. A. Braatz, S. Muller, J. Ott, and R. Q. Mao, "The density, the cosmic microwave background, and the proton-to-electron mass ratio in a cloud at redshift 0.9," Astron. Astrophys. **500**, 725 (2009).

[316] H. L. Bethlem, M. Kajita, B. Sartakov, G. Meijer, and W. Ubachs, "Prospects for precision measurements on ammonia molecules in a fountain," Eur. Phys. J.-Spec. Top. **163**, 55 (2008).

[317] M. G. Kozlov, A. V. Lapinov, and S. A. Levshakov, "Sensitivity of microwave spectra of deuterated ammonia to the variation of the electron-to-proton mass ratio," J. Phys. B-At. Mol. Opt. Phys. **43**, 074003 (2010).

[318] R. Mauersberger, C. Henkel, and T. L. Wilson, "Vibrationally excited ammonia toward Orion-KL," Astron. Astrophys. **205**, 235 (1988).

[319] P. Schilke, R. Mauersberger, C. M. Walmsley, and T. L. Wilson, "Vibrationally excited ammonia in the Galaxy," Astron. Astrophys. **227**, 220 (1990).

[320] P. Schilke, R. Gusten, A. Schulz, E. Serabyn, and C. M. Walmsley, "Submillimeter observations of vibrationally excited NH_3 towards Orion-KL," Astron. Astrophys. **261**, L5 (1992).

[321] K. M. Menten, R. Guesten, S. Leurini, S. Thorwirth, C. Henkel, B. Klein, C. L. Carilli, and M. J. Reid, "Submillimeter water and ammonia absorption by the peculiar $z \approx 0.89$ interstellar medium in the gravitational lens of the PKS 1830-211 system," Astron. Astrophys. **492**, 725 (2008).

[322] P. Molaro, S. A. Levshakov, and M. G. Kozlov, "Stringent bounds to spatial variations of the electron-to-proton mass ratio in the Milky Way," Nucl. Phys. B-Proc. Suppl. **194**, 287 (2009).

[323] S. A. Levshakov, A. V. Lapinov, C. Henkel, P. Molaro, D. Reimers, M. G. Kozlov, and I. I. Agafonova, "Searching for chameleon-like scalar fields with the ammonia method II. Mapping of cold molecular cores in NH_3 and HC_3N lines.," Astron. Astrophys. **524**, A32 (2010).

[324] S. A. Levshakov, P. Molaro, A. V. Lapinov, D. Reimers, C. Henkel, and T. Sakai, "Searching for chameleon-like scalar fields with the ammonia method," Astron. Astrophys. **512**, A44 (2010).

[325] S. A. Levshakov, D. Reimers, C. Henkel, B. Winkel, A. Mignano, M. Centurion, and P. Molaro, "Limits on the spatial variations of the electron-to-proton mass ratio in the Galactic plane," Astron. Astrophys. **559**, A91 (2013).

[326] Š. Urban, V. Špirko, D. Papoušek, R. S. McDowell, N. G. Nereson, S. P. Belov, L. I. Gershstein, A. V. Maslovskij, A. F. Krupnov, J. Curtis, et al., "Coriolis and l-type interactions in the ν_2, $2\nu_2$, and ν_4 states of $^{14}NH_3$," J. Mol. Spectrosc. **79**, 455 (1980).

[327] H. Sasada, Y. Hasegawa, T. Amano, and T. Shimizu, "High-resolution infrared and microwave spectroscopy of the ν_4 and $2\nu_2$ bands of $^{14}NH_3$ and $^{15}NH_3$," J. Mol. Spectrosc. **96**, 106 (1982).

[328] H. Sasada, Y. Endo, E. Hirota, R. L. Poynter, and J. S. Margolis, "Microwave and Fourier-transform infrared spectroscopy of the $\nu_4 = 1$ and $\nu_2 = 2\,s$ states of NH_3," J. Mol. Spectrosc. **151**, 33 (1992).

[329] E. A. C. Mills and M. R. Morris, "Detection of widespread hot ammonia in the Galactic center," Astrophys. J. **772**, 105 (2013).

[330] D. C. Lis, P. Schilke, E. A. Bergin, M. Gerin, J. H. Black, C. Comito, M. De Luca, B. Godard, R. Higgins, F. Le Petit, et al., "Widespread rotationally-hot hydronium ion in the Galactic interstellar medium," Astrophys. J. **785**, 135 (2014).

[331] T. L. Wilson, C. Henkel, and S. Huettemeister, "The detection of the $(J, K) = (18, 18)$ line of NH_3," Astron. Astrophys. **460**, 533 (2006).

[332] A. Yachmenev, S. N. Yurchenko, I. Paidarova, P. Jensen, W. Thiel, and S. P. A. Sauer, "Thermal averaging of the indirect nuclear spin-spin coupling constants of ammonia: The importance of the large amplitude inversion mode," J. Chem. Phys. **132**, 114305 (2010).

[333] S. N. Yurchenko, R. J. Barber, and J. Tennyson, "A variationally computed line list for hot NH_3," Mon. Not. R. Astron. Soc. **413**, 1828 (2011).

[334] C. Sousa-Silva, N. Hesketh, S. N. Yurchenko, C. Hill, and J. Tennyson, "High temperature partition functions and thermodynamic data for ammonia and phosphine," J. Quant. Spectrosc. Radiat. Transf. **142**, 66 (2014).

[335] S. N. Yurchenko, "A theoretical room-temperature line list for $^{15}NH_3$," J. Quant. Spectrosc. Radiat. Transf. **152**, 28 (2015).

[336] S. N. Yurchenko, J. G. Zheng, H. Lin, P. Jensen, and W. Thiel, "Potential-energy surface for the electronic ground state of NH_3 up to $20\,000\,cm^{-1}$ above equilibrium," J. Chem. Phys. **123**, 134308 (2005).

[337] G. Herzberg, *Infrared and Raman Spectra of Polyatomic Molecules* (D. Van Nostrand Co. Inc., New York, 1945).

[338] M. J. Down, C. Hill, S. N. Yurchenko, J. Tennyson, L. R. Brown, and I. Kleiner, "Re-analysis of ammonia spectra: Updating the HITRAN $^{14}NH_3$ database," J. Quant. Spectrosc. Radiat. Transf. **130**, 260 (2013).

[339] Š. Urban, R. D'Cunha, K. N. Rao, and D. Papoušek, "The $\Delta k = \pm 2$ perturbation-allowed ν_4 band and inversion-rotation energy levels of $^{15}NH_3$," J. Mol. Spectrosc. **111**, 361 (1985).

[340] Š. Urban, R. D'Cunha, K. N. Rao, and D. Papoušek, "The $\Delta k = \pm 2$ "forbidden band" and inversion-rotation energy levels of ammonia," Can. J. Phys. **62**, 1775 (1984).

[341] A. L. Betz, R. A. McLaren, and D. L. Spears, "NH_3 in IRC +10216," Astrophys. J. **229**, L97 (1979).

[342] N. J. Evans, J. H. Lacy, and J. S. Carr, "Infrared molecular spectroscopy toward the Orion IRc2 and IRc7 sources - A new probe of physical conditions and abundances in molecular clouds," Astrophys. J. **383**, 674 (1991).

[343] L. Fusina, G. Di Lonardo, E. Canè, A. Predoi-Cross, H. Rozario, and M. Herman, "The high resolution spectrum of $^{15}NH_3$ in the far-infrared: Rotation-inversion transitions in the ground, $\nu_2 = 1, 2$ and $\nu_4 = 1$ states," J. Quant. Spectrosc. Radiat. Transf. (2017).

[344] H. Fichoux, M. Khelkhal, E. Rusinek, J. Legrand, F. Herlemont, and Š. Urban, "Double resonance sub-Doppler study of the allowed and $\Delta K = -3$ forbidden Q(3,3) transitions to the ν_2 vibrational state of $^{14}NH_3$," J. Mol. Spectrosc. **192**, 169 (1998).

[345] S. P. Belov, L. I. Gershstein, A. F. Krupnov, A. V. Maslovskij, Š. Urban, V. Špirko, and D. Papoušek, "Inversion and inversion-rotation spectrum of $^{14}NH_3$ in the ν_2 excited state," J. Mol. Spectrosc. **84**, 288 (1980).

[346] F. J. Lovas, J. E. Bass, R. A. Dragoset, and K. J. Olsen, "NIST recommended rest frequencies for observed interstellar molecular microwave transitions-2009 revision, (version 3.0),", http://physics.nist.gov/restfreq [2013,12,13], National Institute of Standards and Technology, Gaithersburg, MD. (2009), URL `http://physics.nist.gov/restfreq[2013,12,13]`.

[347] C. M. Persson, J. H. Black, J. Cernicharo, J. R. Goicoechea, G. E. Hassel, E. Herbst, M. Gerin, M. De Luca, T. A. Bell, A. Coutens, et al., "Nitrogen hydrides in interstellar gas *Herschel*/HIFI observations towards G10.6-0.4 (W31C)," Astron. Astrophys. **521**, L45 (2010).

[348] E. A. Cohen and R. L. Poynter, "The microwave spectrum of $^{14}NH_3$ in the $\nu = 000^01^1$ state," J. Mol. Spectrosc. **53**, 131 (1974).

[349] E. A. Cohen, "The ν_4 state inversion spectra of $^{15}NH_3$ and $^{14}NH_3$," J. Mol. Spectrosc. **79**, 496 (1980).

[350] A. R. Al Derzi, T. Furtenbacher, J. Tennyson, S. N. Yurchenko, and A. G. Császár, "MARVEL analysis of the measured high-resolution spectra of $^{14}NH_3$," J. Quant. Spectrosc. Radiat. Transf. **161**, 117 (2015).

[351] M. Quintero-Pérez, T. E. Wall, S. Hoekstra, and H. L. Bethlem, "Preparation of an ultra-cold sample of ammonia molecules for precision measurements," J. Mol. Spectrosc. **300**, 112 (2014).

[352] L. Fusina and S. N. Murzin, "Inversion spectrum and ground state spectroscopic parameters of $^{14}ND_3$," J. Mol. Spectrosc. **167**, 464 (1994).

[353] L. Fusina, M. Carlotti, G. Di Lonardo, S. N. Murzin, and O. N. Stepanov, "Pure inversion and inversion-rotation spectra of $^{15}ND_3$ in the ground state," J. Mol. Spectrosc. **147**, 71 (1991).

[354] Š. Urban, D. Papoušek, M. Bester, K. Yamada, G. Winnewisser, and A. Guarnieri, "Simultaneous analysis of the microwave and infrared spectra of $^{14}ND_3$ and $^{15}ND_3$ for the ν_2 excited state," J. Mol. Spectrosc. **106**, 29 (1984).

[355] P. Helminger and W. Gordy, "Submillimeter-wave spectra of ammonia and phosphine," Phys. Rev. **188**, 100 (1969).

[356] P. Helminger, F. C. De Lucia, and W. Gordy, "Rotational spectra of NH_3 and ND_3 in 0.5-mm wavelength region," J. Mol. Spectrosc. **39**, 94 (1971).

[357] R. Mauersberger, T. L. Wilson, and C. Henkel, "The discovery of an interstellar $^{15}NH_3$ maser," Astron. Astrophys. **160**, L13 (1986).

[358] K. J. Johnston, S. R. Stolovy, T. L. Wilson, C. Henkel, and R. Mauersberger, "VLA observations of the $^{15}NH_3$ maser associated with NGC 7538 IRS 1," Astrophys. J. **343**, L41 (1989).

[359] P. Schilke, C. M. Walmsley, and R. Mauersberger, "Peculiar $^{15}NH_3$ toward NGC 7538-IRS 1," Astron. Astrophys. **247**, 516 (1991).

[360] M. Zeppenfeld, B. G. U. Englert, R. Glöckner, A. Prehn, M. Mielenz, C. Sommer, L. D. van Buuren, M. Motsch, and G. Rempe, "Sisyphus cooling of electrically trapped polyatomic molecules," Nature **491**, 570 (2012).

[361] M. Quintero-Pérez, P. Jansen, T. E. Wall, J. E. van den Berg, S. Hoekstra, and H. L. Bethlem, "Static trapping of polar molecules in a traveling wave decelerator," Phys. Rev. Lett. **110**, 133003 (2013).

[362] P. Jansen, M. Quintero-Pérez, T. E. Wall, J. E. van den Berg, S. Hoekstra, and H. L. Bethlem, "Deceleration and trapping of ammonia molecules in a traveling-wave decelerator," Phys. Rev. A **88**, 043424 (2013).

[363] N. Indriolo, D. A. Neufeld, M. Gerin, P. Schilke, A. O. Benz, B. Winkel, K. M. Menten, E. T. Chambers, J. H. Black, S. Bruderer, et al., "*Herschel* survey of galactic OH^+, H_2O^+, and H_3O^+: Probing the molecular hydrogen fraction and cosmic-ray ionization rate," Astrophys. J. **800**, 40 (2015).

[364] J. M. Hollis, E. B. Churchwell, E. Herbst, and F. C. De Lucia, "An interstellar line coincident with the P(2,1) transition of hydronium (H_3O^+)," Nature **322**, 524 (1986).

[365] A. Wootten, F. Boulanger, M. Bogey, F. Combes, P. J. Encrenaz, M. Gerin, and L. Ziurys, "A search for interstellar H_3O^+," Astron. Astrophys. **166**, L15 (1986).

[366] A. Wootten, J. G. Mangum, B. E. Turner, M. Bogey, F. Boulanger, F. Combes, P. J. Encrenaz, and M. Gerin, "Detection of interstellar H_3O^+ - A confirming line," Astrophys. J. **380**, L79 (1991).

[367] T. G. Phillips, E. F. van Dishoeck, and J. Keene, "Interstellar H_3O^+ and its relation to the O_2 and H_2O abundances," Astrophys. J. **399**, 533 (1992).

[368] R. T. Boreiko and A. L. Betz, "A search for the rotational transitions of H_2D^+ at 1370 GHz and H_3O^+ at 985 GHz," Astrophys. J. **405**, L39 (1993).

[369] J. R. Goicoechea and J. Cernicharo, "Far-infrared detection of H_3O^+ in Sagittarius B2," Astrophys. J. **554**, L213 (2001).

[370] F. F. S. van der Tak, A. Belloche, P. Schilke, R. Güsten, S. Philipp, C. Comito, P. Bergman, and Nyman, L. -Å., "APEX mapping of H_3O^+ in the Sgr B2 region," Astron. Astrophys. **454**, L99 (2006).

[371] F. F. S. van der Tak, S. Aalto, and R. Meijerink, "Detection of extragalactic H_3O^+," Astron. Astrophys. **477**, L5 (2008).

[372] M. Gerin, M. De Luca, J. Black, J. R. Goicoechea, E. Herbst, D. A. Neufeld, E. Falgarone, B. Godard, J. C. Pearson, D. C. Lis, et al., "Interstellar OH^+, H_2O^+ and H_3O^+ along the sight-line to G10.6-0.4," Astron. Astrophys. **518**, L110 (2010).

[373] H. Gupta, P. Rimmer, J. C. Pearson, S. Yu, E. Herbst, N. Harada, E. A. Bergin, D. A. Neufeld, G. J. Melnick, R. Bachiller, et al., "Detection of OH^+ and H_2O^+ towards Orion KL," Astron. Astrophys. **521**, L47 (2010).

[374] S. Aalto, F. Costagliola, F. van der Tak, and R. Meijerink, "H_3O^+ line emission from starbursts and AGNs," Astron. Astrophys. **527**, A69 (2011).

[375] E. González-Alfonso, J. Fischer, S. Bruderer, H. S. P. Müller, J. Graciá-Carpio, E. Sturm, D. Lutz, A. Poglitsch, H. Feuchtgruber, S. Veilleux, et al., "Excited OH^+, H_2O^+, and H_3O^+ in NGC 4418 and Arp 220," Astron. Astrophys. **550**, A25 (2013).

[376] R. Timmermann, T. Nikola, A. Poglitsch, N. Geis, G. J. Stacey, and C. H. Townes, "Possible discovery of the 70 micron H_3O^+ $4_3^- \rightarrow 4_3^+$ transition in Orion BN-IRc2," Astrophys. J. **463**, L109 (1996).

[377] M. G. Kozlov and S. A. Levshakov, "Sensitivity of the H_3O^+ inversion-rotational spectrum to changes in the electron-to proton mass ratio," Astrophys. J. **726**, 65 (2011).

[378] D. Uy, E. T. White, and T. Oka, "Observation of $\Delta|k-l|=3$ transitions in the ν_3 band of H_3O^+," J. Mol. Spectrosc. **183**, 240 (1997).

[379] J. Tang and T. Oka, "Infrared spectroscopy of H_3O^+: The fundamental ν_1 band," J. Mol. Spectrosc. **196**, 120 (1999).

[380] M. Araki, H. Ozeki, and S. Saito, "Microwave spectrum of the inversion-rotation transitions of the D_3O^+ ion: $\Delta k=\pm 3n$ interaction and equilibrium structure," Mol. Phys. **97**, 177 (1999).

[381] T. Furuya and S. Saito, "Laboratory measurement of the $J, K = 1, 0^- - 0, 0^+$ transition of ortho-D$-3O^+$," Astron. Astrophys. **441**, 1039 (2005).

[382] S. Yu, B. J. Drouin, J. C. Pearson, and H. M. Pickett, "Terahertz spectroscopy and global analysis of H_3O^+," Astrophys. J. Suppl. Ser. **180**, 119 (2009).

[383] S. Yu and J. C. Pearson, "Terahertz measurements of the hot hydronium ion with an extended negative glow discharge," Astrophys. J. **786**, 133 (2014).

[384] A. Owens, S. N. Yurchenko, W. Thiel, and V. Špirko, "Accurate prediction of the ammonia probes of a variable proton-to-electron mass ratio," Mon. Not. R. Astron. Soc. **450**, 3191 (2015).

[385] D. Papoušek, Š. Urban, V. Špirko, and K. N. Rao, "The $\Delta k = \pm 2$ and $\delta k = \pm 3$ forbidden transitions in the vibrational-rotational spectra of symmetric top molecules NH_3 and H_3O^+," J. Mol. Struct. **141**, 361 (1986).

[386] O. L. Polyansky, K. Bielska, M. Ghysels, L. Lodi, N. F. Zobov, J. T. Hodges, and J. Tennyson, "High-accuracy CO_2 line intensities determined from theory and experiment," Phys. Rev. Lett. **114**, 243001 (2015).

[387] J. M. Bowman, X. Huang, and S. Carter, "Full dimensional calculations of vibrational energies of H_3O^+ and D_3O^+," Spectrochim. Acta, Part A **58**, 839 (2002).

[388] X. Huang, S. Carter, and J. M. Bowman, "*Ab initio* potential energy surface and vibrational energies of H_3O^+ and its isotopomers," J. Phys. Chem. B **106**, 8182 (2002).

[389] X. Huang, S. Carter, and J. M. Bowman, "*Ab initio* potential energy surface and rovibrational energies of H_3O^+ and its isotopomers," J. Chem. Phys. **118**, 5431 (2003).

[390] T. Rajamäki, A. Miani, and L. Halonen, "Six-dimensional *ab initio* potential energy surfaces for H_3O^+ and NH_3: Approaching the subwave number accuracy for the inversion splittings," J. Chem. Phys. **118**, 10929 (2003).

[391] V. Špirko and W. P. Kraemer, "Anharmonic potential function and rotation-inversion energy levels of H_3O^+," J. Mol. Spectrosc. **134**, 72 (1989).

[392] A. I. Pavlyuchko, S. N. Yurchenko, and J. Tennyson, "A hybrid variational-perturbation calculation of the ro-vibrational spectrum of nitric acid," J. Chem. Phys. **142**, 094309 (2015).

[393] A. I. Pavlyuchko, S. N. Yurchenko, and J. Tennyson, "ExoMol molecular line lists - XI. The spectrum of nitric acid," Mon. Not. R. Astron. Soc. **452**, 1702 (2015).

[394] A. I. Pavlyuchko, S. N. Yurchenko, and J. Tennyson, "Hybrid variational-perturbation method for calculating ro-vibrational energy levels of polyatomic molecules," Mol. Phys. **113**, 1559 (2015).

[395] A. F. Al-Refaie, Thesis, University College London, UK, (2016).

[396] C. Sousa-Silva, A. F. Al-Refaie, J. Tennyson, and S. N. Yurchenko, "ExoMol line lists - VII. The rotation-vibration spectrum of phosphine up to 1500 K," Mon. Not. R. Astron. Soc. **446**, 2337 (2015).

[397] A. F. Al-Refaie, O. L. Polyansky, R. I. Ovsyannikov, J. Tennyson, and S. N. Yurchenko, "ExoMol line lists - XV. A new hot line list for hydrogen peroxide," Mon. Not. R. Astron. Soc. **461**, 1012 (2016).

[398] S. N. Yurchenko, L. Lodi, J. Tennyson, and A. V. Stolyarov, "Duo: A general program for calculating spectra of diatomic molecules," Comput. Phys. Commun. **202**, 262 (2016).

[399] J. Tennyson, M. A. Kostin, P. Barletta, G. J. Harris, O. L. Polyansky, J. Ramanlal, and N. F. Zobov, "DVR3D: a program suite for the calculation of rotation–vibration spectra of triatomic molecules," Comput. Phys. Commun. **163**, 85 (2004).

Appendix A

Table A.1: Assigned $J = 0$ vibrational term values (in cm^{-1}) for $CH_3{}^{35}Cl$ and $CH_3{}^{37}Cl$ computed using the CBS-35^{HL} and CBS-37^{HL} PESs, respectively. The basis contribution corresponds to the TROVE assignment.

Mode	Sym.	CBS-35^{HL}	CBS-37^{HL}	Basis contribution
ν_3	A_1	733.22	727.40	0.94
ν_2	A_1	1355.01	1354.82	0.94
$2\nu_3$	A_1	1457.54	1446.12	0.92
$2\nu_6$	A_1	2029.46	2028.68	0.78
$\nu_2 + \nu_3$	A_1	2080.98	2074.90	0.88
$3\nu_3$	A_1	2173.09	2156.31	0.90
$\nu_5 + \nu_6$	A_1	2465.28	2464.85	0.61
$2\nu_2$	A_1	2694.61	2694.22	0.90
$\nu_3 + 2\nu_6$	A_1	2751.74	2745.26	0.76
$\nu_2 + 2\nu_3$	A_1	2797.64	2785.81	0.82
$2\nu_5$	A_1	2879.31	2879.81	0.71
$4\nu_3$	A_1	2880.47	2858.14	0.87
ν_1	A_1	2969.16	2969.14	0.88
$3\nu_6$	A_1	3060.62	3059.47	0.71
$\nu_3 + \nu_5 + \nu_6$	A_1	3190.27	3184.10	0.60
$\nu_2 + 2\nu_6$	A_1	3373.57	3372.58	0.75
$2\nu_2 + \nu_3$	A_1	3414.02	3407.71	0.81
$2\nu_3 + 2\nu_6$	A_1	3464.69	3452.79	0.72
$\nu_5 + 2\nu_6$	A_1	3474.85	3473.97	0.45
$3\nu_3 + \nu_2$	A_1	3505.14	3487.67	0.76
$5\nu_3$	A_1	3578.55	3551.95	0.85
$\nu_3 + 2\nu_5$	A_1	3608.77	3602.92	0.72
$\nu_1 + \nu_3$	A_1	3702.43	3696.58	0.87
$\nu_3 + 3\nu_6$	A_1	3776.82	3770.04	0.69

(*Continued*)

Mode	Sym.	CBS-35 ^{HL}	CBS-37 ^{HL}	Basis contribution
$\nu_2 + \nu_5 + \nu_6$	A_1	3811.29	3810.65	0.60
$2\nu_3 + \nu_5 + \nu_6$	A_1	3906.26	3894.37	0.60
$3\nu_2$	A_1	4020.97	4020.38	0.86
$\nu_4 + \nu_6$	A_1	4042.96	4041.92	0.69
$4\nu_6$	A_1	4057.05	4055.79	0.52
$\nu_2 + \nu_3 + 2\nu_6$	A_1	4090.60	4084.12	0.69
$2\nu_2 + 2\nu_3$	A_1	4123.75	4111.58	0.72
$3\nu_3 + 2\nu_6$	A_1	4168.72	4151.54	0.70
$\nu_2 + 2\nu_5$	A_1	4231.18	4230.90	0.71
$\nu_2 + 4\nu_3$	A_1	4203.62	4180.58	0.70
$6\nu_3$	A_1	4268.42	4237.53	0.83
$\nu_1 + \nu_2$	A_1	4323.57	4323.40	0.85
$2\nu_3 + 2\nu_5$	A_1	4328.70	4317.26	0.71
$3\nu_5$	A_1	4337.34	4337.23	0.65
$\nu_2 + 3\nu_6$	A_1	4399.27	4397.92	0.69
$\nu_1 + 2\nu_3$	A_1	4426.97	4415.51	0.86
$2\nu_3 + 3\nu_6$	A_1	4483.87	4471.19	0.66
$3\nu_3 + \nu_5 + \nu_6$	A_1	4613.10	4596.21	0.58
$2\nu_2 + 2\nu_6$	A_1	4703.21	4701.96	0.72
$3\nu_2 + \nu_3$	A_1	4734.15	4727.65	0.74
$\nu_3 + \nu_4 + \nu_6$	A_1	4778.45	4770.27	0.59
$2\nu_2 + 3\nu_3$	A_1	4823.93	4805.94	0.65
$4\nu_3 + 2\nu_6$	A_1	4863.59	4841.51	0.68
$\nu_2 + \nu_3 + 2\nu_5$	A_1	4952.27	4946.10	0.68
$\nu_2 + 5\nu_3$	A_1	4891.07	4862.73	0.68
$\nu_1 + 2\nu_6$	A_1	4985.90	4985.09	0.72
$\nu_1 + \nu_2 + \nu_3$	A_1	5048.98	5042.84	0.74
$3\nu_3 + 2\nu_5$	A_1	5039.82	5023.11	0.66
$\nu_3 + 3\nu_5$	A_1	5062.68	5056.81	0.65
$\nu_4 + 2\nu_6$	A_1	5063.83	5062.54	0.71
$7\nu_3$	A_1	4951.21	4916.63	0.87
$\nu_2 + \nu_3 + 3\nu_6$	A_1	5111.23	5104.65	0.63

(*Continued*)

Mode	Sym.	CBS-35 $^{\mathrm{HL}}$	CBS-37 $^{\mathrm{HL}}$	Basis contribution
$2\nu_2 + \nu_5 + \nu_6$	A_1	5141.45	5140.60	0.58
$\nu_1 + 3\nu_3$	A_1	5142.84	5126.02	0.84
$3\nu_3 + 3\nu_6$	A_1	5180.97	–	0.63
$4\nu_2$	A_1	5335.27	5334.45	0.81
$\nu_5 + 4\nu_6$	A_1	5522.77	5521.13	0.55
$2\nu_2 + 2\nu_5$	A_1	5562.75	5562.28	0.68
$\nu_1 + 2\nu_2$	A_1	5658.93	5658.52	0.79
$\nu_2 + 3\nu_5$	A_1	5680.91	5680.58	0.63
$\nu_2 + 2\nu_3 + 2\nu_5$	A_1	5663.56	5651.65	0.62
$5\nu_3 + 2\nu_6$	A_1	5550.28	5524.23	0.70
$2\nu_2 + 3\nu_6$	A_1	5723.89	5722.30	0.67
$4\nu_3 + 2\nu_5$	A_1	5741.82	5720.29	0.55
$2\nu_3 + 3\nu_5$	A_1	5779.06	5767.63	0.64
$8\nu_3$	A_1	5620.62	5577.93	0.65
$2\nu_1$	A_1	5881.04	5880.96	0.52
$2\nu_4$	A_1	6018.47	6018.29	0.89
$2\nu_4 + 2\nu_5$	A_1	8877.25	–	0.51
$3\nu_4$	A_1	9079.28	9078.84	0.89
$\nu_5 + \nu_6$	A_2	2467.85	2467.43	0.94
$3\nu_6$	A_2	3060.85	3059.70	0.71
$\nu_3 + \nu_5 + \nu_6$	A_2	3193.18	3187.02	0.91
$\nu_5 + 2\nu_6$	A_2	3473.51	3472.71	0.43
$\nu_3 + 3\nu_6$	A_2	3777.02	3770.25	0.69
$\nu_2 + \nu_5 + \nu_6$	A_2	3813.05	3812.43	0.90
$2\nu_3 + \nu_5 + \nu_6$	A_2	3909.61	3900.07	0.88
$\nu_4 + \nu_6$	A_2	4054.83	4054.42	0.86
$3\nu_5$	A_2	4335.96	4335.87	0.65
$\nu_2 + 3\nu_6$	A_2	4399.70	4398.34	0.69
$\nu_5 + 3\nu_6$	A_2	4482.64	4482.71	0.71
$2\nu_3 + 3\nu_6$	A_2	4484.87	4471.18	0.66
$\nu_2 + \nu_3 + \nu_5 + \nu_6$	A_2	4531.96	4525.58	0.84
$3\nu_3 + \nu_5 + \nu_6$	A_2	4616.33	4599.68	0.82

(*Continued*)

Mode	Sym.	CBS-35 ^{HL}	CBS-37 ^{HL}	Basis contribution
$\nu_3 + \nu_4 + \nu_6$	A_2	4785.23	4779.05	0.84
$\nu_3 + 3\nu_5$	A_2	5061.41	5055.56	0.65
$\nu_4 + 2\nu_6$	A_2	5063.30	5062.05	0.72
$\nu_2 + \nu_3 + 3\nu_6$	A_2	5111.56	5104.98	0.63
$2\nu_2 + \nu_5 + \nu_6$	A_2	5142.49	5141.65	0.85
$\nu_3 + \nu_5 + 3\nu_6$	A_2	5195.90	5189.08	0.62
$3\nu_3 + 3\nu_6$	A_2	5181.25	5163.98	0.63
$3\nu_5 + \nu_6$	A_2	5310.98	5310.60	0.66
$\nu_5 + 4\nu_6$	A_2	5522.72	5521.09	0.55
$\nu_2 + 3\nu_5$	A_2	5679.44	5679.12	0.64
$2\nu_2 + 3\nu_6$	A_2	5724.41	5722.82	0.67
$2\nu_3 + 3\nu_5$	A_2	5777.88	5766.49	0.65
ν_6	E	1018.05	1017.66	0.87
ν_5	E	1452.56	1452.53	0.87
$\nu_3 + \nu_6$	E	1745.78	1739.64	0.85
$2\nu_6$	E	2038.37	2037.59	0.79
$\nu_3 + \nu_5$	E	2183.30	2177.47	0.86
$\nu_2 + \nu_6$	E	2367.90	2367.32	0.85
$\nu_5 + \nu_6$	E	2461.98	2461.78	0.62
$2\nu_3 + \nu_6$	E	2464.65	2452.76	0.81
$\nu_3 + 2\nu_6$	E	2760.42	2753.96	0.77
$\nu_2 + \nu_5$	E	2803.96	2803.73	0.85
$2\nu_5$	E	2898.22	2898.19	0.77
$2\nu_3 + \nu_5$	E	2905.14	2893.71	0.84
ν_4	E	3038.19	3037.71	0.79
$3\nu_6$	E	3045.76	3044.97	0.59
$\nu_2 + \nu_3 + \nu_6$	E	3089.19	3082.87	0.79
$3\nu_3 + \nu_6$	E	3174.22	3157.29	0.80
$\nu_3 + \nu_5 + \nu_6$	E	3187.63	3181.44	0.63
$\nu_2 + 2\nu_6$	E	3382.80	3381.83	0.76
$\nu_5 + 2\nu_6$	E	3469.23	3468.74	0.53
$2\nu_3 + 2\nu_6$	E	3473.52	3461.26	0.73

(*Continued*)

Mode	Sym.	CBS-35 $^{\mathrm{HL}}$	CBS-37 $^{\mathrm{HL}}$	Basis contribution
$\nu_5 + 2\nu_6$	E	3483.31	3482.48	0.70
$\nu_2 + \nu_3 + \nu_5$	E	3527.41	3521.30	0.80
$3\nu_3 + \nu_5$	E	3618.18	3601.43	0.82
$\nu_3 + 2\nu_5$	E	3626.37	3620.53	0.76
$2\nu_2 + \nu_6$	E	3702.80	3702.01	0.81
$\nu_3 + 3\nu_6$	E	3759.07	3752.30	0.65
$\nu_3 + \nu_4$	E	3776.04	3769.61	0.88
$\nu_2 + 2\nu_3 + \nu_6$	E	3801.73	3790.16	0.70
$\nu_2 + \nu_5 + \nu_6$	E	3809.12	3808.47	0.61
$2\nu_5 + \nu_6$	E	3886.75	3886.25	0.50
$4\nu_3 + \nu_6$	E	3875.39	3853.47	0.77
$2\nu_3 + \nu_5 + \nu_6$	E	3903.97	3892.33	0.62
$2\nu_5 + \nu_6$	E	3908.52	3908.05	0.67
$\nu_1 + \nu_6$	E	3980.97	3980.56	0.80
$\nu_4 + \nu_6$	E	4049.83	4048.99	0.75
$4\nu_6$	E	4084.96	4083.43	0.65
$\nu_2 + \nu_3 + 2\nu_6$	E	4099.37	4092.86	0.70
$2\nu_2 + \nu_5$	E	4138.86	4138.44	0.82
$3\nu_3 + 2\nu_6$	E	4177.02	4159.97	0.62
$\nu_3 + \nu_5 + 2\nu_6$	E	4202.77	4182.76	0.69
$\nu_2 + 2\nu_5$	E	4245.82	4245.54	0.73
$\nu_2 + 2\nu_3 + \nu_5$	E	4241.38	4229.53	0.73
$3\nu_5$	E	4304.73	4304.69	0.60
$4\nu_3 + \nu_5$	E	4322.68	4300.74	0.81
$2\nu_3 + 2\nu_5$	E	4345.57	4334.16	0.75
$\nu_2 + 3\nu_6$	E	4379.54	4378.44	0.56
$\nu_2 + \nu_4$	E	4385.90	4385.04	0.73
$\nu_1 + \nu_5$	E	4416.81	4417.11	0.77
$2\nu_2 + \nu_3 + \nu_6$	E	4419.02	4412.44	0.71
$2\nu_3 + 3\nu_6$	E	4466.51	4454.31	0.60
$2\nu_3 + \nu_4$	E	4495.34	–	0.87
$5\nu_3 + \nu_6$	E	4567.86	4541.48	0.75

(*Continued*)

Mode	Sym.	CBS-35 ^{HL}	CBS-37 ^{HL}	Basis contribution
$3\nu_3 + \nu_5 + \nu_6$	E	4611.83	4594.42	0.61
$\nu_3 + 2\nu_5 + \nu_6$	E	4631.00	4624.81	0.67
$\nu_1 + \nu_3 + \nu_6$	E	4708.88	4702.70	0.79
$2\nu_2 + 2\nu_6$	E	4712.74	4711.54	0.73
$\nu_3 + \nu_4 + \nu_6$	E	4783.16	4775.60	0.50
$\nu_3 + 4\nu_6$	E	4795.02	4760.90	0.62
$\nu_2 + \nu_5 + 2\nu_6$	E	4822.63	–	0.66
$2\nu_2 + \nu_3 + \nu_5$	E	4855.84	4849.49	0.74
$4\nu_3 + 2\nu_6$	E	4871.98	4850.06	0.67
$2\nu_3 + \nu_5 + 2\nu_6$	E	4913.30	4897.96	0.66
$\nu_2 + 3\nu_3 + \nu_5$	E	4946.16	4928.65	0.70
$\nu_1 + 2\nu_6$	E	4995.08	4994.28	0.73
$3\nu_2 + \nu_6$	E	5024.73	5023.72	0.77
$\nu_3 + 3\nu_5$	E	5031.24	5025.35	0.60
$5\nu_3 + \nu_5$	E	5018.26	4991.77	0.80
$3\nu_3 + 2\nu_5$	E	5056.00	5039.28	0.74
$\nu_2 + \nu_3 + \nu_4$	E	5108.14	5100.13	0.56
$2\nu_2 + \nu_5 + \nu_6$	E	5139.97	–	0.61
$\nu_1 + \nu_3 + \nu_5$	E	5147.53	–	0.76
$3\nu_3 + 3\nu_6$	E	5164.13	5146.65	0.53
$\nu_3 + \nu_4 + \nu_5$	E	5209.03	5202.22	0.58
$3\nu_3 + \nu_4$	E	5223.55	5202.73	0.84
$\nu_2 + 2\nu_5 + \nu_6$	E	5249.39	5248.70	0.64
$2\nu_3 + 2\nu_5 + \nu_6$	E	5344.52	5333.17	0.66
$6\nu_3 + \nu_6$	E	5252.98	5223.68	0.79
$3\nu_2 + \nu_5$	E	5460.15	5459.52	0.77
$2\nu_2 + 2\nu_5$	E	5575.55	5575.08	0.72
$\nu_2 + 3\nu_5$	E	5654.71	5654.32	0.51
$\nu_2 + 2\nu_3 + 2\nu_5$	E	5677.58	5665.69	0.67
$5\nu_3 + 2\nu_6$	E	5558.47	5532.56	0.71
$\nu_2 + 4\nu_3 + \nu_5$	E	5640.36	5617.37	0.66
$2\nu_2 + \nu_4$	E	5711.12	5711.19	0.81

(*Continued*)

Mode	Sym.	CBS-35 $^{\mathrm{HL}}$	CBS-37 $^{\mathrm{HL}}$	Basis contribution
$2\nu_3 + 3\nu_5$	E	5748.70	5737.82	0.59
$3\nu_2 + \nu_3 + \nu_6$	E	5736.60	5730.95	0.57
$4\nu_3 + 2\nu_5$	E	5757.54	5735.23	0.74
$6\nu_3 + \nu_5$	E	5706.20	5675.51	0.81
$\nu_1 + \nu_4$	E	5875.98	5875.78	0.52
$\nu_4 + 2\nu_5$	E	5923.37	5923.05	0.53
$2\nu_1 + \nu_5$	E	7311.08	7311.15	0.40
$2\nu_4 + \nu_5$	E	7445.86	7445.13	0.73

Table A.2: Calculated vibrational transition moments (in Debye) and frequencies (in cm^{-1}) from the vibrational ground state for $CH_3{}^{35}Cl$ and $CH_3{}^{37}Cl$ computed using the CBS-35 $^{\mathrm{HL}}$ and CBS-37 $^{\mathrm{HL}}$ PESs, respectively.

Mode	Sym.	CBS-35 $^{\mathrm{HL}}$	$\mu_{if}^{^{35}\mathrm{Cl}}$	CBS-37 $^{\mathrm{HL}}$	$\mu_{if}^{^{37}\mathrm{Cl}}$
ν_3	A_1	733.22	1.147E-1	727.40	1.142E-1
ν_6	E	1018.05	3.707E-2	1017.66	3.724E-2
ν_2	A_1	1355.01	5.260E-2	1354.82	5.275E-2
ν_5	E	1452.56	5.451E-2	1452.53	5.449E-2
$2\nu_3$	A_1	1457.54	6.950E-3	1446.12	7.391E-3
$\nu_3 + \nu_6$	E	1745.78	8.262E-4	1739.64	8.698E-4
$2\nu_6$	A_1	2029.46	3.742E-5	2028.68	6.348E-5
$2\nu_6$	E	2038.37	6.358E-4	2037.59	6.441E-4
$\nu_2 + \nu_3$	A_1	2080.98	3.619E-3	2074.90	3.589E-3
$3\nu_3$	A_1	2173.09	4.546E-4	2156.31	5.100E-4
$\nu_3 + \nu_5$	E	2183.30	4.593E-4	2177.47	4.560E-4
$\nu_2 + \nu_6$	E	2367.90	6.991E-3	2367.32	6.972E-3
$\nu_5 + \nu_6$	E	2461.98	6.235E-3	2461.78	6.248E-3
$2\nu_3 + \nu_6$	E	2464.65	1.057E-3	2452.76	1.015E-3
$\nu_5 + \nu_6$	A_1	2465.28	4.914E-3	2464.85	4.900E-3
$\nu_5 + \nu_6$	A_2	2467.85	1.389E-15	2467.43	4.451E-16
$2\nu_2$	A_1	2694.61	2.072E-4	2694.22	2.089E-4

(*Continued*)

Mode	Sym.	CBS-35 $^{\mathrm{HL}}$	$\mu_{if}^{^{35}\mathrm{Cl}}$	CBS-37 $^{\mathrm{HL}}$	$\mu_{if}^{^{37}\mathrm{Cl}}$
$\nu_3 + 2\nu_6$	A_1	2751.74	1.951E-3	2745.26	1.921E-3
$\nu_3 + 2\nu_6$	E	2760.42	8.572E-5	2753.96	6.799E-5
$\nu_2 + 2\nu_3$	A_1	2797.64	1.884E-3	2785.81	1.707E-3
$\nu_2 + \nu_5$	E	2803.96	4.126E-3	2803.73	4.124E-3
$2\nu_5$	A_1	2879.31	2.217E-2	2879.81	2.451E-2
$4\nu_3$	A_1	2880.47	1.051E-2	2858.14	1.184E-3
$2\nu_5$	E	2898.22	4.083E-3	2898.19	4.038E-3
$2\nu_3 + \nu_5$	E	2905.14	3.594E-4	2893.71	7.064E-4
ν_1	A_1	2969.16	5.296E-2	2969.14	5.296E-2
ν_4	E	3038.19	3.108E-2	3037.71	2.939E-2
$3\nu_6$	E	3045.76	2.268E-2	3044.97	2.474E-2
$3\nu_6$	A_1	3060.62	2.135E-3	3059.47	2.145E-3
$3\nu_6$	A_2	3060.85	4.098E-14	3059.70	1.170E-14
$\nu_2 + \nu_3 + \nu_6$	E	3089.19	3.870E-3	3082.87	4.478E-3
$3\nu_3 + \nu_6$	E	3174.22	4.311E-4	3157.29	5.182E-4
$\nu_3 + \nu_5 + \nu_6$	E	3187.63	7.392E-5	3181.44	5.534E-5
$\nu_3 + \nu_5 + \nu_6$	A_1	3190.27	1.068E-3	3184.10	1.085E-3
$\nu_3 + \nu_5 + \nu_6$	A_2	3193.18	1.385E-15	3187.02	3.890E-16
$\nu_2 + 2\nu_6$	A_1	3373.57	1.541E-3	3372.58	1.543E-3
$\nu_2 + 2\nu_6$	E	3382.80	1.105E-4	3381.83	1.114E-4
$2\nu_2 + \nu_3$	A_1	3414.02	9.106E-4	3407.71	8.702E-4
$2\nu_3 + 2\nu_6$	A_1	3464.69	3.761E-4	3452.79	3.893E-4
$\nu_5 + 2\nu_6$	E	3469.23	1.206E-3	3468.74	1.208E-3
$\nu_5 + 2\nu_6$	A_2	3473.51	2.622E-14	3472.71	7.741E-15
$2\nu_3 + 2\nu_6$	E	3473.52	2.068E-4	3461.26	2.090E-4
$\nu_5 + 2\nu_6$	A_1	3474.85	6.695E-5	3473.97	4.758E-5
$\nu_5 + 2\nu_6$	E	3483.31	3.448E-4	3482.48	3.432E-4
$3\nu_3 + \nu_2$	A_1	3505.14	1.882E-4	3487.67	1.831E-4
$\nu_2 + \nu_3 + \nu_5$	E	3527.41	2.939E-4	3521.30	2.827E-4
$5\nu_3$	A_1	3578.55	1.235E-4	3551.95	9.459E-5
$\nu_3 + 2\nu_5$	A_1	3608.77	1.808E-3	3602.92	1.801E-3
$3\nu_3 + \nu_5$	E	3618.18	8.408E-5	3601.43	6.805E-5

(*Continued*)

Mode	Sym.	CBS-35 $^{\mathrm{HL}}$	$\mu_{if}^{^{35}\mathrm{Cl}}$	CBS-37 $^{\mathrm{HL}}$	$\mu_{if}^{^{37}\mathrm{Cl}}$
$\nu_3 + 2\nu_5$	E	3626.37	6.914E-4	3620.53	6.900E-4
$\nu_1 + \nu_3$	A_1	3702.43	4.766E-3	3696.58	4.747E-3
$2\nu_2 + \nu_6$	E	3702.80	8.163E-4	3702.01	8.054E-4
$\nu_3 + 3\nu_6$	E	3759.07	8.688E-4	3752.30	8.055E-4
$\nu_3 + \nu_4$	E	3776.04	4.044E-3	3769.61	3.952E-3
$\nu_3 + 3\nu_6$	A_1	3776.82	1.852E-4	3770.04	1.867E-4
$\nu_3 + 3\nu_6$	A_2	3777.02	6.439E-15	3770.25	2.043E-15
$\nu_2 + 2\nu_3 + \nu_6$	E	3801.73	9.104E-4	3790.16	1.225E-3
$\nu_2 + \nu_5 + \nu_6$	E	3809.12	1.291E-3	3808.47	1.254E-3
$\nu_2 + \nu_5 + \nu_6$	A_1	3811.29	1.390E-3	3810.65	1.387E-3
$\nu_2 + \nu_5 + \nu_6$	A_2	3813.05	3.202E-15	3812.43	6.199E-16
$4\nu_3 + \nu_6$	E	3875.39	2.485E-4	3853.47	1.995E-4
$2\nu_5 + \nu_6$	E	3886.75	2.124E-3	3886.25	2.120E-3
$2\nu_3 + \nu_5 + \nu_6$	E	3903.97	1.816E-4	3892.33	3.139E-4
$2\nu_3 + \nu_5 + \nu_6$	A_1	3906.26	1.180E-4	3894.37	2.075E-4
$2\nu_5 + \nu_6$	E	3908.52	3.077E-4	3908.05	3.026E-4
$2\nu_3 + \nu_5 + \nu_6$	A_2	3909.61	1.448E-15	3900.07	2.389E-15
$\nu_1 + \nu_6$	E	3980.97	3.459E-3	3980.56	3.462E-3
$3\nu_2$	A_1	4020.97	2.283E-3	4020.38	2.283E-3
$\nu_4 + \nu_6$	A_1	4042.96	3.428E-3	4041.92	3.272E-3
$\nu_4 + \nu_6$	E	4049.83	1.602E-3	4048.99	1.546E-3
$\nu_4 + \nu_6$	A_2	4054.83	2.007E-15	4054.42	7.230E-16
$4\nu_6$	A_1	4057.05	4.041E-3	4055.79	4.085E-3
$4\nu_6$	E	4084.96	1.742E-4	4083.43	1.761E-4
$\nu_2 + \nu_3 + 2\nu_6$	A_1	4090.60	1.524E-3	4084.12	1.730E-3
$\nu_2 + \nu_3 + 2\nu_6$	E	4099.37	5.806E-4	4092.86	6.327E-4
$2\nu_2 + 2\nu_3$	A_1	4123.75	2.385E-4	4111.58	2.295E-4
$2\nu_2 + \nu_5$	E	4138.86	2.564E-3	4138.44	2.560E-3
$3\nu_3 + 2\nu_6$	A_1	4168.72	2.461E-4	4151.54	2.712E-4
$3\nu_3 + 2\nu_6$	E	4177.02	9.934E-5	4159.97	1.011E-4

Appendix B

Comprehensive tables of all investigated transitions between the $2\nu_2$ and ν_4 vibrational states of $^{14}NH_3$ are provided. In total, sensitivity coefficients have been calculated for over 350 microwave, submillimetre and far infrared transitions up to $J = 15$. All rotation-vibration energy levels have a vibrational state (v), symmetry (Γ), parity (p), rotational quantum number (J), and projection onto the molecule-fixed z axis (K) label. For all transitions there is a TROVE computed frequency $\nu_{\rm calc}$ and corresponding sensitivity coefficient $T_{\rm calc}$, and a MARVEL substituted experimental frequency $\nu_{\rm exp}$ and corresponding sensitivity coefficient $T_{\rm exp}$ where possible. Upper and lower states are labelled with a $'$ and $''$, respectively. Aside from Table 1 which contains the observed frequencies from Ref. [327, 328], transitions have been grouped together according to Einstein A coefficient in Tables 2, 3 and 4. Note that in relation to the standard Herzberg convention [337] which uses the normal mode quantum numbers v_1, v_2, v_3, v_4, l_3 and l_4, the $2\nu_2$ state corresponds to the doubly excited inversion mode $v_2 = 2$, whilst ν_4 is the singly excited antisymmetric bending mode $v_4 = |l_4| = 1$ (see Down et al. [338] for more details).

Table B.1: Observed vibration-rotation-inversion frequencies (ν), Einstein A coefficients (A) and sensitivity coefficients (T) of $^{14}NH_3$ for transitions between the $2\nu_2$ and ν_4 vibrational states. Experimental frequencies are from Ref. [328] unless stated otherwise.

v'	Γ'	p'	J'	K'	v''	Γ''	p''	J''	K''	ν_{calc}/MHz	ν_{exp}/MHz	A/s^{-1}	T_{calc}	T_{exp}
ν_4	E''	+	9	9	$2\nu_2$	E'	+	9	8	132 031.60	124 829.13 [a,b]	2.167E-5	−29.98	-31.71
ν_4	E'	+	8	8	$2\nu_2$	E''	+	8	7	160 886.62	154 415.54 [a]	3.036E-5	−28.97	-30.19
ν_4	E'	+	9	8	$2\nu_2$	E''	+	9	7	185 115.85	177 312.18	4.845E-5	−22.66	-23.66
ν_4	A_2''	+	7	7	$2\nu_2$	A_2'	+	7	6	204 389.50	198 997.44	4.284E-5	−26.52	-27.24
ν_4	A_2''	+	9	7	$2\nu_2$	A_2'	+	9	6	214 465.53	206 314.26	5.749E-5	−20.53	-21.34
$2\nu_2$	A_2''	+	10	9	ν_4	A_2'	+	10	10	205 993.39	210 104.63	9.220E-5	14.34	14.06
ν_4	A_2''	+	8	7	$2\nu_2$	A_2'	+	8	6	220 233.54	213 191.30	6.121E-5	−22.26	-22.99
$2\nu_2$	E'	+	10	4	ν_4	E''	+	10	5	215 008.15	219 719.96	2.321E-5	14.39	14.09
ν_4	E'	+	9	6	$2\nu_2$	E''	+	9	5	232 288.19	223 905.49	5.161E-5	−19.94	-20.68
$2\nu_2$	E''	+	2	1	ν_4	E'	+	1	0	233 283.50	231 528.17	1.180E-6	27.70	27.91
ν_4	E''	+	9	5	$2\nu_2$	E'	+	9	4	244 124.00	235 545.72	3.788E-5	−20.19	-20.92
$2\nu_2$	E'	+	11	10	ν_4	E''	+	11	11	234 782.46	240 987.16	1.228E-4	13.70	13.34
ν_4	A_2'	+	9	4	$2\nu_2$	A_2''	+	9	3	252 734.04	243 884.52	2.227E-5	−21.14	-21.91
ν_4	E''	+	9	3	$2\nu_2$	E'	+	9	2	257 497.74	248 518.72	9.251E-6	−22.53	-23.35
$2\nu_2$	E'	+	10	8	ν_4	E''	+	10	9	247 568.61	251 505.03	1.272E-4	12.71	12.51
ν_4	E'	+	8	6	$2\nu_2$	E''	+	8	5	260 843.42	253 418.53	7.117E-5	−19.97	-20.55
$2\nu_2$	E''	+	10	5	ν_4	E'	+	10	6	250 530.56	255 218.89	5.420E-5	13.24	13.00
ν_4	E'	+	6	6	$2\nu_2$	E''	+	6	5	265 487.21	261 535.38	5.745E-5	−22.94	-23.29
ν_4	E'	+	7	6	$2\nu_2$	E''	+	7	5	272 436.40	266 540.95	7.700E-5	−20.74	-21.20
$2\nu_2$	E''	+	12	11	ν_4	E'	+	12	12	258 846.80	267 188.68	1.536E-4	12.87	12.47
$2\nu_2$	E''	+	10	7	ν_4	E'	+	10	8	266 662.39	270 799.22	1.222E-4	12.40	12.21
$2\nu_2$	A_2'	+	10	6	ν_4	A_2''	+	10	7	267 702.67	272 146.04	9.216E-5	12.61	12.41
ν_4	E''	+	8	5	$2\nu_2$	E'	+	8	4	294 171.35	286 489.22	6.298E-5	−18.94	-19.45
$2\nu_2$	A_2''	+	11	9	ν_4	A_2'	+	11	10	285 705.21	291 851.94	1.775E-4	12.20	11.95
$2\nu_2$	E''	+	14	13	ν_4	E'	+	14	14	291 137.45	303 522.59	2.101E-4	11.11	10.66
ν_4	A_2'	+	8	4	$2\nu_2$	A_2''	+	8	3	325 490.67	317 688.65	4.406E-5	−18.41	-18.86
ν_4	E''	+	7	5	$2\nu_2$	E'	+	7	4	328 122.85	321 934.98	8.437E-5	−18.27	-18.62
$2\nu_2$	E'	+	11	8	ν_4	E''	+	11	9	317 129.46	323 758.48	1.849E-4	11.91	11.67
$2\nu_2$	E'	+	12	10	ν_4	E''	+	12	11	318 361.60	326 815.17	2.298E-4	11.57	11.27
ν_4	E''	+	6	5	$2\nu_2$	E'	+	6	4	344 695.37	340 322.94	9.137E-5	−18.29	-18.52
$2\nu_2$	E''	+	11	7	ν_4	E'	+	11	8	333 147.37	340 449.73	1.570E-4	12.05	11.79
$2\nu_2$	A_2'	+	11	6	ν_4	A_2''	+	11	7	332 808.60	340 787.72	1.099E-4	12.50	12.21
ν_4	E''	+	5	5	$2\nu_2$	E'	+	5	4	345 142.06	342 797.10	7.054E-5	−19.09	-19.22
ν_4	E''	+	8	3	$2\nu_2$	E'	+	8	2	353 734.11	346 476.00	2.037E-5	−16.96	-17.32
$2\nu_2$	A_2''	+	12	9	ν_4	A_2'	+	12	10	362 254.22	371 521.86	2.544E-4	11.28	11.00
ν_4	A_2'	+	7	4	$2\nu_2$	A_2''	+	7	3	381 473.91	375 174.47	6.887E-5	−16.71	-16.99
$2\nu_2$	A_2'	+	14	12	ν_4	A_2''	+	14	13	363 477.37	376 477.33	3.281E-4	10.34	9.98
ν_4	E'	+	0	0	$2\nu_2$	E''	+	1	1	376 860.11	379 596.53	4.703E-6	−18.84	-18.70

[a] Ref. [327]. [b] MARVEL analysis [350] reports a frequency of 123 705.91 MHz resulting in $T = -32.00$.

Table B.2: Vibration-rotation-inversion frequencies (ν), Einstein A coefficients (A) and sensitivity coefficients (T) of $^{14}NH_3$ for transitions between the $2\nu_2$ and ν_4 vibrational states. Experimental frequencies have been obtained using energy levels from the MARVEL analysis [350].

v'	Γ'	p'	J'	K'	v''	Γ''	p''	J''	K''	$\nu_{\rm calc}$/MHz	$\nu_{\rm exp}$/MHz	A/s^{-1}	$T_{\rm calc}$	$T_{\rm exp}$
ν_4	E'	+	12	12	$2\nu_2$	E''	+	12	11	98 604.7		1.232E-5	−28.19	
ν_4	E''	+	15	15	$2\nu_2$	E'	+	15	14	105 113.2		1.498E-5	−24.50	
$2\nu_2$	E'	−	11	5	ν_4	E''	−	12	6	114 532.7	116 719.3	1.236E-6	1.32	1.29
ν_4	E'	−	10	3	$2\nu_2$	E''	−	9	4	122 078.5	113 519.2	1.211E-6	-10.89	-11.71
$2\nu_2$	A_2''	−	10	0	ν_4	A_2'	+	11	2	135 815.0	143 327.4	1.120E-6	11.78	11.17
ν_4	E'	+	13	12	$2\nu_2$	E''	+	13	11	142 611.3		3.425E-5	−19.76	
ν_4	E''	+	10	3	$2\nu_2$	E'	+	10	2	151 734.0	142 903.4	2.438E-6	−30.51	-32.40
ν_4	A_2''	−	10	2	$2\nu_2$	A_2'	−	9	3	158 134.5	148 964.7	3.712E-6	-8.29	-8.80
ν_4	E''	+	10	9	$2\nu_2$	E'	+	10	8	162 964.2		4.001E-5	−22.28	
$2\nu_2$	A_2''	+	10	3	ν_4	A_2'	+	10	4	165 035.7	169 236.3	6.421E-6	16.36	15.95
ν_4	E''	+	11	9	$2\nu_2$	E'	+	11	8	166 276.9		4.090E-5	−19.42	
$2\nu_2$	E'	+	9	8	ν_4	E''	+	9	9	174 047.5		6.374E-5	14.47	
ν_4	E'	−	10	1	$2\nu_2$	E''	−	9	2	174 877.9	165 720.4	6.185E-6	-7.11	-7.51
ν_4	E''	−	10	0	$2\nu_2$	E'	−	9	1	186 039.2	176 739.5	9.006E-6	-5.91	-6.22
ν_4	E'	+	10	6	$2\nu_2$	E''	+	10	5	190 719.0		2.944E-5	−20.13	
$2\nu_2$	E''	+	9	5	ν_4	E'	+	9	6	203 574.1		4.550E-5	12.45	
ν_4	A_2''	−	12	4	$2\nu_2$	A_2'	−	11	3	217 415.5	213 858.1	5.839E-6	-5.96	-6.06
$2\nu_2$	A_2''	+	11	3	ν_4	A_2'	+	11	4	222 988.6	232 096.7	6.801E-6	17.97	17.27
ν_4	E'	+	9	2	$2\nu_2$	E''	+	9	1	262 162.5	252 726.0	2.652E-6	−24.30	-25.20
$2\nu_2$	E''	−	10	2	ν_4	E'	−	11	3	263 484.6	272 824.7	1.490E-6	4.33	4.18
$2\nu_2$	E'	+	11	2	ν_4	E''	+	11	3	272 133.6	284 989.4	2.189E-6	14.28	13.64
$2\nu_2$	E'	+	11	4	ν_4	E''	+	11	5	278 363.3	287 246.1	2.573E-5	14.93	14.47
$2\nu_2$	E'	+	12	2	ν_4	E''	+	12	3	294 309.3	308 379.8	8.639E-6	14.56	13.90
$2\nu_2$	E'	+	15	14	ν_4	E''	+	15	15	299 984.3		2.345E-4	10.22	
$2\nu_2$	E'	+	12	2	ν_4	E''	+	12	3	302 808.4	312 803.4	1.413E-6	13.25	12.83
ν_4	A_2'	−	15	13	$2\nu_2$	A_2''	−	14	12	309 565.7	304 019.2	1.384E-5	3.67	3.73
$2\nu_2$	E''	+	11	5	ν_4	E'	+	11	6	314 599.2	323 076.1	6.149E-5	13.37	13.02
$2\nu_2$	E'	−	10	1	ν_4	E''	−	11	2	326 336.1	326 806.8	4.222E-5	-0.61	-0.61
$2\nu_2$	A_2''	−	11	6	ν_4	A_2'	−	12	7	332 994.5	334 687.7	3.212E-5	-1.55	-1.54
ν_4	E'	−	12	3	$2\nu_2$	E''	−	11	2	333 920.8		1.505E-5	-5.53	
$2\nu_2$	A_2''	+	12	3	ν_4	A_2'	+	12	4	342 021.2	355 894.6	6.644E-6	15.02	14.43
ν_4	A_2''	−	9	2	$2\nu_2$	A_2'	+	9	0	351 803.5	339 058.1	3.077E-6	−18.80	-19.51
ν_4	A_2''	−	11	2	$2\nu_2$	A_2'	+	11	0	367 917.3	350 853.0	6.345E-6	−14.65	-15.36
$2\nu_2$	E''	+	15	13	ν_4	E'	+	15	14	375 768.9	390 891.3	3.693E-4	9.77	9.39
$2\nu_2$	E'	+	12	4	ν_4	E''	+	12	5	376 818.1	390 488.2	2.550E-5	13.38	12.92
ν_4	E'	+	8	2	$2\nu_2$	E''	+	8	1	380 133.8	372 905.3	7.163E-6	−16.73	-17.06
ν_4	A_2''	−	15	2	$2\nu_2$	A_2'	+	15	0	389 106.6	376 629.1	5.421E-6	−6.98	-7.21
$2\nu_2$	E'	+	12	8	ν_4	E''	+	12	9	394 583.8	404 951.6	2.354E-4	11.28	10.99
$2\nu_2$	E'	+	13	10	ν_4	E''	+	13	11	399 548.4	411 594.9	3.240E-4	10.67	10.36
$2\nu_2$	E''	+	12	5	ν_4	E'	+	12	6	405 328.4	418 467.6	6.459E-5	12.35	11.97
$2\nu_2$	E''	+	12	7	ν_4	E'	+	12	8	413 941.4	425 387.4	1.852E-4	11.43	11.12
$2\nu_2$	E''	+	12	1	ν_4	E'	+	12	2	415 167.6		1.147E-6	9.59	
$2\nu_2$	E''	−	15	8	ν_4	E'	+	15	4	416 085.0	432 973.2	6.532E-6	4.17	4.00
$2\nu_2$	A_2'	+	12	6	ν_4	A_2''	+	12	7	417 976.6	430 386.5	1.219E-4	11.76	11.42
ν_4	A_2'	+	6	4	$2\nu_2$	A_2''	+	6	3	418 270.4	413 748.1	9.006E-5	−15.80	-15.98
ν_4	E''	−	12	2	$2\nu_2$	E'	−	11	1	424 005.5	411 879.2	1.470E-5	-5.76	-5.93
ν_4	A_2''	−	13	2	$2\nu_2$	A_2'	+	13	0	431 191.5	410 204.9	2.552E-5	−5.95	-6.25
$2\nu_2$	E''	−	10	2	ν_4	E'	−	11	3	432 930.3	432 248.1	1.132E-4	-1.72	-1.72

(*Continued*)

v'	Γ'	p'	J'	K'	v''	Γ''	p''	J''	K''	ν_{calc}/MHz	ν_{exp}/MHz	A/s^{-1}	T_{calc}	T_{exp}
$2\nu_2$	E''	+	14	11	ν_4	E'	+	14	12	433 760.7	448 408.6	4.013E-4	9.79	9.47
ν_4	E''	+	7	3	$2\nu_2$	E'	+	7	2	436 515.8	430 468.6	4.113E-5	−15.08	-15.29
ν_4	A_2'	+	5	4	$2\nu_2$	A_2''	+	5	3	437 616.0	434 941.1	9.782E-5	−15.50	-15.59
ν_4	A_2'	+	4	4	$2\nu_2$	A_2''	+	4	3	442 676.5	441 874.1	7.796E-5	−15.66	-15.68
$2\nu_2$	A_2''	+	13	9	ν_4	A_2'	+	13	10	448 069.8	461 549.9	3.198E-4	10.55	10.25
$2\nu_2$	A_2'	+	15	12	ν_4	A_2''	+	15	13	452 668.6	469 935.8	4.668E-4	9.62	9.27
$2\nu_2$	E'	−	14	13	ν_4	E''	+	14	11	453 538.0		1.459E-4	5.23	
$2\nu_2$	A_2''	+	13	3	ν_4	A_2'	+	13	4	471 333.7	489 078.7	2.981E-6	10.89	10.49
ν_4	E'	+	7	2	$2\nu_2$	E''	+	7	1	484 698.5	478 994.6	1.719E-5	−14.13	-14.29
$2\nu_2$	E'	+	13	8	ν_4	E''	+	13	9	488 083.1	503 099.1	2.741E-4	10.45	10.14
$2\nu_2$	A_2''	+	3	3	ν_4	A_2'	+	2	2	491 165.0	489 672.2	4.360E-6	12.69	12.72
ν_4	A_2'	−	13	7	$2\nu_2$	A_2''	−	12	6	491 180.0	485 978.4	6.061E-5	-2.69	-2.72
ν_4	E''	+	6	3	$2\nu_2$	E'	+	6	2	493 089.6	488 661.3	6.308E-5	−13.99	-14.12
$2\nu_2$	A_2''	−	15	12	ν_4	A_2'	+	15	10	494 630.6	512 454.4	1.437E-5	3.19	3.08
$2\nu_2$	E'	+	14	2	ν_4	E''	−	14	2	508 969.6	524 718.7	8.777E-6	9.69	9.40
$2\nu_2$	E'	+	13	4	ν_4	E''	+	13	5	512 279.4	530 229.9	2.025E-5	10.59	10.23
ν_4	A_2''	+	7	1	$2\nu_2$	A_2'	+	7	0	512 816.0	507 179.0	9.573E-6	−13.86	-14.01
$2\nu_2$	E''	+	13	7	ν_4	E'	+	13	8	516 209.6		2.015E-4	10.36	
$2\nu_2$	E''	+	13	5	ν_4	E'	+	13	6	527 994.5	545 753.3	5.975E-5	10.38	10.05
$2\nu_2$	A_2'	+	13	6	ν_4	A_2''	+	13	7	529 772.2	546 912.7	1.235E-4	10.32	10.00
ν_4	E''	+	5	3	$2\nu_2$	E'	+	5	2	530 045.1	527 333.3	8.219E-5	−13.25	-13.31
$2\nu_2$	E'	−	14	13	ν_4	E''	+	14	11	532 701.2	548 704.9	2.808E-4	4.61	4.48
ν_4	A_2''	−	14	10	$2\nu_2$	A_2'	−	13	9	532 974.0	529 031.5	6.325E-5	-0.59	-0.59
$2\nu_2$	E''	+	15	11	ν_4	E'	+	15	12	534 682.8	554 512.8	5.162E-4	9.28	8.95
$2\nu_2$	A_2''	+	14	9	ν_4	A_2'	+	14	10	545 853.1	564 260.5	3.434E-4	9.50	9.19
ν_4	E''	+	4	3	$2\nu_2$	E'	+	4	2	549 801.4	548 781.8	9.102E-5	−12.92	-12.94
$2\nu_2$	E''	+	13	1	ν_4	E'	+	13	2	551 357.3	568 811.3	4.039E-6	8.08	7.83
$2\nu_2$	E''	+	11	1	ν_4	E'	−	11	3	552 562.5	557 067.9	1.128E-6	2.65	2.63
ν_4	E''	+	3	3	$2\nu_2$	E'	+	3	2	556 807.5	557 275.3	7.623E-5	−12.88	-12.87
ν_4	E'	+	10	2	$2\nu_2$	E''	−	9	4	560 587.9	557 554.9	1.270E-6	−3.67	-3.69
ν_4	E'	+	6	2	$2\nu_2$	E''	+	6	1	563 310.0	559 214.0	3.027E-5	−12.64	-12.73
$2\nu_2$	A_2'	−	12	9	ν_4	A_2''	+	12	5	566 089.1	577 705.1	2.592E-6	1.75	1.72
ν_4	A_2'	−	15	13	$2\nu_2$	A_2''	+	14	9	566 272.0	557 190.6	3.342E-6	−6.55	-6.66
$2\nu_2$	A_2'	−	10	3	ν_4	A_2''	−	11	4	568 097.7	567 172.6	2.545E-4	-1.87	-1.88
ν_4	E'	+	12	2	$2\nu_2$	E''	−	11	2	574 213.5		9.890E-5	−2.48	
$2\nu_2$	E'	−	11	7	ν_4	E''	−	12	8	589 721.7	591 039.0	1.809E-4	-2.16	-2.16
$2\nu_2$	E'	+	14	8	ν_4	E''	+	14	9	602 274.1	622 391.0	2.893E-4	9.28	8.98
ν_4	E'	+	14	6	$2\nu_2$	E''	−	14	10	604 954.2	588 757.6	4.244E-6	−4.21	-4.33
$2\nu_2$	E'	+	15	10	ν_4	E''	+	15	11	619 826.9	641 982.3	5.033E-4	8.66	8.36
ν_4	E'	+	5	2	$2\nu_2$	E''	+	5	1	621 217.9	618 776.8	4.583E-5	−11.62	-11.66
ν_4	E'	−	11	9	$2\nu_2$	E''	−	10	10	624 116.9	615 826.8	3.863E-6	-1.35	-1.37
ν_4	A_2''	+	11	1	$2\nu_2$	A_2'	−	10	3	632 208.3		4.048E-5	−3.70	
$2\nu_2$	A_2''	+	13	9	ν_4	A_2'	−	12	5	639 466.3	653 650.6	1.787E-6	6.71	6.57
$2\nu_2$	E''	−	8	2	ν_4	E'	+	9	0	639 730.1	646 252.4	1.557E-6	1.88	1.86
$2\nu_2$	E''	+	14	7	ν_4	E'	+	14	8	643 933.2	665 196.4	1.991E-4	8.90	8.62
$2\nu_2$	A_2''	−	13	12	ν_4	A_2'	−	14	13	647 671.6	651 484.6	1.246E-4	-4.68	-4.66
ν_4	E''	−	15	4	$2\nu_2$	E'	+	15	4	653 373.7		2.997E-6	−8.94	
$2\nu_2$	E''	+	12	1	ν_4	E'	−	12	3	655 460.2	669 113.6	2.964E-6	6.72	6.58
ν_4	E'	+	4	2	$2\nu_2$	E''	+	4	1	658 707.0	657 787.0	6.078E-5	−11.06	-11.07
$2\nu_2$	A_2'	+	14	6	ν_4	A_2''	+	14	7	670 120.1	691 897.2	1.111E-4	8.52	8.25
$2\nu_2$	E'	+	3	2	ν_4	E''	+	2	1	673 351.8	672 644.4	3.223E-5	8.89	8.89
ν_4	A_2''	+	5	1	$2\nu_2$	A_2'	+	5	0	674 404.1	672 376.5	2.542E-5	−10.83	-10.86
$2\nu_2$	A_2'	−	8	3	ν_4	A_2''	−	9	2	674 766.9	679 711.7	1.384E-4	0.94	0.93
$2\nu_2$	E'	+	14	4	ν_4	E''	+	14	5	676 784.5	698 111.4	1.154E-5	7.88	7.64

(*Continued*)

v'	Γ'	p'	J'	K'	v''	Γ''	p''	J''	K''	ν_{calc}/MHz	ν_{exp}/MHz	A/s^{-1}	T_{calc}	T_{exp}
ν_4	E'	+	3	2	$2\nu_2$	E''	+	3	1	678 679.2	679 163.4	6.964E-5	−10.80	-10.79
$2\nu_2$	E''	+	14	5	ν_4	E'	+	14	6	680 837.7	702 457.3	4.641E-5	8.17	7.92
$2\nu_2$	E'	−	10	1	ν_4	E''	+	11	3	681 314.3	686 273.1	4.382E-6	2.05	2.03
ν_4	E''	−	13	6	$2\nu_2$	E'	−	12	5	685 946.1	680 012.7	1.377E-4	-2.85	-2.88
ν_4	E'	+	2	2	$2\nu_2$	E''	+	2	1	686 189.0	687 852.5	6.318E-5	−10.73	-10.70
$2\nu_2$	E''	−	14	8	ν_4	E'	+	14	4	688 887.1	661 641.0	5.510E-5	0.58	0.60
ν_4	A_2'	−	12	1	$2\nu_2$	A_2''	+	12	3	694 772.0		9.461E-6	−8.76	
$2\nu_2$	E''	−	9	2	ν_4	E'	+	10	2	698 999.1	702 125.4	1.683E-5	1.47	1.47
ν_4	E''	−	15	2	$2\nu_2$	E'	+	15	4	701 865.1	686 876.9	4.513E-5	−8.78	-8.97
$2\nu_2$	E''	−	12	10	ν_4	E'	−	13	11	706 269.1	708 727.7	2.235E-4	-3.36	-3.35
$2\nu_2$	E'	+	15	2	ν_4	E''	−	15	2	707 705.1	720 609.5	1.218E-5	6.38	6.27
$2\nu_2$	A_2''	+	15	9	ν_4	A_2'	+	15	10	711 914.2	735 227.6	4.144E-4	7.20	6.97
$2\nu_2$	A_2''	−	8	0	ν_4	A_2'	−	9	1	712 843.5	721 065.6	5.050E-4	0.11	0.11
$2\nu_2$	E'	−	8	1	ν_4	E''	−	9	0	714 033.7	722 303.2	4.761E-4	0.17	0.17
$2\nu_2$	E''	−	8	2	ν_4	E'	−	9	1	716 965.7	724 899.9	3.951E-4	0.34	0.33
$2\nu_2$	E'	+	15	8	ν_4	E''	+	15	9	724 328.6	748 607.8	2.274E-4	7.41	7.17
ν_4	A_2''	−	11	8	$2\nu_2$	A_2'	−	10	9	735 774.6	727 288.4	2.146E-5	-1.89	-1.91
$2\nu_2$	E''	−	10	4	ν_4	E'	−	11	5	735 948.5	734 922.7	5.368E-4	-1.95	-1.95
ν_4	E''	−	15	12	$2\nu_2$	E'	−	14	11	741 087.0	734 546.6	1.865E-4	-0.25	-0.25
$2\nu_2$	E''	−	8	4	ν_4	E'	−	9	3	742 169.2	749 245.6	2.163E-4	0.47	0.47
$2\nu_2$	E''	+	14	1	ν_4	E'	+	14	2	745 838.7	759 442.8	1.168E-5	5.74	5.64
$2\nu_2$	E'	−	8	5	ν_4	E''	−	9	4	757 599.5	764 122.9	1.374E-4	0.41	0.40
ν_4	E''	+	13	3	$2\nu_2$	E'	−	12	1	770 619.5	761 683.1	2.912E-6	−4.32	-4.37
ν_4	A_2''	+	3	1	$2\nu_2$	A_2'	+	3	0	774 058.1	774 889.5	4.660E-5	−9.60	-9.59
$2\nu_2$	A_2''	−	8	6	ν_4	A_2'	−	9	5	785 351.3	791 493.8	8.082E-5	0.18	0.18
$2\nu_2$	E''	+	15	7	ν_4	E'	+	15	8	795 136.5	820 833.3	1.733E-4	7.30	7.07
ν_4	E'	+	12	2	$2\nu_2$	E''	−	11	2	800 805.6		1.586E-4	−3.13	
$2\nu_2$	A_2''	−	14	12	ν_4	A_2'	+	14	10	802 556.4	817 431.8	5.121E-5	0.42	0.42
$2\nu_2$	A_2'	−	8	3	ν_4	A_2''	+	9	1	817 078.3	821 302.6	1.975E-4	0.42	0.42
$2\nu_2$	E''	+	13	1	ν_4	E'	−	13	3	819 449.7	837 081.4	5.860E-6	5.82	5.70
ν_4	E'	−	11	7	$2\nu_2$	E''	−	10	8	820 370.1	811 608.6	6.793E-5	-2.21	-2.23
ν_4	A_2''	+	1	1	$2\nu_2$	A_2'	+	1	0	822 000.9	824 624.2	6.427E-5	−9.16	-9.13
$2\nu_2$	E'	−	13	13	ν_4	E''	+	13	11	824 474.2	838 064.7	8.400E-6	−1.17	-1.16
$2\nu_2$	E'	−	8	7	ν_4	E''	−	9	6	829 606.7	835 209.1	4.188E-5	-0.16	-0.16
$2\nu_2$	A_2'	+	15	6	ν_4	A_2''	+	15	7	835 632.5	861 357.9	8.630E-5	6.74	6.54
$2\nu_2$	A_2'	−	11	9	ν_4	A_2''	+	11	5	836 453.9	845 821.7	1.129E-6	0.40	0.40
$2\nu_2$	E'	−	15	7	ν_4	E''	+	15	3	838 738.4	857 668.9	1.272E-5	2.64	2.59
ν_4	E'	−	14	9	$2\nu_2$	E''	−	13	8	839 029.2	831 788.8	2.630E-4	-1.75	-1.76
ν_4	A_2''	+	10	1	$2\nu_2$	A_2'	−	9	3	841 574.4	833 197.0	1.540E-6	−3.43	-3.46
$2\nu_2$	E''	+	3	1	ν_4	E'	+	2	0	843 046.4	842 667.6	1.210E-4	6.91	6.91
ν_4	E'	−	13	5	$2\nu_2$	E''	−	12	4	845 468.7	838 820.7	2.002E-4	-2.95	-2.98
$2\nu_2$	A_2'	+	15	0	ν_4	A_2''	+	15	1	855 355.8		4.298E-6	0.33	
$2\nu_2$	E''	+	15	5	ν_4	E'	+	15	6	857 007.7	880 193.2	2.848E-5	6.21	6.05
$2\nu_2$	E'	+	15	4	ν_4	E''	+	15	5	858 045.0	881 947.1	3.491E-6	5.59	5.44
ν_4	E'	+	15	0	$2\nu_2$	E''	+	15	1	865 195.0		1.230E-5	−7.66	
ν_4	E'	+	15	6	$2\nu_2$	E''	−	15	10	876 629.1	857 387.9	2.319E-5	−3.65	-3.73
ν_4	E''	−	11	6	$2\nu_2$	E'	−	10	7	884 234.9	875 140.7	1.594E-4	-2.38	-2.41
$2\nu_2$	E''	−	11	8	ν_4	E'	−	12	9	887 979.3	888 965.3	5.942E-4	-2.40	-2.40
$2\nu_2$	E''	−	8	8	ν_4	E'	−	9	7	895 998.7	902 654.5	1.557E-5	-0.59	-0.58
ν_4	E''	+	15	1	$2\nu_2$	E'	+	15	2	898 460.0		6.512E-5	−7.43	
ν_4	E''	−	14	2	$2\nu_2$	E'	+	14	4	898 879.7	880 934.1	1.336E-4	−7.61	-7.77

Table B.3: Vibration-rotation-inversion frequencies (ν), Einstein A coefficients (A) and sensitivity coefficients (T) of $^{14}NH_3$ for transitions between the $2\nu_2$ and ν_4 vibrational states. Experimental frequencies have been obtained using energy levels from the MARVEL analysis [350].

v'	Γ'	p'	J'	K'	v''	Γ''	p''	J''	K''	$\nu_{\rm calc}$/MHz	$\nu_{\rm exp}$/MHz	$A/{\rm s}^{-1}$	$T_{\rm calc}$	$T_{\rm exp}$
ν_4	E'	−	14	3	$2\nu_2$	E''	−	14	8	6223.7		5.840E-11	-217.22	
$2\nu_2$	E''	−	12	8	ν_4	E'	−	13	9	17 103.2	20 755.7	3.391E-9	-17.35	-14.30
ν_4	E''	−	10	6	$2\nu_2$	E'	−	9	7	19 036.8	11 683.4	9.298E-10	-51.85	-84.48
$2\nu_2$	E''	+	15	11	ν_4	E'	−	14	7	27 634.9	46 788.8	2.313E-11	191.99	113.40
ν_4	E'	+	11	2	$2\nu_2$	E''	−	10	2	32 848.3	28 291.4	4.250E-9	−57.62	-66.90
ν_4	E'	−	8	3	$2\nu_2$	E''	+	8	1	33 250.0	25 603.0	5.274E-9	−160.99	-209.07
$2\nu_2$	E'	+	8	2	ν_4	E''	+	8	3	39 392.7	49 374.3	6.298E-11	156.58	124.93
ν_4	E''	+	12	3	$2\nu_2$	E'	−	11	1	45 301.6	38 428.3	7.179E-10	−52.51	-61.91
$2\nu_2$	E''	−	9	8	ν_4	E'	−	10	7	45 829.3	53 966.1	6.295E-9	13.90	11.80
ν_4	E'	+	12	6	$2\nu_2$	E''	−	12	10	48 053.7	37 036.2	5.298E-9	−24.87	-32.27
ν_4	E''	+	12	3	$2\nu_2$	E'	−	11	1	53 797.8	42 851.8	2.761E-10	−49.29	-61.89
$2\nu_2$	E'	+	9	2	ν_4	E''	+	9	3	56 597.8	68 679.3	3.476E-10	101.43	83.59
ν_4	A_2'	+	13	4	$2\nu_2$	A_2''	−	12	0	60 738.0	51 342.8	2.565E-10	−44.17	-52.26
$2\nu_2$	E''	+	9	1	ν_4	E'	−	9	1	63 289.2		5.474E-9	79.00	
$2\nu_2$	E'	+	2	2	ν_4	E''	+	1	1	63 924.7	61 712.7	1.042E-8	104.21	107.95
$2\nu_2$	E'	+	10	2	ν_4	E''	+	10	3	64 989.0	77 575.0	6.839E-10	71.99	60.31
ν_4	A_2'	−	10	5	$2\nu_2$	A_2''	−	9	6	65 933.4	58 158.6	7.357E-8	-18.50	-20.97
ν_4	E''	+	14	5	$2\nu_2$	E'	−	13	1	66 655.9		2.448E-11	−44.25	
ν_4	E'	−	12	5	$2\nu_2$	E''	−	11	4	68 478.6	65 641.3	2.187E-7	-10.90	-11.37
$2\nu_2$	E'	+	13	2	ν_4	E''	−	13	2	71 605.4		4.559E-9	70.67	
ν_4	E''	−	12	2	$2\nu_2$	E'	+	12	2	75 895.5	60 647.6	4.231E-9	−53.72	-67.22
$2\nu_2$	E'	−	13	13	ν_4	E''	−	12	6	75 925.4	89 116.6	1.724E-11	-3.08	-2.62
$2\nu_2$	A_2'	+	11	0	ν_4	A_2''	+	11	1	76 408.1		7.566E-9	69.42	
$2\nu_2$	E'	+	12	8	ν_4	E''	+	11	3	82 910.6	89 509.4	1.362E-11	56.90	52.70
$2\nu_2$	E''	+	11	1	ν_4	E'	+	11	2	86 783.9	96 528.3	1.320E-8	47.28	42.51
$2\nu_2$	E'	+	15	14	ν_4	E''	−	14	12	96 401.3		2.589E-11	13.55	
ν_4	E''	−	10	4	$2\nu_2$	E'	−	9	5	99 908.8	91 668.2	4.346E-7	-13.36	-14.56
ν_4	E'	+	15	12	$2\nu_2$	E''	−	15	14	104 471.7	86 839.9	1.426E-7	−5.36	-6.45
ν_4	E''	+	15	7	$2\nu_2$	E'	−	14	5	104 981.3	87 564.5	1.117E-10	−30.73	-36.84
$2\nu_2$	E''	−	13	4	ν_4	E'	+	14	6	108 998.5	124 181.3	1.328E-10	26.25	23.04
ν_4	E'	−	7	3	$2\nu_2$	E''	+	7	1	117 602.6	110 957.2	9.461E-8	−51.03	-54.08
ν_4	E'	+	13	2	$2\nu_2$	E''	−	13	8	119 041.6	109 711.6	4.915E-11	−9.75	-10.58
ν_4	A_2'	+	8	4	$2\nu_2$	A_2''	−	7	6	122 869.9	120 732.7	1.752E-11	−6.46	-6.57
ν_4	E'	−	15	1	$2\nu_2$	E''	−	15	8	125 130.4	111 510.3	1.255E-7	-17.01	-19.09
ν_4	E'	+	10	2	$2\nu_2$	E''	+	10	1	133 512.6	123 427.8	4.745E-7	−40.78	-44.11
$2\nu_2$	A_2'	−	9	9	ν_4	A_2''	−	10	8	135 065.5	141 945.6	4.751E-8	1.22	1.16
$2\nu_2$	E''	−	13	8	ν_4	E'	−	13	3	149 050.8	158 558.5	1.436E-8	9.91	9.32
$2\nu_2$	E''	−	8	4	ν_4	E'	+	9	2	160 418.9	162 319.1	5.872E-9	7.00	6.91
$2\nu_2$	E''	+	10	1	ν_4	E'	−	10	1	161 435.2	168 626.8	3.602E-8	19.48	18.65
$2\nu_2$	E'	+	11	2	ν_4	E''	+	11	3	165 899.2	174 547.8	8.989E-7	22.32	21.21
ν_4	E'	−	6	3	$2\nu_2$	E''	+	6	1	174 647.1	169 341.3	2.539E-8	−36.43	-37.57
ν_4	E''	−	10	4	$2\nu_2$	E'	+	11	8	178 151.7		6.768E-10	−17.61	
$2\nu_2$	E''	+	12	1	ν_4	E'	+	12	2	188 575.5		4.254E-9	26.85	
ν_4	E''	−	11	2	$2\nu_2$	E'	+	11	2	189 082.1	184 918.5	3.358E-8	−11.16	-11.41
$2\nu_2$	E''	+	8	7	ν_4	E'	−	7	5	198 702.4	203 766.3	8.527E-11	16.21	15.80
ν_4	E'	−	5	3	$2\nu_2$	E''	+	5	1	209 318.1	205 609.0	8.205E-9	−31.22	-31.78
ν_4	A_2''	+	9	1	$2\nu_2$	A_2'	+	9	0	209 489.0	197 467.1	7.478E-8	−30.17	-32.01
ν_4	E'	+	10	0	$2\nu_2$	E''	−	9	2	219 921.8	211 671.7	4.588E-7	−10.52	-10.93

(*Continued*)

v'	Γ'	p'	J'	K'	v''	Γ''	p''	J''	K''	ν_{calc}/MHz	ν_{exp}/MHz	A/s^{-1}	T_{calc}	T_{exp}
$2\nu_2$	E''	$-$	7	4	ν_4	E'	$+$	8	0	221 192.9	226 050.6	1.446E-9	4.95	4.84
ν_4	E'	$-$	3	3	$2\nu_2$	E''	$+$	3	1	221 639.6	221 261.9	2.673E-10	−30.81	-30.86
ν_4	E'	$-$	4	3	$2\nu_2$	E''	$+$	5	5	222 383.0	221 629.8	2.688E-11	−30.49	-30.60
ν_4	E'	$-$	4	3	$2\nu_2$	E''	$+$	4	1	223 276.4	221 209.4	2.001E-9	−29.92	-30.20
$2\nu_2$	E''	$-$	11	10	ν_4	E'	$+$	11	6	228 058.1	236 952.0	4.881E-7	2.22	2.14
ν_4	A_2''	$-$	3	2	$2\nu_2$	A_2'	$+$	3	0	231 898.5	231 697.2	4.217E-10	−30.10	-30.12
$2\nu_2$	E''	$+$	10	7	ν_4	E'	$-$	11	11	232 641.9	231 001.8	1.039E-10	0.57	0.58
ν_4	A_2''	$-$	5	2	$2\nu_2$	A_2'	$+$	5	0	240 790.3	236 429.8	4.767E-10	−28.56	-29.09
$2\nu_2$	A_2''	$+$	10	9	ν_4	A_2'	$-$	9	7	246 042.7	245 788.3	1.394E-9	1.18	1.18
ν_4	A_2''	$-$	7	2	$2\nu_2$	A_2'	$+$	7	0	256 343.5	246 617.0	9.753E-9	−26.06	-27.09
ν_4	E'	$-$	10	1	$2\nu_2$	E''	$-$	9	4	265 637.1	265 500.3	2.065E-8	0.91	0.91
$2\nu_2$	E'	$+$	15	2	ν_4	E''	$+$	15	3	271 177.3	295 527.8	1.948E-7	19.97	18.33
ν_4	E''	$-$	11	2	$2\nu_2$	E'	$+$	12	8	272 070.6	269 956.9	1.176E-11	−11.49	-11.58
ν_4	A_2''	$-$	5	4	$2\nu_2$	A_2'	$+$	6	6	273 695.5	271 413.1	1.013E-10	−23.91	-24.11
ν_4	A_2'	$-$	14	1	$2\nu_2$	A_2''	$+$	14	3	284 161.3	262 580.4	6.415E-7	−21.29	-23.04
ν_4	E''	$+$	9	7	$2\nu_2$	E'	$+$	8	2	289 050.9	278 543.2	1.050E-11	−21.95	-22.78
ν_4	E''	$-$	15	4	$2\nu_2$	E'	$+$	15	4	293 553.8	273 373.9	3.777E-7	−15.55	-16.69
$2\nu_2$	E''	$+$	7	5	ν_4	E'	$-$	6	1	299 067.0	306 213.1	1.727E-10	16.65	16.26
$2\nu_2$	A_2'	$+$	7	6	ν_4	A_2''	$-$	6	4	299 741.5	304 232.2	2.560E-10	14.71	14.50
ν_4	A_2''	$+$	15	13	$2\nu_2$	A_2'	$-$	15	15	310 977.7	292 218.4	8.819E-7	0.42	0.44
$2\nu_2$	E'	$-$	14	13	ν_4	E''	$-$	13	6	370 468.5	386 366.5	1.634E-7	6.52	6.25
$2\nu_2$	E''	$+$	11	1	ν_4	E'	$-$	11	3	383 116.8	397 644.4	7.878E-7	8.74	8.43
$2\nu_2$	E'	$-$	9	1	ν_4	E''	$+$	10	1	391 133.2	399 006.5	5.035E-8	4.54	4.46
ν_4	E''	$-$	14	4	$2\nu_2$	E'	$+$	14	4	391 573.9	369 051.4	9.071E-9	−13.83	-14.68
ν_4	E'	$-$	8	3	$2\nu_2$	E''	$+$	9	7	393 819.4	386 248.0	7.438E-10	−11.20	-11.42
ν_4	A_2''	$-$	10	4	$2\nu_2$	A_2'	$-$	10	9	395 977.9	399 753.4	1.409E-11	7.58	7.51
ν_4	E''	$-$	12	4	$2\nu_2$	E'	$+$	12	4	400 546.7	382 835.1	2.160E-10	−13.26	-13.88
$2\nu_2$	E''	$-$	12	2	ν_4	E'	$-$	13	5	404 821.7	411 541.5	3.784E-11	3.60	3.55
$2\nu_2$	E''	$+$	2	1	ν_4	E'	$-$	1	1	411 785.9	410 294.2	2.933E-10	15.50	15.56
ν_4	E''	$-$	13	4	$2\nu_2$	E'	$+$	13	4	412 766.2	391 603.0	1.298E-9	−13.63	-14.37
$2\nu_2$	E'	$+$	3	2	ν_4	E''	$-$	2	0	418 312.4	418 044.7	3.347E-10	15.03	15.04
$2\nu_2$	E'	$+$	5	4	ν_4	E''	$-$	4	2	426 211.9	427 780.8	2.998E-10	13.77	13.72
$2\nu_2$	A_2'	$+$	13	0	ν_4	A_2''	$+$	13	1	427 273.2	444 607.4	8.633E-7	5.14	4.94
ν_4	E'	$-$	13	3	$2\nu_2$	E''	$-$	13	8	432 732.4	422 088.3	1.336E-9	-3.24	-3.32
ν_4	E''	$-$	7	6	$2\nu_2$	E'	$+$	8	8	436 285.0	429 917.9	1.476E-9	−12.77	-12.96
$2\nu_2$	A_2''	$-$	14	12	ν_4	A_2'	$+$	13	4	436 303.0	447 998.1	1.222E-10	1.36	1.32
ν_4	E''	$+$	8	1	$2\nu_2$	E'	$-$	7	5	449 011.2	444 718.8	4.822E-9	−3.44	-3.48
$2\nu_2$	E''	$-$	10	8	ν_4	E'	$-$	10	1	471 678.5		3.126E-10	-3.36	
ν_4	E''	$+$	11	1	$2\nu_2$	E'	$-$	10	1	472 739.7	462 948.4	1.469E-7	−6.20	-6.33
$2\nu_2$	E'	$+$	13	2	ν_4	E''	$+$	13	3	473 783.0	488 310.8	6.262E-11	9.78	9.49
$2\nu_2$	E'	$+$	11	2	ν_4	E''	$+$	12	9	477 572.4	489 990.1	1.758E-11	7.19	7.01
ν_4	E''	$-$	13	0	$2\nu_2$	E'	$-$	13	7	479 838.8	467 282.5	6.591E-9	-2.32	-2.38
$2\nu_2$	E''	$-$	8	4	ν_4	E'	$-$	9	1	485 870.6		5.687E-9	-0.51	
ν_4	E''	$+$	14	5	$2\nu_2$	E'	$+$	15	10	486 677.1	467 668.0	8.877E-10	−12.98	-13.51
$2\nu_2$	E''	$-$	11	8	ν_4	E'	$-$	11	3	490 061.7	490 267.1	2.737E-9	-3.19	-3.19
$2\nu_2$	E''	$-$	10	10	ν_4	E'	$+$	10	6	492 622.0	499 709.3	7.714E-8	−0.36	-0.35
ν_4	A_2''	$-$	11	10	$2\nu_2$	A_2'	$+$	10	6	494 681.5	496 832.3	8.060E-9	−1.76	-1.76
$2\nu_2$	E''	$+$	12	7	ν_4	E'	$+$	11	0	495 889.7	509 581.8	7.614E-11	8.86	8.62
$2\nu_2$	E'	$+$	13	8	ν_4	E''	$-$	12	2	498 381.0	515 446.1	3.328E-11	9.41	9.10
ν_4	E''	$+$	14	9	$2\nu_2$	E'	$+$	13	4	502 008.5	481 006.5	1.541E-11	−13.17	-13.74
ν_4	E''	$-$	3	0	$2\nu_2$	E'	$+$	4	4	509 875.0	509 939.3	2.820E-11	−14.19	-14.19
$2\nu_2$	E'	$-$	14	1	ν_4	E''	$-$	15	6	513 775.3	529 792.8	2.948E-10	4.18	4.05
$2\nu_2$	E''	$+$	12	7	ν_4	E'	$-$	11	1	518 473.1		7.981E-11	8.20	
$2\nu_2$	A_2'	$+$	9	6	ν_4	A_2''	$-$	8	2	520 115.9	530 125.8	6.108E-9	6.67	6.54

(*Continued*)

v'	Γ'	p'	J'	K'	v''	Γ''	p''	J''	K''	$\nu_{\rm calc}$/MHz	$\nu_{\rm exp}$/MHz	A/s^{-1}	$T_{\rm calc}$	$T_{\rm exp}$
ν_4	A_2''	−	11	10	$2\nu_2$	A_2'	+	12	12	527 967.5	522 798.6	5.244E-9	−6.89	-6.96
ν_4	A_2''	+	14	5	$2\nu_2$	A_2'	−	13	3	529 679.3	519 268.7	2.848E-8	−6.78	-6.92
ν_4	E'	−	9	1	$2\nu_2$	E''	−	8	4	544 495.1	536 665.8	5.798E-11	-2.32	-2.36
ν_4	A_2'	−	8	7	$2\nu_2$	A_2''	+	9	9	547 699.8	541 374.3	4.911E-9	−8.93	-9.03
$2\nu_2$	E'	−	10	7	ν_4	E''	−	10	0	551 917.9	562 160.3	2.505E-11	-0.39	-0.39
ν_4	E''	+	8	5	$2\nu_2$	E'	−	7	7	553 180.0	550 518.3	1.517E-9	−1.67	-1.68
$2\nu_2$	E''	−	11	2	ν_4	E'	+	12	4	554 034.4		4.035E-8	3.69	
$2\nu_2$	E'	+	11	10	ν_4	E''	−	10	8	556 948.4	552 032.8	6.561E-11	−0.65	-0.66
$2\nu_2$	A_2''	−	14	6	ν_4	A_2'	+	15	8	558 315.5	575 254.6	1.019E-8	4.32	4.20
$2\nu_2$	A_2''	+	12	9	ν_4	A_2'	−	13	13	563 019.2	565 112.9	7.362E-9	1.73	1.73
$2\nu_2$	E'	−	15	13	ν_4	E''	−	14	6	566 197.0	583 213.0	1.775E-8	0.14	0.13
ν_4	A_2'	+	12	8	$2\nu_2$	A_2''	+	11	3	574 312.4	561 928.1	8.085E-11	−8.53	-8.72
ν_4	E''	−	10	0	$2\nu_2$	E'	+	10	2	588 510.6	581 667.0	9.235E-8	−6.84	-6.92

Table B.4: Vibration-rotation-inversion frequencies (ν), Einstein A coefficients (A) and sensitivity coefficients (T) of $^{14}NH_3$ for transitions between the $2\nu_2$ and ν_4 vibrational states. Experimental frequencies have been obtained using energy levels from the MARVEL analysis [350].

v'	Γ'	p'	J'	K'	v''	Γ''	p''	J''	K''	$\nu_{\rm calc}$/MHz	$\nu_{\rm exp}$/MHz	A/s^{-1}	$T_{\rm calc}$	$T_{\rm exp}$
$2\nu_2$	A_2'	−	14	9	ν_4	A_2''	+	14	5	2869.0	13 943.5	2.496E-12	770.89	158.62
ν_4	E''	+	5	3	$2\nu_2$	E'	+	5	2	3540.5	389.9	1.894E-15	−1843.25	-16,737.52
$2\nu_2$	A_2''	−	13	12	ν_4	A_2'	+	12	4	3654.5	12 450.3	2.167E-18	125.08	36.71
$2\nu_2$	E'	+	6	2	ν_4	E''	+	6	3	7362.9	12 687.9	6.231E-14	877.49	509.21
$2\nu_2$	A_2''	+	13	9	ν_4	A_2'	−	14	13	8783.9	13 385.9	7.203E-13	260.35	170.84
ν_4	E''	+	4	3	$2\nu_2$	E'	+	4	2	10 441.8	9235.5	9.301E-15	−630.49	-712.84
ν_4	E''	+	12	7	$2\nu_2$	E'	−	11	7	13 244.8	3258.0	5.271E-18	−131.57	-534.87
ν_4	E''	+	3	3	$2\nu_2$	E'	+	3	2	13 727.5	14 116.6	2.066E-15	−484.00	-470.66
ν_4	A_2'	−	11	5	$2\nu_2$	A_2''	+	12	9	18 889.9	9313.7	3.659E-12	−233.82	-474.24
ν_4	E'	+	13	8	$2\nu_2$	E''	+	14	11	21 809.9	10 121.4	5.243E-21	−222.12	-478.64
$2\nu_2$	E'	+	7	2	ν_4	E''	+	7	3	22 031.7	29 771.2	4.761E-12	288.71	213.65
ν_4	E'	+	13	10	$2\nu_2$	E''	−	12	10	22 511.4	11 390.1	1.900E-17	−45.36	-89.65
$2\nu_2$	E''	−	11	8	ν_4	E'	+	11	2	24 283.2	29 727.5	6.991E-17	44.14	36.05
ν_4	A_2''	−	7	2	$2\nu_2$	A_2'	+	8	6	33 193.0	25 452.1	3.082E-13	−140.17	-182.79
ν_4	E''	−	12	8	$2\nu_2$	E'	−	12	11	37 009.4	34 972.4	5.319E-20	45.86	48.53
ν_4	E'	+	5	2	$2\nu_2$	E''	+	6	5	37 758.9	35 875.2	4.280E-17	−158.57	-166.89
ν_4	E'	+	10	8	$2\nu_2$	E''	+	9	1	42 879.3	29 604.5	3.786E-15	−142.81	-206.85
ν_4	E''	+	14	1	$2\nu_2$	E'	−	14	7	44 774.0	26 546.7	6.005E-13	−65.86	-111.08
$2\nu_2$	A_2''	−	15	6	ν_4	A_2'	−	15	1	47 199.3	59 449.2	9.114E-12	17.21	13.67
$2\nu_2$	E''	+	10	7	ν_4	E'	+	9	2	47 382.2	47 660.4	1.134E-16	74.98	74.55
$2\nu_2$	E''	+	8	7	ν_4	E'	+	7	4	49 067.0	53 771.1	3.235E-19	96.03	87.62
$2\nu_2$	E'	−	14	11	ν_4	E''	−	13	0	50 673.9	64 280.5	1.837E-17	-4.85	-3.82
ν_4	E''	+	10	7	$2\nu_2$	E'	+	11	10	53 258.1	49 792.6	7.021E-19	−73.12	-78.21
$2\nu_2$	E''	+	8	1	ν_4	E'	−	9	7	55 815.4	66 964.1	2.485E-14	106.98	89.17
$2\nu_2$	E'	+	5	4	ν_4	E''	−	4	0	60 051.4	63 043.9	5.157E-14	102.78	97.90
ν_4	E''	+	9	3	$2\nu_2$	E'	−	8	5	64 134.6	58 861.4	5.937E-16	−21.57	-23.50
$2\nu_2$	A_2''	+	10	3	ν_4	A_2'	+	11	8	65 303.8	72 587.6	2.485E-13	43.28	38.94
ν_4	E''	−	9	8	$2\nu_2$	E'	+	8	2	66 883.7	57 708.2	7.717E-17	−47.24	-54.75

(*Continued*)

v'	Γ'	p'	J'	K'	v''	Γ''	p''	J''	K''	ν_{calc}/MHz	ν_{exp}/MHz	A/s^{-1}	T_{calc}	T_{exp}
ν_4	E'	+	15	6	$2\nu_2$	E''	−	14	2	67 144.5	53 783.2	3.293E-12	−47.41	-59.18
ν_4	E'	−	10	1	$2\nu_2$	E''	+	11	7	68 862.3	59 127.9	2.090E-15	−53.67	-62.51
ν_4	E''	−	7	0	$2\nu_2$	E'	−	6	5	69 644.8	64 096.1	4.241E-15	-3.43	-3.73
$2\nu_2$	E'	+	9	8	ν_4	E''	−	8	6	72 271.0	78 005.7	3.767E-12	26.51	24.56
ν_4	E''	+	10	1	$2\nu_2$	E'	−	11	11	73 958.8	64 546.6	5.011E-17	−7.00	-8.02
$2\nu_2$	E'	+	12	4	ν_4	E''	+	13	9	77 781.2	94 457.9	1.745E-14	70.00	57.64
ν_4	E''	−	15	10	$2\nu_2$	E'	+	15	10	79 259.1	57 282.5	9.514E-16	−76.85	-106.33
$2\nu_2$	E'	+	15	8	ν_4	E''	−	14	0	82 460.9	103 540.2	4.726E-15	49.65	39.54
ν_4	E'	−	15	7	$2\nu_2$	E''	+	15	7	82 880.6	56 099.2	2.551E-16	−76.46	-112.96
ν_4	E''	+	13	9	$2\nu_2$	E'	+	12	2	86 193.3	72 994.5	3.558E-14	−52.03	-61.44
$2\nu_2$	A_2''	+	15	9	ν_4	A_2'	−	14	1	89 976.7	111 115.7	1.566E-18	60.20	48.75
ν_4	E''	+	10	9	$2\nu_2$	E'	+	9	4	93 115.5	81 629.4	3.945E-20	−49.44	-56.40
$2\nu_2$	E'	+	10	8	ν_4	E''	+	9	5	96 563.2	97 613.4	7.541E-20	35.95	35.56
ν_4	E''	−	8	2	$2\nu_2$	E'	−	7	5	104 453.7	103 325.9	2.312E-13	-7.79	-7.87
ν_4	E'	−	14	7	$2\nu_2$	E''	+	14	7	110 323.6	87 142.1	9.221E-16	−56.88	-72.01
ν_4	E'	+	10	0	$2\nu_2$	E''	+	11	7	113 903.1	105 079.2	3.443E-13	−41.85	-45.36
ν_4	A_2'	−	14	1	$2\nu_2$	A_2''	−	15	12	127 303.9	111 657.5	3.416E-16	-14.68	-16.74
ν_4	E''	−	12	0	$2\nu_2$	E'	−	12	7	128 808.8	116 841.5	2.621E-12	-5.35	-5.90
ν_4	E''	−	14	10	$2\nu_2$	E'	−	14	13	129 717.2	113 927.7	2.815E-15	-24.72	-28.14
ν_4	E'	−	13	7	$2\nu_2$	E''	+	13	7	137 931.5		2.502E-15	−42.72	
$2\nu_2$	E''	+	10	5	ν_4	E'	−	11	9	143 648.6	150 832.9	6.730E-18	23.80	22.66
$2\nu_2$	E''	−	10	4	ν_4	E'	+	11	4	147 482.9	156 281.9	2.428E-12	13.13	12.39
ν_4	A_2'	−	2	1	$2\nu_2$	A_2''	+	3	3	147 719.7	149 449.7	1.315E-12	−47.21	-46.66

Appendix C

Comprehensive tables of all investigated transitions of $H_3{}^{16}O^+$, $H_3{}^{18}O^+$ and $D_3{}^{16}O^+$ are provided. For all transitions, a TROVE computed frequency $\nu_{\rm calc}$ and corresponding sensitivity coefficient $T_{\rm calc}$ is given, and if available an experimental frequency $\nu_{\rm exp}$ and corresponding sensitivity coefficient $T_{\rm exp}$. Upper and lower states are labelled with a $'$ and $''$, respectively. Apart from the pure inversion transitions, all rotation-vibration energy levels have a symmetry (Γ), parity (p), rotational quantum number (J), and projection onto the molecule-fixed z axis (K) label. Einstein A coefficients are also provided.

Table C.1: Inversion frequencies (ν), Einstein coefficients (A), and sensitivities (T) of $H_3{}^{16}O^+$ in the ground vibrational state.

J	K	ν_{calc}/GHz	A/s^{-1}	T_{calc}	J	K	ν_{calc}/GHz	A/s^{-1}	T_{calc}
1	1	1655.8577	0.859E-1	-1.940	9	4	1299.1987	0.156E-1	-1.851
2	1	1632.1427	0.275E-1	-1.935	9	5	1361.3791	0.277E-1	-1.867
2	2	1657.2795	0.115E+0	-1.940	9	6	1440.7479	0.465E-1	-1.887
3	1	1597.1617	0.130E-1	-1.927	9	7	1539.6082	0.758E-1	-1.909
3	2	1621.8135	0.540E-1	-1.932	9	8	1660.8177	0.122E+0	-1.933
3	3	1663.6273	0.130E+0	-1.941	9	9	1807.9346	0.194E+0	-1.960
4	1	1551.6036	0.718E-2	-1.917	10	1	1116.0095	0.517E-3	-1.794
4	2	1575.6236	0.299E-1	-1.922	10	2	1133.9754	0.218E-2	-1.800
4	3	1616.3635	0.722E-1	-1.931	10	3	1164.3403	0.528E-2	-1.810
4	4	1674.9135	0.141E+0	-1.942	10	4	1207.1102	0.104E-1	-1.823
5	1	1496.3542	0.433E-2	-1.904	10	5	1265.3697	0.185E-1	-1.840
5	2	1519.6085	0.181E-1	-1.909	10	6	1339.7326	0.311E-1	-1.861
5	3	1559.1102	0.436E-1	-1.918	10	7	1432.3974	0.508E-1	-1.884
5	4	1615.7120	0.854E-1	-1.930	10	8	1546.0712	0.818E-1	-1.909
5	5	1691.1924	0.151E+0	-1.944	10	9	1684.1080	0.131E+0	-1.936
6	1	1432.4704	0.274E-2	-1.888	10	10	1850.6608	0.208E+0	-1.964
6	2	1454.8402	0.114E-1	-1.894	11	1	1028.6003	0.341E-3	-1.762
6	3	1492.7651	0.276E-1	-1.902	11	2	1045.3255	0.144E-2	-1.768
6	4	1547.2271	0.541E-1	-1.914	11	3	1067.9266	0.344E-2	-1.754
6	5	1619.8437	0.958E-1	-1.929	11	4	1112.7743	0.689E-2	-1.791
6	6	1712.5291	0.160E+0	-1.947	11	5	1166.9778	0.123E-1	-1.809
7	1	1361.1517	0.178E-2	-1.869	11	6	1236.1629	0.207E-1	-1.831
7	2	1382.5344	0.745E-2	-1.875	11	7	1322.4210	0.339E-1	-1.855
7	3	1419.9413	0.177E-1	-1.873	11	8	1428.3078	0.547E-1	-1.881
7	4	1470.7199	0.353E-1	-1.896	11	9	1556.9798	0.876E-1	-1.909
7	5	1540.1308	0.625E-1	-1.912	11	10	1712.3208	0.140E+0	-1.939
7	6	1628.7283	0.105E+0	-1.930	11	11	1899.1299	0.224E+0	-1.969
7	7	1739.0173	0.170E+0	-1.951	12	1	940.6819	0.222E-3	-1.725
8	1	1283.7070	0.118E-2	-1.848	12	2	956.1391	0.943E-3	-1.733
8	2	1304.0163	0.492E-2	-1.853	12	3	982.2569	0.231E-2	-1.744
8	3	1338.4028	0.119E-1	-1.863	12	4	1017.6294	0.454E-2	-1.755
8	4	1387.5621	0.234E-1	-1.875	12	5	1067.6920	0.810E-2	-1.774
8	5	1453.4769	0.414E-1	-1.891	12	6	1131.5933	0.137E-1	-1.797
8	6	1537.6131	0.696E-1	-1.910	12	7	1211.3128	0.225E-1	-1.822
8	7	1642.3757	0.113E+0	-1.931	12	8	1309.2553	0.364E-1	-1.850
8	8	1770.7731	0.181E+0	-1.955	12	9	1428.3843	0.585E-1	-1.879
9	1	1201.5193	0.780E-3	-1.822	12	10	1572.3335	0.937E-1	-1.910
9	2	1220.6846	0.327E-2	-1.829	12	11	1745.5500	0.151E+0	-1.942
9	3	1247.2272	0.736E-2	-1.769	12	12	1953.5372	0.243E+0	-1.974

Table C.2: Inversion frequencies (ν), Einstein coefficients (A), and sensitivities (T) of $H_3{}^{18}O^+$ in the ground vibrational state.

J	K	ν_{calc}/GHz	A/s^{-1}	T_{calc}	J	K	ν_{calc}/GHz	A/s^{-1}	T_{calc}
1	1	1608.7744	0.788E-1	-1.956	9	4	1249.7781	0.139E-1	-1.863
2	1	1584.8777	0.252E-2	-1.951	9	5	1311.5302	0.248E-1	-1.881
2	2	1610.0266	0.105E+0	-1.956	9	6	1390.4774	0.419E-1	-1.901
3	1	1549.6465	0.119E-1	-1.943	9	7	1488.9820	0.687E-1	-1.924
3	2	1574.2941	0.495E-1	-1.948	9	8	1609.9871	0.111E+0	-1.949
3	3	1616.1228	0.120E+0	-1.957	9	9	1757.1626	0.178E+0	-1.976
4	1	1503.7957	0.655E-2	-1.933	10	1	1067.7086	0.455E-3	-1.804
4	2	1527.7903	0.273E-1	-1.938	10	2	1085.4457	0.191E-2	-1.811
4	3	1568.5089	0.661E-1	-1.946	10	3	1115.4586	0.466E-2	-1.821
4	4	1627.0739	0.130E+0	-1.958	10	4	1157.7924	0.919E-2	-1.834
5	1	1448.2441	0.393E-2	-1.919	10	5	1215.5004	0.164E-1	-1.852
5	2	1471.4472	0.164E-1	-1.925	10	6	1289.2850	0.278E-1	-1.874
5	3	1510.9033	0.397E-1	-1.933	10	7	1381.3957	0.457E-1	-1.897
5	4	1567.4392	0.781E-1	-1.946	10	8	1494.6172	0.740E-1	-1.924
5	5	1642.9342	0.139E+0	-1.961	10	9	1632.4068	0.119E+0	-1.952
6	1	1384.0878	0.248E-2	-1.903	10	10	1799.0512	0.191E+0	-1.981
6	2	1406.3764	0.104E-1	-1.908	11	1	980.8269	0.297E-3	-1.770
6	3	1444.1869	0.250E-1	-1.917	11	2	997.2851	0.125E-2	-1.778
6	4	1498.5317	0.493E-1	-1.930	11	3	1020.2468	0.302E-2	-1.769
6	5	1571.0658	0.875E-1	-1.945	11	4	1063.8066	0.605E-2	-1.801
6	6	1663.7686	0.147E+0	-1.964	11	5	1117.3373	0.108E-1	-1.820
7	1	1312.5691	0.160E-2	-1.883	11	6	1185.7894	0.184E-1	-1.842
7	2	1333.8368	0.670E-2	-1.889	11	7	1271.2962	0.303E-1	-1.867
7	3	1372.3392	0.152E-1	-1.849	11	8	1376.4827	0.491E-1	-1.895
7	4	1421.6592	0.319E-1	-1.911	11	9	1504.5995	0.793E-1	-1.924
7	5	1490.8797	0.568E-1	-1.927	11	10	1659.6530	0.128E+0	-1.954
7	6	1579.3572	0.957E-1	-1.946	11	11	1846.6000	0.206E+0	-1.986
7	7	1689.6703	0.156E+0	-1.967	12	1	893.7115	0.191E-3	-1.732
8	1	1235.0417	0.105E-2	-1.860	12	2	908.8659	0.813E-3	-1.740
8	2	1255.1996	0.440E-2	-1.866	12	3	934.5041	0.200E-2	-1.752
8	3	1289.3581	0.107E-1	-1.876	12	4	969.2948	0.394E-2	-1.763
8	4	1338.2431	0.210E-1	-1.889	12	5	1018.5693	0.707E-2	-1.783
8	5	1403.8511	0.374E-1	-1.906	12	6	1081.5894	0.120E-1	-1.807
8	6	1487.7198	0.631E-1	-1.925	12	7	1160.3673	0.199E-1	-1.833
8	7	1592.3211	0.103E+0	-1.947	12	8	1257.3680	0.323E-1	-1.862
8	8	1720.7555	0.167E+0	-1.971	12	9	1375.6386	0.524E-1	-1.893
9	1	1152.9337	0.692E-3	-1.834	12	10	1518.9249	0.847E-1	-1.925
9	2	1171.9093	0.290E-2	-1.841	12	11	1691.8180	0.137E+0	-1.958
9	3	1200.2604	0.685E-2	-1.819	12	12	1900.0058	0.223E+0	-1.991

Table C.3: The rotation-inversion frequencies (ν), Einstein coefficients (A), and sensitivities (T) of $H_3{}^{16}O^+$ in the ground vibrational state[a].

Γ'	p'	J'	K'	Γ''	p''	J''	K''	$\nu_{\rm calc}$/MHz	$\nu_{\rm exp}$/MHz	A/s^{-1}	$T_{\rm calc}$	$T_{\rm exp}$
E'	0^-	1	1	E''	0^+	2	1	308483.172	307192.410[b]	0.556E-3	-5.992	-6.017
E'	0^+	3	2	E''	0^-	2	2	362865.643	364797.427[b,c]	0.432E-3	3.227	3.210
E''	0^+	3	1	E'	0^-	2	1	386507.906	388458.641	0.838E-3	2.891	2.876
A_2'	0^+	3	0	A_2''	0^-	2	0	394315.581	396272.412[d]	0.100E-2	2.788	2.775
A_2''	0^-	0	0	A_2'	0^+	1	0	985361.418	984711.888	0.362E-1	-2.575	-2.577
A_2''	0^+	4	3	A_2'	0^-	3	3	1028722.980	1031293.719	0.803E-2	0.492	0.491
E'	0^+	4	2	E''	0^-	3	2	1067224.066	1069826.484	0.155E-1	0.392	0.391
E''	0^+	4	1	E'	0^-	3	1	1089903.366	1092523.071	0.207E-1	0.336	0.335
A_2''	0^+	5	3	A_2'	0^-	4	3	1741874.136	1745127.371	0.589E-1	-0.154	-0.153
E'	0^+	5	2	E''	0^-	4	2	1778525.083	1781805.268	0.829E-1	-0.198	-0.197
E''	0^+	5	1	E'	0^-	4	1	1800111.519	1803407.189	0.986E-1	-0.223	-0.222
A_2'	0^+	5	0	A_2''	0^-	4	0	1807154.483	1810454.545	0.104E+0	-0.231	-0.230
E''	0^+	7	5	E'	0^-	6	5	3073339.801	3077891.800	0.255E+0	-0.521	-0.520
A_2''	0^-	2	0	A_2'	0^+	1	0	2970878.114	2972100[e]	0.399E+0	-1.515	-1.515
E'	0^-	2	1	E''	0^+	1	1	2979517.263	2980725[e]	0.301E+0	-1.518	-1.517
E''	0^-	3	2	E'	0^+	2	2	3641958.615	3643830[f]	0.437E+0	-1.422	-1.421
E'	0^-	3	1	E''	0^+	2	1	3615812.275	3617711[f]	0.687E+0	-1.416	-1.415
A_2'	0^-	4	3	A_2''	0^+	3	3	4308712.151	4311203[f]	0.591E+0	-1.356	-1.355
E''	0^-	4	2	E'	0^+	3	2	4264661.127	4267265[f]	0.990E+0	-1.347	-1.346
E'	0^-	4	1	E''	0^+	3	1	4238668.671	4241306[f]	0.122E+1	-1.341	-1.341
A_2''	0^-	4	0	A_2'	0^+	3	0	4230078.747	4232743[f]	0.130E+1	-1.340	-1.339
E''	0^-	5	4	E'	0^+	4	4	4979729.095	4982921[f]	0.768E+0	-1.309	-1.308

[a] If not stated otherwise, the experimental frequencies have been taken from Yu and Pearson [383]. [b] Also observed astronomically in van der Tak et al. [370] [c] Also observed astronomically in Wootten et al. [366] [d] Also observed astronomically in Phillips et al. [367] [e] Astronomical observation from Goicoechea and Cernicharo [369]. [f] Astronomical observation from González-Alfonso et al. [375].

Table C.4: The rotation-inversion frequencies (ν), Einstein coefficients (A), and sensitivities (T) of $H_3{}^{18}O^+$ in the ground vibrational state.

Γ'	p'	J'	K'	Γ''	p''	J''	K''	ν_{calc}/MHz	A/s^{-1}	T_{calc}
A_2''	0^-	0	0	A_2'	0^+	1	0	939604	0.314E-1	-2.633
E'	0^-	2	1	E''	0^+	1	1	2929768	0.287E+0	-1.520
A_2''	0^-	2	0	A_2'	0^+	1	0	2921121	0.379E+0	-1.518
E'	0^-	1	1	E''	0^+	2	1	263884	0.349E-3	-6.765
E''	0^-	3	2	E'	0^+	2	2	3590704	0.419E+0	-1.423
E'	0^-	3	1	E''	0^+	2	1	3564536	0.659E+0	-1.416
E'	0^+	3	2	E''	0^-	2	2	406384	0.607E-3	2.728
E''	0^+	3	1	E'	0^-	2	1	430012	0.116E-2	2.452
A_2'	0^+	3	0	A_2''	0^-	2	0	437812	0.137E-2	2.367
A_2'	0^-	4	3	A_2''	0^+	3	3	4255872	0.570E+0	-1.356
E''	0^-	4	2	E'	0^+	3	2	4211784	0.955E+0	-1.347
E'	0^-	4	1	E''	0^+	3	1	4185782	0.118E+1	-1.341
A_2''	0^-	4	0	A_2'	0^+	3	0	4177192	0.125E+1	-1.339
A_2''	0^+	4	3	A_2'	0^-	3	3	1071240	0.908E-2	0.414
E'	0^+	4	2	E''	0^-	3	2	1109700	0.174E-1	0.320
E''	0^+	4	1	E'	0^-	3	1	1132340	0.233E-1	0.268
E''	0^-	5	4	E'	0^+	4	4	4925223	0.744E+0	-1.309
A_2'	0^+	5	0	A_2''	0^+	4	3	4703383	0.813E-3	-1.020
A_2'	0^-	5	3	A_2''	0^+	4	3	4862806	0.128E+1	-1.296
E'	0^+	5	4	E''	0^-	4	4	1730710	0.322E-1	-0.121
E''	0^-	5	2	E'	0^+	4	2	4819190	0.165E+1	-1.288
E'	0^-	5	1	E''	0^+	4	1	4793510	0.187E+1	-1.283
A_2''	0^+	5	3	A_2'	0^-	4	3	1783394	0.633E-1	-0.185
E''	0^+	5	2	E'	0^-	4	2	1819952	0.889E-1	-0.228
E''	0^+	5	1	E'	0^-	4	1	1841471	0.106E+0	-0.252
A_2'	0^+	5	0	A_2''	0^-	4	0	1848471	0.111E+0	-0.260
A_2'	0^-	5	3	A_2''	0^-	4	0	2007895	0.113E-3	-0.990

Table C.5: The frequencies (ν), Einstein coefficients (A), and sensitivities (T) of the strongest 'forbidden' rotation-inversion transitions in the ground vibrational state of $H_3{}^{16}O^+$.

Γ'	p'	J'	K'	Γ''	p''	J''	K''	$\nu_{\rm calc}$/MHz	$A/{\rm s}^{-1}$	$T_{\rm calc}$
A_2'	0^+	7	0	A_2''	0^+	6	3	6013041	0.532E-1	-1.012
A_2'	0^-	7	3	A_2''	0^-	6	0	3320905	0.115E-1	-0.982
A_2''	0^+	8	3	A_2'	0^+	7	0	3986710	0.132E-1	-0.985
A_2''	0^-	8	0	A_2'	0^-	7	3	6509745	0.713E-1	-0.980
A_2'	0^+	9	0	A_2''	0^+	8	3	7288334	0.473E+0	-1.011
E'	0^-	9	1	E''	0^-	8	4	7989021	0.354E-2	-0.974
A_2'	0^-	9	3	A_2''	0^-	8	0	4609322	0.133E+0	-0.962
E''	0^+	10	1	E'	0^+	9	2	7028329	0.327E-2	-0.991
E''	0^+	10	1	E'	0^+	9	4	8788561	0.292E-2	-0.996
E''	0^-	10	2	E'	0^-	9	5	9456048	0.352E-2	-0.970
E'	0^-	10	1	E''	0^-	9	4	8605372	0.737E-2	-0.971
A_2''	0^-	10	0	A_2'	0^-	9	3	7767436	0.758E+0	-0.983
A_2''	0^+	10	3	A_2'	0^+	9	0	5280810	0.218E+0	-0.969
A_2'	0^-	11	3	A_2''	0^-	10	6	10906889	0.460E-2	-0.964
E''	0^-	11	2	E'	0^-	10	5	10058374	0.717E-2	-0.967
E''	0^+	11	1	E'	0^+	10	4	9392283	0.509E-2	-0.990
A_2'	0^+	11	0	A_2''	0^+	10	3	8521500	0.203E+0	-0.991
E'	0^-	11	1	E''	0^-	10	4	9213773	0.138E-1	-0.967
A_2'	0^-	11	3	A_2''	0^-	10	0	5884393	0.687E-1	-0.970
E'	0^-	12	5	E''	0^-	11	8	13229315	0.464E-2	-0.965
E''	0^-	12	4	E'	0^-	11	7	12356185	0.663E-2	-0.963
A_2'	0^-	12	3	A_2''	0^-	11	6	11498974	0.917E-2	-0.963
E'	0^+	12	2	E''	0^+	11	5	10862715	0.255E-2	-0.986
E''	0^-	12	2	E'	0^-	11	5	10651877	0.132E-1	-0.962
E''	0^+	12	1	E'	0^+	11	4	9985895	0.813E-2	-0.983
E'	0^-	12	1	E''	0^-	11	4	9813803	0.238E-1	-0.963
A_2'	0^-	12	0	A_2''	0^-	11	3	8987776	0.381E+0	-0.967
E'	0^+	12	4	E''	0^+	11	1	5706783	0.502E-2	-0.979
A_2''	0^+	12	3	A_2'	0^+	11	0	6554476	0.142E+0	-0.975

Table C.6: Combination differences (CD) of the 'forbidden' ($\Delta|k-l|=3$) and allowed ($\Delta|k-l|=0$) transitions between the ν_3 and ground vibrational states in $H_3{}^{16}O^+$ [a].

Allowed	ν_{calc}/cm^{-1}	ν_{exp}/cm^{-1}	A/s^{-1}	Forbidden	ν_{calc}/cm^{-1}	ν_{exp}/cm^{-1}	A/s^{-1}	CD/cm^{-1}
$^{r}P(3,0)^{+}$	3457.025		0.390E+3	$^{o}P(3,3)^{-}$	3447.266		0.826E-1	9.7594
$^{r}Q(3,0)^{+}$	3523.544		0.964E+3	$^{o}Q(3,3)^{-}$	3513.785		0.189E-1	9.7594
$^{r}R(3,0)^{+}$	3610.441		0.530E+3	$^{o}R(3,3)^{-}$	3600.682		0.326E-1	9.7594
$^{p}P(3,3)^{-}$	3474.787		0.934E+3	$^{s}P(3,0)^{+}$	3484.546		0.420E-1	9.7594
$^{p}Q(3,3)^{-}$	3539.922		0.233E+3	$^{s}Q(3,0)^{+}$	3549.681		0.142E+0	9.7594
$^{p}R(3,3)^{-}$	3626.725		0.246E+2	$^{s}R(3,0)^{+}$	3636.484		0.222E+0	9.7594
$^{r}R(3,3)^{-}$	3564.692		0.730E+3	$^{u}R(3,0)^{+}$	3574.452		0.104E-1	9.7594
$^{r}P(5,0)^{+}$	3409.061		0.434E+3	$^{o}P(5,3)^{-}$	3402.343		0.543E+0	6.7184
$^{r}Q(5,0)^{+}$	3520.120		0.954E+3	$^{o}Q(5,3)^{-}$	3513.402		0.206E-1	6.7184
$^{r}R(5,0)^{+}$	3649.203		0.508E+3	$^{o}R(5,3)^{-}$	3642.485		0.558E+0	6.7184
$^{p}P(5,3)^{-}$	3428.386		0.577E+3	$^{s}P(5,0)^{+}$	3435.104		0.441E+0	6.7184
$^{r}P(5,3)^{-}$	3366.353		0.222E+2	$^{u}P(5,0)^{+}$	3373.071		0.110E-1	6.7184
$^{p}Q(5,3)^{-}$	3536.580		0.375E+3	$^{s}Q(5,0)^{+}$	3543.298		0.130E+0	6.7184
$^{r}Q(5,3)^{-}$	3474.807		0.274E+3	$^{u}Q(5,0)^{+}$	3481.525		0.153E+0	6.7184
$^{p}R(5,3)^{-}$	3666.517		0.650E+2	$^{s}R(5,0)^{+}$	3673.236		0.673E+0	6.7184
$^{r}R(5,3)^{-}$	3604.698		0.540E+3	$^{u}R(5,0)^{+}$	3611.416		0.356E+0	6.7184
$^{r}P(7,0)^{+}$	3359.844		0.441E+3	$^{o}P(7,3)^{-}$	3357.106		0.877E+1	2.7377
$^{r}Q(7,0)^{+}$	3515.328		0.930E+3	$^{o}Q(7,3)^{-}$	3512.590		0.965E+1	2.7377
$^{r}R(7,0)^{+}$	3685.519		0.482E+3	$^{o}R(7,3)^{-}$	3682.782		0.104E+2	2.7377
$^{p}P(7,3)^{-}$	3381.138	3385.075	0.442E+3	$^{s}P(7,0)^{+}$	3383.876	3387.725	0.762E+1	2.7377(2.650)
$^{r}P(7,3)^{-}$	3319.319	3323.231	0.664E+2	$^{u}P(7,0)^{+}$	3322.056	3325.884	0.111E+1	2.7377(2.653)
$^{p}Q(7,3)^{-}$	3531.771	3535.834	0.421E+3	$^{s}Q(7,0)^{+}$	3534.508	3538.495	0.205E+1	2.7377(2.661)
$^{r}Q(7,3)^{-}$	3470.509		0.340E+3	$^{u}Q(7,0)^{+}$	3473.246		0.617E+1	2.7377
$^{p}R(7,3)^{-}$	3704.670		0.851E+2	$^{s}R(7,0)^{+}$	3707.407		0.387E+1	2.7377
$^{r}R(7,3)^{-}$	3642.850		0.445E+3	$^{u}R(7,0)^{+}$	3645.587		0.903E+1	2.7377
$^{r}P(9,0)^{+}$	3309.424	3313.435	0.424E+3	$^{o}P(9,3)^{-}$	3311.889	3315.944	0.311E+2	2.4653(2.509)
$^{r}Q(9,0)^{+}$	3509.010	3513.136	0.833E+3	$^{o}Q(9,3)^{-}$	3511.475	3515.651	0.856E+2	2.4653(2.515)
$^{r}R(9,0)^{+}$	3719.122		0.449E+3	$^{o}R(9,3)^{-}$	3721.587		0.287E+2	2.4653
$^{p}P(9,3)^{-}$	3333.778	3337.640	0.350E+3	$^{s}P(9,0)^{+}$	3331.312	3335.123	0.292E+2	2.4653(2.517)
$^{r}P(9,3)^{-}$	3271.958	3275.802	0.946E+2	$^{u}P(9,0)^{+}$	3269.492	3273.280	0.752E+1	2.4653(2.522)
$^{p}Q(9,3)^{-}$	3525.875	3529.900	0.394E+3	$^{s}Q(9,0)^{+}$	3523.410	3527.384	0.540E+2	2.4653(2.516)
$^{r}Q(9,3)^{-}$	3465.261	3469.262	0.340E+3	$^{u}Q(9,0)^{+}$	3462.796	3466.750	0.241E+2	2.4653(2.512)
$^{p}R(9,3)^{-}$	3741.744		0.958E+2	$^{s}R(9,0)^{+}$	3739.278		0.351E+1	2.4653
$^{r}R(9,3)^{-}$	3679.393		0.375E+3	$^{u}R(9,0)^{+}$	3676.927		0.222E+2	2.4653
$^{r}P(11,0)^{+}$	3258.726		0.445E+3	$^{o}P(11,3)^{-}$	3266.211		0.861E+1	7.4847
$^{r}Q(11,0)^{+}$	3501.923		0.856E+3	$^{o}Q(11,3)^{-}$	3509.407		0.340E+2	7.4847
$^{r}R(11,0)^{+}$	3750.757		0.456E+3	$^{o}R(11,3)^{-}$	3758.241		0.527E+1	7.4847
$^{p}P(11,3)^{-}$	3286.368	3290.155	0.317E+3	$^{s}P(11,0)^{+}$	3278.883	3282.529	0.937E+1	7.4847(7.626)
$^{r}P(11,3)^{-}$	3224.017	3227.779	0.121E+3	$^{u}P(11,0)^{+}$	3216.532	3220.154	0.295E+1	7.4847(7.625)
$^{p}Q(11,3)^{-}$	3518.513		0.433E+3	$^{s}Q(11,0)^{+}$	3511.028		0.310E+2	7.4847
$^{r}Q(11,3)^{-}$	3458.662		0.353E+3	$^{u}Q(11,0)^{+}$	3451.178		0.502E+1	7.4847
$^{p}R(11,3)^{-}$	3777.943		0.975E+2	$^{s}R(11,0)^{+}$	3770.459		0.343E+0	7.4847
$^{r}R(11,3)^{-}$	3714.190		0.261E+3	$^{u}R(11,0)^{+}$	3706.706		0.738E-1	7.4847

[a] Experimental frequencies from Tang and Oka [379] and Uy et al. [378]. Experimental CD data in parentheses. Transitions with $\Delta J=-1,0,+1$ are described using the labels P, Q, R respectively, whilst the superscript o,p,q,r,s,t,u notation corresponds to transitions with $\Delta K=-2,-1,0,+1,+2,+3,+4$ respectively. All transitions are between states of A_2' and A_2'' symmetry, where $+(-)\rightarrow+(-)$ are allowed, and $+(-)\rightarrow-(+)$ are forbidden.

Table C.7: The 'forbidden' combination differences (ν) and sensitivities (T) of the $H_3{}^{16}O^+$ and $H_3{}^{18}O^+$ ground vibrational state transitions[a].

Γ'	p'	J'	K'	Γ''	p''	J''	K''	$\nu_{\rm calc}$/MHz	$\nu_{\rm exp}$/MHz	$T_{\rm calc}$	$T_{\rm exp}$
								$H_3{}^{16}O^+$			
A_2''	0^+	8	3	A_2''	0^-	8	6	2490592	2499819	-0.492	-0.490
A_2''	0^+	9	3	A_2''	0^-	9	6	2549767	2557200	-0.536	-0.534
E'	0^+	7	4	E'	0^-	7	7	3257694	3261952	-0.566	-0.565
E'	0^+	8	4	E'	0^-	8	7	3311613	3316064	-0.597	-0.596
E'	0^+	8	4	E'	0^-	8	7	3311613	3316124	-0.597	-0.596
E''	0^+	7	7	E''	0^-	5	4	2096835	2100526	-0.196	-0.196
E''	0^-	7	4	E''	0^+	7	7	6467432	6471380	-1.241	-1.240
E''	0^-	7	4	E''	0^+	7	7	6467432	6473688	-1.241	-1.239
E''	0^-	8	4	E''	0^+	8	7	6341551	6347955	-1.222	-1.221
A_1'	0^-	3	3	A_2'	0^+	3	0	292579		-6.094	
A_2'	0^-	5	3	A_2'	0^+	5	0	201415		-7.803	
A_2'	0^-	7	3	A_2'	0^+	7	0	82072	79535	-15.416	-15.907
A_2'	0^-	7	3	A_2'	0^+	7	0	82072	79445	-15.416	-15.925
A_2'	0^-	7	3	A_2'	0^+	7	0	82072	79775	-15.416	-15.859
A_2'	0^-	9	3	A_2'	0^+	9	0	73906	75308	10.518	10.322
A_2'	0^-	9	3	A_2'	0^+	9	0	73906	75608	10.518	10.281
A_2'	0^-	9	3	A_2'	0^+	9	0	73906	75458	10.518	10.302
A_2'	0^-	9	3	A_2'	0^+	9	0	73906	75428	10.518	10.306
A_2'	0^-	9	3	A_2'	0^+	9	0	73906	75218	10.518	10.344
A_2'	0^-	9	3	A_2'	0^+	9	0	73906	75398	10.518	10.310
A_2'	0^-	11	3	A_2'	0^+	11	0	224387	228592	2.508	2.462
A_2'	0^-	11	3	A_2'	0^+	11	0	224387	228622	2.508	2.461
								$H_3{}^{18}O^+$			
A_2'	0^-	3	3	A_2'	0^+	3	0	251040		-6.858	
A_2'	0^-	5	3	A_2'	0^+	5	0	159424		-9.453	
A_2'	0^-	7	3	A_2'	0^+	7	0	42250		-26.035	
A_2'	0^-	9	3	A_2'	0^+	9	0	111874		7.280	
A_1'	0^-	11	3	A_2'	0^+	11	0	263960		1.933	

[a] Experimental frequencies from Tang and Oka [379] and Uy et al. [378].

Table C.8: Inversion frequencies (ν), Einstein coefficients (A), and sensitivities (T) of $D_3{}^{16}O^+$ in the ground vibrational state.

J	K	ν_{calc}/MHz	A/s^{-1}	T_{calc}	J	K	ν_{calc}/MHz	A/s^{-1}	T_{calc}
1	1	461457.7	0.202E-2	-2.594	9	3	396223.5	0.262E-3	-2.532
2	1	457746.8	0.659E-3	-2.591	9	-3	396307.6	0.262E-3	-2.533
2	2	462036.6	0.271E-2	-2.595	9	4	404995.9	0.495E-3	-2.541
3	1	452238.3	0.318E-3	-2.586	9	5	416478.0	0.837E-3	-2.552
3	2	456477.0	0.131E-2	-2.590	9	6	430926.5	0.133E-2	-2.565
3	3	463624.8	0.307E-2	-2.596	9	7	448609.6	0.202E-2	-2.580
3	-3	463624.9	0.307E-2	-2.596	9	8	469861.2	0.301E-2	-2.597
4	1	445000.1	0.182E-3	-2.580	9	9	495091.4	0.441E-2	-2.617
4	2	449171.5	0.749E-3	-2.583	10	1	371355.7	0.197E-4	-2.506
4	3	456206.1	0.176E-2	-2.589	10	2	374847.8	0.811E-4	-2.510
4	-3	456205.3	0.176E-2	-2.589	10	3	380737.2	0.191E-3	-2.516
4	4	466229.2	0.333E-2	-2.597	10	-3	380588.7	0.191E-3	-2.515
5	1	436120.3	0.115E-3	-2.572	10	4	389060.1	0.361E-3	-2.525
5	2	440209.4	0.471E-3	-2.575	10	5	400099.1	0.610E-3	-2.536
5	3	447102.0	0.111E-2	-2.581	10	6	413989.0	0.968E-3	-2.549
5	-3	447105.0	0.111E-2	-2.581	10	7	430988.1	0.148E-2	-2.564
5	4	456929.3	0.209E-2	-2.590	10	8	451417.0	0.220E-2	-2.582
5	5	469861.8	0.354E-2	-2.600	10	9	475669.3	0.322E-2	-2.601
6	1	425705.7	0.765E-4	-2.562	10	10	504223.5	0.469E-2	-2.622
6	2	429698.4	0.314E-3	-2.565	11	1	355354.7	0.145E-4	-2.488
6	3	436431.4	0.739E-3	-2.572	11	2	358700.1	0.595E-4	-2.492
6	-3	436422.5	0.739E-3	-2.571	11	3	364095.1	0.140E-3	-2.497
6	4	446021.4	0.140E-2	-2.580	11	-3	364342.1	0.140E-3	-2.498
6	5	458648.4	0.236E-2	-2.590	11	4	372266.1	0.265E-3	-2.507
6	6	474539.6	0.374E-2	-2.603	11	5	382838.8	0.448E-3	-2.518
7	1	413879.5	0.529E-4	-2.550	11	6	396141.0	0.711E-3	-2.531
7	2	417762.9	0.217E-3	-2.554	11	7	412420.4	0.108E-2	-2.547
7	3	424290.4	0.511E-3	-2.560	11	8	431984.1	0.161E-2	-2.564
7	-3	424311.5	0.511E-3	-2.560	11	9	455208.5	0.237E-2	-2.584
7	4	433633.4	0.966E-3	-2.568	11	10	482551.0	0.345E-2	-2.605
7	5	445914.1	0.163E-2	-2.579	11	11	514564.3	0.500E-2	-2.629
7	6	461368.9	0.259E-2	-2.592	12	1	338716.8	0.106E-4	-2.468
7	7	480284.7	0.395E-2	-2.607	12	2	341909.8	0.438E-4	-2.472
8	1	400778.6	0.375E-4	-2.537	12	3	347292.8	0.103E-3	-2.479
8	2	404541.2	0.154E-3	-2.541	12	-3	346901.5	0.103E-3	-2.477
8	3	410886.1	0.363E-3	-2.547	12	4	354781.7	0.195E-3	-2.487
8	-3	410841.9	0.363E-3	-2.547	12	5	364869.9	0.330E-3	-2.498
8	4	419907.3	0.686E-3	-2.556	12	6	377561.1	0.524E-3	-2.512
8	5	431804.8	0.116E-2	-2.566	12	7	393092.4	0.800E-3	-2.527
8	6	446776.9	0.184E-2	-2.579	12	8	411756.9	0.119E-2	-2.545
8	7	465101.3	0.280E-2	-2.594	12	9	433913.7	0.175E-2	-2.565
8	8	487124.4	0.417E-2	-2.612	12	10	459998.3	0.255E-2	-2.587
9	1	386551.6	0.271E-4	-2.523	12	11	490536.8	0.369E-2	-2.610
9	2	390183.3	0.111E-3	-2.526	12	12	526162.6	0.535E-2	-2.635

Table C.9: The frequencies (ν), Einstein coefficients (A), and sensitivities (T) of the rotation-inversion transitions in the ground vibrational state of $D_3{}^{16}O^+$.

Γ'	p'	J'	K'	Γ''	p''	J''	K''	$\nu_{\rm calc}$/MHz	$A/{\rm s}^{-1}$	$T_{\rm calc}$
A_1''	0^-	1	0	A_1'	0^+	0	0	799894[a]	0.703E-2	-1.919
A_2''	0^-	0	0	A_2'	0^+	1	0	122016	0.748E-4	-7.018
E'	0^-	2	1	E''	0^+	1	1	1137348	0.182E-1	-1.644
A_2''	0^-	2	0	A_2'	0^+	1	0	1135859	0.242E-1	-1.643
E''	0^+	2	1	E'	0^-	1	1	218144	0.128E-3	2.352
A_1'	0^+	2	0	A_1''	0^-	1	0	219509	0.174E-3	2.319
E''	0^-	3	2	E'	0^+	2	2	1475670	0.315E-1	-1.496
E'	0^-	3	1	E''	0^+	2	1	1471128	0.501E-1	-1.492
A_1''	0^-	3	0	A_1'	0^+	2	0	1469623	0.562E-1	-1.490
E'	0^+	3	2	E''	0^-	2	2	557156	0.170E-2	0.311
E''	0^+	3	1	E'	0^-	2	1	561143	0.278E-2	0.287
A_2'	0^+	3	0	A_2''	0^-	2	0	562464	0.315E-2	0.279
A_1'	0^-	4	-3	A_1''	0^+	3	-3	1814847	0.479E-1	-1.404
A_2'	0^-	4	3	A_2''	0^+	3	3	1814848	0.479E-1	-1.404
E''	0^-	4	2	E'	0^+	3	2	1807141	0.813E-1	-1.398
A_2''	0^+	4	3	A_2'	0^-	3	3	895017	0.574E-2	-0.183
A_1''	0^+	4	-3	A_1'	0^-	3	-3	895017	0.574E-2	-0.183
E'	0^-	4	1	E''	0^+	3	1	1802568	0.101E+0	-1.394
A_2''	0^-	4	0	A_2'	0^+	3	0	1801051	0.108E+0	-1.393
E'	0^+	4	2	E''	0^-	3	2	901493	0.101E-1	-0.203
E''	0^+	4	1	E'	0^-	3	1	905329	0.128E-1	-0.215
A_1'	0^+	4	0	A_1''	0^-	3	0	906601	0.137E-1	-0.219
E''	0^-	5	4	E'	0^+	4	4	2154875	0.675E-1	-1.342
E'	0^+	5	4	E''	0^-	4	4	1231716	0.126E-1	-0.403
A_2'	0^-	5	3	A_2''	0^+	4	3	2143872	0.119E+0	-1.334
A_1'	0^-	5	-3	A_1''	0^+	4	-3	2143874	0.119E+0	-1.334
E''	0^-	5	2	E'	0^+	4	2	2136144	0.154E+0	-1.328
A_2''	0^+	5	3	A_2'	0^-	4	3	1240564	0.230E-1	-0.423
A_1''	0^+	5	-3	A_1'	0^-	4	-3	1240564	0.230E-1	-0.423
E'	0^-	5	1	E''	0^+	4	1	2131556	0.176E+0	-1.325
A_1''	0^-	5	0	A_1'	0^+	4	0	2130034	0.183E+0	-1.324
E'	0^+	5	2	E''	0^-	4	2	1246763	0.307E-1	-0.436
E''	0^+	5	1	E'	0^-	4	1	1250435	0.354E-1	-0.443
A_2'	0^+	5	0	A_2''	0^-	4	0	1251654	0.370E-1	-0.446

[a] Experimental value of 798713.814 MHz measured in Furuya and Saito [381]. Note that states with $K = +3$ are of A_2 symmetry, whilst those with $K = -3$ are of A_1 symmetry.

Table C.10: The frequencies (ν), Einstein coefficients (A), and sensitivities (T) of the strongest 'forbidden' rotation-inversion transitions in the ground vibrational state of $D_3{}^{16}O^+$.

Γ'	p'	J'	K'	Γ''	p''	J''	K''	$\nu_{\rm calc}$/MHz	$A/{\rm s}^{-1}$	$T_{\rm calc}$
A_1''	0^-	9	0	A_1'	0^-	8	-3	3688528	0.170E-3	-0.989
A_1'	0^+	10	0	A_1''	0^+	9	-3	4042517	0.147E-3	-1.000
A_2''	0^-	10	0	A_2'	0^-	9	3	4016397	0.375E-3	-0.987
E'	0^-	11	1	E''	0^-	10	4	4785669	0.151E-3	-0.985
A_2'	0^+	11	0	A_2''	0^+	10	3	4368847	0.288E-3	-0.997
A_1''	0^-	11	0	A_1'	0^-	10	-3	4342344	0.754E-3	-0.985
A_1''	0^+	11	-3	A_1'	0^+	10	0	3024066	0.275E-3	-0.991
E''	0^-	12	2	E'	0^-	11	5	5551457	0.191E-3	-0.983
E'	0^-	12	1	E''	0^-	11	4	5107776	0.289E-3	-0.983
A_1'	0^+	12	0	A_1''	0^+	11	-3	4692929	0.520E-3	-0.994
A_2''	0^-	12	0	A_2'	0^-	11	3	4666233	0.140E-2	-0.983
A_2''	0^+	12	3	A_2'	0^+	11	0	3354397	0.556E-3	-0.989
A_1'	0^-	12	-3	A_1''	0^-	11	0	3347266	0.160E-3	-0.985

Note that states with $K = +3$ are of A_2 symmetry, whilst those with $K = -3$ are of A_1 symmetry.

Table C.11: The 'forbidden' combination differences (ν) and sensitivities (T) of the $D_3{}^{16}O^+$ ground vibrational state transitions[a] .

Γ'	p'	J'	K'	Γ''	p''	J''	K''	$\nu_{\rm calc}$/MHz	$\nu_{\rm exp}$/MHz	$T_{\rm calc}$	$T_{\rm exp}$
A_2'	0+	8	6	A_2'	0+	7	6	2711462	2714369	-1.004	-1.003
A_2'	0+	7	6	A_2'	0+	6	6	2376103	2378622	-1.006	-1.005
E'	0+	6	4	E'	0+	5	4	2035287	2037351	-1.005	-1.004
A_2''	0+	4	3	A_2''	0+	3	3	1358641	1360071	-1.006	-1.005
A_1''	0+	4	-3	A_1''	0+	3	-3	1358642	1360071	-1.006	-1.005
E'	0+	3	2	E'	0+	2	2	1019193	1020224	-1.006	-1.005
E'	0+	5	2	E'	0+	4	2	1695934	1697704	-1.005	-1.004

[a] Experimental frequencies from Araki et al. [380].